EXPERT REPORT

Prepared for United States Department of Justice
Robinson v. United States

Prepared by:

BRUCE A. EBERSOLE, P.E.
United States Army Corps of Engineers
Chief, Flood and Storm Protection Division
Coastal and Hydraulics Laboratory
Engineer Research and Development Center
Vicksburg, MS
December 17, 2008

Expert Report – Bruce A. Ebersole

			Page
Executive Summary			5
I.	**Introduction**		7
	a.	Scope of the Report	7
	b.	Study Area	7
	c.	Approach	8
II.	**Hurricane Katrina Storm Surge and Waves (Regional Perspective)**		11
	a.	Measured Water Levels	11
		i. High Water Marks – Indicators of Maximum Water Level	11
		ii. Hydrographs – Variation of Water Level with Time	14
	b.	Computer Simulation of Waves and Surge	15
		i. Models Used – Corps' Approach	15
		ii. Evolution of the Storm Surge (Synoptic View)	16
		iii. Maximum Water Level (Synoptic View)	25
		iv. Evolution of the Storm Waves (Synoptic View)	29
		v. Maximum Wave Height and Corresponding Period (Synoptic View)	37
	c.	Best Estimates of Water Level and Wave Conditions for Selected Locations	39
		i. Along the MRGO Reach 2 Levee	39
		ii. At IHNC Breach Sites	43

III. Surf Zone Dynamics – Implications for Levee Erosion 44

a. Wave Breaking, Run-up and Overtopping During the Storm 44

b. Visualization of Wave Overtopping and Overflow 47

c. Results from High-Resolution Modeling of Velocities at the MRGO Reach 2 Levee 49

IV. Levee Response 52

a. Data Sources 52

b. Factors that Influence Levee Erodability 53

c. Erodability as a Function of Freeboard and Sediment Type 55

i. Levees Along GIWW (East of Michoud Canal) 57

ii. Levees Along MRGO Reach 2 59

iii. Summary 63

d. Erodability – Results from ILIT Flume Tests 63

i. Applicability of the EFA Erosion Flume 63

ii. Sample Collection, Preparation and Testing Methods 64

iii. Results for Sample S-4 72

iv. Results for Samples S-5 and S-6 73

v. Results for Sample S-15 74

vi. Results for Sample S-3 75

vii. Summary 76

e. Influence of Placement Method on Erodability 77

f. Influence of Sediment Heterogeneity on Erodability 78

g. Modes of Erosion for Different Hydrodynamic Regimes 78

i. Front-Side Erosion by Currents (No Waves) 79

ii. Front-Side Erosion by Wave Action 80

1. Surficial Erosion Band 81

2. Calculation of Wave-Induced Erosion 82

3. Wave-Induced Bench Cutting 85

4. Summary 90

iii. Back Side Erosion by Wave Overtopping and Overflow 91

1. Head-Cutting Process 91

2. Levee Damage as a Function of Mean Overtopping Rate – Current Guidance 94

3. Overtopping Rate Calculations – Implications for Levee Damage 96

4. Summary 103

h. Analysis of Eroded Sediment Volume 103

i. Primary Cause for Levee Erosion and Degradation - Rationale 110

i. Erosion Potential – Front Side Versus Back Side 110

ii. Timing and Magnitude of Back Side and Front Side Erosion 110

iii. Visual Evidence 113

V. Erosion at Floodwalls 124

a. Overtopping Jet and Fluid Velocities 124

b. Erosion Due to Overtopping 125

VI. Influence of the MRGO on Critical Levee and Wall Breaches 130

a. Major Sources of Floodwater into the St. Bernard Polder 130

b. Breaching of the MRGO Reach 2 Levee and Walls 133

c. IHNC Breaches (East Side) 149

i. North Breach 149

ii. South Breach 154

APPENDIX A: Oblique Photos - MRGO Reach 2 Levees and Floodwalls

APPENDIX B: 3D Renderings of Post-Storm Levee Condition Based on LIDAR Data

APPENDIX C: Aerial Photos and Analysis of Pre- and Post-Storm LIDAR Data by Surfbreak Engineering Sciences, Inc.

APPENDIX D: Review of Levee Erosion Modeling Described in Declaration and Technical Reports by Robert Bea

REFERENCES

Curriculum Vitae

Executive Summary

Analysis and interpretation of the data and other information presented in this report, and conclusions drawn from them, are based on my professional experience and judgment. The opinions expressed in this report are based upon a reasonable degree of scientific certainty. I have not read all the expert reports; therefore, I reserve the right to alter my opinions based on the content of those reports. This report does not include analysis of Plaintiffs' experts' depositions regarding their final reports. Therefore, I reserve the right to amend and supplement this report in response. I am not being compensated for this work.

Hurricane Katrina produced unparalleled wave and storm surge conditions for the New Orleans vicinity (IPET, 2006). Katrina was a very large Category 3 storm (on the Saffir-Simpson wind intensity scale) when it passed the New Orleans area on the morning of 29 August 2005. Twenty-four hours earlier this storm had been the largest Category 5 and most intense storm on record within the northern Gulf of Mexico. The large size of Katrina during its movement through the Gulf, its intensity, and its track and landfall location, enabled this hurricane to produce the largest storm surge (reliable observations up to 28 ft) that has ever been observed within the Gulf of Mexico, as determined from analyses of historical records. Due east of the Mississippi River delta, a deepwater National Oceanic and Atmospheric Administration (NOAA) buoy recorded the highest significant wave height (55 ft) ever measured in the Gulf of Mexico.

Along the exposed eastern side of the hurricane protection system surrounding the St. Bernard polder, the reach adjacent to the Mississippi River Gulf Outlet (MRGO), Katrina produced maximum storm surge levels of 17.5 to 18.3 ft which overwhelmed the levee and walls. These peak water levels exceeded, by nearly 5 ft, those for which this levee reach was designed. Design water levels were 12.9 to 13.4 ft. Wave conditions created by Katrina along this levee reach were characterized by significant wave heights of 6 to 7 ft and mean wave periods of 5 to 6 sec. These conditions were quite similar to those factored into the levee's design, wave heights of 6.6 to 7 ft and periods of 6.2 to 6.4 sec. But the extreme storm surge created by Katrina completely overwhelmed this reach of the levee/wall system, exceeding levee and wall crests by up to 4 ft in places. Within the Inner Harbor Navigation Canal (IHNC), Katrina generated maximum water levels of 14.3 to 15.4 ft, which exceeded the design water level of 13.5 ft by approximately 1 to 2 ft. Katrina's storm surge also overwhelmed this part of the hurricane protection system.

Extensive analyses of photographs, pre- and post-storm levee elevation data, results obtained from numerical storm surge and wave prediction models, data from soil borings; review of scientific and engineering literature, and engineering calculations led to the conclusion that overtopping and overflow associated with the extremely high water levels and energetic wave conditions caused widespread destruction and breaching of the eastern levees and walls. Waves were considered as an erosion mechanism on the levee front side; and there were relatively minor signatures of wave-induced erosion evident on the front face. However, the velocity regime on the front side was much less erosive than the velocity regime created on the levee back side, once overtopping of the levee began.

When water levels were halfway up the levee front face, overtopping became the dominant erosion mechanism, and that dominance continued as both water levels and wave heights increased. Once the storm surge reached levels that were 1 to 1.5 ft below the levee crest, significant head-cutting and degradation occurred due to wave overtopping, lowering levee crests. As the storm surge rose above levee and wall crests, steady overflow commenced. Overflow occurred nearly everywhere between Bayou Bienvenue and Bayou Dupre, as well as at other locations south of Bayou Dupre. Overflow, pulsating with each passing wave crest, began a self-reinforcing and exacerbating process of erosion and degradation. Crest lowering led to higher overflow rates and higher, more erosive back-side velocities, which led to breach widening and deepening, which led to more crest lowering, and so on. The degree of levee and wall breaching was dictated by the magnitude and duration of overtopping and overflow, the quality of grass cover, and by the resistance to erosion of soil comprising the levee.

Flooding in the Lower 9th Ward and Chalmette areas of the St. Bernard polder can be characterized as early inundation due to water which entered through two breaches on the east side of the IHNC and much greater inundation that began a short time later, due to water that entered the polder as a result of the widespread severe breaching along the eastern levee. Water that entered the polder through the breached levee was, by far, the greatest source of flood water, greatly exceeding all other sources. The majority of this water came through breaches between Bayou Bienvenue and Bayou Dupre where the storm surge exceeded the height of levees and walls by the greatest amounts and for the longest duration. Flood water propagated across the Central Wetlands region between the eastern levee and the interior 40-Arpent levee, which surrounded the heavily populated areas. This water flowed over the 40-Arpent levee and massively flooded the entire Chalmette area, including the Lower 9th Ward.

The MRGO channel, and wetland changes that have occurred since its construction, had negligible effects on damage to the eastern levee and wall system. Even complete removal of the MRGO, and restoration of the wetland to its 1958 condition, which was simulated using storm surge and wave numerical models, reduced the maximum storm surge levels of 17.5 to 18.3 ft by only a few inches along the critical Bayou Dupre to Bayou Bienvenue reach. These small reductions had little influence on the magnitude and duration of overtopping and overflow, on levee erosion, and therefore on levee/wall breaching. Reduction of the MRGO channel cross-section to its authorized dimensions had an even lesser, negligible, influence on maximum water levels, magnitude and duration of overtopping and overflow, and levee/wall breaching. It is my opinion, to a reasonable degree of scientific certainty, that the MRGO did not significantly alter the breaching which occurred along the eastern levee during Katrina.

It is my opinion, to a reasonable degree of scientific certainty, that neither MRGO removal, nor changes in wetland condition that have occurred since 1958, nor changes in MRGO cross-section that have occurred since its construction, altered the occurrences of either the north or south breaches along the eastern side of the IHNC during Katrina, which led to early flooding in the Lower 9th Ward area of the St. Bernard polder.

I. Introduction

a. Scope of the Report

This expert report examines the following issues: 1) effect of the Mississippi River Gulf Outlet (MRGO) navigation channel and historic changes to the surrounding wetlands that have occurred since its construction, on the water levels, wave conditions, and overtopping/overflow produced by Katrina around the periphery of the St. Bernard polder (see Figure 1), and 2) effect of the MRGO on levee and floodwall breaches along the eastern-facing levee of the St. Bernard polder and along the east side of the Inner Harbor Navigation Canal (IHNC), which resulted in significant flood water entering that polder.

I believe the data and information presented in this report are factual. Analysis and interpretation of these data and other information, and conclusions drawn from them, are based on my professional experience and judgment. I will be prepared to speak to any other matter within my area of expertise that is raised at deposition or trial.

b. Study Area

The MRGO is a navigation project that was intended to serve waterborne commerce for the region. A navigation channel is the primary project feature. The Lake Pontchartrain, Louisiana and Vicinity Hurricane Protection Project (LPV), which surrounds portions of St. Bernard, Orleans, Jefferson, and St. Charles Parishes, is intended to reduce damages due to hurricanes. The LPV project is comprised of many features; grass-covered earthen levees along much of its length, as well as steel sheet-pile walls, concrete walls and gates. Sections of the LPV project are located adjacent to the MRGO and to other navigable waterways, the Gulf Intracoastal Waterway (GIWW) and the IHNC, in St. Bernard and Orleans Parishes. Figure 1 shows the region considered in this report. Storm surge and wave conditions experienced during Katrina, around the St. Bernard polder periphery, are examined. The Lower 9th Ward is the westernmost section of the St. Bernard Polder, adjacent to the IHNC.

The MRGO is divided into two channel reaches for the purposes of this report. One is MRGO Reach 2 (Reach 2), which has a southeast-to-northwest alignment and it extends from Breton Sound to the point where it meets the GIWW. A second reach, here called GIWW/MRGO Reach 1 (Reach 1), has an east-west alignment and it extends from the point were the MRGO and GIWW waterways merge to its confluence with the IHNC. In this channel reach, the two waterways (GIWW and MRGO) occupy the same area. Other sites of interest are also shown in Figure 1. The Michoud Canal is the truncated canal seen just to the east of Paris Road Bridge, along the New Orleans East polder.

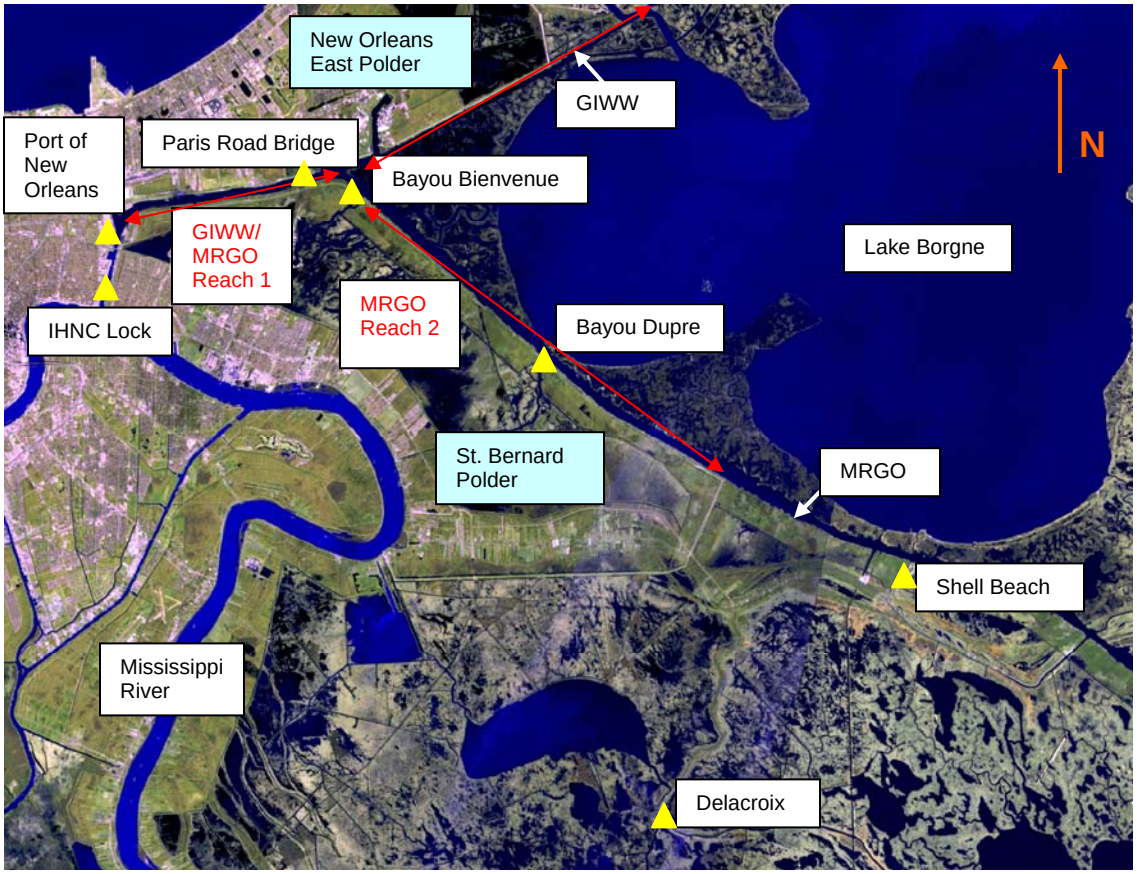


Figure 1. Location map for the study area

c. Approach

This report frequently refers to work done by the Interagency Performance Evaluation Task Force (IPET, 2006, 2007), a multi-agency, university, private sector interdisciplinary team, which was commissioned by the U.S. Army Corps of Engineers (USACE) to examine performance of the southeastern Louisiana hurricane protection system performance in response to Katrina. Details of the IPET work can be found in the extensive reports that were produced. Several data and analysis results are repeated here, or displayed in different formats, to make certain points. Information presented in the report by the Independent Levee Investigation Team (ILIT, 2006), an independent examination, is also utilized. Data derived from additional analyses and model simulations that have been done since the work of the IPET are utilized as well.

The IPET assembled a considerable amount of data and information following Hurricane Katrina. The team performed extensive technical analyses of those data and results obtained from applications of comprehensive, detailed computer models of hurricane winds, storm surge and waves. Models were used to examine the regional storm surge and wave conditions and hydrodynamic loadings on levees and floodwalls. The work of IPET was closely scrutinized and critically reviewed by two teams of national and international technical experts. Members from one team, formed by the

American Society of Civil Engineers, were imbedded in the IPET technical teams to facilitate a detailed and transparent review of the work. A second team was comprised of members selected by the National Research Council (NRC). NRC team members were not closely engaged in the IPET work, by design. They performed a "higher-altitude," at-arms-distance technical review.

In the first parts of this report, hydrodynamic and coastal processes that are germane to performance of the hurricane protection system and sources of floodwater, such as waves, water levels, water velocities, overtopping, scour and erosion, etc., are examined and discussed, focusing on conditions during Katrina. The physical condition of the levees and floodwalls, before and after the storm, are examined. Those aspects of the physical conditions and processes that are most relevant to the issue of flooding in the St. Bernard polder are discussed, supported with data and analysis. Once the important processes and conditions are understood and the hydrodynamic loadings created by Katrina are characterized, causes of system response and flooding in the St. Bernard polder can be better understood, as can the linkage between cause and effect.

With that baseline information, one can then examine how the MRGO might have altered the important processes and how those changes might have contributed to a different outcome in terms of hurricane protection system response and flooding. Computer models enable this to be done, facilitating investigation of hypothetical "what-if" scenarios. This analysis was performed by first applying the numerical storm surge and wave models for conditions as they existed when Katrina struck in 2005 (the baseline condition). Then, the model application was modified by "removing" the MRGO channel or making physical changes attributed to the MRGO; and simulations were made of Katrina for these hypothetical conditions. Results for base line and hypothetical cases were compared. In this way, changes induced by the MRGO and any effects of those changes on system response and breaching were assessed.

The effect of the MRGO on overtopping and overflow of the levees and walls adjacent to MRGO Reach 2 is a central issue. Model simulations were made to investigate changes to water level, wave conditions, and overtopping/overflow conditions along Reach 2 and at the site of IHNC breaches (east side). Five cases were examined in this report:

1) Case H1 (Base Case): occurrence of Katrina for the levee and MRGO channel and wetland conditions that existing at the time the hurricane struck on August 29, 2005.

2) Case H2: occurrence of Katrina for a hypothetical condition that assumes the MRGO navigation channel did not exist, wetlands were in their 2005 condition, with the LPV levees/walls at their pre-Katrina locations and actual elevations. This case was designed to examine any direct effect of the MRGO channel itself.

3) Case H3: occurrence of Katrina for a hypothetical condition that assumes the MRGO navigation channel did not exist, wetlands were in their pre-MRGO

condition (1958), with the LPV levees/walls at their pre-Katrina locations and actual elevations. This case was designed to examine both the direct effects of the MRGO channel and effects of changes to wetlands that have occurred since MRGO construction.

4) Case H5: occurrence of Katrina for a hypothetical condition that assumes the MRGO navigation channel was at its authorized dimensions (eliminating effects of side bank erosion and changes to cross-sectional area that have occurred), wetlands were in their 2005 condition, with the LPV levees/walls at their pre-Katrina locations and actual elevations.

5) Case H6: occurrence of Katrina for a hypothetical condition that assumes the MRGO navigation channel was at its authorized dimensions (eliminating effects of side bank erosion and changes to cross-sectional area that have occurred), wetlands were in their pre-MRGO condition (1958), with the LPV levees/walls at their pre-Katrina locations and actual elevations.

II. Hurricane Katrina Storm Surge and Waves (Regional Perspective)

a. Measured Water Levels

i. High Water Marks – Indicators of Maximum Water Level

Elevation of the mean water surface (an average over the time scale of tens of minutes), relative to the crest elevation of levees and floodwalls, is the most important water variable that dictates levee and floodwall performance, followed by wave conditions and duration of loading. Figure 2 shows high water marks that were recorded in the region of interest by a number of organizations, the USACE, United States Geological Survey (USGS) and Louisiana State University (LSU). All marks cite water surface elevations referenced to the new vertical datum that has been established for the region, NAVD88 2004.65. Information about each mark was carefully reviewed by an IPET interagency expert team comprised of engineers and scientists from the USACE, National Atmospheric and Oceanic Administration (NOAA), and the USGS. Team members had extensive experience in collecting, analyzing and interpreting high water marks that are identified and recorded following storms. The marks, which are displayed in the figure with a white background, were those rated by the expert panel as being excellent indicators of storm surge level, e.g., those recovered from protected areas inside a structure. These marks are our best indicators of the maximum mean water level (also referred to in this report as peak storm surge level, or peak surge). The team believed they reflected minimal effects of wind or wave action. Where two excellent marks were recorded in close proximity to one another, each is listed. Where more than two marks were acquired in close proximity to one other, the range of elevations reflected in the set of marks is listed. Each of the marks displayed with a light blue background was rated by the expert team to be a fair or poor indicator of storm surge. They are shown because they provide some useful information in key areas along the levee system where excellent marks were not available. In each of these particular cases, the review team believed the mark was strongly influenced by local wave action.

Considering only the marks rated as excellent, the highest recorded peak storm surge level in the region was at Shell Beach (marks of 18.1 and 18.7 ft). At a point just west of Shell Beach, the next highest excellent-rated mark was recorded, 17.1 ft. At Delacroix, two excellent marks showed peak surge levels of 16.5 and 16.7 ft. A trend in this region is evident, with high water marks increasing from west to east through this area.

High water marks recorded on the south side of the south-facing levee of St. Bernard show considerable variability, but they also show an identifiable trend, increasing peak surge levels from west to east along the western half of this levee. These high water marks reflect debris (primarily vegetation) left on the levee due to elevated water level and the wave conditions that interacted with the south-side levee face.

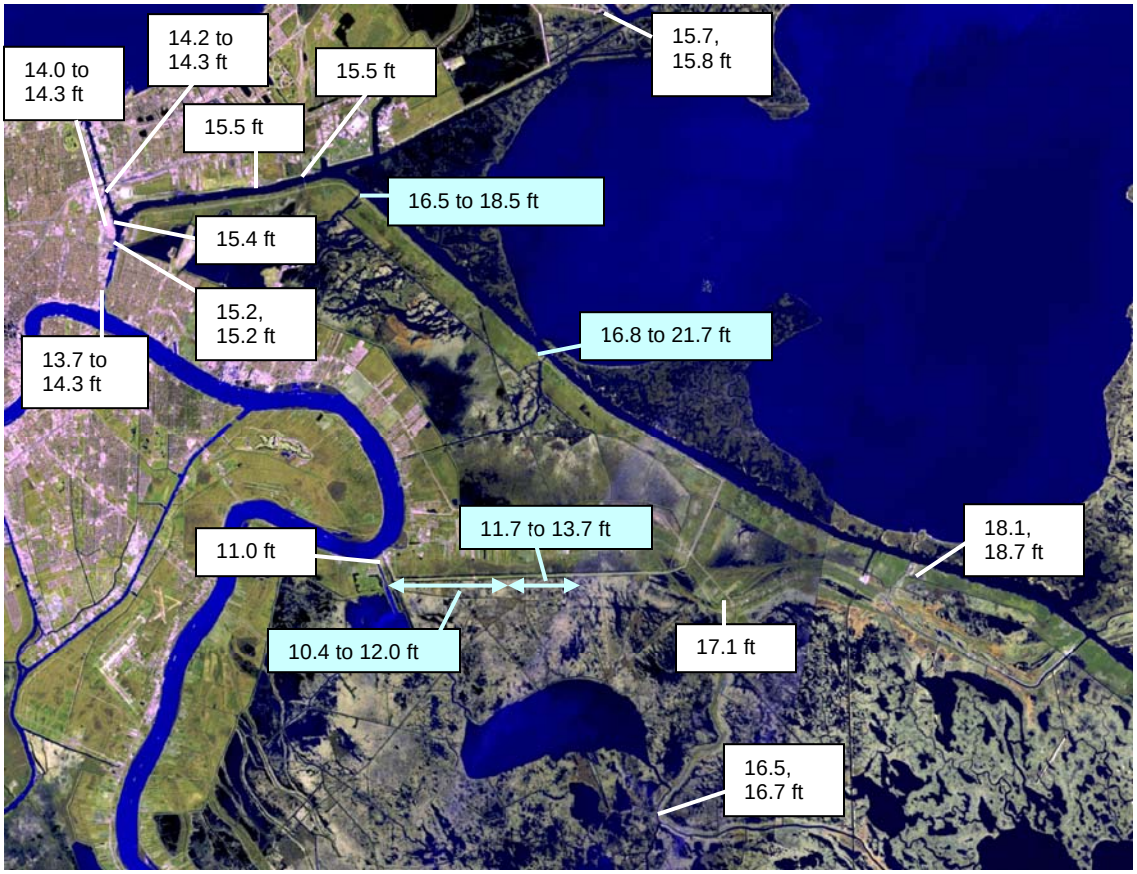


Figure 2. High water marks in feet, NAVD88 2004.65 (data from IPET 2006, Volume IV).

These debris lines are uncertain as an indicator of peak storm surge level since they likely include the effects of wave run-up on the levee face. At the far western end of the south-facing levee of St. Bernard, an excellent mark of 11.0 ft was recorded at Caernarvon. The fair/poor marks nearby are consistent with this excellent mark, and they confirm the trend for increasing peak water levels from west to east. A very large gradient in peak water level is evident, a change on the order of 6 ft (11 ft to 17 ft) over the length of this levee reach.

High water marks recorded at the Bayou Bienvenue and Dupre gate structures, along MRGO Reach 2, varied greatly. Accuracy of marks at both sites, as indicators of peak storm surge level, is highly uncertain. The fair/poor-rated marks reflected accumulation of debris (primarily vegetation) that was left on railings or sills. The lower of the high water marks at both sites reflected marsh grass accumulation on a lower railing. The higher marks reflected vegetation accumulation on an upper railing or some other exposed part of a structure. Debris left on railing, and debris deposited on top of something, might not be a good indicator of peak storm level because the debris can be left during a time of falling water level following the peak. The marks also reflect water surface fluctuations due to short-period wind wave action because of the completely open exposure of these sites. During the storm, high winds blew from an easterly direction

creating significant wave energy at both sites. Exposure to wave action contributes to the high degree of variability reflected in the marks.

Along the GIWW, two excellent-rated high water marks recorded along the Chef Menteur Pass indicated peak surge levels of 15.7 and 15.8 ft. Peak surge indicated by a mark near Paris Road Bridge along the north shore of the GIWW/MRGO reach 1 was 15.5 ft. Just to the west of Paris Road Bridge, a second excellent mark in the vicinity along the north bank indicated the same water level, 15.5 ft.

At the confluence of the GIWW/MRGO Reach 1 with the IHNC, east of the Port of New Orleans (PONO) floodwall, peak surge levels were approximately 15.2 to 15.4 ft. A single mark east of the PONO floodwall recorded a level of 15.4 ft. The two marks that recorded 15.2 ft were acquired just north of the Florida Avenue Bridge on the west side of the IHNC. There were a number of high water marks measured west of the PONO floodwall (but east of the LPV levee), all in the 14.0 to 14.3 ft range. At the IHNC Lock, several high water marks ranged from 13.7 to 14.3 ft. The highest mark of 14.3 is considered to be the most reliable mark because the lock operator read it from a staff gage throughout the storm. Two excellent marks from locations nearby indicated slightly lower water levels, 13.8 and 13.7 ft.

A group of five excellent high water marks north of the IHNC-GIWW/MRGO Reach 1 confluence but south of the I-10 crossing over the IHNC ranged from 14.2 to 14.3 ft. Immediately north of the Danzinger Bridge crossing over the IHNC, several high water marks ranged from 12.4 to 12.6 ft (not shown in Figure 2). Within the IHNC, it was water levels at and south of the I-10 crossing that had the greatest effect on flooding into New Orleans East from this side of the IHNC. At the Lake Pontchartrain entrance to the IHNC, there were a number of excellent high water marks that indicated maximum water levels of 11.8 ft, on average.

In the IHNC, peak water levels exceeded the crest heights of most sections of the hurricane protection system south of the confluence. In light of the widespread flow over the walls and several breaches that formed, and the large areas in polders available to receive the overflowing water volume, a considerable amount of water steadily flowed from the IHNC into adjacent populated areas at the peak of the storm. Therefore peak surge levels were reduced in the southern part of the IHNC and west of the PONO floodwall. A gradient in water level along the IHNC was created, increasing from 14.3 ft at the IHNC Lock to 15.4 ft at the confluence of the IHNC with GIWW/MRGO Reach 1. A water level gradient also existed north of the confluence (see IPET, 2006). It was caused by the lower water levels at the entrance to IHNC in Lake Pontchartrain, by the constriction formed at the railroad bridge south of the I-10 crossing, and by energy losses associated with other features of the highly irregular nature of infrastructure along the IHNC in this region.

ii. Hydrographs – Variation of Water Level with Time

Figure 3 shows hydrographs (variation of water level with time) measured at several locations in the region of interest, along with some spot elevation measurements that were derived from post-storm analysis of digital photographs taken by the IHNC Lock operator during Katrina. The staff gage at the IHNC Lock, which was read each hour throughout the storm by the operator, was the only source for a complete hydrograph for the entire region of interest. This hydrograph is the most accurate information available for characterizing the temporal variation of storm surge levels within the IHNC in the vicinity of the lock, and it is confirmed by data extracted from the digital photos.

At other locations, computed results (from the ADCIRC model), were scaled based on differences between model predictions of water level maximums and measured high water marks. In this report, the words "observed" or "measured" are used to describe water levels derived from a high water mark or from a recorded/observed hydrograph. The word "calculated" or "computed" refers to a model generated water level; the word "estimated" is used to refer to a water level that was derived from a model-generated result and then scaled using measured water level data.

The peak surge recorded at the IHNC staff gage was logged at about 9:00 am CDT on August 29, 2005 (1400 UTC). Since water levels were recorded hourly, the peak level may not have been recorded; however the recorded observation of 14.3 ft at 9:00 a.m. is very consistent with nearby excellent high water marks. The rate of rise reflected in the recorded water levels between 7:00 and 8:00 a.m. suggest the peak water level occurred before 9:00 a.m., at a slightly higher peak value.

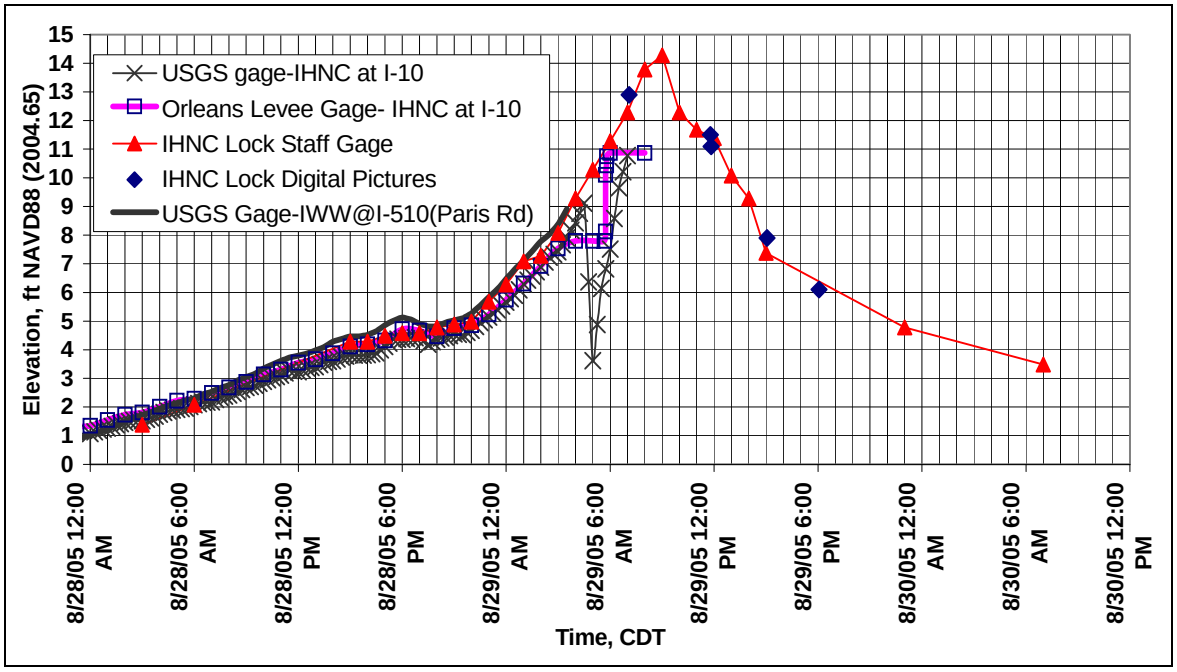


Figure 3. Measured hydrographs (water level versus time)

b. Computer Simulation of Waves and Surge

i. Models Used – Corps' Approach

The regional storm surge and wave modeling done by the IPET team received high marks from both the ASCE and NRC reviewers. That modeling work, which included considerable validation of the models for Hurricane Katrina using an extensive data set, is thoroughly documented in IPET (2006). Validation is extremely important in establishing the credibility of any modeling of such complex processes and understanding the inherent uncertainties and inaccuracies of model results.

The IPET and other USACE studies that have been done since the work of IPET have continued to utilize numerical storm surge and wave models (the ADCIRC SL15 storm surge model application coupled to an STWAVE shallow water wave model application). The models complement the measured data and provide information on how hurricane storm surge and waves evolve with time, throughout southeast Louisiana and Mississippi. The models are coupled to treat the important effects of storm surge on wave propagation and breaking (through changing water depth), and the momentum transfer from waves back to the storm surge associated with wave breaking (through consideration of radiation stresses in the surge modeling). Details of the basic modeling methodology that was applied to produce the results shown here are extensively documented in IPET (2006). The hurricane storm surge (ADCIRC SL15) and wave (STWAVE) model applications used to support this report are more highly resolved, improved, and refined applications of models that were originally applied by the IPET. The storm surge and wave modeling work done in support of this report are described in greater detail in the expert reports by Westerink (2008) and Resio (2008), respectively.

The ADCIRC storm surge model, which was applied in support of this report, uses the SL15 grid mesh. Model accuracy is generally related to model resolution; the higher the resolution the greater the accuracy. The SL15 model application is a much more refined and higher resolution application of the ADCIRC model than the IPET application. Winds, which are the primary forcing for storm surge and waves were the same high-quality wind fields developed by the NOAA Hurricane Research Division and Oceanweather, Inc., for the IPET work. These wind fields provide the most accurate depiction of winds throughout the storm, from the time it entered the Gulf of Mexico through the time it made landfall in Mississippi and moved inland.

Validation is critical for establishing credibility of the model and its application. Validation of the more detailed coupled models (including the SL15 ADCIRC storm surge application) has been repeated for Katrina, and independently validated for Hurricane Rita as well (see Bunya et al 2008 and Dietrich et al 2008).

To support the work done to prepare this report, the full-plane version of the STWAVE model (which considers wave generation and transformation for the full 360-

degree plane) was applied, an improvement over the half-plane wave modeling approach taken by the IPET for several model domains.

ii. Evolution of the Storm Surge (Synoptic View)

Measured water level data are rarely, if ever, available at every location where information is sought for a post-storm analysis. For example, a number of excellent high water marks were available at discrete locations, but none along the MRGO Reach 2 levee. And as noted above, variation of water level throughout the entire storm was measured at only a single point, the IHNC Lock, which was situated well away from more exposed levees and walls that were subjected to higher storm surge and wave conditions, and where substantial breaching occurred.

Measured data, acquired using the monitoring techniques and sensor technologies available today, never fully capture the complete space-time picture of how a storm surge evolves. Computer models are extremely valuable for this purpose. Later in this section, a series of figures are presented, a progression of storm surge snap-shots in time, which were generated with the SL15 ADCIRC application (coupled to STWAVE). This series of figures show how the Katrina storm surge developed and evolved in the region of interest. The figures show color-shaded contours of computed mean water surface elevation, in feet NAVD88 2004.64, using the scale shown on the left of each figure (from 0 to 30 ft). Individual water surface elevation contour lines are shown as continuous black lines. Small black vectors show the wind speed, in knots, and direction (wind speed scale is also shown). The time of each snap-shot is listed in the caption (both local daylight, CDT, and universal, Z or UTC, times are listed).

Before discussing surge evolution, it is informative to examine the characteristics of wind prior to arrival of the storm into the region. Winds prior to landfall were the main contributor to the early build-up of storm surge and waves. Figure 4 shows the near-surface, over-water winds measured at NOAA NDBC buoy 42007, which is located in the Gulf of Mexico, east of and offshore of New Orleans, in open water near the northern tip of the Chandeleur barrier islands. For several days prior to Katrina's landfall winds had directions from 60 deg to 110 deg (blowing out of the east-northeast, east, and east-southeast directions). This pattern of predominant easterly winds was persistent for the four days prior to the storm's arrival at the coast. Wind speeds gradually increased during this period of time. Wind speeds four days prior to landfall were approximately 5 to 10 knots; 20 knots at a time 24 hours prior to landfall; and 30 knots at a time 12 hours prior to landfall.

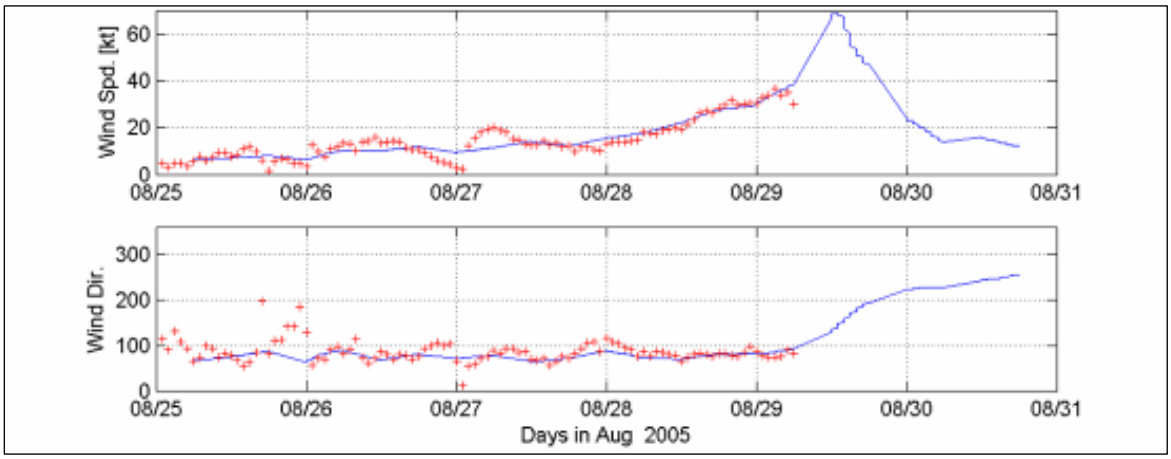


Figure 4. Wind speed and direction at NOAA NDBC Buoy 42007. Red symbols are actual measurements. A direction of 90 degrees indicates winds blowing out of the east; 0 degrees is winds out of the north.

Figure 5 shows the storm surge at 2:00 a.m. on 29 August, 2005, approximately four hours prior to the first landfall of Katrina's eye in Buras, LA to the south. Storm surge in the MRGO, GIWW and IHNC was 7 to 8 ft, and it was rather uniform along the east-facing levee of St. Bernard Parish, the MRGO Reach 2, with water levels slightly greater than 8 ft. These calculated water levels are consistent with the water levels measured at a number of gages in the region (see Figure 3). Considerable water was being blown into the region from the east. This is due to the counterclockwise rotation of winds around the hurricane center which, in the area of interest, results in winds out of the east. This east-to-west movement of water was the dominant pattern of movement prior to landfall. Winds out of the east persisted for several days prior to landfall, and they pushed water into the region for several days prior to arrival of the core of the hurricane.

The wetlands of southeastern Louisiana have low elevations. Based on the measured data shown in Figure 3, the entire wetland system east of the Mississippi River was nearly completely inundated once water levels reached about 3 ft, which occurred one day prior to landfall. Note that winds were blowing water away from the south-facing levee in St. Bernard Parish, and penetration of the storm surge had not yet reached the levee. This is evident by the white-shaded region just south of the levee, which shows areas that were not yet inundated.

Figure 6 shows the storm surge three hours later at 5:00 a.m. on 29 August, approximately one hour prior to first landfall. Winds were steadily increasing and the water continued to be pushed into the region from the east over the inundated wetlands. Computed storm surge levels along the MRGO Reach 2 levee were about 12 ft. As the surge rose in Lake Borgne and along the levee adjacent to the MRGO, the surge also rose in the MRGO/GIWW and the IHNC. Measurements in Figure 3 show that water level at the IHNC lock reached 10 ft at this time. This level is consistent with the computed level.

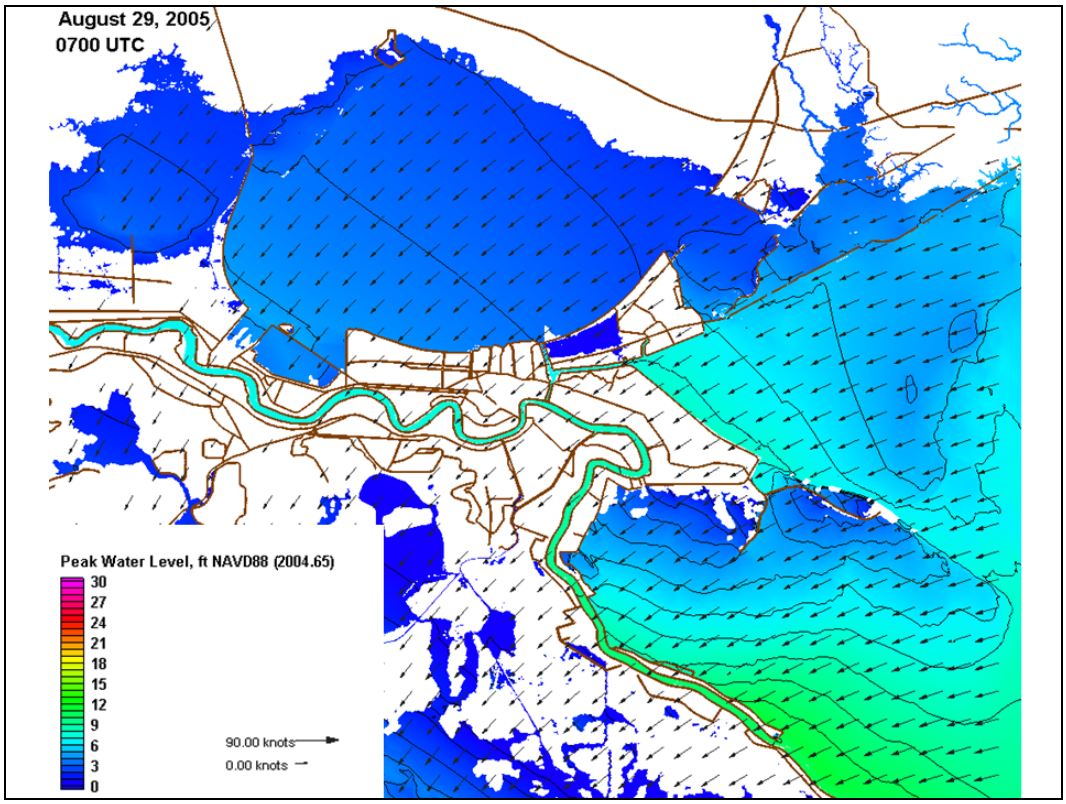


Figure 5. Storm surge snap-shot at 8/29/0700Z (2:00 am CDT August 29, 2005)

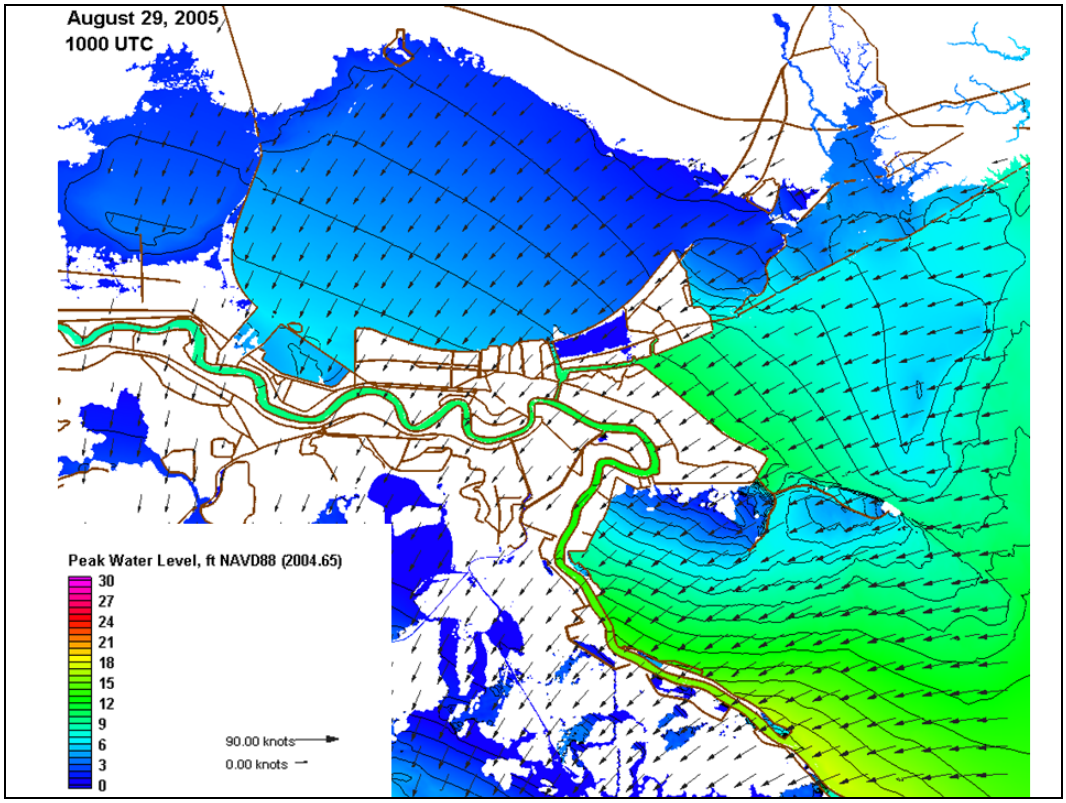


Figure 6. Storm surge snap-shot at 8/29/1000Z (5:00 am CDT August 29, 2005)

Water levels in the GIWW/MRGO Reach 1 channel and in the IHNC were less than levels along the east-facing levee of St. Bernard polder because of the fact that the IHNC has an open connection to Lake Pontchartrain. At this phase of the storm, water levels in Lake Pontchartrain were lower than those along the east-facing levees. The hydraulic connectivity between the two lakes created a gradient in peak storm surge level though the system of channels, from Lake Borgne to Lake Pontchartrain. The gradient was small from Paris Road Bridge to the confluence of GIWW/MRGO Reach 1 and IHNC. The gradient was higher north of the confluence.

Winds were very strong and out of the northeast at this time, and they acted to push water against the MRGO Reach 2 levee. Winds out of the northeast were nearly perpendicular to the levee (See Figure 6), which is aligned in a northwest-southeast orientation. The storm surge along the MRGO Reach 2 levee was primarily the result of a balance in momentum between the wind stress and the slope of the water surface that arose because water was being pushed against the levee. Storm surge contour lines are nearly parallel to the levee and nearly perpendicular to the wind direction. A similar momentum balance is in place within Lake Pontchartrain; surge is being pushed against the southwest shoreline of the lake. Note that the distance between the water level contour lines (1 ft intervals) was greater in Lake Pontchartrain (i.e., a smaller water surface slope) than the distance between contour lines in Lake Borgne (i.e., a greater water surface slope). This difference arose because the wind speed magnitude in Lake Pontchartrain was less than in Lake Borgne. In the momentum balance, the higher the wind speed (or wind stress) the higher the water surface slope.

While the MRGO Reach 2 levee was being subjected to a 12-ft storm surge, the wetlands south of the south-facing levee were still dry for the most part. Winds were blowing from the northeast away from the south-facing levee, and storm surge had not yet penetrated into this area. However, storm surge penetration from the east was beginning (the white shaded area is decreasing in extent) in response to the water surface gradients that had formed. Water was being driven toward this area from the east and southeast, flowing from areas of high surge adjacent to the MRGO Reach 2 levee and from the southeast in conjunction with the approaching core winds of the hurricane.

The snap shot in Figure 7 is at 6:00 a.m. CDT, about 10 minutes prior to the time of first landfall. Winds continued to increase in speed, wind stress increased, and wind directions in Lake Borgne and Lake Pontchartrain were still primarily out of the northeast. As a result the water surface slopes became greater in both lakes as wind speeds increased, increasing maximum surge levels. Winds continued to force water into the region from the east over the inundated wetlands. Peak water levels along the MRGO Reach 2 levee in St. Bernard Parish were slightly greater than 14 ft. The surge also rose in the MRGO/GIWW and the IHNC. At the IHNC lock, measured surge levels were about 11 ft. South of the south-facing levee in St. Bernard Parish, strong winds continued to push water away from this levee, while water surface gradients in the storm surge field acted to force water into this wetland area.

Figure 8 shows surge conditions at 7:00 a.m. CDT. Winds increased with the approaching storm core. The hurricane eye is seen at the very bottom of the figure. The momentum balance continued to be the dominant feature of the storm surge in Lake Borgne; wind continued to drive water into the region from the east. The water surface slope formed in Lake Borgne, balancing the wind stress, is near its greatest magnitude (i.e., this is the near the time of maximum surge along the MRGO Reach 2 levee). Computed peak surge was almost 16 ft, and this level was fairly uniform along much of the MRGO Reach 2 levee. The area of maximum storm surge was in the vicinity of the Bayou Dupre gate and just to the south of it. Peak surge was about 0.5 to 1 ft lower near the north and south ends of the levee. The computed peak water level near Paris Rd Bridge was about 14.4 ft, consistent with, but slightly less than, the measured high water mark value of 15.5 ft. In the IHNC, the measured water level at this time was 12.5 ft. Storm surge was building from the south at Shell Beach (about 12 ft) and at Delacroix (about 14 ft). The easternmost third of the south-facing levee of St. Bernard Parish was experiencing a growing storm surge (strong winds blowing away from the levee act to drive surge away but this was countered by storm surge gradients that acted to drive water into the region from the east and toward the region from the south). The westernmost two-thirds of the levee had yet to experience any storm surge at all, despite this being the time of peak surge along MRGO Reach 2.

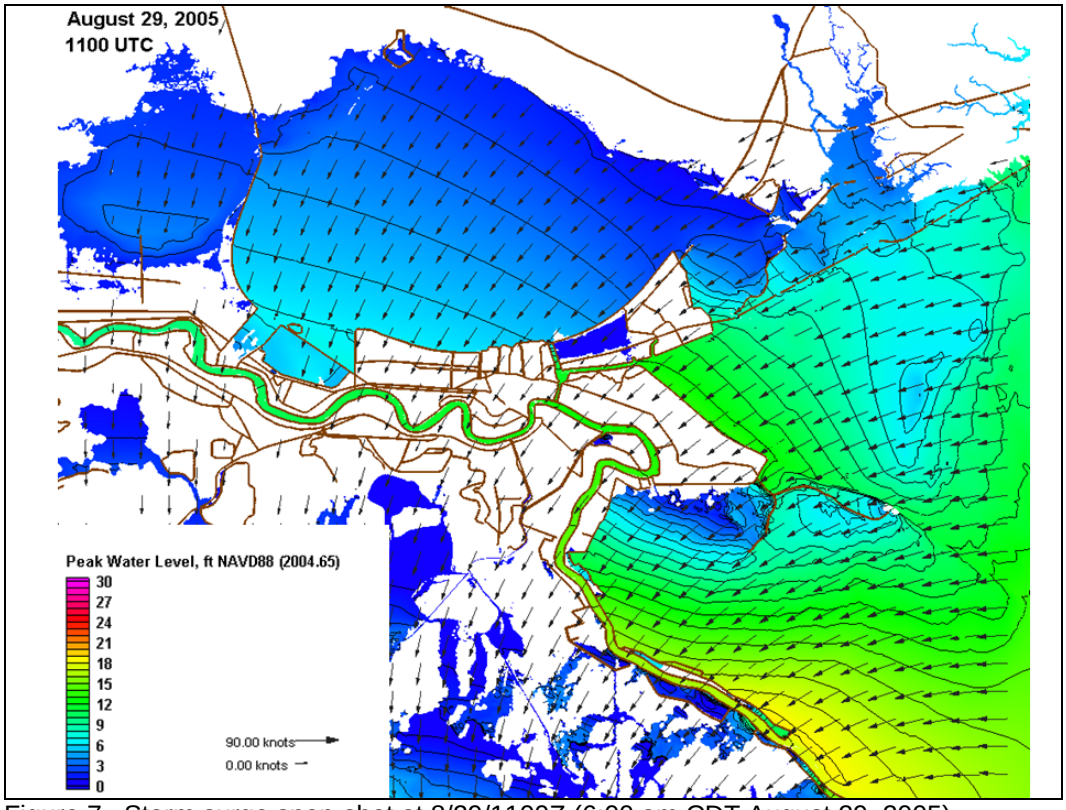


Figure 7. Storm surge snap-shot at 8/29/1100Z (6:00 am CDT August 29, 2005)

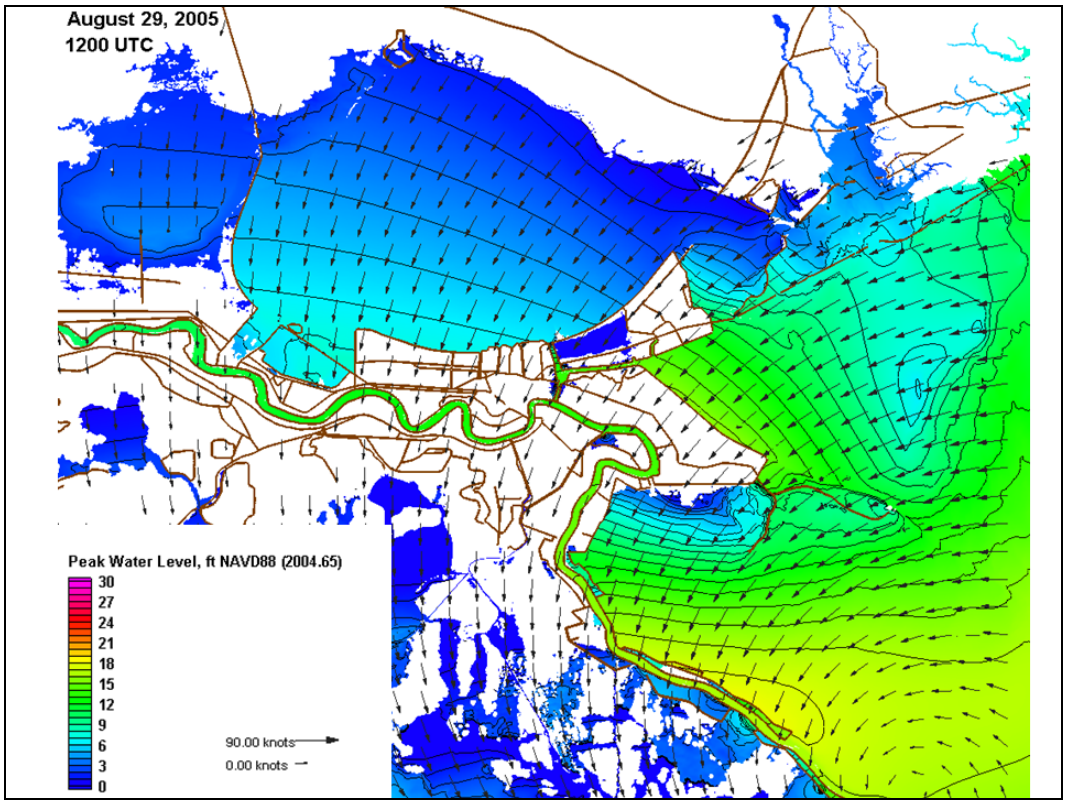


Figure 8. Storm surge snap-shot at 8/29/1200Z (7:00 am CDT August 29, 2005)

Figure 9 shows conditions at 8:00 a.m. CDT. The center of the hurricane was tracking toward the north, southeast of the St. Bernard polder. Winds were changing direction, rotating, as the eye approached. The momentum balance between wind stress and water surface slope was still in place in Lake Pontchartrain. With shifting wind directions, winds were out of the north, and the surge was stacked against the southern Lake shoreline. Winds in Lake Pontchartrain were growing and the water surface slope increased, raising water levels along the south shore. The southernmost portions of the MRGO Reach 2 levee continued to experience high water levels (about 16 ft). Computed water levels at Paris Road Bridge decreased slightly, to about 14.0 ft. Measured water levels at the IHNC lock were nearly 14 ft. As the winds acting to blow water away from the south-facing levee of St. Bernard Parish decreased and began to change direction, as the core of the storm arrived, the surge rapidly propagated into this area.

Figure 10 shows the storm surge at 9:00 a.m. CDT. The zone of peak storm surge in Lake Pontchartrain was positioned along the southern shoreline at the entrance to the IHNC; the water surface slope in Lake Pontchartrain was near its greatest magnitude, so water level at the entrance to the IHNC was near its maximum value (11.8 ft based on high water marks). Measured water level at the IHNC Lock was 14.3 ft. The eye of the hurricane was sitting over Lake Borgne, about 45 minutes from making second landfall in Mississippi. Because winds blow counterclockwise around the eye of the hurricane, winds in the region were shifting rapidly as the storm center moved through.

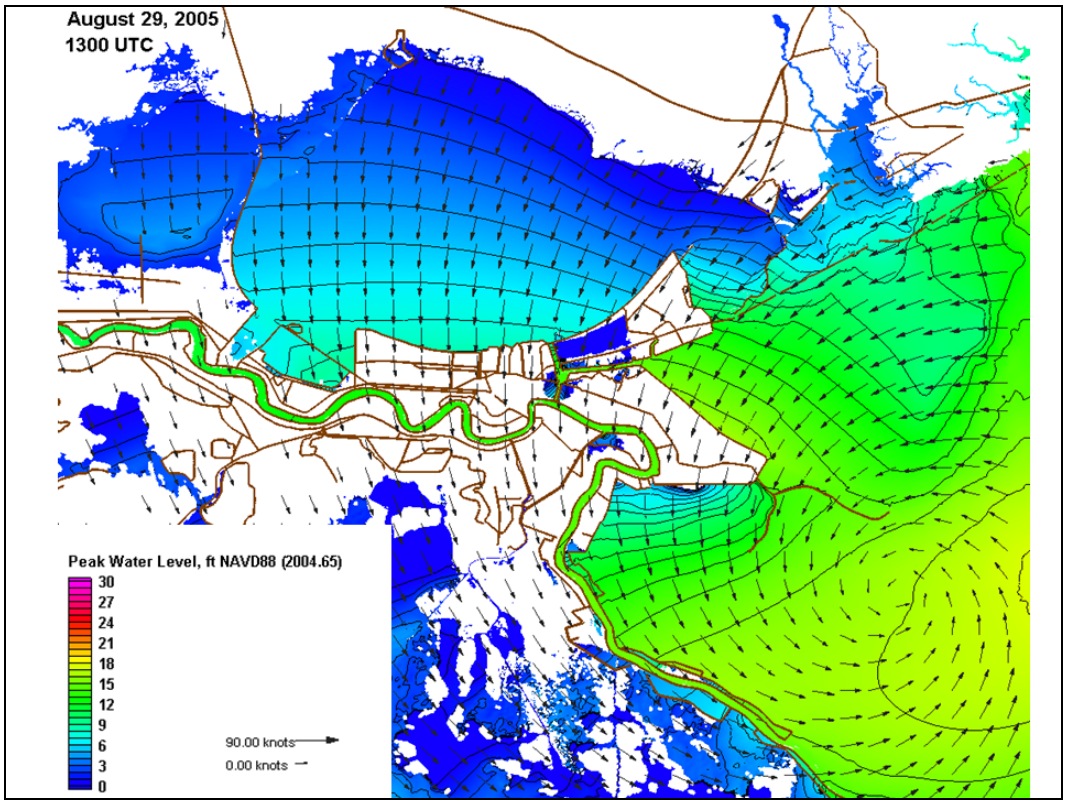


Figure 9. Storm surge snap-shot at 8/29/1300Z (8:00 am CDT August 29, 2005)

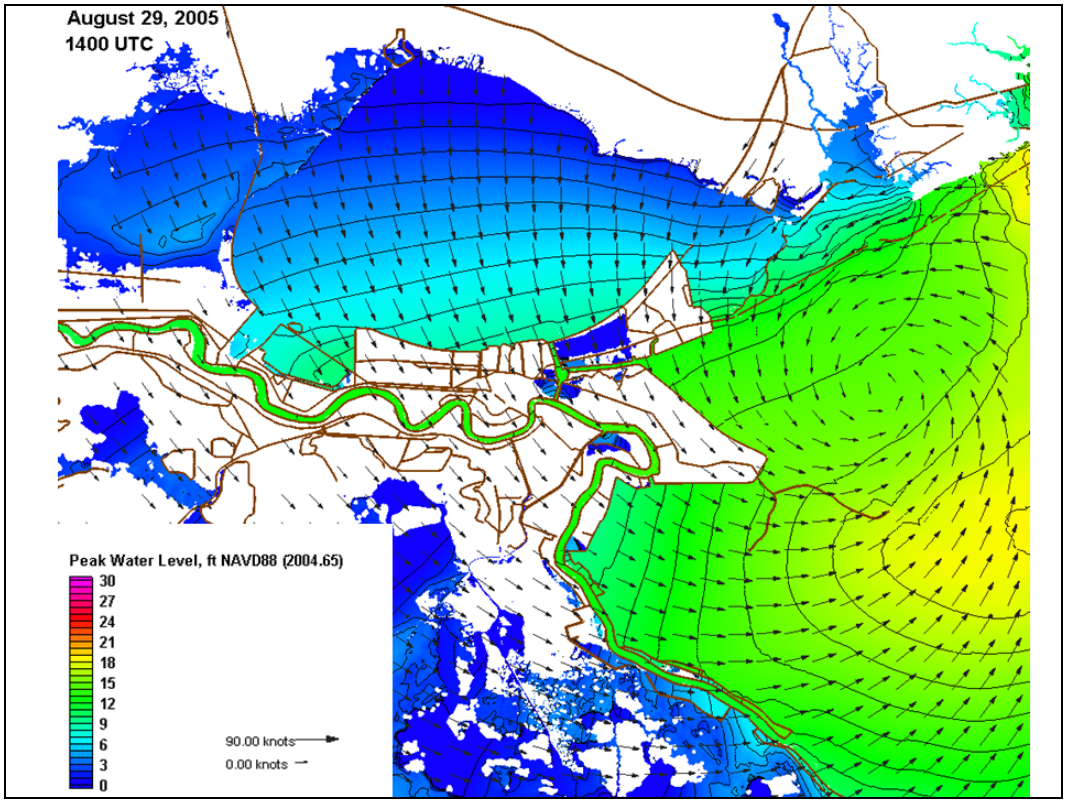


Figure 10. Storm surge snap-shot at 8/29/1400Z (9:00 am CDT August 29, 2005)

Winds were beginning to blow water away from the MRGO Reach 2 levee, and surge began to decrease. Computed water level at Paris Rd Bridge was 13 to 13.5 ft, and decreasing. Computed levels along MRGO Reach 2 were 13.5 to 16 ft, increasing from north to south. Surge was increasing along the south-facing levee, and a gradient in water level existed along the levee, from 11 ft in the east to 15 ft in the west. This gradient was qualitatively similar to the gradient in the high water marks, and similar in magnitude.

Figure 11 shows conditions at 10:00 a.m. CDT, approximately 15 minutes after second landfall in Mississippi. Winds shifted to northwesterly and westerly directions following passage of the eye through the region. Water levels along the MRGO Reach 2 levee continued to decrease. A gradient in water level existed along MRGO Reach 2, from 11.5 ft in the north to 14 ft at the southeastern end. Measured water levels at the IHNC lock were 12 ft and decreasing. Computed levels at Paris Rd Bridge were 11.5 ft and decreasing. A gradient existed along the south-facing levee, from 11 ft in the west to 14.5 ft in the east.

Figure 12 shows the storm surge field at 11:00 a.m. CDT. Water level continued to decrease along the MRGO Reach 2 and at the IHNC Lock. Measured water level at the lock was 11.5 ft. Computed surges along the MRGO Reach 2 were 11 to 13.5 ft. Figures 13 and 14 show the surge field at 12:00 p.m. and 3:00 p.m. CDT, respectively. Storm surge continued to decrease throughout the region. Water levels were 11.5 and 7.5 ft at the IHNC Lock at 12:00 p.m. and 3:00 p.m., respectively.

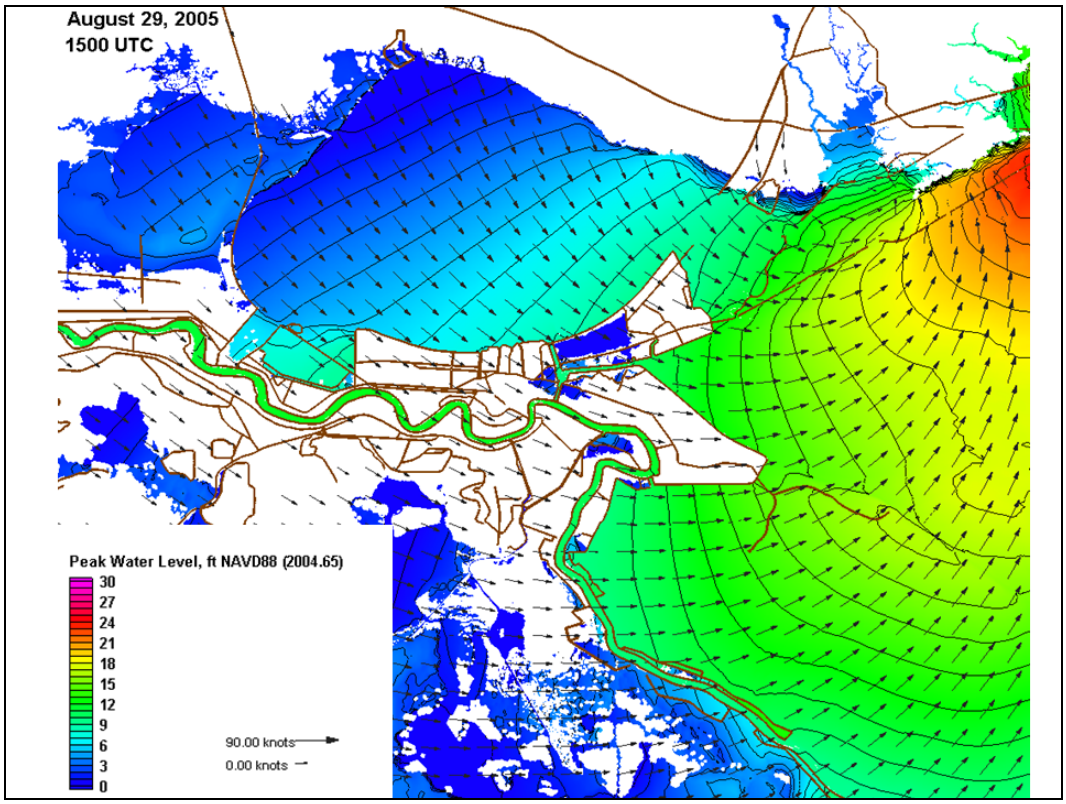


Figure 11. Storm surge snap-shot at 8/29/1500Z (10:00 am CDT August 29, 2005)

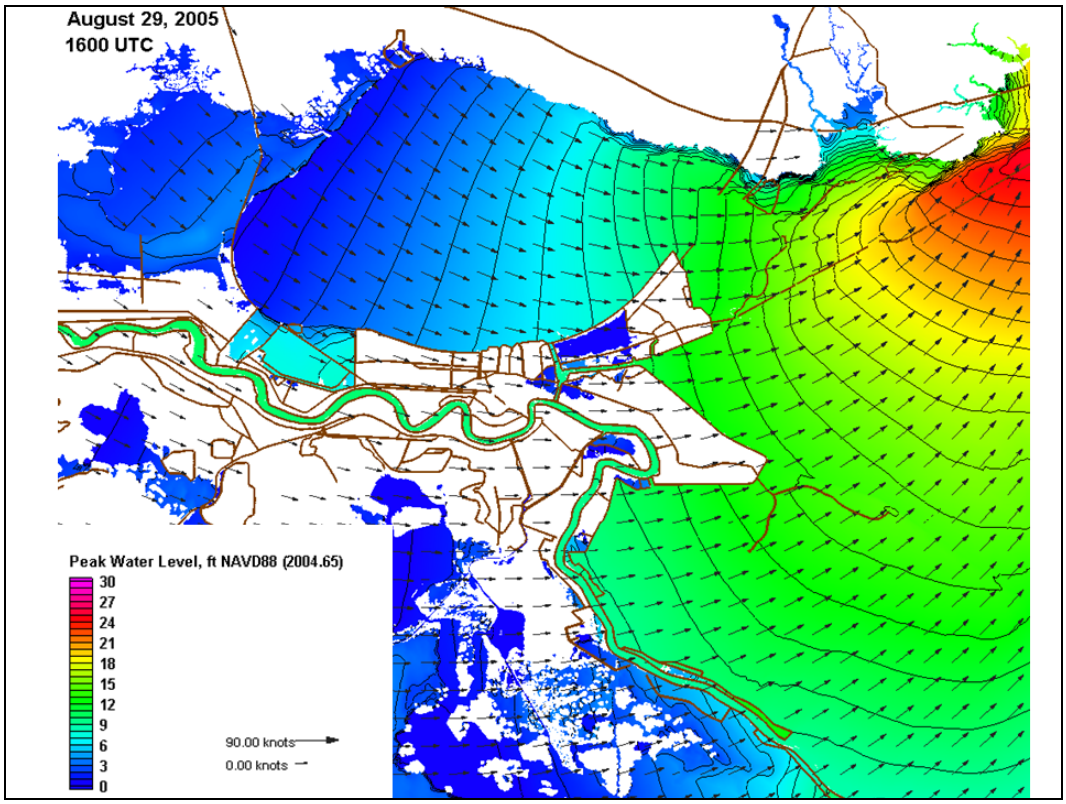


Figure 12. Storm surge snap-shot at 8/29/1600Z (11:00 am CDT August 29, 2005)

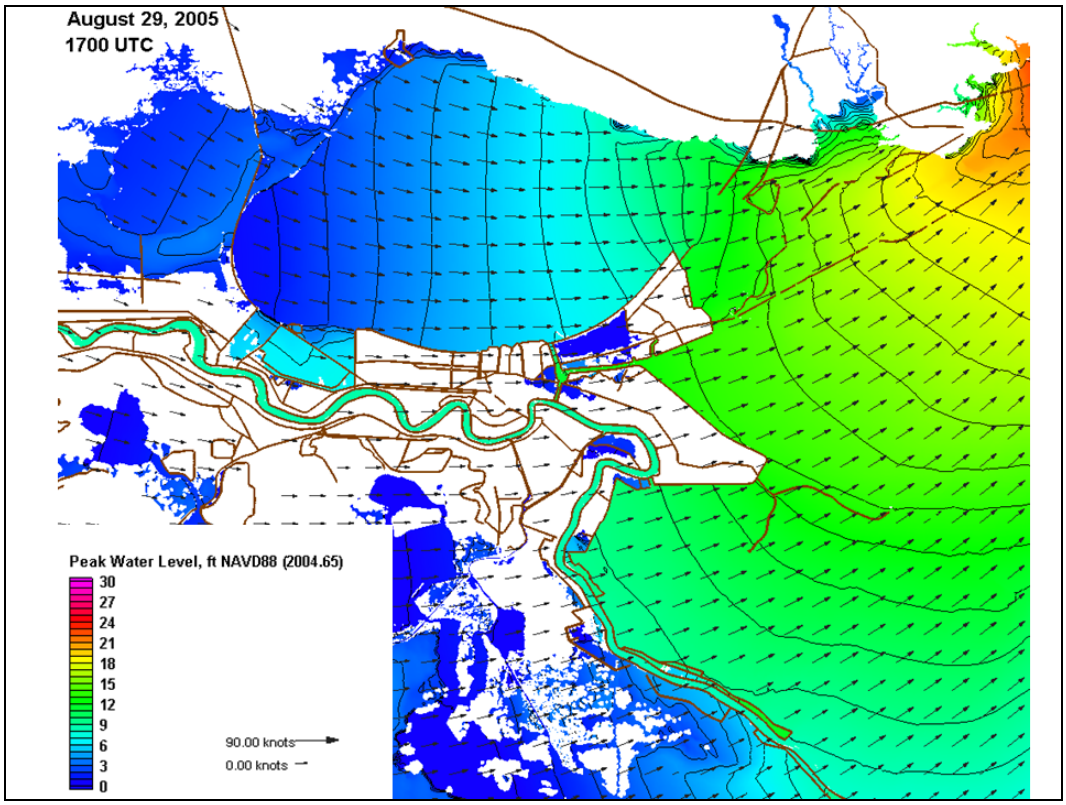


Figure 13. Storm surge snap-shot at 8/29/1700Z (12:00 pm CDT August 29, 2005)

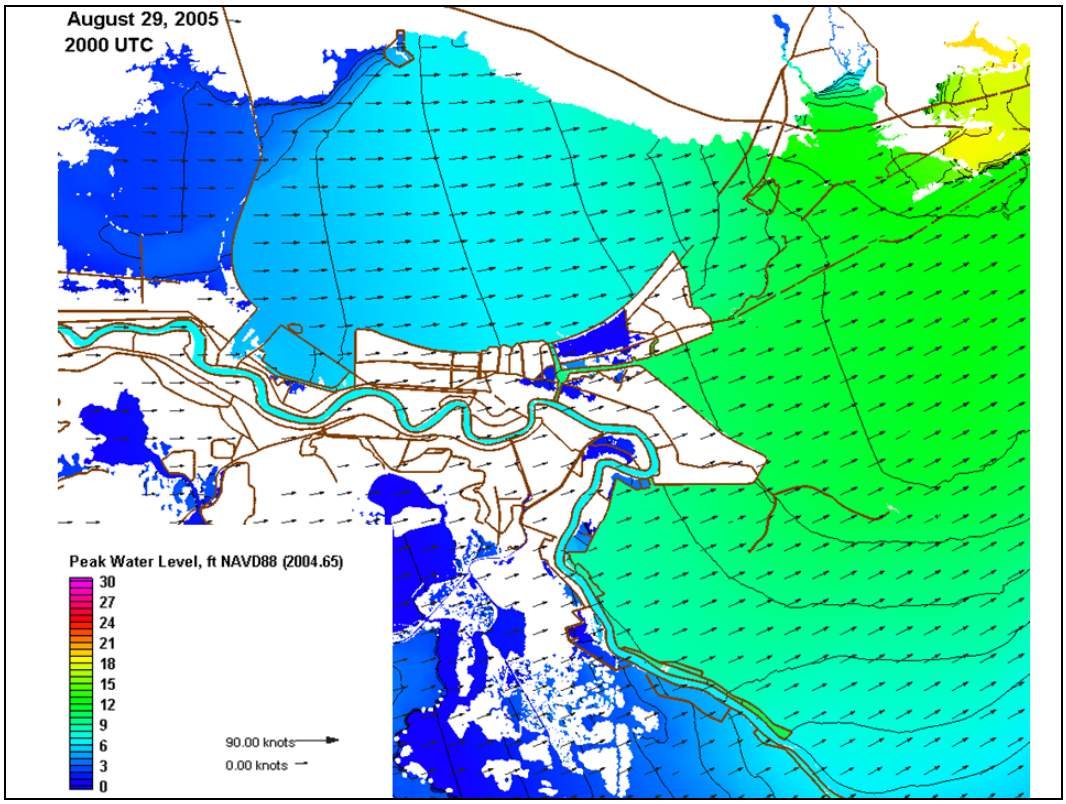


Figure 14. Storm surge snap-shot at 8/29/2000Z (3:00 pm CDT August 29, 2005)

iii. Maximum Water Level (Synoptic View)

Figure 15 shows peak water levels throughout the region of interest computed using the ADCIRC SL15 application. The shaded colors reflect maximum water surface elevations, in feet NGVD88 2004.65. Individual contour lines of computed maximum water levels are shown as black labeled solid lines. These values reflect peak levels computed at each location throughout the model domain. These water levels account for the contribution of wave breaking to the mean water surface away from the levees, through coupling between wave and surge models; however, they do not include the additional contribution to the mean water surface associated with wave breaking right at the levee. Several aspects of the spatial pattern reflected in computed peak surge levels are qualitatively consistent with the pattern evident in the distribution of excellent-rated high water marks (refer back to Figure 2).

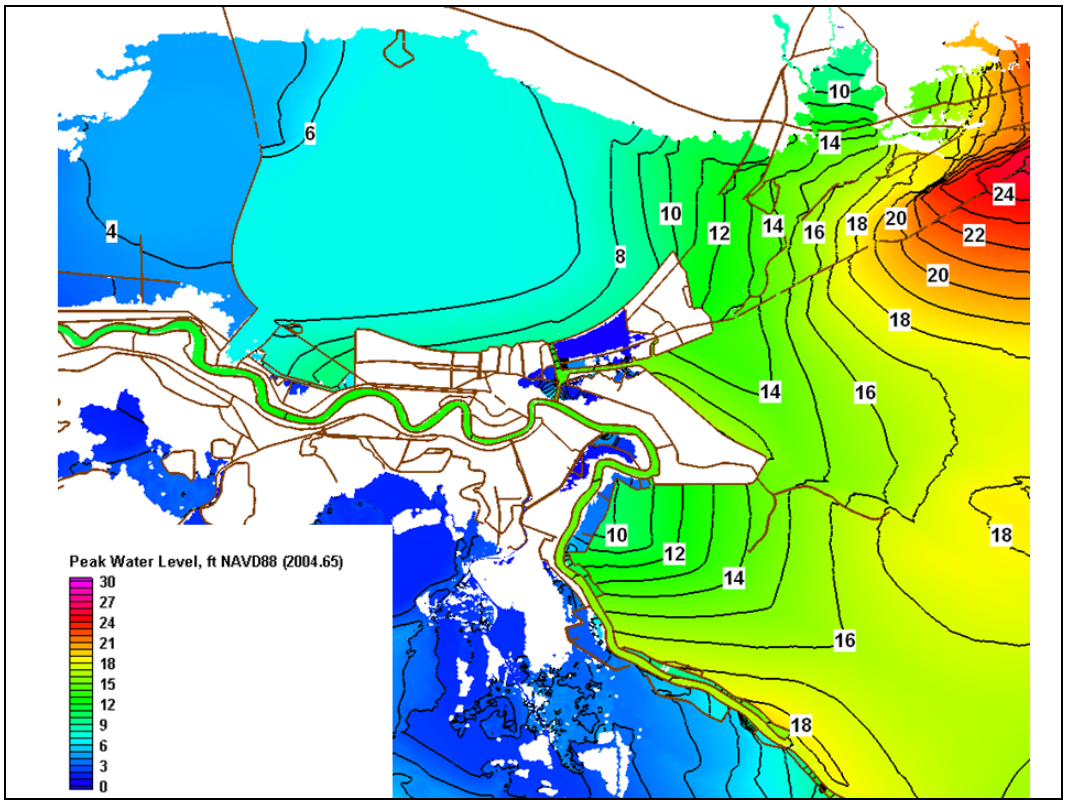


Figure 15. Spatial distribution of computed peak water levels

The maximum computed peak water level for the region shown in Figure 2 was located to the southeast of Shell Beach. That pattern was also evident in the model calculations. The highest of the most reliable high water marks in the region was found in this vicinity (at Shell Beach); high water marks were 18.1 and 18.7 ft. Computed peak levels in this same location are 15.4 to 15.2 ft, a difference of 2.7 and 3.5 ft, respectively. At Delacroix, the computed peak surge is 14.0 and 14.2 ft (differences of 2.5 feet in both instances); and at Reggio, due west of Shell Beach, the computed peak surge is 14.7 ft and the measured value is 17.1 ft (a difference of 2.4 ft). There is a trend of increasing storm surge from west to east evident in this group of high water marks, and the same trend is evident in the model results. Computed peak water levels are consistently less than measured values.

Table 1 summarizes comparisons between computed peak mean water surface elevations and measured high water marks for the region. Marks are grouped according to geographical location. Percent differences are computed for each pair of measured/computed water levels, and an average percent difference is computed for each geographically distinct set of water levels. Model results are biased low by 4 to 17%. To estimate the actual water levels, computed levels were adjusted upward to account for the bias.

Table 1. Comparison of Measured High Water Marks and Computed Maximum Water Surface Elevations

Location	Measured (ft)	Computed (ft)	Difference (ft)	Difference (%)
Chef Menteur S	15.7	13.2	-2.5	-16
Chef Menteur N	15.8	12.9	-2.9	-18
				Avg -17
Paris Rd Br	15.5	14.4	-1.1	-7
W of Paris Rd Br	15.5	14.2	-1.3	-9
				Avg -8
Shell Beach E	18.7	15.2	-3.5	-19
Shell Beach W	18.1	15.4	-2.7	-15
Reggio	17.1	14.7	-2.4	-14
				Avg -16
Delacroix N	16.5	14.0	-2.5	-15
Delacroix S	16.7	14.2	-2.5	-13
				Avg -14
Caernarvon	11.0	11.0	0	0
PONO – E -1	15.4	13.5	-1.9	-12
PONO – E - 2	15.2	13.6	-1.6	-11
PONO – E -3	15.2	13.6	-1.6	-11
				Avg -11
PONO – W -1	14.3	13.6	-0.7	-5
PONO – W -2	14.1	13.5	-0.6	-4
PONO – W - 3	14.3	13.5	-0.8	-6
PONO – W - 4	14.1	13.4	-0.7	-5
				Avg -5
IHNC Lock -1	13.7	13.7	0	0
IHNC Lock -2	13.8	13.8	0	0
IHNC Lock -3	14.3*	13.8	-0.5	-4
				Use -4

* Observations made by IHNC Lock operator

Along the MRGO Reach 2 levee, estimation of the actual peak water level is more difficult and uncertain because of the absence of excellent-rated high water marks. However, the local pattern evident in the calculated peak surge field and differences between observed and calculated peak water levels aid in making a reasonable estimate. As seen in Figure 15, the peak water level contours indicate that model-generated maxima are fairly uniform along most of this levee section, deceasing with increasing proximity to both the northwestern and southeastern ends. Calculated peak water levels are fairly uniform along MRGO Reach 2; they ranged from 15.0 to 15.7 ft, with the maximum located where the levee makes a slight bend south of Bayou Dupre. The

average differences for the two clusters of open-exposure high water marks near Shell Beach and Chef Menteur Pass are 16% and 17%, respectively. Average differences near Paris Road Bridge are less, approximately 8%. Model results are consistently less than measured values. Based on this information alone, an estimate for the peak surge level along the Reach 2 levee is 16.6 to 17.6 ft, using differences for the more open-exposure sites. The calculated peak water level contour pattern for the region provides additional information. The pattern of water level contours suggests that the peak value along MRGO Reach 2 should be higher than the value of 15.5 ft at Paris Road Bridge, less than the 18.1 and 18.7 ft marks at Shell Beach, and higher than the 17.1 ft mark at Reggio. Considering all these factors, a best estimate for the actual maximum water level along the MRGO Reach 2, is 17.6 ft, just to the south of Bayou Dupre. ADCIRC hydrographs were scaled upward by a factor of 1.12 to make estimates of actual hydrographs along the MRGO Reach 2 levee.

Along the GIWW, high water marks at Chef Menteur Pass (15.7 and 15.8 ft) are 2.6 and 2.9 ft greater than calculated peak levels (an average difference of 17%). High water marks at Paris Road Bridge (15.5 ft) and just west of the Bridge (also 15.5 ft) are 1.1 and 1.3 ft higher than the corresponding model results (an average difference of 8%). High water marks at Paris Road Bridge and Chef Menteur Pass are quite similar, differing by only tenths of a foot. An average of the high water marks at Paris Road Bridge and Chef Menteur Pass is 15.6 ft. Therefore a value of 15.6 ft is a reasonable estimate of the peak water level for the levee reach between Michoud Canal and the easternmost end of the levee adjacent to the GIWW. Computed peak water levels are approximately 14.0 ft near Michoud Canal and 13.2 ft at the eastern end. Therefore, for this levee reach, computed hydrographs were scaled upward by a factor of approximately 1.15 to estimate actual hydrographs.

The measured peak level at Paris Road Bridge is 15.5 ft; a second value of 15.5 ft was also recorded at a location west of Paris Road Bridge. An excellent-rated high water mark in the IHNC closest to the confluence of MRGO/GIWW Reach 1 and the IHNC had a value of 15.4 ft. The difference between the peak level at the confluence and the peak level at Paris Road Bridge is only 0.1 ft. Model results show a larger change of 0.9 ft from Paris Road Bridge (14.4 ft) to the confluence (13.5 ft). Both the high water marks and the model results suggest the spatial gradient of peak water level within this section of channel is rather small. Peak water levels, along the south shore of Lake Pontchartrain at the entrance to the IHNC, were under-predicted by nearly 3 ft in the ADCIRC SL15 application. This low bias influences the computed water level gradient in the northern half of the IHNC. For this reason, more weight was placed on the high water marks recorded east of PONO flood wall and the marks near Paris Road Bridge. In light of the low gradient evident in the high water marks, a best estimate of peak storm surge level throughout the MRGO/GIWW Reach 1 channel is 15.5 ft. Computed hydrographs were scaled upward by a factor of 1.08 to estimate actual hydrographs in the GIWW/MRGO Reach 1.

There were numerous excellent-rated high water marks available in the IHNC. From the confluence north to the I-10 crossing over the IHNC, peak storm surge levels decreased from 15.4 to 14.3 ft (a difference of 1.1 ft). From the confluence south to Florida Avenue Bridge, the observed peak level decreased from 15.4 to 15.2 ft, and from there southward they decreased to 14.3 ft at the IHNC Lock. At the lock, water level observations recorded by the lock operator were given greatest weight relative to other nearby measured high water marks. Computed peak water levels south of the confluence show an increase from 13.5 ft at the confluence to 13.8 ft at the Lock. However, note that the ADCIRC SL15 application does not consider the effects of breaches that occurred along this section of waterway. For this reason and those cited above, more weight is placed on high waters marks collected east of the PONO floodwall. Between Florida Avenue Bridge and the confluence, computed hydrographs were scaled upward by a factor of 1.11 to estimate hydrographs. South of the Florida Avenue Bridge, to the IHNC Lock, computed hydrographs were scaled upward by a factor of 1.04 to estimate actual hydrographs.

Along the southern levee of the St. Bernard polder, a trend of increasing peak surge from west to east is reflected in the both the model results and the measured high water marks. The spatial gradient in peak water level reflected in the high water marks is about 6 ft (11.0 to 17.1 ft); whereas the gradient reflected in the model results is less, nearly 4 ft (11.0 to 14.7 ft). The gradient in peak levels is very high. The computed peak surge for Caernarvon, at the westernmost end of this levee segment, matches the measured high water mark. However, at the eastern end of the levee, model results are approximately 14% to 15% lower than the measured high water marks. A reasonable approach to estimating hydrographs for the western third of the southern is levee reach is to scale the model hydrographs upward by a factor of 1.02, 1.06 for the central third of the levee, and 1.12 for the eastern third.

iv. Evolution of the Storm Waves (Synoptic View)

The only nearshore wave measurements that were made during the storm were made in Lake Pontchartrain, offshore of the 17th Street Canal. No shallow-water wave measurements were available in the vicinity of Lake Borgne. The closest wave measurements were available from a site well offshore, at NDBC Buoy 42007, which is located just off the northern end of the Chandeleur barrier islands in water having a depth of about 45 ft. Wave measurements this far away, and in deeper water, are not indicative of conditions along the levee system. The buoy failed to capture wave conditions at the peak of the storm. Incident wave conditions along the MRGO Reach 2 levee were calculated using the full-plane version of the STWAVE shallow water wave model, linked and coupled with the SL15 ADCIRC storm surge model.

Figures 16 through 28 show the temporal evolution of the incident wave conditions (significant wave height, mean wave period, and mean wave direction) as the core hurricane winds arrived and passed through the region. Color contours show the significant wave heights (in feet) or the mean wave period (in seconds); black vectors indicate the mean wave direction. Figures 16 and 17 show the distribution of wave

height and wave period, respectively, at 2:00 a.m. CDT August 29, approximately four hours before the time of first landfall in Louisiana. Mean wave directions were generally aligned with the direction of the wind; and waves approached perpendicular to the MRGO Reach 2 levee. The most energetic wave conditions (significant incident heights of 4 ft) were in the vicinity of Bayou Dupre. Wave heights were reduced over the wetlands due primarily to wave breaking and energy dissipation.

Figures 18 (5:00 a.m. CDT) and 19 (6:00 a.m. CDT) show changes in significant wave height and mean wave direction as the storm made landfall to the south. Spatial variability and patterns of significant wave height and mean wave direction were similar to those for preceding times. Wave heights steadily increased during this time, reaching maximum heights along the MRGO Reach 2 levee, near Bayou Dupre, of 7 ft. Heights along the other areas of MRGO Reach 2 were slightly less. Increasing winds and water levels resulted in increasing wave heights. Depth-induced breaking over the shallower wetlands remained a dominant process.

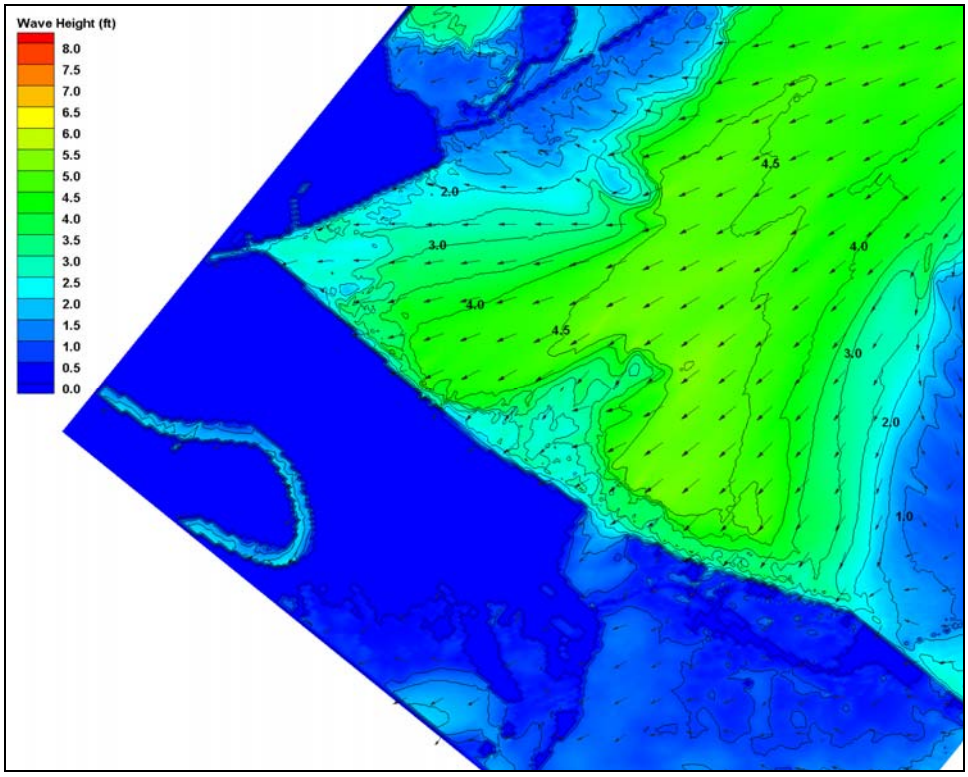


Figure 16. Significant wave height snap-shot at 8/29/0700Z (2:00 am CDT August 29, 2005)

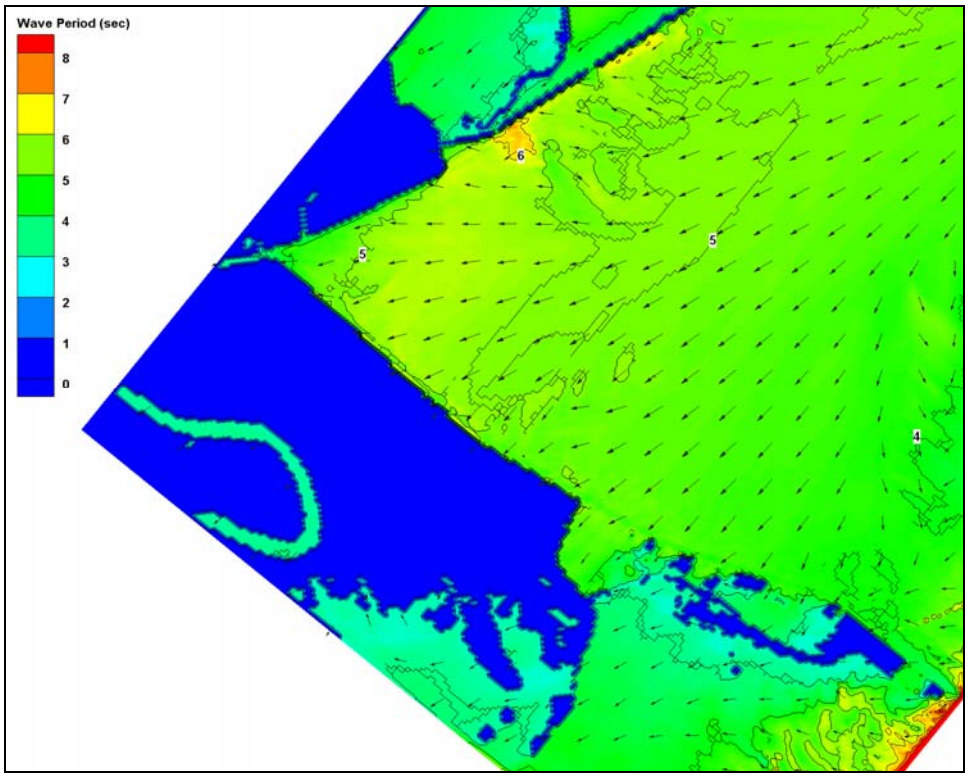


Figure 17. Mean wave period snap-shot at 8/29/0700Z (2:00 am CDT August 29, 2005)

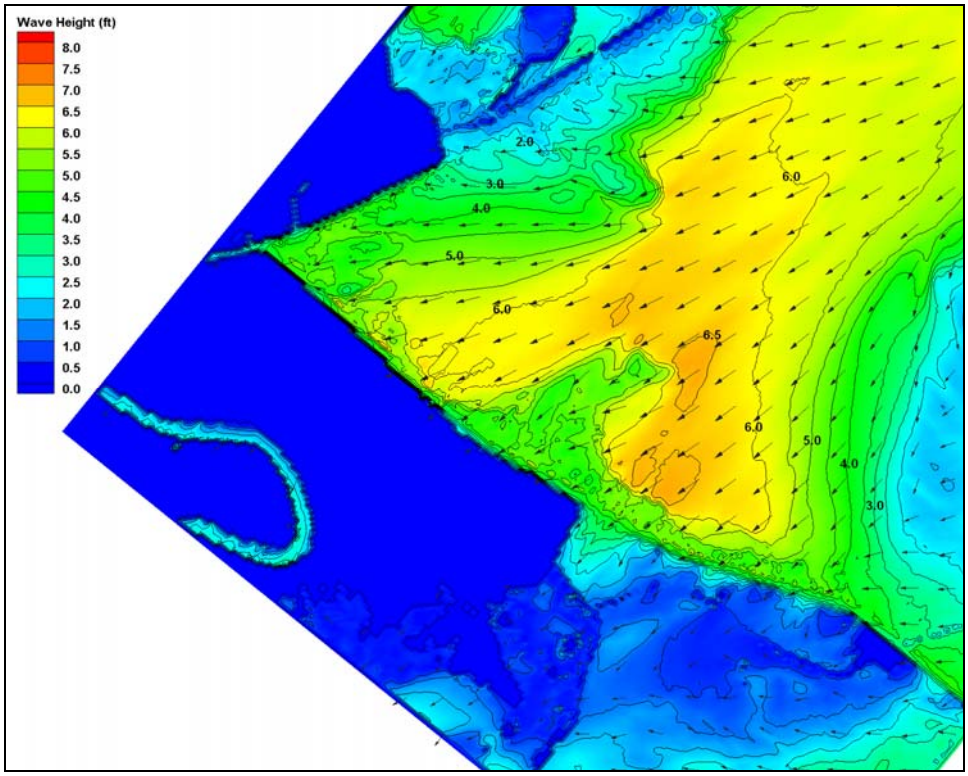


Figure 18. Significant wave height snap-shot at 8/29/1000Z (5:00 am CDT August 29, 2005)

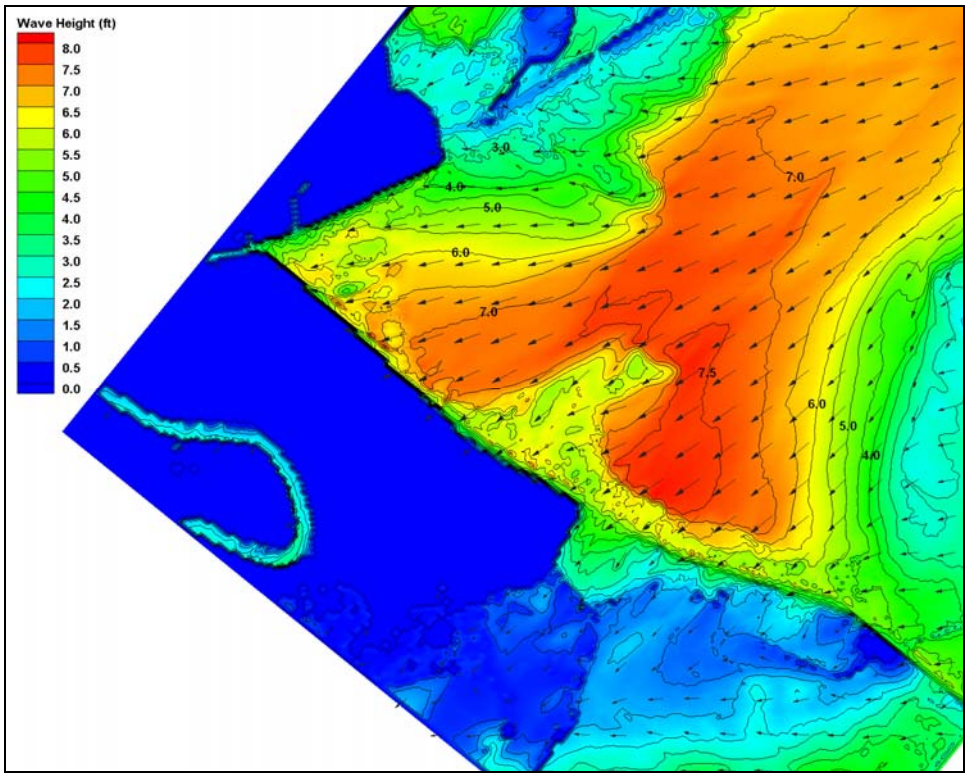


Figure 19. Significant wave height snap-shot at 8/29/1100Z (6:00 am CDT August 29, 2005)

Figures 20 and 21 show the significant wave height, mean wave period, and mean wave direction near the time of peak surge at 7:00 a.m. CDT. Increasing water levels and winds resulted in increased wave heights. Spatial variability and patterns of significant wave height and mean wave direction are similar to those for preceding times. Significant wave heights reached maximum values of 7 ft along the MRGO Reach 2 levee; maximum mean periods were approximately 5 to 6 seconds. Heights along the MRGO Reach 2 levee ranged from 5 to 7 feet. Depth-induced breaking over the shallower wetlands remains a dominant process.

Figures 22 through 28 show evolution of the wave field as the hurricane eye moved through the region, toward the north. As wind direction changed rapidly (from out of the east to out of the west) with passage of the storm, wave conditions changed rapidly because they were strongly wind-driven. Wave heights decreased considerably; wave periods also decreased; and mean wave direction changed to directions out of the west, aligned with the wind direction.

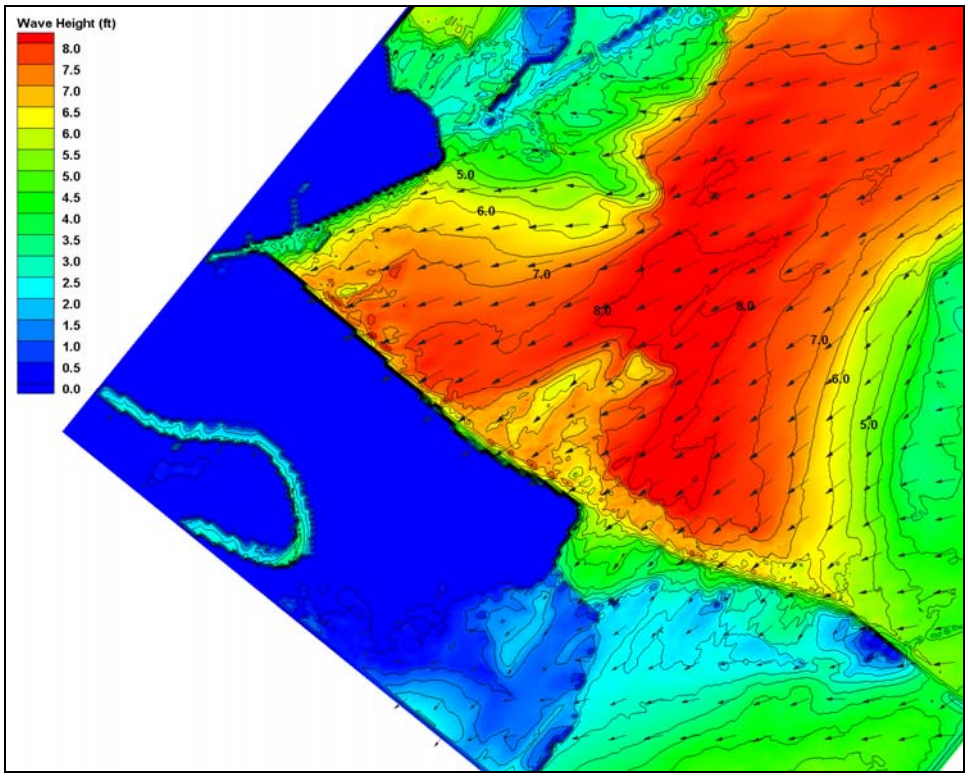


Figure 20. Significant wave height snap-shot at 8/29/1200Z (7:00 am CDT August 29, 2005)

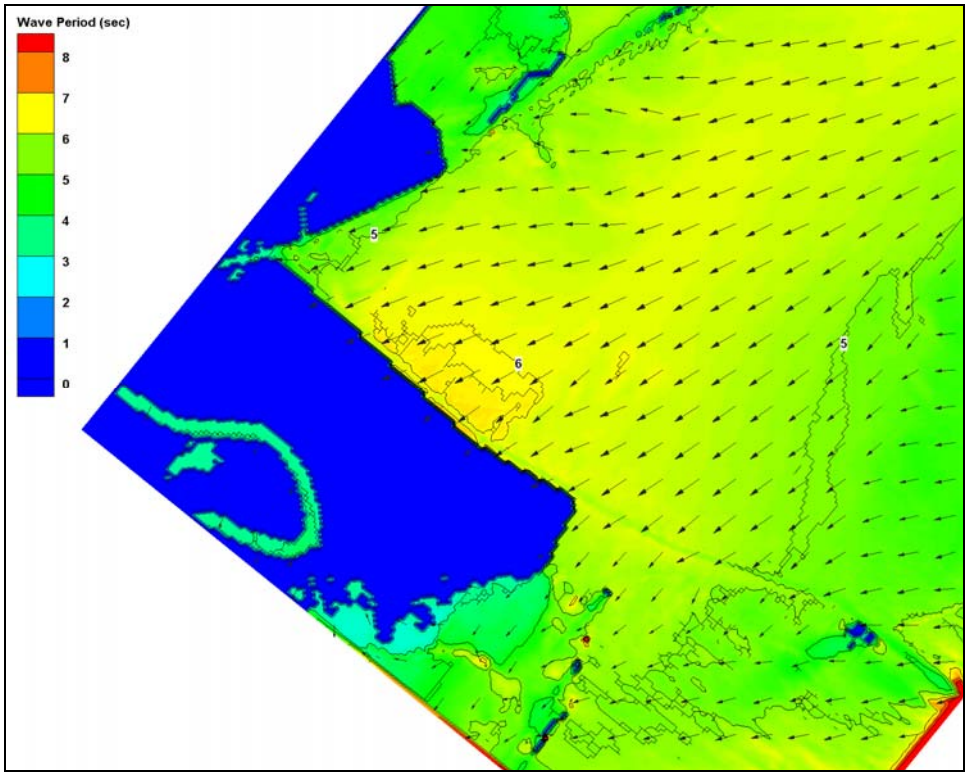


Figure 21. Mean wave period snap-shot at 8/29/1200Z (7:00 am CDT August 29, 2005)

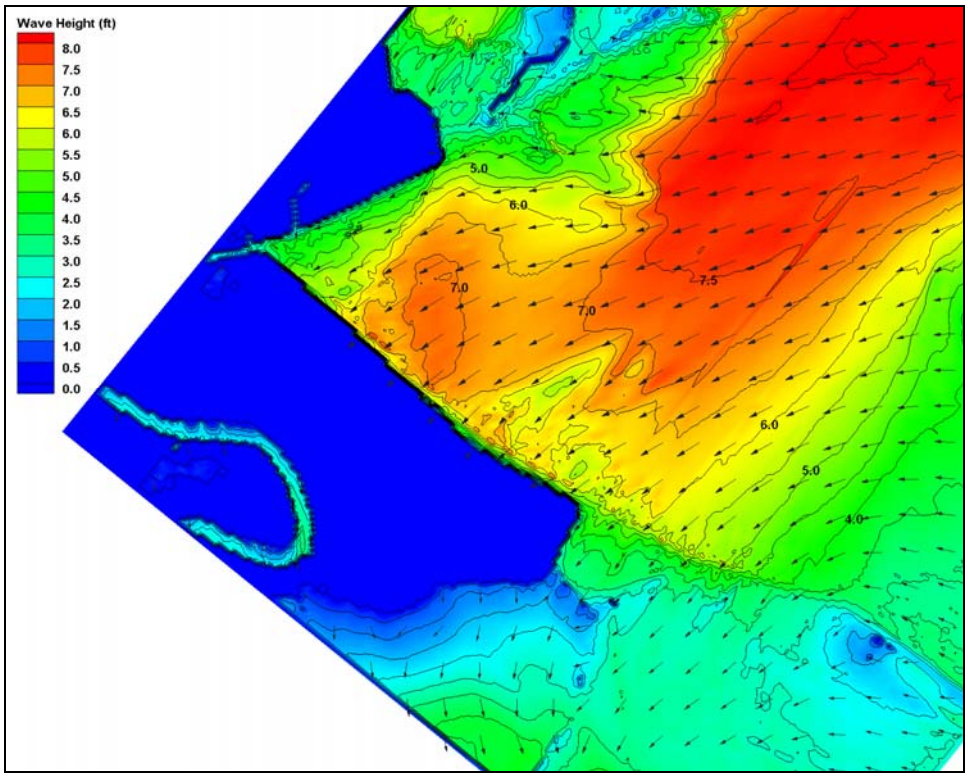


Figure 22. Significant wave height snap-shot at 8/29/1300Z (8:00 am CDT August 29, 2005)

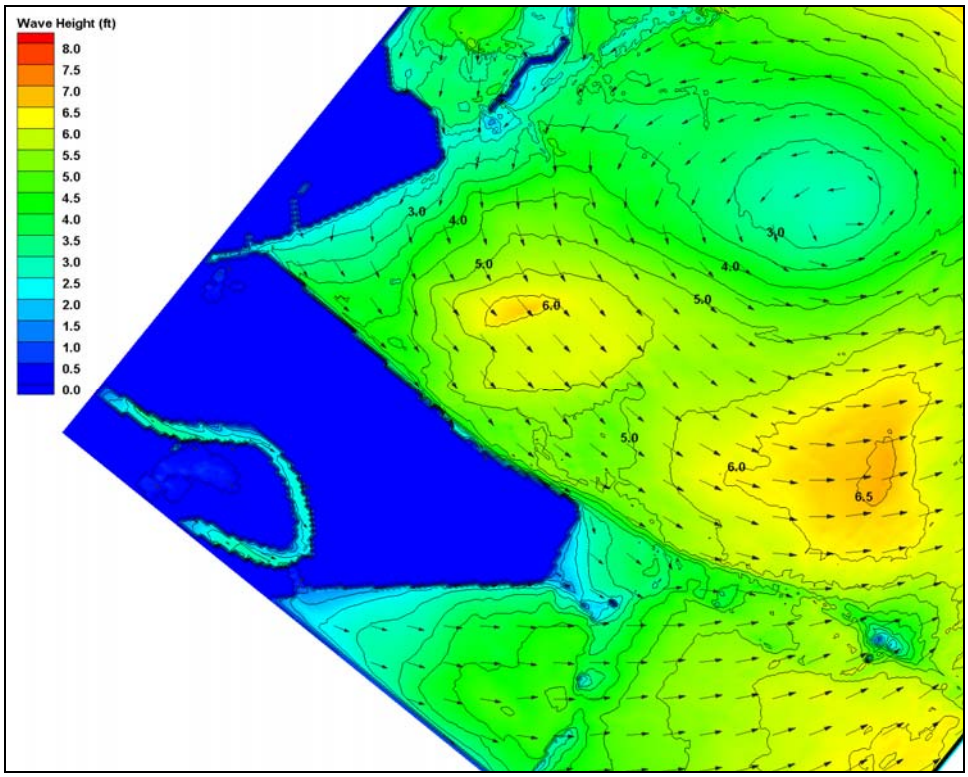


Figure 23. Significant wave height snap-shot at 8/29/1400Z (9:00 am CDT August 29, 2005)

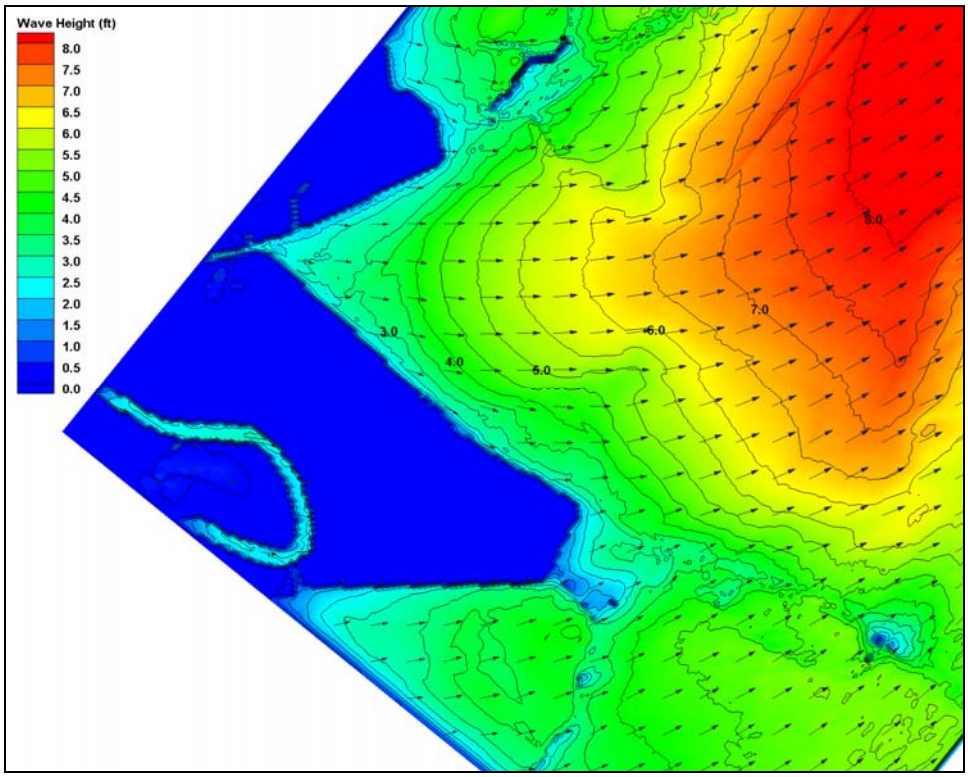


Figure 24. Significant wave height snap-shot at 8/29/1500Z (10:00 am CDT August 29, 2005)

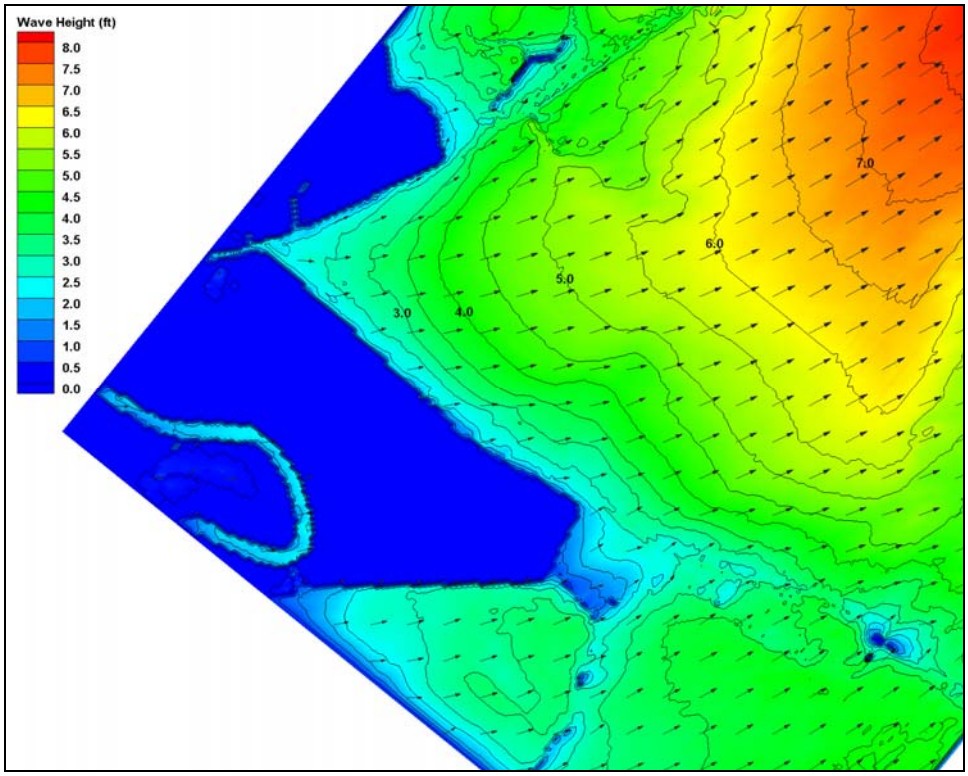


Figure 25. Significant wave height snap-shot at 8/29/1600Z (11:00 am CDT August 29, 2005)

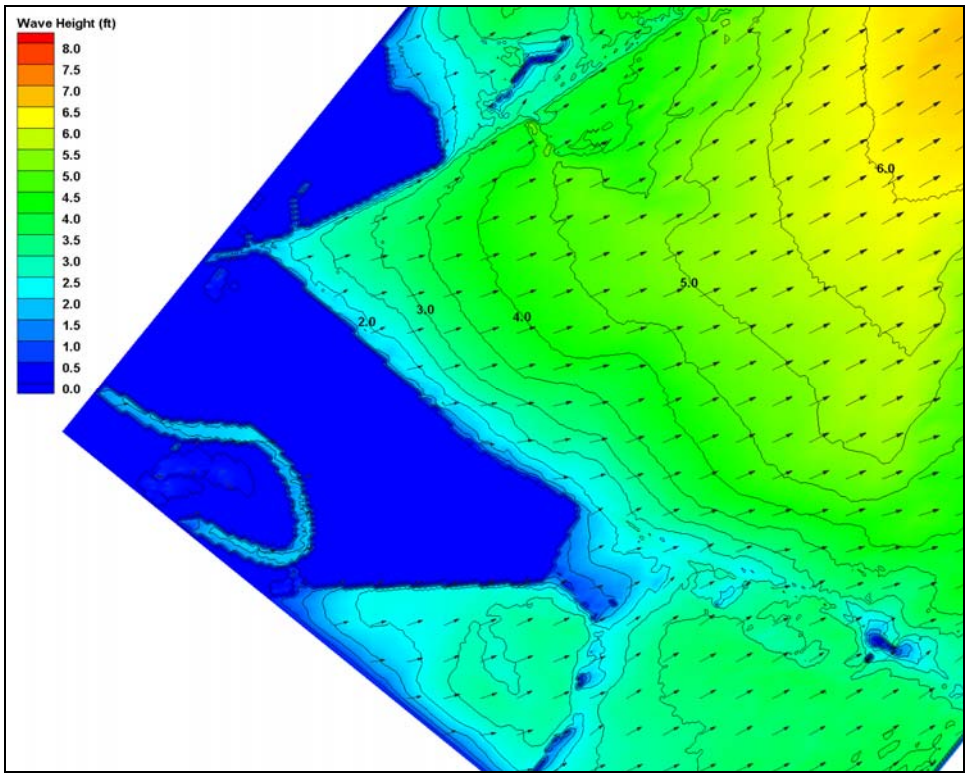


Figure 26. Significant wave height snap-shot at 8/29/1700Z (12:00 pm CDT August 29, 2005)

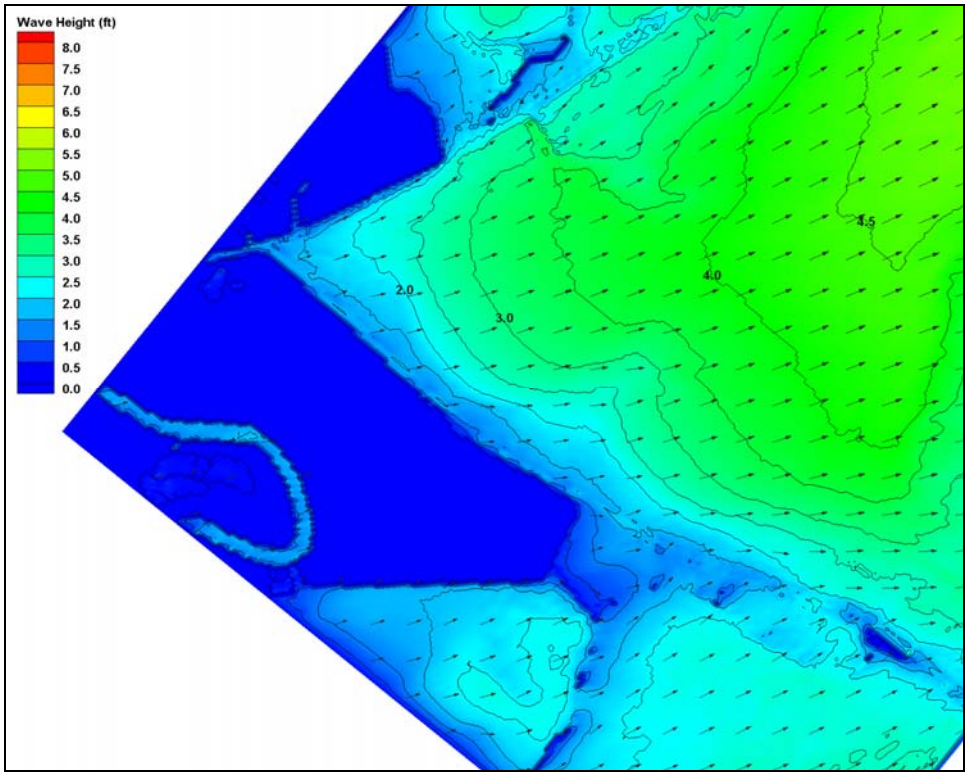


Figure 27. Significant wave height snap-shot at 8/29/2000Z (3:00 pm CDT August 29, 2005)

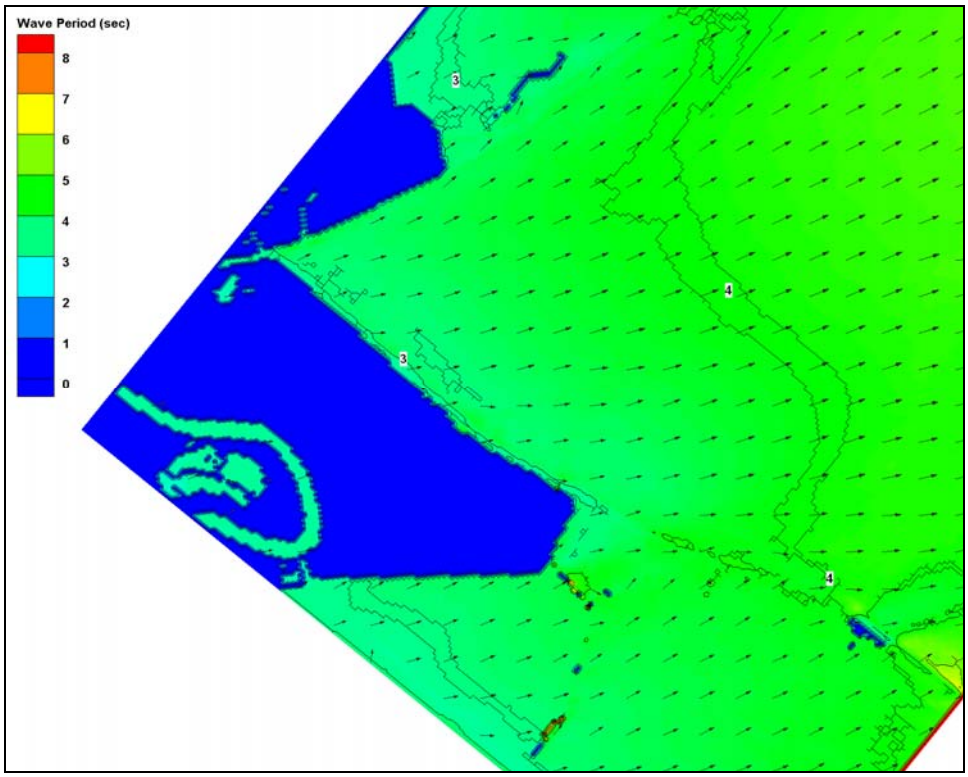


Figure 28. Mean wave period snap-shot at 8/29/2000Z (3:00 pm CDT August 29, 2005)

v. Maximum Wave Height and Corresponding Period (Synoptic View)

Figures 29 and 30 show the spatial distribution of maximum significant wave height and corresponding mean wave period, respectively, for the region. Both figures also show the mean wave direction (indicated by the black vectors) at the time of maximum wave height. Peak wave heights were between Bayou Bienvenue and Bayou Dupre (6.5 to 7.5 ft). The highest incident waves were just to the north of Bayou Dupre. Peak wave heights were 5.5 to 6.5 ft, but rather uniform in height, along the levee south of Bayou Dupre. Significant wave heights decreased north of Bayou Bienvenue, with maximum wave heights at the confluence of approximately 4 ft. Waves with greater significant heights have greater potential for runup and overtopping.

At the time wave heights were greatest, waves approached nearly perpendicular to the entire MRGO Reach 2 levee; this was the case throughout the time during which surge built up to high levels against this levee. Normal wave incidence maximizes the potential for runup and overtopping, compared to waves that approach obliquely to a levee. Mean wave periods corresponding to the time of maximum wave height were 6 to 6.5 sec along the central third of the MRGO Reach 2 levee, and slightly less, 5 to 6 sec along the northern and southern thirds. The highest wave periods were just south of Bayou Dupre. Waves with longer periods have greater potential for runup and overtopping than do shorter periods.

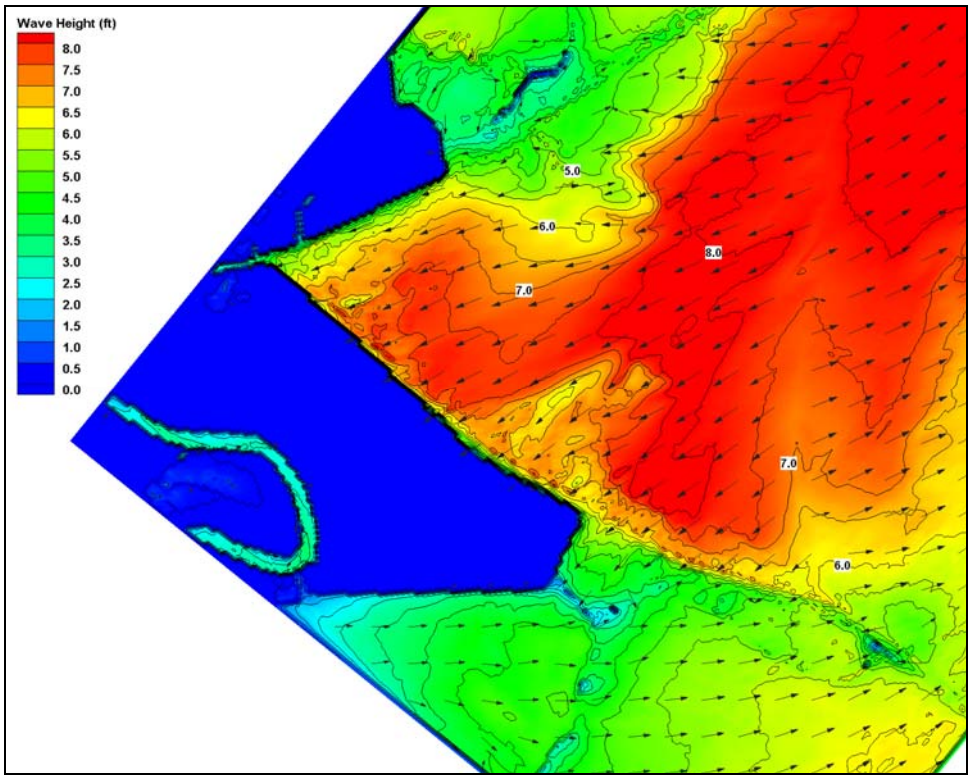


Figure 29. Maximum significant wave height and corresponding mean wave direction

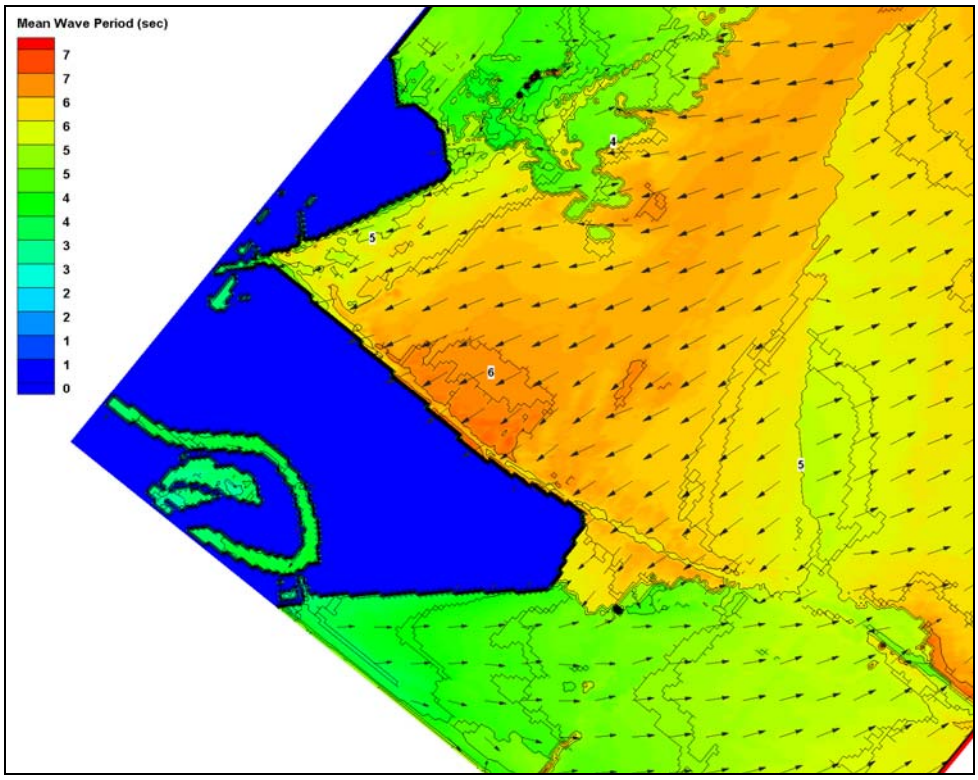


Figure 30. Mean wave period and direction corresponding to the maximum wave height

In light of the high water levels and wave heights that were experienced along the MRGO Reach 2, these levees and floodwalls were subjected to severe wave runup and overtopping. In terms of wave conditions and water levels only (without consideration of levee crest elevation) the maximum potential for runup and overtopping was in the vicinity of Bayou Dupre.

c. Best Estimates of Water Level and Wave Conditions for Selected Locations

i. Along the MRGO Reach 2 Levee

Figures 31 through 33 show the temporal variation of computed water level and wave conditions (significant height and mean wave period) along the MRGO Reach 2 levee. Results are shown for these three sites:

1) MRGO Reach 2 channel at Bayou Bienvenue (Figure 31)
2) MRGO Reach 2 channel at Bayou Dupre (Figure 32)
3) MRGO Reach 2 channel at the southeastern end of the levee (Figure 33)

Water level hydrographs shown are the computed hydrographs, scaled upward using the appropriate scale factor, to better approximate the actual hydrograph. The contribution of wave set up to the mean water surface is included in these figures. Maximum mean wave setup was 0.5 to 0.9 ft along the MRGO Reach 2 levee.

The surge hydrograph at Bayou Bienvenue (Figure 31) had two peaks. The first was associated with the arrival of the core hurricane winds, which built surge against the MRGO Reach 2 levee. Once the core arrived, surge increased rapidly. Between the time the surge reached 8 ft and the time of peak surge, the average rate of water level rise was 1.5 to 2 ft/hr. Computed peak surge was 14.8 ft. Actual peak surge was estimated to be 16.6 ft using the scaling factor of 1.12. An additional contribution to the mean water surface (i.e., wave setup) of several tenths of a foot occurred right at the levee due to wave breaking on the levee. The amount depends on the degree of overtopping. This water level estimate is consistent with the fair/poor high water marks at this site (16.5 to 18.5 ft).

The time of peak surge is between 7:00 and 7:30 a.m. CDT. The surge level fell just as rapidly as it rose as the hurricane center moved through Lake Borgne toward a second landfall in Mississippi. The second peak of lesser magnitude was created as the build-up of storm surge along the Mississippi coast, which was pushed against the coastline by high winds, propagated back away from the coast as the storm moved inland and wind speeds at the coast dropped quickly. The propagation of surge back toward the Gulf created the second peak, increasing water levels in Lake Borgne which had already fallen once the hurricane moved north of the region. Peak significant wave heights at Bayou Bienvenue were 5.5 ft, with a corresponding mean wave period of 4.5 sec. Peak

waves arrived slightly before peak surge. At the time of peak surge, significant wave heights were 5 ft.

The surge at Bayou Dupre was quite similar, although the second peak was less pronounced than it was at Bayou Bienvenue. The computed peak surge was 15.5 ft, corresponding to an estimated actual peak surge of 17.4 ft using the 1.12 scaling factor. An additional contribution to the mean water surface of approximately 0.8 ft occurred right at the levee due to wave breaking on the levee. This elevation is consistent with the fair/poor high water marks recorded at this site (16.8 to 21.7 ft). The rate of rise is similar and the time of peak surge is about 7:30 a.m. CDT. Peak significant wave heights at Bayou Dupre were 6.9 ft with a corresponding mean wave period of 5.8 sec. Peak waves arrived 0.5 hour before the time of peak surge. At the time of peak surge, significant wave heights were still 6.9 ft.

At the southeastern end of the levee along MRGO Reach 2, the second surge peak was much less pronounced. The computed peak surge at this location, 15.1 ft, was less than the value at Bayou Dupre, but similar to the value at Bayou Bienvenue, corresponding to an estimated actual surge of 17.0 ft. The time of peak surge was 7:30 a.m. CDT. Peak significant wave heights were 6 ft and the corresponding mean wave period was 5.6 sec. An additional contribution to the mean water surface of 0.5 ft occurred right at the levee due to wave breaking on the levee. Peak waves occurred at or just slightly before the time of peak storm surge.

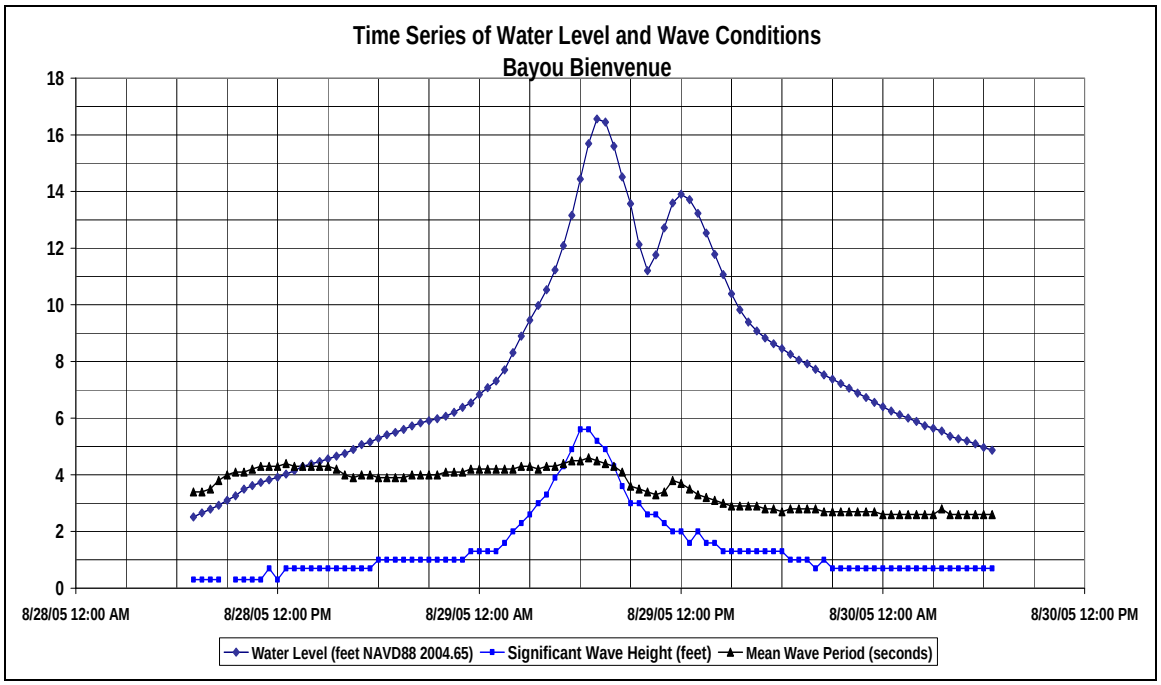


Figure 31. Temporal variation of estimated water level and computed incident wave conditions at Bayou Bienvenue

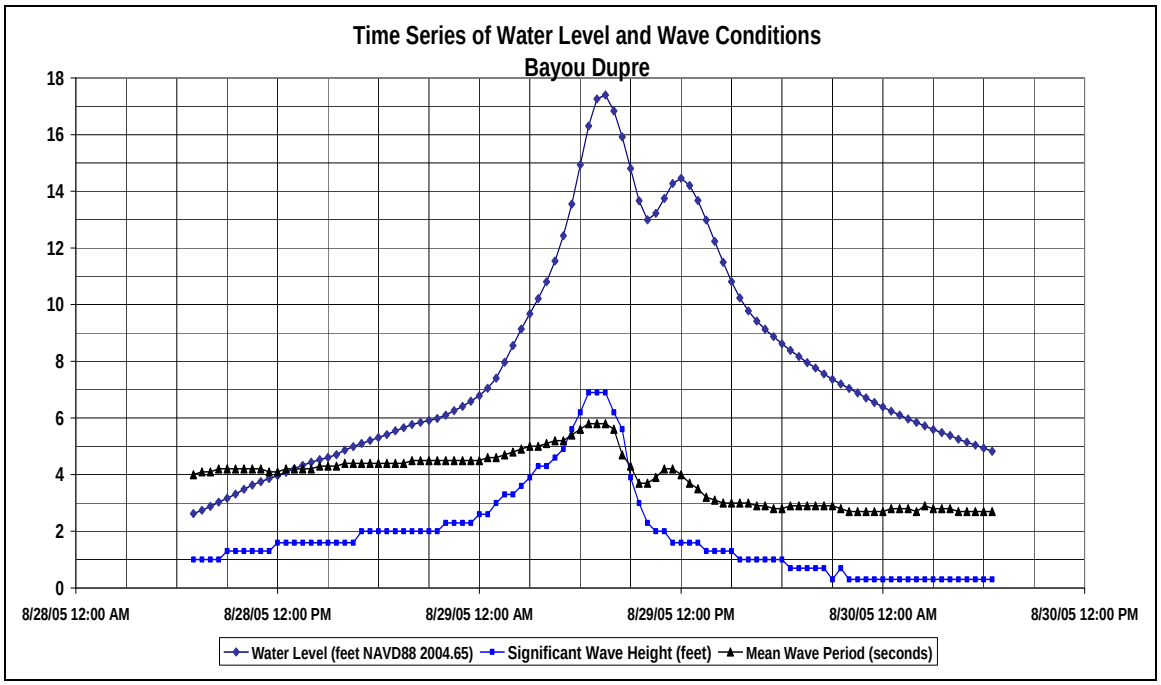


Figure 32. Temporal variation of estimated water level and computed incident wave conditions at Bayou Dupre

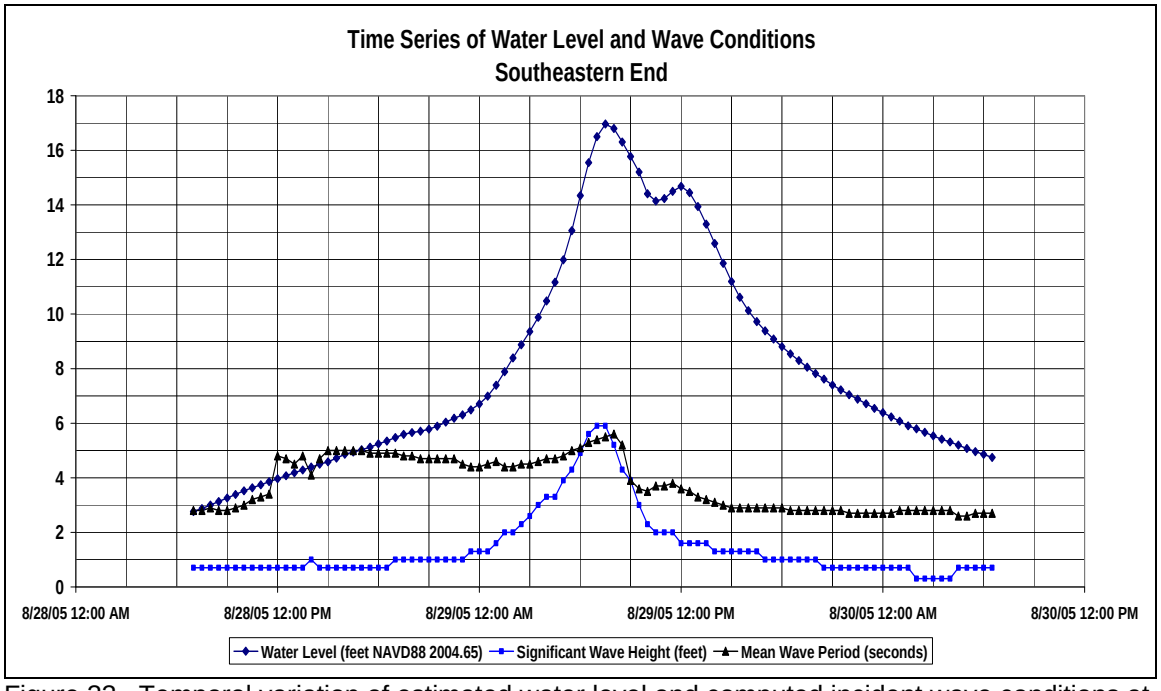


Figure 33. Temporal variation of estimated water level and computed incident wave conditions at southeastern end of MRGO Reach 2 levee

Figure 34 shows variation along the entire MRGO Reach 2 levee for estimated actual maximum total water level, maximum significant wave height and the maximum mean wave period. In the figure, Bayou Bienvenue is near location #2 and Bayou Dupre is near location #11. The water level curve in Figure 34 reflects computed surge elevations, which are first scaled up using a factor of 1.12, plus an additional contribution to the mean water surface associated with wave setup due to wave breaking right at the levee.

The maximum total water level is fairly uniform along the levee, decreasing gradually near the northwestern and southeastern ends. The highest value (18.3 ft NAVD88 2004.65) was in the vicinity of Bayou Dupre. Significant wave heights were slightly greater for the northern half compared to the southern half of this levee reach. The maximum wave heights (7 ft) were located just to the north of Bayou Dupre as were the maximum wave periods (6 sec). Incident wave directions all along MRGO Reach 2 were from 65 to 70 degrees true north, i.e., from the east-northeast direction, perpendicular to the levee alignment.

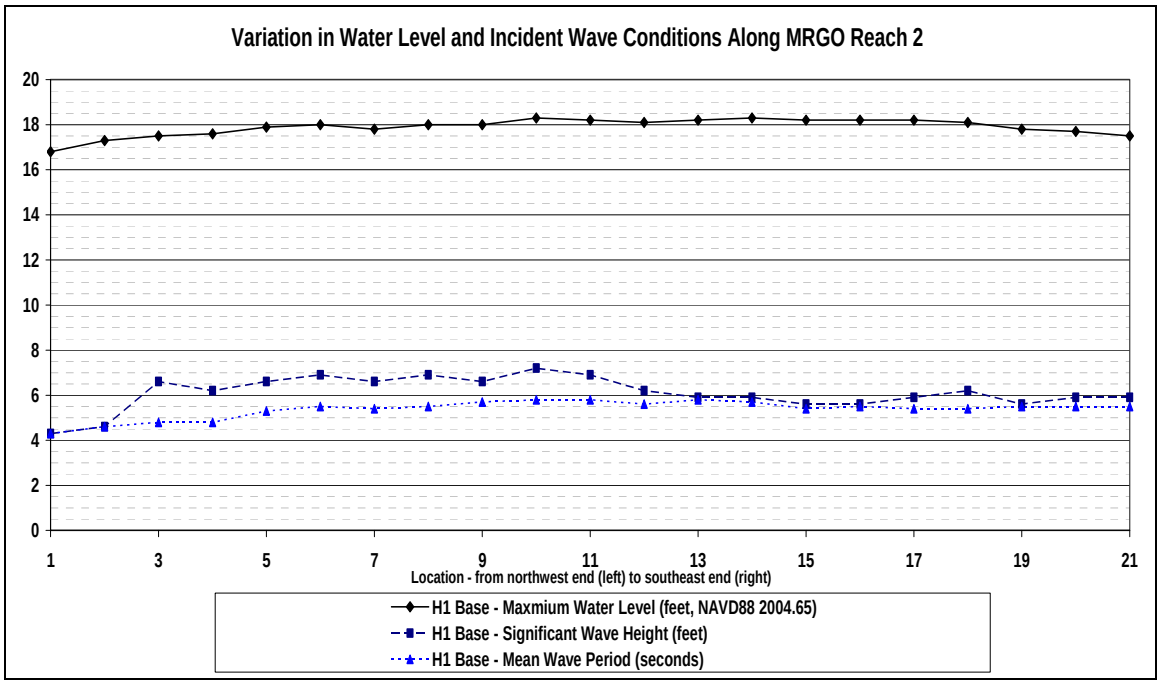


Figure 34. Variation in estimated maximum total water level (including wave setup) and computed peak wave conditions along the MRGO Reach 2 levee

ii. At IHNC Breach Sites

Figure 35 shows the estimated hydrograph at the IHNC breach sites, based on model computations. The computed hydrograph was scaled upward using a factor of 1.04 so that water level maximum matched the maximum water level recorded at the IHNC Lock. The hydrograph shows arrival of the peak surge between 7:30 and 8:00 a.m. CDT, earlier than the IHNC hydrograph. The computed hydrograph shows two peaks; whereas, the hydrograph measured at the IHNC Lock showed a single peak.

This discrepancy is attributed to several factors. One, the ADCIRC SL15 model under-predicted peak surge along the south shore of Lake Pontchartrain at the entrance to the IHNC (simulated maximum value of 9 ft versus the approximately 11.8 ft maximum which was reflected in several excellent high water marks at the entrance). The time of maximum surge at the Lake Pontchartrain entrance to the IHNC occurred at approximately 9:00 a.m., lagging behind the time of peak surge in Lake Borgne. With a maximum surge of near 12 ft in Lake Pontchartrain at approximately 9:00 a.m., the water level gradient through the IHNC would have been much less than that simulated by the model. Wind from the north in Lake Pontchartrain also was acting to set up the water surface within the IHNC according to the momentum balance that was in place within the lake at around 9:00 a.m. Water levels in the flooded St. Bernard polder also acted to keep water levels higher in the IHNC as water flowed back out from the polder to the IHNC following movement of the hurricane to the north. Feedback between the water levels in the inundated St. Bernard polder and in the IHNC, via the breaches, was not simulated in the ADCIRC model. Some or all of these factors appear to have acted to keep water levels higher in the IHNC during the time the model predicted a dip in water level.

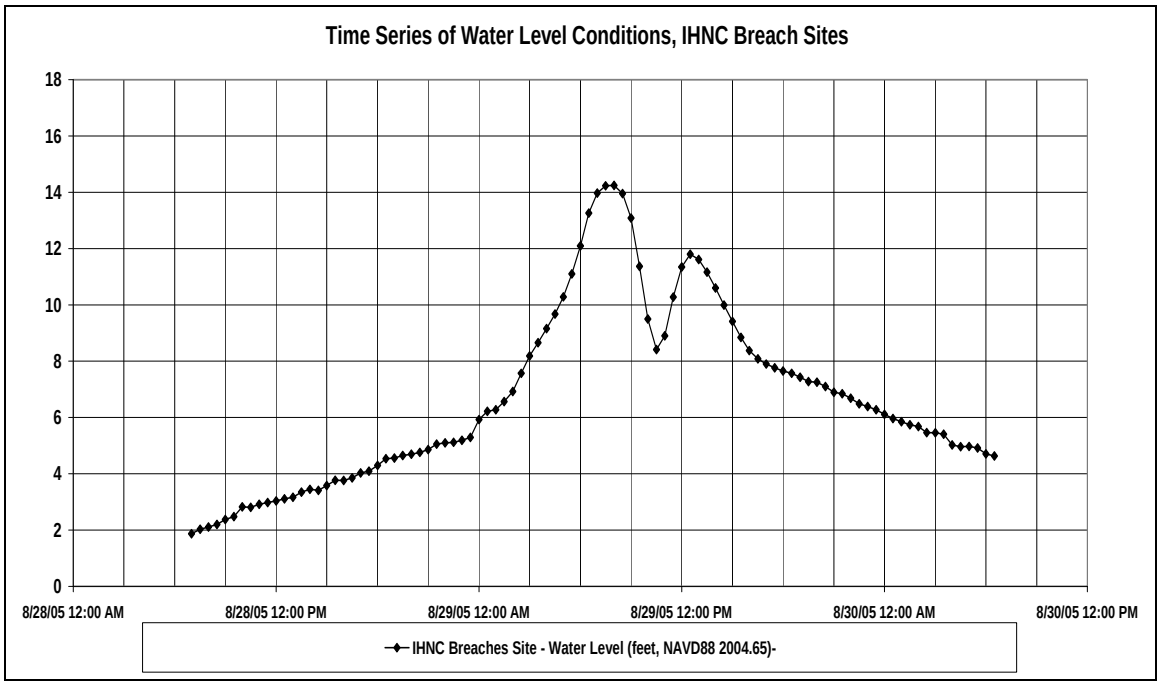


Figure 35. Temporal variation of computed water level at the IHNC Breach Sites

III. Surf Zone Dynamics – Implications for Levee Erosion

a. Wave Breaking, Run-up and Overtopping During the Storm

The rapidly rising water level and increasing wave energy just seaward of the MRGO Reach 2 levee toe dictated the hydrodynamic regime and loadings experienced on the levee. As winds built the storm surge, waves also increased in height and energy (the two are directly related). During the rise in water level and wave conditions, wave energy was dissipated on the more gently sloping berm that fronted the steeper front face of the levee. Wave breaking and dissipation on the berm limited the amount of wave energy that actually reached the levee; the degree of dissipation was strongly influenced by the depth of water on the berm. Significant wave height is limited to a value that is approximately equal to 0.4 to 0.6 times the local water depth, due to wave breaking, depending on slope.

Table 2 shows estimated water levels (excluding wave setup) and incident wave conditions, as a function of time, every 30 minutes, for a location between Bayou Bienvenue and Bayou Dupre, which is representative of conditions found along the MRGO Reach 2 levee. Local time is listed in CDT, water level is referenced to feet NAVD88 2004.65, and the wave height values are significant heights, in feet. Assuming an elevation of 9 ft on the berm just seaward of the levee toe, the depth-limited significant wave height approaching the toe is conservatively computed as 0.6 times the local water depth (water level minus the berm elevation). As the water level increased during the storm, the water depth increased on the berm and the wave energy that reached the toe and impacted the levee also increased. Wave energy at the levee toe was small until the water level rose high enough to allow significant wave energy to reach the levee.

Figure 36 illustrates the evolving water level and wave conditions at the toe of the MRGO Reach 2 levee at hourly intervals using data from Table 2. Wave heights and water levels shown in the figure are scaled approximately. At 4:00 a.m., incident significant wave heights were 3.3 ft. The water level was 11.3 ft, therefore the depth of water over the berm was quite shallow, with a depth just seaward of the toe equal to 2.3 ft. The shallow water on the berm greatly limited the wave energy that reached the levee; the depth-limited significant wave height was 1.4 ft at the toe. The toe would have been at the inner portion of the surf zone. Small waves would have been breaking on the levee face near the toe and running up the levee front face; the larger waves would have been breaking seaward of the toe. This is a very low wave energy condition on the front face, from the standpoint of erosion potential and overtopping potential.

Table 2. Evolution of Hydrodynamic Conditions at the Levee Toe			
Time, CDT	**Water Level (ft)**	**Incident Wave Height (ft)**	**Wave Height at Levee Toe (ft)***
8/29/05 3:00 AM	10.1	3	0.7
8/29/05 3:30 AM	10.7	3	1.0
8/29/05 4:00 AM	11.3	3.3	1.4
8/29/05 4:30 AM	12.1	3.6	1.9
8/29/05 5:00 AM	12.9	4.3	2.3
8/29/05 5:30 AM	13.9	4.6	2.9
8/29/05 6:00 AM	15.5	5.2	3.9
8/29/05 6:30 AM	16.8	5.9	4.7
8/29/05 7:00 AM	17.5	6.2	5.1
8/29/05 7:30 AM	17.5	6.6	5.1
8/29/05 8:00 AM	16.9	6.2	4.7
8/29/05 8:30 AM	15.9	4.9	4.1
8/29/05 9:00 AM	14.5	3.6	3.3
8/29/05 9:30 AM	13.1	3	2.5
8/29/05 10:00 AM	12.4	2	2
8/29/05 10:30 AM	12.7	2	2
8/29/05 11:00 AM	13.0	2	2
* Assumes elevation of sloping berm in front of the levee is 9 ft and assumes depth-limited significant wave height at the toe is 0.6 times the local water depth			

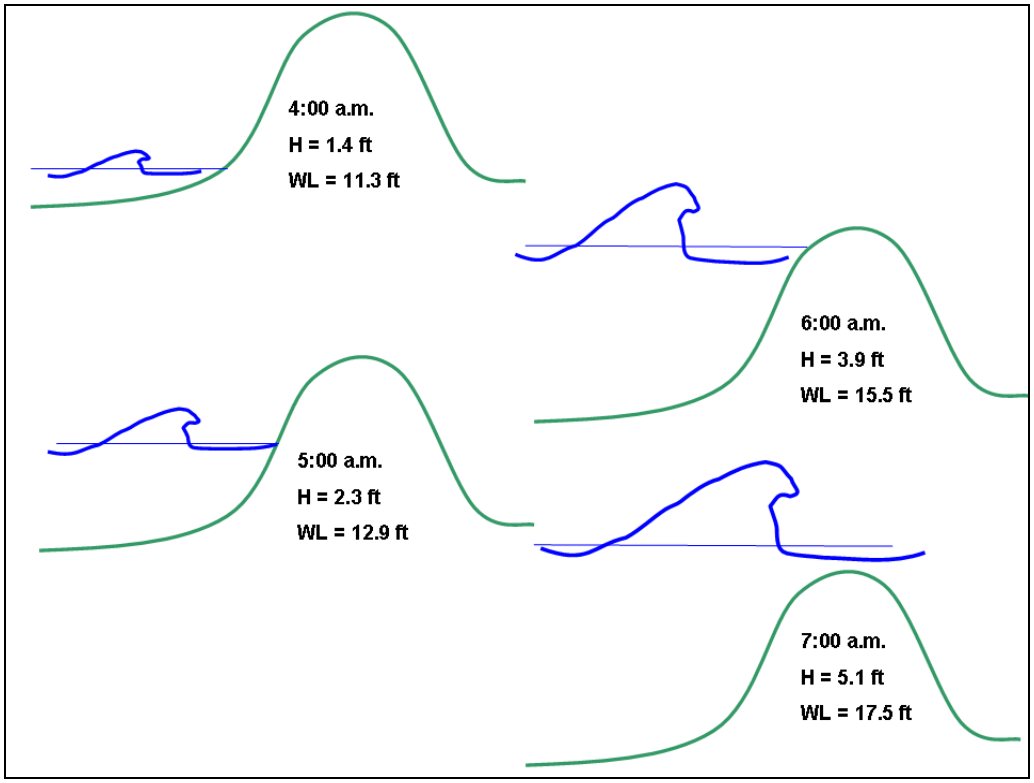


Figure 36. Sketch of temporal variation of surf zone conditions at the levee toe

One hour later, at 5:00 a.m. the water level had increased by 1.6 ft to a level of 12.9 ft. The levee between Bayou Bienvenue and Bayou Dupre had crest heights less than 16 ft at many locations. At this point in time, for a levee with a crest elevation of 16 ft, the water level would have been halfway up the levee front face. The water depth on the berm just seaward of the toe increased to 3.9 ft, still rather shallow. The incident significant wave height was higher, 4.3 ft. However, in light of the shallow water depth, considerable energy was still being dissipated on the berm fronting the levee. The depth-limited significant wave height near the levee toe was 2.3 ft. Wave energy acting on the levee face remained rather low, from an erosion standpoint. But because of the elevated water level, broken wave bores in the swash zone advanced up the slope and began to overtop the levee crest, for levees having a 16-ft crest height or less. Overtopping was more severe for lower levees at this time.

With the water level increasing at a rate of nearly 2 ft/hr, the location of the swash zone was advancing up the levee face at a similar rate. Duration of hydrodynamic loading within the surf and swash zones, and persistence at a single location, are both important in dictating the degree of front side erosion that occurs. Erosion depends upon the magnitude of oscillatory wave velocities, turbulence, and mean currents, including the mean undertow that is generated on the front face and is directed down the slope, and the duration of loadings. Erosion is also strongly influenced by the grass cover, and by the character and properties of soil comprising the levee.

One hour later at 6:00 a.m. the water level was rising at a faster rate, increasing by another 2.6 ft to a level of 15.5 ft, approaching the crest of the levee at many locations between Bayou Bienvenue and Bayou Dupre. The incident significant wave height was 5.2 ft. Water depth at the levee toe was 6.5 ft, so much more wave energy was reaching the levee; less was being dissipated on the fronting berm. The significant wave height seaward of the levee toe was still limited by breaking to a value of 3.9 ft, which was twice the magnitude of the wave height just one hour earlier. With the water level near the levee crest (assuming a 16-ft height), the highest waves would have been breaking on the levee front face. Many of the waves would have been breaking on the levee crest or on the back side of the crest. Nearly all unbroken or partially broken waves would have passed over the levee crest. As wave energy was increasing and creating more potential for erosion, overtopping was also increasing greatly.

Once overtopping began, it quickly became the dominant loading condition on the MRGO Reach 2 levee. The onset of overtopping depends strongly on the elevation difference between water level and levee crest (difference is called freeboard) and on the incident wave characteristics. Positive freeboard conditions are when the levee crest elevation is above the mean water surface. As the mean water surface rose above a point midway up the levee front face, to within several feet of the levee crest, wave overtopping began. At first, overtopping was intermittent with the passage of some wave crests over the crest of the levee, which then cascaded down the back side. Waves that did not pass over the levee crest ran up and then back down the front face. Water in each overtopping wave crest has a high velocity, and that water was further accelerated down the entire back side of the levee by gravity, exposing the entire back side to extremely

high flow speeds, creating much greater erosion potential. The higher erosion pressure on the back side, much greater in magnitude than on the front side, acts on the entire levee back slope unlike the front side where the most erosive zone is the breaking zone where high velocities last just for a fraction of each wave period. As the water level gets closer and closer to the levee crest, more and more individual waves overtop the levee. There will not be nearly as many down rushing waves to interact with the up rushing waves on the front side, so the intensity of the swash zone on the front side will diminish as overtopping increases and wave breaking will be concentrated on the crest and back side of the crest.

In a period of just two hours, from 4:00 a.m. to 6:00 a.m., hydrodynamic loading conditions on the levee changed from conditions having minor erosion potential on the front side (limited by lower velocities and short duration) to persistent and potentially very damaging overtopping/overflow and velocity conditions on the levee back side.

Another hour later, at 7:00 a.m. near the time of maximum surge and maximum wave conditions, the water level was 17.5 feet and water was steadily flowing over the levee crest, pulsating with the passage of each wave over the crest. The incident significant wave height was 6.2 ft. Water depth on the berm just seaward of the levee toe was 8.5 ft, so the wave energy would still have been limited somewhat due to breaking of the very largest waves on the berm in front of the levee. Significant wave heights near the toe would have been higher at this time, reaching their maximum value of 5.1 ft. At this water level, many of the waves would have broken directly on the levee crest and on the back side of the crest. Most waves would have propagated over the levee crest and down the back side. There would not have been a swash zone on the front side, since the mean water level was higher than the levee crest height. Since steady overflow is occurring, water is constantly accelerated down the backside slope, with repetitive pulses of even higher speed water associated with each overtopping wave. The pulses are accelerated down the back side. The potential for erosion in this loading situation is much greater and it is constantly exerted on the entire back side of the levee.

b. Visualization of Wave Overtopping and Overflow

The video file (.avi file titled “S1H6T10_Rollup-LowRes”) that accompanies this report illustrates a number of the points just made regarding hydrodynamic loadings on the levee. The video shows waves impacting a levee in a scaled physical-model simulation of conditions that are quite similar to those which occurred during Katrina along the MRGO Reach 2 levee at the peak of the storm. Model tests were performed at the U.S. Army Engineer Research and Development Centers’ Coastal and Hydraulics Laboratory. The first frame of the video (Figure 37) illustrates the model setup. The levee used in the test was quite similar to the lower spots on the MRGO Reach 2 levee: crest height 15 ft; crest width 10 ft; 1:4.25 front slope, and 1:3 back slope. For this test, the still water level was 1 ft above the levee crest, which is quite similar to conditions that were experienced during Katrina for much of the Reach 2 levee between 6:00 a.m. and 7:00 a.m. CDT. The incident significant wave height and wave period were 6 ft and 10

sec, respectively. Irregular waves are simulated. This wave height is quite similar to the maximum incident significant wave heights that were calculated along the MRGO Reach 2 levee (5 to 7 ft). The wave period in the test was longer (10 sec versus 6 sec). This test involved examination of the performance of a concrete mat on the levee slope; the prototype weight of the mat is 1 ton per linear foot of levee crest length. The extreme power of storm waves is illustrated by the impact of the waves on the heavy concrete mat. The reason for including the video is that it illustrates several key features of the loadings and velocity regimes.

An irregular sea state is created during hurricanes; both high and low waves occur, all of which impact the levee. The location of breaking is highly dependent upon the heights of individual waves, and local water depth. As seen in the video, a few of the waves break on the upper third of the levee slope, introducing higher speed orbital velocities and turbulence to the levee surface on the front side; these high velocities last for a relatively short duration (a fraction of each wave period). Most of the waves break right on the levee crest; some break on the upper region of the back side slope. A few smaller waves surge over the crest without breaking. At this still water level, every wave runs up and over the crest and down the back side. Considerable turbulence and high velocities are associated with breaking waves and these loadings are introduced to the levee crest and back side for most of the waves.

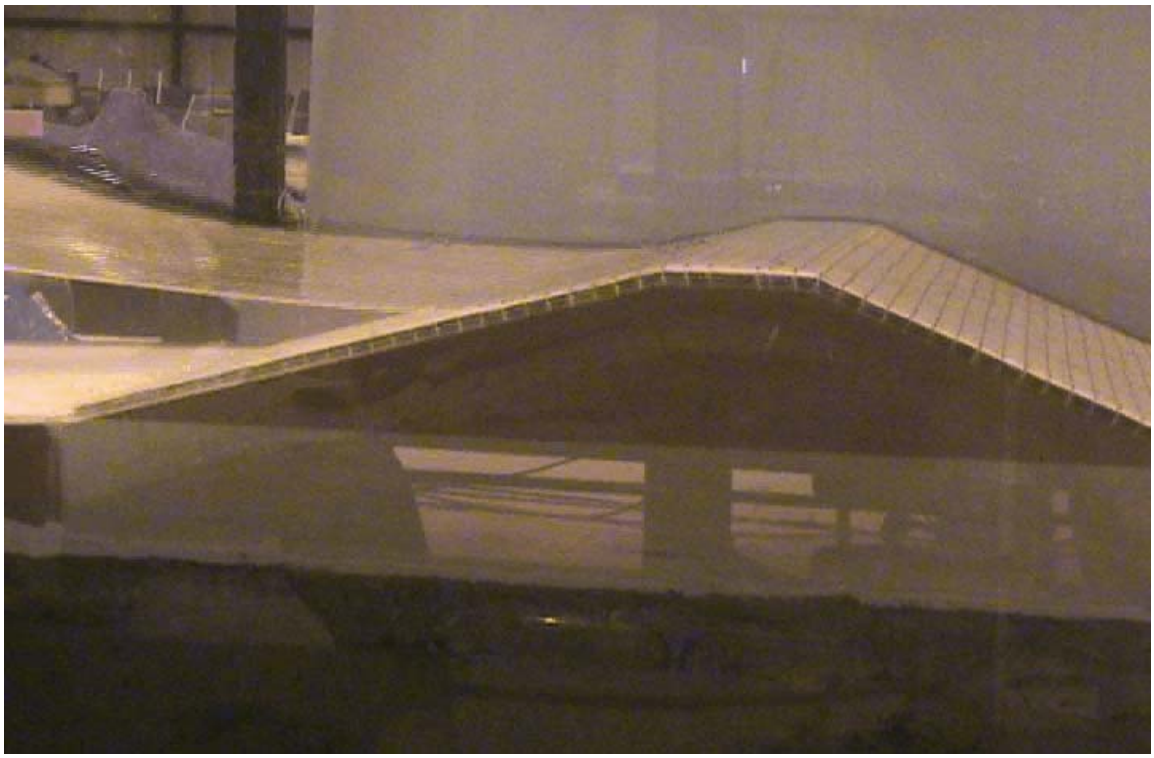


Figure 37. Scale-model setup for the video “S1H6T10_Rollup-LowRes” that demonstrates hydrodynamic loadings on the MRGO Reach 2 levees.

As waves propagate over the crest, the water in them is accelerated down the back side by the force of gravity. The same is true for the steady flow component that arises because the still water level exceeds the crest height; that flow is also accelerated down the back side by gravity. With the passage of each wave, the steady flow down the back side pulsates. In the video, these pulses enable one to see the acceleration of water and just how fast the fluid is moving down the back side (it is less apparent without wave pulses).

The pulsating supercritical flow is persistent everywhere on the back side, unlike the velocities associated with the intermittent, short-duration, and less frequent breaking waves on the front side which occur at different locations. The video shows why the back side hydrodynamic regime is so much more erosive, because of the much more persistent high fluid velocities and turbulence, compared to the velocity regime on the front side which is dominated by a few high waves with short duration bursts of high velocity and turbulence.

c. Results from High-Resolution Modeling of Velocities at the MRGO Reach 2 Levee

To examine the effects of waves on the velocity regime along the MRGO Reach 2 levee, a state-of-the art Boussinesq-type wave model, COULWAVE, was applied to compute hydrodynamic loadings on levee cross-sections that were representative of those along this reach of levee. This work is more fully described in the expert report by Resio (2008). This type of ultra-high-resolution wave modeling, which has been extensively validated, provides reliable estimates of water velocities that are acting to erode the levee, as well as mean overtopping rates and other surf zone wave and current properties. The model was applied to simulate a number of cases of irregular wave overtopping and overflow when the surge level was both below and above the levee crest. Results shown here are for water level, wave and levee conditions between Bayou Bienvenue and Bayou Dupre, the critical reach of the MRGO Reach 2 levee.

IPET (2006) showed that, prior to the mean water surface exceeding the levee crest height (positive freeboards of 1 to 2 ft), mean velocities on the front side were near zero and average peak velocities associated with passage of individual waves (both up rushing and down rushing water) were 3 to 5 ft/sec. Peak velocities only occurred for short periods of time during the passage of each wave, a fraction of each wave period. Notably, results showed that whenever overtopping occurred due to wave action alone, the mean velocities on the crest and back side were of greater magnitude than those on the front side, and the average peak velocities also were significantly greater on the crest and back side. Any water in a wave that overtops the levee is accelerated down the back side by gravity, producing higher velocities as a result of the acceleration compared to velocities on the front side. Non-zero mean velocities on the back side, and the bursts of higher velocity associated with each overtopping wave bore, exerted much more persistent erosion pressure on the back side than the intermittent bursts of higher wave velocities on the front side, and which had a near-zero mean.

IPET (2006) also showed that, once the mean water surface exceeded the levee crest height (negative freeboard situations), front side velocities increased, but crest and back side velocities always increased more to even greater velocities. Both mean and average peak crest and back side velocities were always equal to or greater than front side means or average peaks in situations where both overflow and wave overtopping occurred. Crest and back-side velocities were always the dominant velocity regime from the perspective of levee erosion, whenever overtopping occurred.

Figures 38 and 39 show the temporal variation through the storm of a velocity measure at both the levee crest and back-side, respectively, for a range of levee crest heights. Velocities shown in these figures were computed as the average of velocity-cubed for each of a series of 30-min time blocks during the storm; then the cube root of that value was calculated to derive an average velocity condition. Data are shown for several different locations (loading conditions) between Bayou Bienvenue and Bayou Dupre. Locations/conditions were selected for levee crest heights that had integer values. Even though results are not for the same location (i.e. not exactly the same incident wave and water level conditions), they illustrate how crest and back side velocities varied with levee crest elevation. Note that the values shown in the figures are mean values; velocities associated with the passage of individual waves would be much higher than the mean value.

Figure 38 shows results for velocities at the levee crest. Velocities are greatest for the lower crest heights, and less for the higher crest heights. The pattern of increasing mean crest velocity for decreasing levee crest height is expected. For the lowest levees along this critical reach (crest heights of 14 and 15 ft), at 6:00 a.m., well before the time of peak water level at 7:30 a.m., mean velocities of water flowing over the crest are already 5 to 6 ft/sec. Compare this magnitude of velocity (a mean quantity with intermittent velocities of much higher magnitude) with intermittent wave velocities on the front side of approximately 5 ft/sec. This illustrates the much higher velocity regime on the crest, compared to the front side, once overtopping occurred. Changes in maximum mean crest velocity, with decreasing levee crest height, are substantial, e.g., a maximum average velocity of 15 ft/sec for a 14-ft levee compared to 6.5 ft/sec maximum average velocity for a 16-ft levee.

Figure 39 shows results for velocities on the levee back side. They are much higher on the back side because of the acceleration down the back side, by force of gravity. Average velocities on the back side for a levee crest of 14 ft are 25 ft/sec, and above 10 ft/sec for levees with crest heights of 15 and 16 ft, which was common along the critical levee reach between Bayou Dupre and Bayou Bienvenue. These are mean velocities; pulses of much higher velocity occurred with the passage of each wave. At 6:00 a.m., mean velocities on the back side were 5 to 10 ft/sec for levees with crest of 15 and 14 ft, respectively. Even for a levee with crest height of 19 ft, at the time of maximum water level, the mean velocity on the back side is 4 ft/sec, comparable to the intermittent peak wave velocities on the front side of 5 ft/sec. The velocity regime on the back side is dominant over the velocity regime on the front side.

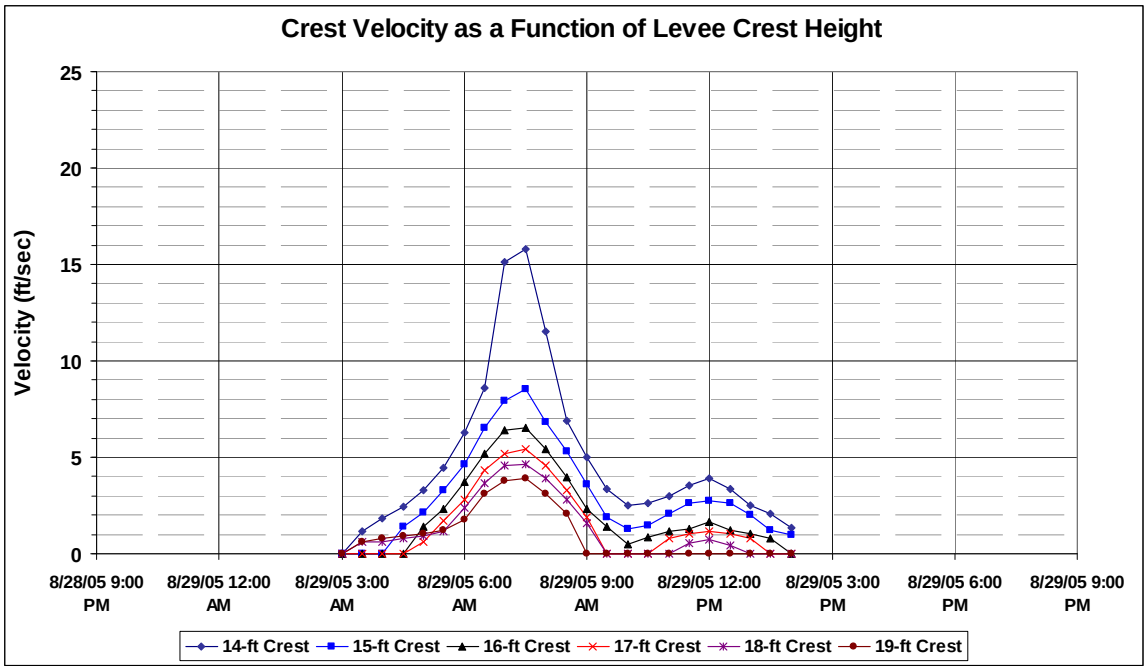


Figure 38. Mean crest velocities, through time, as a function of levee crest height

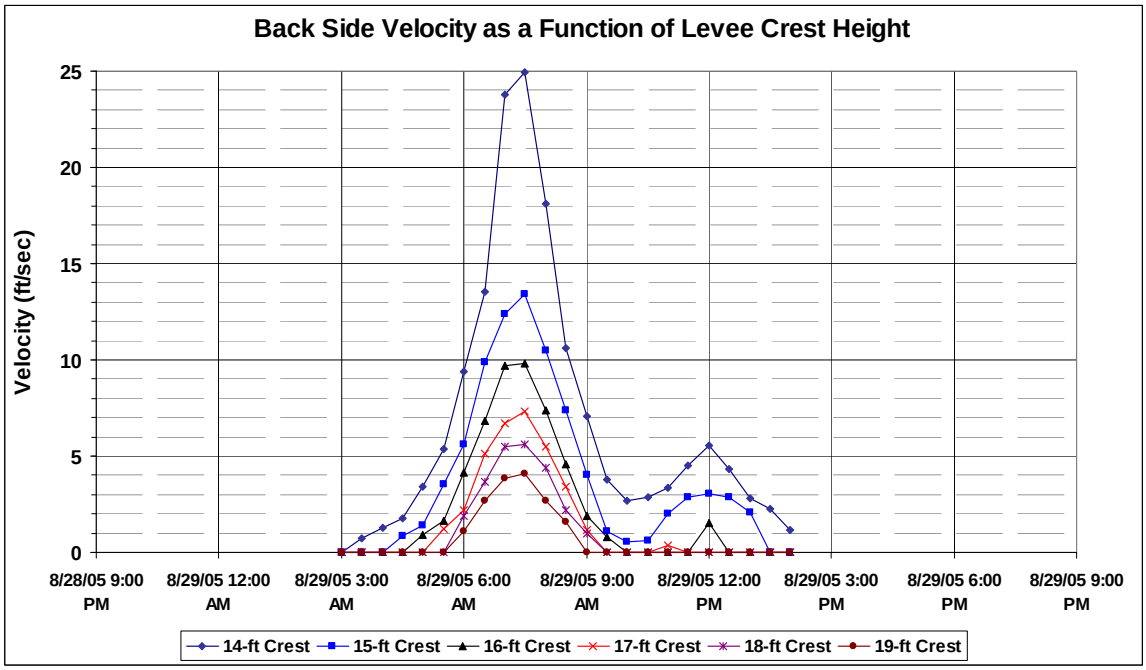


Figure 39. Mean back side velocities, through time, as a function of levee crest height

IV. Levee Response

a. Data Sources

Appendices A, B and C provide valuable visual information for examining levee and floodwall responses during Katrina. They shed light on erosion processes that occurred, and they facilitate enhanced understanding of what took place, where, and why.

Appendix A shows a series of 50 oblique aerial photographs taken shortly after Hurricane Katrina, along the entire stretch of levee adjacent to MRGO Reach 2. The first photo begins at the Bayou Bienvenue gate structure and the last one ends at the southeastern end of this levee section where the hurricane protection levee turns westward. The photos are fairly evenly spaced along the entire stretch of levee/floodwall system, so they provide a representative characterization of the levee and wall responses to the effects of erosive forces that acted on them. Each photo is annotated to provide an interpretation of what erosion processes and levee responses were prevalent at the location of each photo. Several photos are discussed in much greater detail in subsequent sections.

Appendix B shows graphical three-dimensional renderings of the post-storm levee topography, based on the 2005 LIDAR data. These figures present an oblique aerial perspective of the degraded levees, along the entire perimeter of the levee/floodwall system, from Caernarvon along the southern levee of St. Bernard polder, along MRGO Reach 2, along the GIWW and for some distance along the IHNC (east side). Each figure is annotated in the caption to provide additional information on the following: pre-storm crest height of levees and walls; how much of a levee reach had elevations that were above or below certain values; crest elevations in the low spots of the reach. The images provide a regional perspective on levee degradation and damage, enabling regional differences to be assessed.

Appendix C shows results from analyses of the pre-and post-storm LIDAR data performed by Dr. William Dally, Surfbreak Engineering Sciences, Inc along the entire MRGO Reach 2 levee/wall system. Information shown in the appendix was generated by creating closely spaced, cross-sectional slices through the point LIDAR data, in which the closest actual LIDAR data points were assigned to the slice, and then subsequent analysis of those cross-sections was performed. Polynomial fits to the cross-section data also were computed and used as input to the analyses to examine sensitivity of calculations to the choice of method for defining levee cross-section. Graphs are presented which show eroded volumes for both the front and rear sections of the levee. Front and rear were delineated by the position of the highest elevation on the levee cross-section in the pre-storm data. Total erosion volumes are displayed. Along-levee variability in eroded volume is shown at very high density. Higher-altitude aerial photos of each section of the MRGO Reach 2 levee also are shown. These data provide an excellent depiction of the spatial variability in levee crest elevation, eroded sill elevation, and of the degree of levee degradation as reflected by eroded volume.

b. Factors that Influence Levee Erodability

Based on the past two decades of experience with design, performance, and evaluation of USACE coastal storm damage reduction projects along U.S. coastlines, which have primarily involved beach nourishment (with sand) and dune construction, the maximum storm-induced water level was found to be the single most important hydrodynamic parameter that defines beach erosion and dune response. Incident wave conditions and duration of high water levels and wave conditions were also found to be important loading parameters. The same was true for this levee erosion situation.

Figure 40 shows pre-and post-storm elevations along the levee centerline for the entire length of MRGO Reach 2 levee/wall system, from Bayou Bienvenue to its southeastern end. Locations and lengths of floodwall are delineated by the black triangles at the bottom of the figure. Much of the levee south of Bayou Dupre, which is identified by the small wall section located at a distance of approximately 35,000 ft, was noticeably higher (by up to several feet, on average) than much of the levee between Bayou Bienvenue and Bayou Dupre. Overall, levee degradation/erosion is different for these two regions as evidenced by post-storm elevation data; there is less degradation, overall, along the southern one-third of the levee compared to the northern two-thirds. The estimated maximum total water level along the MRGO Reach 2 levee was rather uniform, 16.8 to 18.3 ft. The along-levee variation in maximum water level also is displayed in Figure 40. For much of the northern half of the levee/wall system, maximum water levels of this magnitude exceeded the height of the levee/walls. The graphical images in both Appendices A and B show these regional differences in erosion and levee degradation. These observations also indicate the importance of freeboard on erosion and levee damage; although it is not the only parameter that is important in determining levee response.

Figure 40 illustrates the amount of variability in pre-storm levee crest elevation over relatively short (on the order of 1000 ft) distances, compared to the overall length of this entire reach, 65,000 ft. Variations in crest elevation over this shorter length scale are as much as 2 ft. Considering all the low spots in the levee, and the magnitude of total mean water level (16.8 to 18.3 ft), and the potential for run-up elevations to be 3 to 4 ft, or more, above the mean water level, many locations were subjected to overtopping and steady overflow. Wave overtopping alone, and even more so in conjunction with steady overflow, created a very erosive hydrodynamic regime on the back side of the levee beginning at the low spots. This loading condition led to severe back-side erosion and scour, and formation and deepening and widening of many breaches. The number of areas subjected to damaging wave overtopping and overflow grew as the water level and wave energy increased. As levee crests were eroded and lowered in response to these forces, the magnitude of overtopping and overflow increased; this was a self-reinforcing and exacerbating process that led to widespread breaching and rapid levee destruction, the results of which are shown in Figure 40. The red curve shows the elevation of the levee along its centerline following the storm. Levee crests were degraded by amounts of 5 to 10 ft in many areas along the 12-mile stretch of levee. Breaching occurred along the entire MRGO Reach 2 levee, except at the southernmost end.

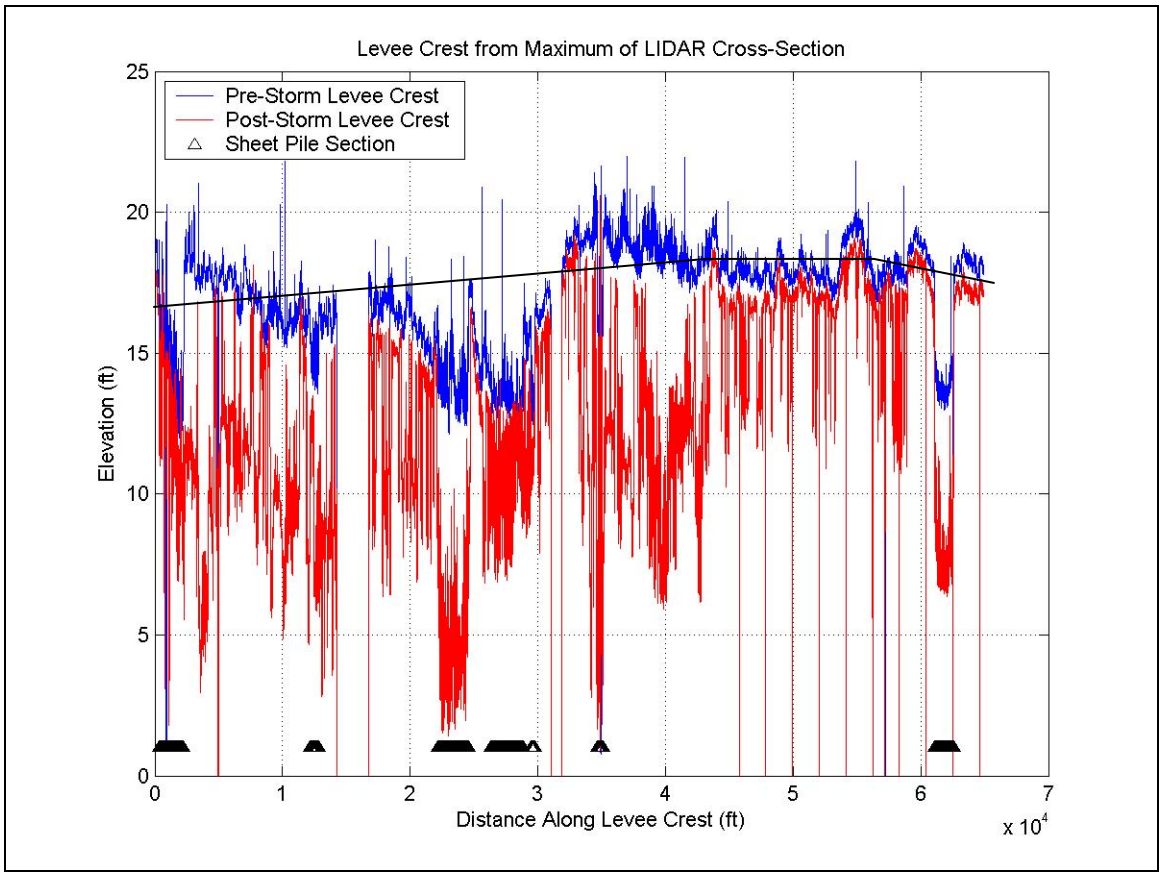


Figure 40. Pre- and post-storm elevations along the MRGO Reach 2 levee centerline. The estimated maximum mean water level along the reach is shown with a solid black line.

The water velocity regime on the levee back side was much higher than on the front side. Erosion is non-linearly related to velocity. For example, as an approximate rule of thumb, increasing velocity by a factor of 2 does not mean the erosion will increase by a factor of 2. Erosion will increase by a factor of 8 (i.e. erosion related to velocity raised to the third power). For these reasons, the much higher velocity regime on levee back side was so much more erosive and damaging than water velocities were on the front side.

In addition to erosion and breaching initiated by wave overtopping and overflow, breach widening was an important process. Water levels on the Lake Borgne side of the levee were higher than water levels in the interior of the polder, creating a hydraulic gradient or slope in the water surface from front side to back side. As breaches formed, flow was directed along adjacent higher levee sections toward the breaches in response to this hydraulic gradient. This flow of water toward the breach and acceleration of water through breach caused breaches to widen and deepen. The hydraulic gradient drove tremendous flows at high speeds over degrading levees and walls and through breaches as they formed, allowing a massive volume of water to enter and inundate the entire St. Bernard polder.

The degree of erosion and degradation also is dependent upon erodability of the sediment, or soil, comprising the levee, and by the grass cover (how it resists the onset of erosion of the underlying sediment). The words sediment and soil are used interchangeably in this report. Erodability is defined here as the degree to which levee sediments resist erosion by the imposed fluid stresses acting on them. Technical information and design guidance on quantifying erodability of fine-grained, mixed sediment under loading by waves (unsteady, oscillatory fluid motions with fluid accelerations) and combined wave-current flow regimes, particularly for sloping levee surfaces, is relatively sparse. More information and guidance exists for unidirectional steady flow conditions acting on flat vegetated earthen surfaces.

Erosion of mixed sediments is highly sensitive to local sediment properties. For example, non-cohesive silts and sands would be expected to be readily erode when subjected to typical storm wave-induced peak orbital velocities of 6 to 8 ft/sec; whereas denser clayey type sediments might not be eroded at all, or be eroded to a lesser degree, at these same velocities. Clay is the preferred material for construction of earthen levees because of its ability to be compacted to high density, its inter-particle bonding, and it relatively high resistance to erosion. Erodability of clayey sediments is very much related to the density, clay mineralogy, which can vary significantly for different types and sources of clay, natural and mechanical compaction, organic content, and to its moisture content. Research has shown that even small amounts of certain types of clay added to quartz sand can dramatically reduce the erodability of the mixed sediment (Lick et al, 2004).

c. Erodability as a Function of Freeboard and Sediment Type

Limited information about the types of sediment that comprised the heavily degraded levee reaches was available in the form of core logs from borings made at different times prior to the storm along the levee centerline. Analyses performed on the cores identified discrete sediment strata, characterized each stratum in terms of a soil classification, and cited other properties based on traditional geotechnical analyses done on extracted samples. While informative, data derived from the core samples were of very limited use from the standpoint of assessing sediment erodability. For example, existing information does not adequately characterize the crucial parameter of sediment density throughout the upper 10 ft of the sediment column, the portion of the levee that was most heavily eroded. Available tests and analyses done on the samples do not provide information on all the important sediment properties that are relevant to formation of a relationship between unsteady wave and current-induced fluid velocities, shear stresses and sediment erosion. They do not enable a relationship to be developed in any quantifiable and reliable way, for the wide range of sediment conditions that existed, and for the hydrodynamic loadings that were experienced during the hurricane.

Despite the limitations in available data regarding sediment erodability, the possibility of a relationship between sediment type and maximum water level (through its influence on freeboard) was examined in light of past USACE experience which has identified the importance of this particular parameter in the response of beach nourishment projects. In this analysis, freeboard is used as a surrogate for hydrodynamic loading. Positive free board conditions are when the levee crest is above the maximum mean water level; negative freeboard conditions when the maximum mean water level exceeds the levee crest height. Maximum water level is calculated as the sum of estimated peak surge level plus the contribution of wave-setup. Estimated peak water level for the New Orleans East back levee along the GIWW (east of Michoud Canal) is 16 ft (15.6 ft plus 0.4 ft wave setup), and the peak water level along the MRGO Reach 2 is 18.5 ft (17.5 ft plus approximately 1 ft wave setup). The actual maximum water level at any particular location could be several tenths of a foot different than these values.

Tables 3 and 4 present information at a number of locations along levees adjacent to GIWW east of Michoud Canal (Table 3) and MRGO Reach 2 (Table 4). Core samples at wall sections were not considered in these tables. Information about the sediment cores is from IPET (2007). The following information is shown in both tables:

Column 1: core identifier number and location of the sample described in terms of two different referencing systems (stationing used for the core location and in the analysis of pre- and post-storm elevation data), other descriptive information regarding sample location.

Column 2: type of sediment found in different strata (or zones, or lenses) using standard unified soil classification types. A stratum, lens or zone, is defined by the range of depth below the levee surface in which the stratum is located.

Column 3: approximate levee crest elevation in close proximity to the location of the sample.

Column 4: freeboard at the core sample location. Intermittent wave overtopping might occur for positive freeboard values; overflow and wave overtopping would occur for negative freeboard values.

Column 5: Description of the degree of erosion and levee degradation at the location of the core sample.

i. Levees Along GIWW (East of Michoud Canal)

Core log results in Table 3 for samples 42-U and 43-U show a thin 1-ft layer of lean clay, underlain by several feet of silt or sand. There was no significant erosion or levee degradation at either of these two sites. Both sample locations are along the GIWW, east of Michoud Canal and west of Pump Station OP-15, along a large stretch of levee that was undamaged. The most notable observation at both sites is the freeboard. Positive values of +1 to +1.5 ft indicate only intermittent wave overtopping and no steady overflow. Hydrodynamic loadings at both sites were not sufficient to strip the vegetation cover and erode the lean clay layer.

The reach of levee east of Pump Station OP-15 was heavily damaged. At the location of sample 44-U, just to the east of OP-15, there was a thin 1.5-ft layer of fat clay at the surface, underlain with a silty sand layer 2 ft thick, underlain by lean and fat clays down to 10 ft. The levee crest elevations at this location were much lower; freeboard was negative, -0.5 to -1 ft indicating significant overflow and wave overtopping at this location. Levees in the vicinity of this site were heavily eroded and degraded (7.5 to 8 ft of vertical erosion) and there was considerable breaching in this general region; however, at the sample site there was no significant erosion. At the sample location, the thin fat clay layer at the surface was able to resist erosion by the hydrodynamic loadings. However, the hydrodynamic regime on the back side created by overflow and wave overtopping was severe enough to erode the levee in many places in this general vicinity.

At the location of sample 45-U, near the eastern end of the levee adjacent to the GIWW, the levee was severely degraded, 7 to 7.5 ft of vertical erosion occurred, as it was in most places near this sample location. The freeboard was negative, -0.5 to -1 ft, indicating overflow and wave overtopping. The sediment was lean clay for the upper 7 ft. Here the hydrodynamic loading associated with wave overtopping and overflow was severe enough to completely erode the lean clay layer, down to the approximate elevation of the fat clay layer. Differences between levee response at this location and at sites 42-U and 43-U (all three had lean clay surface layers) show the importance of freeboard in dictating levee response.

Results for levees adjacent to the GIWW, east of Michoud Canal, suggest that the most severely degraded levees were subjected to overflow and wave overtopping associated with negative freeboard values, -0.5 to -1 ft. All samples had clay in the surface layer. Three of the four samples showed a prevalence of lean and fat clay in the upper 10 ft. Several of the sediment cores showed lenses of sand, silt, or silty sand, which would be expected to be much more erodable than clayey sediments, once the clay layer eroded.

Table 3. Sediment Properties, Freeboard and Levee Response Along the GIWW				
Sample Identifier	**Sediment Description, by layer (in feet below the levee**	**Levee Crest Elev (feet) +/- 100 ft**	**Free-board (feet) +/- 100 ft**	**Description of degradation at sample location**
42-U New Orleans East 65,400 832+00 Midway between Michoud Canal and Pump OP-15	0 to 1 lean clay 1 to 3 silt 3 to 9 lean clay	17 to 17.5	+1 to +1.5	No vertical erosion at the sample site; no vertical erosion for several hundred feet to either side of the sampling location. Generally no erosion for several thousand feet west of this site.
43-U New Orleans East 62,400 872+00 Just west of Pump Station OP-15	0 to 1 lean clay 1 to 6 sand 6 to 9 lean clay	17	+1	No vertical erosion at the sample site; no vertical erosion for several hundred feet to either side of the sampling location.
44-U New Orleans East 57,300 913+00 east of Pump Station OP-15	0 to 1.5 fat clay 1.5 to 3.5 silty sand 3.5 to 5 lean clay 5 to 10 fat clay	15 to 15.5	-0.5 to -1	No vertical erosion within 100 ft to either side of the site; but severe degradation and breaches down to elevations of +7.5 ft (7.5 to 8 ft of vertical erosion) within 200 ft on either side of the sampling location. Considerable breaching along this stretch
45-U New Orleans East 48,500 1003+00 Easternmost end of the levee adjacent to GIWW	0 to 7 lean clay 7 to 10 fat clay	15 to 15.5	-0.5 to -1	Levee significantly degraded at the site and for several hundred feet to either side; vertical erosion down to elevation 8 ft at the site and for 300 ft to either side is quite uniform (magnitude of vertical erosion equal to 7 to 7.5 ft)

One sample, 43-U, showed a very thick layer of sand in the core log. However, these more erodable lenses were not at the surface at any of the sample locations. Even levees with a lean clay layer at the surface eroded under loadings associated with negative freeboards of -0.5 to -1 ft, i.e. overflow and wave overtopping. Only a surface fat clay layer appears to have been capable of resisting erosion under the same degree of hydrodynamic loading. Levees that had positive freeboard values, +1 to +1.5 ft, which meant they were subjected to much less if any wave overtopping and no steady overflow, and which were comprised of a lean clay layer at the surface, were relatively undamaged. For those levees with lean clay at the surface, it appears as though the amount of freeboard was very important in dictating whether or not the levee experienced severe erosion and degradation. The location with fat clay at the surface was able to withstand the loading associated with a negative freeboard of -0.5 to -1.0 ft.

ii. Levees Along MRGO Reach 2

The first five samples listed in Table 4 were acquired at sites between Bayou Bienvenue and Bayou Dupre along the centerline of the levee (sample locations are shown in Figure 1 of Appendix C). The last sample was acquired from the southernmost end of the MRGO Reach 2 levee. Its location is shown in the same figure. When considering the freeboard condition along the GIWW (east of Michoud Canal) and along MRGO Reach 2, it is important to recognize that the wave contribution to overtopping was greater along MRGO Reach 2 than along the GIWW.

At the location of sample 9BU-CHBD, the levee was comprised of lean and fat clay throughout the upper 10 ft; with a 2-ft layer of lean clay at the surface, underlain by 3 ft of fat clay, 2 ft of lean clay, and 3 more feet of fat clay. The freeboard at this location was -1 to -1.5 ft; indicating substantial overflow and wave overtopping. The levee was severely degraded at this site under this hydrodynamic loading, down to elevations of 10 to 12.5 ft (vertical erosion of approximately 5 to 7 ft) and the upper lean and fat clay layers were eroded down to the lower fat clay layer.

At the location of sample 11BU-CHBD, the 2.5-ft thick surface layer was comprised of fat clay, underlain by a 1-ft layer of sand, and then by a 6.5-ft layer of lean clay. Freeboard was -1.5 to -2 ft at this site. The levee was heavily degraded at this location. Hydrodynamic loadings due to overflow and wave overtopping were even higher at his site, sufficient enough to erode the surface fat clay layer and erode the underlying sand and lean clay layers, down to elevations of 5 to 8 ft. Vertical erosion was 8 to 12 ft. The larger free-board amount implies earlier onset and therefore longer duration of wave overtopping and overflow-induced erosion.

Table 4. Sediment Properties, Freeboard and Levee Response Along MRGO Reach 2				
Sample Identifier	**Sediment Description, by layer (in feet below the levee surface)**	**Levee Crest Elev (feet) +/- 100 ft**	**Free-board (feet) +/- 100 ft**	**Degradation at sample location**
9BU-CHBD MRGO Reach 2 13,900 445+00 Approx 6,000 ft south of Bayou Bienvenue	0 to 2 lean clay 2 to 5 fat clay 5 to 7 lean clay 7 to 10 fat clay	17 to 17.5	-1 to -1.5	Levee significantly degraded at this site and for several hundred feet to either side; at the site vertical erosion down to elevations of +10 to +12 ft (vertical erosion of 5 to 7.5 ft). Levee severely degraded throughout the region.
11BU-CHBD MRGO Reach 2 20,500 509+00 Approx 13,000 ft south of Bayou Bienvenue	0 to 2.5 fat clay 2.5 to 3.5 sand 3.5 to 10 lean clay	16.5 to 17	-1.5 to -2	Levee significantly degraded at this site and for several hundred feet to either side; vertical erosion at the site down to elevations ranging from +5 to +8 (vertical erosion of 8 to 12 ft). Levee severely degraded throughout the region.
12BU-CHBD MRGO Reach 2 26,400 570+00 Approx 19,000 ft south of Bayou Bienvenue; midway between Bayou Bienvenue and Bayou Dupre	0 to 1.5 lean clay 1.5 to 6 fat clay 6 to 7 lean clay 7 to 10 fat clay	16	-2.5	Levee degraded at this site; vertical erosion down to elevations ranging from +7.5 to +10 (vertical erosion of 6 to 8 ft). Levee degraded intermittently to the north; extensively to the south.

Table 4 (continued). Sediment Properties, Freeboard and Levee Response Along MRGO Reach 2				
Sample Identifier	**Sediment Description, by layer (in feet below the levee surface)**	**Levee Crest Elev (feet) +/- 100 ft**	**Free-board (feet) +/- 100 ft**	**Degradation at sample location**
18-UBD MRGO Reach 2 29,200 596+00 Approx 13,000 ft north of Bayou Dupre	0 to 6 silty sand 6 to 7.5 fat clay 7.5 to 9 silt and silty sand	14 to 15.5	-3 to -4.5	Levee degraded at this site; vertical erosion down to elevations ranging from +7 to +11.5 (vertical erosion of 4 to 7.5 ft). Widespread erosion and degradation to the south with vertical erosion of 7 to 8 ft, and intermittent breaching to the north with vertical erosion of 6 to 8 ft.
13BU-CHBD MRGO Reach 2 32,200 614+00 Approx 10,000 ft north of Bayou Dupre	0 to 10 fat clay	15 to 15.5	- 3 to -3.5	No severe vertical erosion or breaching for several hundred feet to either side. Extensive severe degradation further north; intermittent breaching further to the south.
10-CUI MRGO Reach 2 70,000 989+00 MRGO Reach 2 southernmost end just south of sheet pile wall.	0 to 10 fat clay	18.5	0 (+0.5*)	No vertical erosion at the sample site; no vertical erosion for several hundred feet to either side. No vertical erosion for several thousand feet to the south; wall located to the north. *This site was located at the very southeastern end of the levee. This site had a positive freeboard due to a lower maximum water level at this location (18 ft compared to 18.5 ft at other sites).

At the location of sample 12BU-CHBD, the sediment was comprised entirely of lean and fat clay in the upper 10 ft, a 1.5-ft think surface layer of lean clay underlain by 4.5 ft of fat clay, a 1 ft of lean clay, and 3 more feet of fat clay. The freeboard at this location was -2.5 ft, so hydrodynamic loadings were severe and lasted for longer durations. The levee was heavily degraded, and eroded down to elevations of 7.5 to 10.5 ft; vertical erosion was 6 to 8 ft. The surface lean clay layer was insufficient to resist erosion under these loadings; and as degradation increased and the hydrodynamic loadings increased, even the thicker underlying fat clay layer was eroded.

At the location of sample 18-UBD, the freeboard was -3 to -4.5 ft, indicating a very long duration and high magnitude of overflow and wave overtopping, and the greatest hydrodynamic loadings on any levee location along this stretch of MRGO Reach 2 where core samples were collected. The levee was heavily degraded at this location. At this site sediments in the upper 6 ft were silty sand, which is more erodable than clay, underlain by 1.5 ft of fat clay, and then by 1.5 ft of more erodable silt and silty sand. The levee was eroded to elevations of 7 to 11 ft. Vertical erosion was 4 to 7.5 ft at the sample site. Vertical erosion extended down to about the location of the underlying fat clay layer.

At the location of sample 13BU-CHBD, the entire upper 10 ft of the levee is comprised of fat clay. Freeboard at this location is -3 to -3.5 ft, representing severe hydrodynamic loadings. However, there was no vertical erosion at the site, suggesting that the fat clay at this location was able to withstand the severe persistent hydrodynamic loading. The fat clay and grass cover at this location was more resistant to erosion than fat clay at site 11BU-CHBD, where the fat clay was severely eroded under less severe hydrodynamic loading. This indicates that traditional soil classification type alone can not reliably distinguish between erodable and non-erodable sediments

At the location of sample 10-CUI, the upper 10 ft of the levee was comprised entirely of fat clay. No vertical erosion occurred at this location, for several hundred feet to either side, and for several thousand feet to the south. At this site a freeboard value of +0.5 ft indicates less severe hydrodynamic loading, associated with wave overtopping only. The presence of fat clay at the surface also was a likely factor in explaining the lack of erosion.

Several of the core logs showed strata of sand or silt and silty sand, but most cores were comprised mainly of lean and/or fat clay throughout the upper 10 ft, with the exception of core 18-UBD. This core showed a significant lens of silty sand from the surface down to a depth of 6 ft. Silty sand is likely to be more erodable than lean or fat clay. The levee at this location was heavily eroded. At this site, erosion appears to have occurred down to a fat clay layer 6 to 7.5 ft beneath the surface.

Any site with sediment classified as something other than fat clay at the surface and subjected to negative freeboard conditions, experienced severe erosion and degradation. Generally, the levee eroded for more negative freeboard conditions, except at 13BU-CHBD where the grass cover and fat clay at that site resisted erosion. The lack

of vertical erosion at sample location 13BU-CHBD, despite having severe hydrodynamic loading, illustrates the importance of in-situ sediment properties other than simple soil classification type. Once the levee degraded, and hydrodynamic loading increased, even fat clay layers several feet beneath the surface eroded at several locations.

iii. Summary

Cores indicated that the levee along these two reaches was primarily comprised of lean and fat clays in the upper 10 ft. Some cores indicated lenses of silt, sand or silty sand.

All but one core showed lean or fat clay at the levee surface. The exception, one core along MRGO Reach 2, showed a very think 6-ft lens of silty sand at the surface.

Results indicate that freeboard, the difference between maximum mean water surface elevation and levee crest elevation, is an important parameter in levee response.

Sites with lean or fat clay sediment at the levee surface and positive freeboard conditions did not erode.

Negative freeboard values less than -0.5 ft were prevalent along the GIWW (east of Michoud Canal) and MRGO Reach 2 levees. This level of hydrodynamic loading was clearly capable of eroding all types of sediment except the most erosion resistant of the fat clays.

Once erosion and vertical degradation began, even fat clays were often eroded by the increased hydrodynamic loading. The presence of fat clay appeared to limit vertical erosion at some locations.

In general, fat clays were less erodable than other sediment types.
However, mixed results for fat clay (erosion in some cases and not in others) illustrate the inadequacy of soil classification type alone as an indicator of sediment erodability.

d. Erodability -Results from ILIT Flume Tests

i. Applicability of the EFA Erosion Flume

The most appropriate way to examine and quantify erodability of fine-grained mixed sediments is to conduct experiments, ideally at full scale, on undisturbed sediment samples where the in-situ density structure of the sample is preserved to the greatest extent possible. Hydrodynamic loading must reflect the type of loading that is to be experienced in the field.

The EFA erosion flume used by the ILIT did not simulate the highly erosive turbulence and vortices caused by breaking waves, up rushing and down rushing wave bores in the swash zone, or by cascading water that falls over the edges of steep head-cuts

which were prevalent along the levees during their degradation. On the front side of the MRGO Reach 2 and GIWW levees east of Michoud Canal, within the surf zone on the levee front face, the velocity regime would have been characterized by a mean offshore-directed undertow velocity directed downslope along the levee, superimposed with an unsteady wave orbital velocity component that would have been in the same direction as the undertow (offshore) during a portion of each incident wave cycle and in the opposite direction (shoreward) during the other portion of the wave cycle. The inner swash zone would have been incredibly complex, chaotic and turbulent, with down rushing wave bores constantly colliding with up rushing wave bores. The steady unidirectional fluid motion regime created within the EFA flume was not at all like the unsteady bi-directional wave-dominated regime (with fluid accelerations and breaking-induced turbulence) that was experienced on the front side of the levee along MRGO Reach 2. The steady hydrodynamic regime created in the EFA flume was unlike the intermittent unsteady wave overtopping or the combined action of pulsating and accelerating overflow created on the back side of the levee by overtopping waves. The erodability results obtained with the EFA flume are not so useful for examining erosion and degradation along the MRGO Reach 2 levee.

The flow regime that is created in the EFA erosion flume is somewhat more applicable to flow down the back side of a levee under steady overflow, with little or no wave action present. For this reason results from the flume tests are discussed here. However, even on the back side, applicability is limited because of the highly turbulent erosive environment that is created once the back side begins to erode. This is not simulated in the EFA erosion flume.

ii. Sample Collection, Preparation and Testing Methods

Tests were performed on sediment samples acquired at locations shown in Figure 41 (ILIT Figure 9.36). Figure 42 (ILIT Table 9.10) shows a table summarizing properties of sediment samples tested by the ILIT (2006), which were derived using traditional soil testing methods. Figure 43 shows gross erosion rate results from all the tests which the ILIT team performed and reported (ILIT Figure 9.41).

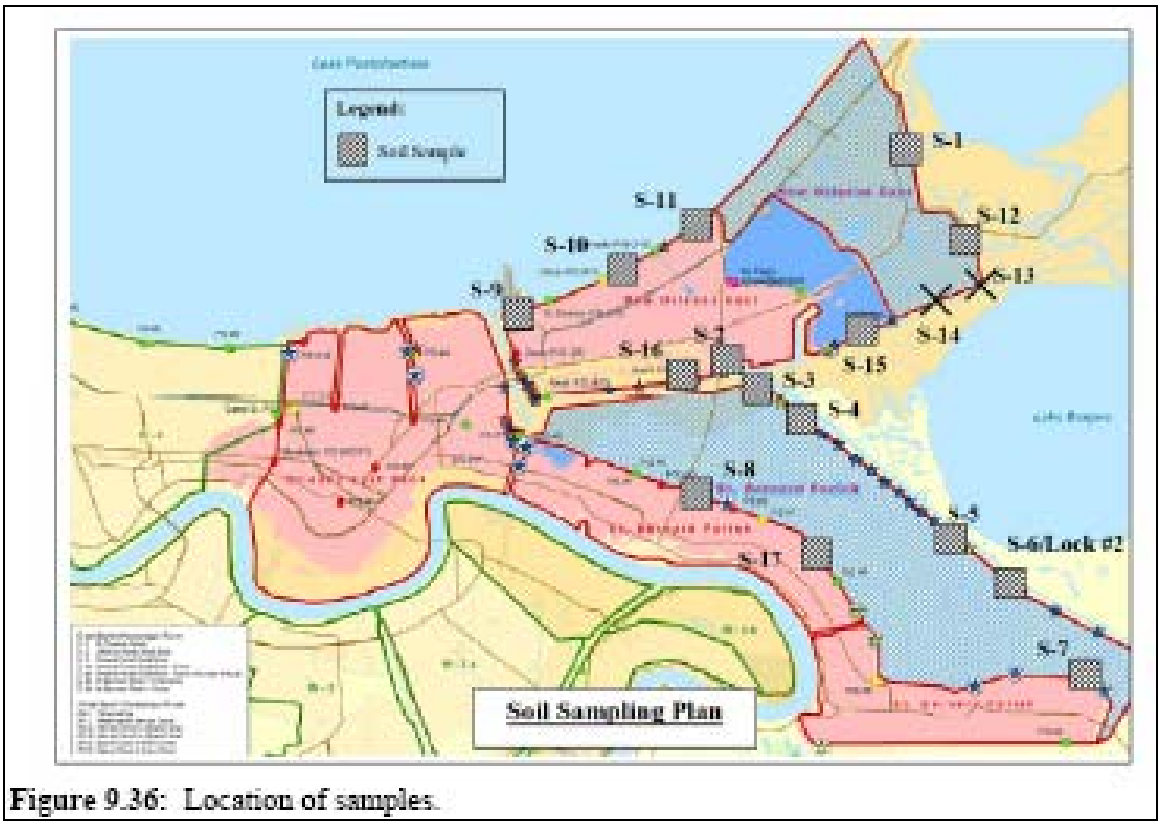


Figure 9.36: Location of samples.

Figure 41. Location of samples (ILIT 2006, Figure 9-36)

The erosion flume was used to develop relationships between imposed shear stress (or shear velocity) and the rate at which sediment was eroded from the surface of a sediment core. A sediment core is pushed upward by the flume operator, through the bottom of the flume and into contact with the flow field, while the flume is re-circulating water. The operator attempts to push the core into the flow field at a rate that is equal to that at which the imposed fluid velocity erodes the sediment surface. This must be done very carefully; it is a highly subjective process based entirely on visual observation and judgment. The quality of results obtained from these tests is extremely dependent upon the operator's skill. In light of the potential for error, repeatability testing is recommended as a standard component of any erosion testing using this type of flume. Velocity and shear stress are estimated from the rate at which water is circulated through the piping system of the flume.

Gross erosion rate is measured in the EFA flume. While results obtained from flume experiments of this type are useful for examining gross sediment erodability; gross erosion rates, alone, are not necessarily very useful for an accurate quantitative assessment of levee erosion or degradation, i.e. morphology change. Erosion rates measured with the flume only provide information on the rate at which sediment is eroded from the sediment surface as a function of imposed velocity or shear stress. Erosion and degradation of a levee or any other sediment feature also is dictated by a number of important processes, including: spatial gradients in sediment transport rates; the difference between what is being transported into and out of a sediment control

volume through sheet flow, bed load and suspended load; the rate at which sediment is being eroded and entrained locally (this is the rate which the erosion flume provides); the rate at which sediment is being deposited; and processes such as armoring of the sediment surface due to local sorting and sediment influxes. All these other processes must be considered in any attempt to properly model the highly complex process of levee erosion and degradation. These processes are <u>not</u> reflected in the gross erosion rates measured in this type of erosion flume. The modeling of erosion described in the Declaration and Technical Report by Robert Bea (Bea 2008, Bea and Storesund, 2008) does not account for these other physical processes. A review of the erosion modeling work by Bea is in Appendix D.

Sample	Soil Description	Classification	γ_t (kN/m3)	γ_{dry} (kN/m3)	w (%)	Tested at Texas A&M University					Tests Performed by STE			
						% fines	LL	PL	PI	Organic Content%	% fines	LL	PL	PI
S1-B1-(0-2ft)-TW	Clay with hard clay grain mixture	CH	20.23	15.37	31.66	-	71	25	46	3.09	89.9	65	22	43
S1-B1-(2-4ft)-SW	Clay with rootlets	CH	19.10	15.69	21.77	-	56	19	37	1.91				
S2-B1-(0-2ft)-TW	Clay with rootlets	CL	19.74	17.00	16.11	-	46	17	29	16.94	67.2	49	17	32
S2-B1-(2-4ft)-SW	Clay	CL	20.26	16.71	21.23	69.1	41	16	25	1.62				
S3-B1-(2-4ft)-SW	Clay	CL-CH	17.60	13.86	27.00	-	48	17	31	2.50	90.3	54	19	35
S3-B2-(0-2ft)-SW	Clay with some sand	CH	20.20	17.26	31.66	-	69	23	46	-				
S3-B3-(0-1ft)-SW	Clay	CL-CH	17.16	13.95	23.00	-	32	12	20	2.60				
S4-(0-0.5ft)-LC-SW	Clat with some sand	CL	13.87	10.42	33.14	90.5	60	30	30	8.16	-	-	-	-
S4-(0-0.5ft)-HC-SW	Clay with some sand		17.69	13.23	33.14									
S5-(0-0.5ft)-LT-SW	Silt-Clay		21.85	18.15	20.40	54.4	-	-	-	0.69	-	-	-	-
S6-(0-0.5ft)-LC-SW	Sand w/Some Clay	SP	13.45	12.79	5.21	8.9	-	-	-	0.71				
S7-B1-(0-2ft)-TW	Clay	CH	17.39	13.73	26.65	-	68	24	44	3.78	90.1	78	32	46
S7-B1-(2-4ft)-SW	Clay with hard clay grain mixture	CH	16.52	13.42	23.04	-	-	-	-	7.14				
S8-B1-(0-2ft)-TW	Clay with 1.5" thick grass on top of sample	CH	17.71	13.38	32.34	-	-	-	-	-	97.3	85	36	49
S8-B1-(2-4ft)-L1-SW	Clay with 2 layers	CH	18.74	14.00	33.87	-	-	-	-	2.28				
S8-B1-(2-4ft)-L2-SW	Clay with 2 layers	CH	18.74	14.00	33.87	-	54	21	33	15.37				
S11-(0-0.5ft)-LC-TW	Sand	SP	12.30	12.23	1.02	0.1	-	-	-	0.32	-	-	-	-
S11-(0-0.5ft)-HC-TW	Sand	SP	13.26	13.12	1.02		-	-	-	0.35				
S12-B1-(0-2ft)-TW	Clay with decomposed wood	CH	14.77	10.19	44.94	-	67	27	40	16.91	92	67	21	46
S12-B1-(2-4ft)-SW	Clay	MH-CH	17.56	12.64	38.94	-	58	32	26	5.28				
S15-CanalSide-(0-0.5ft)-LC-SW	Sand w/Some Clay	SM	13.85	12.21	13.43	29.9	-	-	-	1.28	-	-	-	-
S15-CanalSide-(0-0.5ft)-HC-SW	Sand w/some clay		19.63	17.31	13.43		-	-	-					
S15-LeveeCrown-(0-0.5ft)-LT-SW	Sand w/Some Clay		13.29	11.94	11.29		-	-	-	2.16				
S15-LeveeCrown-(0.5-1ft)-LT-SW	Sand w/Some Clay		13.57	12.46	8.93		-	-	-	1.01				

Figure 42. Results of the soil index property tests (ILIT 2006, Table 9.10)

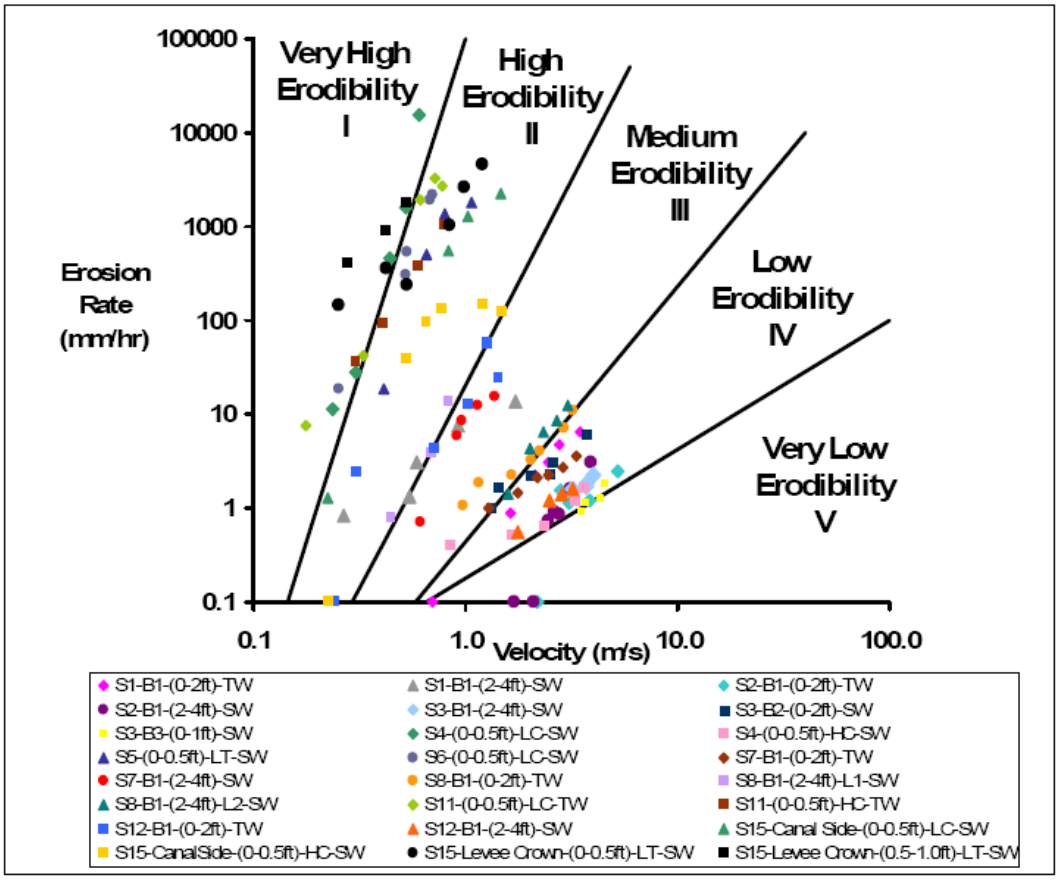


Figure 43. Erosion rate versus velocity results for each sample (ILIT 2006, Figure 9-41)

In light of the need to consider all these other processes, and in light of our lack of knowledge concerning mixed sediment erosion and deposition in response to combined current-wave action on sloping vegetated surfaces, it is not surprising that there are no models presently available which can reliably model erosion of vegetated earthen levees subjected to wave action and combined wave overtopping-steady overflow. At the present time, research progress in this area is being made through the use of field testing and data collection and large-scale laboratory testing, including erosion flumes that can simulate oscillatory flow regimes, such as the work of Seijffert and Verheij (1998) which is discussed later.

In addition to severe limitations associated with applicability of the EFA flume to examine the fluid regime that existed along the key degraded levees, there are severe limitations associated with the sediment sampling and testing procedure that was adopted by the ILIT. These limitations are quite severe, and render test results based on certain samples collected along the degraded levees to be of no use for making reliable erosion predictions. The text in italics below is taken from the ILIT (2006) report; it describes the sediment sampling program and the process used to prepare samples for testing in the flume.

"A total of 11 locations were identified for studying the erosion resistance of the levee soils. Emphasis was placed on levees which were very likely overtopped. These locations are labeled S1 through S15 for Site 1 through Site 15 on Figure 9.36. The samples were taken by pushing a Shelby tube when possible or using a shovel to retrieve soil samples into a plastic bag. For example at Site S1, the drilling rig was driven on top of the levee, stopped at the location of Site 1, a first Shelby tube was pushed with the drilling rig from 0 to 2 ft depth and then a second Shelby tube was pushed from 2 to 4 ft depth in the same hole. These two Shelby tubes belonged to boring B1. The drilling rig advanced a few feet and a second location B2 at Site S1 was chosen; then two more Shelby tubes were collected in the same way as for B1. This process at Site S1 generated 4 Shelby tube samples designated:

- *S1-B1-(0-2ft)*
- *S1-B1-(2-4ft)*
- *S1-B2-(0-2ft)*
- *S1-B2-(2-4ft)*

Four such Shelby tubes were collected from sites S1, S2, S3, S7, S8, and S12. In a number of cases, Shelby tube samples could not be obtained because access for the drilling rig was not possible (e.g., access by light boat for the MRGO levee) or pushing a Shelby tube did not yield any sample (clean sands). In these cases, grab samples were collected by using a shovel and filling a plastic bag. The number of bags collected varied from 1 to 4. Plastic bag samples were collected from sites S4, S5, S6, S11, and S15. The total number of sites sampled for erosion testing was therefore 11. These 11 sites generated a total of 23 samples. One of the samples, S8-B1-(2-4ft), exhibited two distinct layers during the EFA tests and therefore lead to two EFA curves. All in all 24 EFA curves were obtained from these 23 samples: 14 performed on Shelby tube samples and 10 on bag samples.

No special sample preparation was necessary for the samples which were in Shelby tubes. The Shelby tube was simply inserted in the hole on the bottom side of the rectangular cross section pipe of the EFA (described previously). For bag samples obtained by using a shovel to collect the soil, there was a need to reconstruct the sample. These samples were prepared by re-compacting the soil in the Shelby tube (Figure 9.37). The same process as the one used to prepare a sample for a Proctor compaction test was used. Since it was not known what the compaction level was in the field, two extreme levels of compaction energy were used to re-compact the samples. The goal was to bracket the erosion response of the intact soil.

For the high compaction effort (100% of Modified Proctor compaction effort), the sample was compacted in an 18-inch long Shelby tube as follows:
1) The total sample height was 6 inches. The sample was compacted in eight layers.
2) To form each layer, the soil was poured into the Shelby tube from a height of 1 inch above the top of the tube.

3) The soil was compacted using a 10 lb hammer (Modified Proctor hammer) with a drop height of 1.5 feet. Each layer was compacted by 8 hammer blows, i.e. 8 blows/layer.
4) This process was repeated until a 6 inch sample was obtained.
5) The corresponding compaction energy was equal to the Standard Modified Proctor Compaction energy.

For the low compaction effort (1.63% of Modified Proctor compaction effort), the sample was compacted in an 18-inch long Shelby tube as follows:
1) The total sample height was 6 inches. The sample was compacted in eight layers.
2) To form each layer, the soil was poured into the Shelby tube from a height of 1 inch above the top of the tube.
3) The soil was compacted using a 10 lb hammer (Modified Proctor hammer) with a drop height of 1 inch. Each layer was compacted by 3 hammer blows, i.e. 3 blows/layer.
4) This process was repeated until a 6 inch sample was obtained.
5) The corresponding compaction energy was 1.63% of the Standard Modified Proctor Compaction energy.

Figure 9.41 shows the erosion chart populated with the EFA results for all 24 EFA tests. The legend contains the sample/test designation which starts with the site number (Figure 9.36), followed by the boring number, the depth, and letter symbols including SW, TW, LC, HC, and LT. SW stands for Sea Water and means that the water used in the EFA test was salt water at a salinity of approximately 35000 ppm. TW stands for Tap Water and means that the water used in the EFA test was Tap Water at a salinity of approximately 500 ppm. LC stands for Low Compaction, refers to bag samples only, and means that the sample was prepared using 1.63% of Modified Proctor compaction effort. HC stands for High Compaction, refers to bag samples only, and means that the sample was prepared using 100% of Modified Proctor compaction effort. LT stands for Light Tamping and refers to the preparation of some bag samples used in some early tests; it is very similar to the LC preparation."

Collection of samples using sediment coring is recommended practice for erosion testing of fine-grained and mixed sediments. It is extremely important to collect samples in a way that minimizes disturbance to the sediment, i.e., maximizes the preservation of in situ density structure because of its importance in determining erodability. Sediment coring is the most reliable method for doing so. Erosion results derived from tests on the samples collected in the Shelby-tubes likely had the best chance for yielding reliable erodability results. Handling and transporting of cores also must be done carefully to minimize disturbance to the samples. We have found in our experiences with testing using our erosion flumes of this type that disturbance to a sediment core (handling it roughly, storing it other than in a vertical position, allowing unnatural drying and cracking) can compromise the natural properties of the sediment sample, in terms of its resistance to erosion, and lead to erroneous test results. Minimal disturbance of the

samples is essential to maximize accuracy of the erosion tests. Few details were provided regarding transportation and handling of the sediment cores.

Erosion results for samples that were collected using a shovel, transported to the laboratory, reconstituted, and then artificially compacted, are of no use in conducting a definitive, quantitative, and accurate assessment of actual erodability of intact sediments. The actual in situ density structure, a crucial sediment property, was completely lost in this process. It is unclear if the shoveled samples were dug from undisturbed sections of the levee or shoveled from depositional features. Cohesive and mixed sediments that were eroded, i.e. had physical and chemical bonds broken during the erosion and transporting process, will not have the same properties as they had as in situ sediments. The sampling location and manner of sample acquisition strongly influence the characteristics of the size distribution and properties of sediment contained in the sample. Few details from field notes about each collection site, lack of photos from the actual sample extraction sites, and lack of detail about the sample extraction procedure were included in the ILIT (2006) report.

Unfortunately, all the samples collected at the most heavily degraded levees (S-15, S-4, S-5, S-6) were collected with shovel, and then reconstituted and re-compacted back in the laboratory. The natural level of compaction, i.e. density, for these samples was completely lost. The authors of Chapter 9 of ILIT (2006) acknowledge the limitations of using the reconstituted samples and artificial compaction process. The authors admit that they do not know what the compaction level was for the in situ sediments from the field, in their intact natural state:

> *"Since it was not known what the compaction level was in the field, two extreme levels of compaction energy were used to re-compact the samples. The goal was to bracket the erosion response of the intact soil."*

The ILIT investigators applied two "*extreme*" and artificial levels of compaction to reconstituted samples, in light of their inability to acquire undisturbed core samples. Clearly, the intent of ILIT was to apply extreme low compaction and extreme high compaction to bracket the results, as they state, assuming that the natural level of compaction would fall somewhere between the two extremes. The ILIT authors intended the two degrees of compaction to reflect extreme under- and over-compaction, with the expectation that the actual compaction/density would fall somewhere between the two extremes.

The degree considered by the authors to be an extreme high level of compaction was 100% of the compaction achieved using the Modified Proctor method. The Modified Proctor compaction method is thought to replicate the degree of compaction achieved by heavy compaction equipment in the field. The level of compaction used to form and shape the hurricane protection system levees might not have been as great as that achieved with the Modified Proctor level of compaction. For the extreme low degree of compaction, 1.63% of the compaction achieved using the Modified Proctor compaction

test was imposed on the samples, a factor of 60 less than the upper limit. This is an extremely low level of compaction.

The authors also describe an un-quantified level of compaction called “light tamping” which they stated was similar to the level of compaction achieved with 1.63% of the Modified Proctor method, the extreme lower limit; although the similarity is based on subjective judgment only and nothing quantitative. It appears as though the authors might have initiated testing with an uncontrolled compaction process and then changed to a more structured, systematic compaction approach using the two extreme limits, which is a more quantitative and reproducible approach. The use of “light tamping” versus a more controlled level of compaction also increases the uncertainty in, and diminishes the usefulness of, results from samples for which this rather arbitrary compaction method was applied.

The ILIT authors specifically recommend using results from erosion tests for both extreme levels of compaction to bracket the true estimate of erodability for the intact sediments, which makes sense. However, in the tests done, both extreme levels of compaction were only applied to two of the reconstituted samples (S-4 and S-15) in the areas of primary interest, and not to samples S-5 or S-6. See Figure 44 below (ILIT Figure 9.42) for results from samples tested with both levels of compaction.

Considering that both compaction levels were applied to reconstituted samples from only one of the sample sites along MRGO Reach 2, and not for the others, a bias is created toward the extreme low compaction testing and will be reflected in any subsequent analysis. Any quantitative analysis and interpretation that is done can only have meaning when done along with a similar analysis and interpretation using results for both levels of compaction.

Quite a few of the sediment samples collected along the levees were collected within the uppermost 0.5 ft of the levee surface. The great majority of samples were collected within the upper 2 feet; and all were collected within 4 ft of the surface. In general, sediment deeper into the levee is expected to more compacted and denser, and less erodable, than sediment near the surface, due to the added weight of sediment above it. The levees were 15 to 19 ft high, and in many cases the levees experienced 5 to 10 ft of vertical erosion. Use of only surface samples in the testing also will likely bias test results, and it precludes accurately assessing any decrease in erodability with depth below the surface, which is often the case with fine-grained sediments.

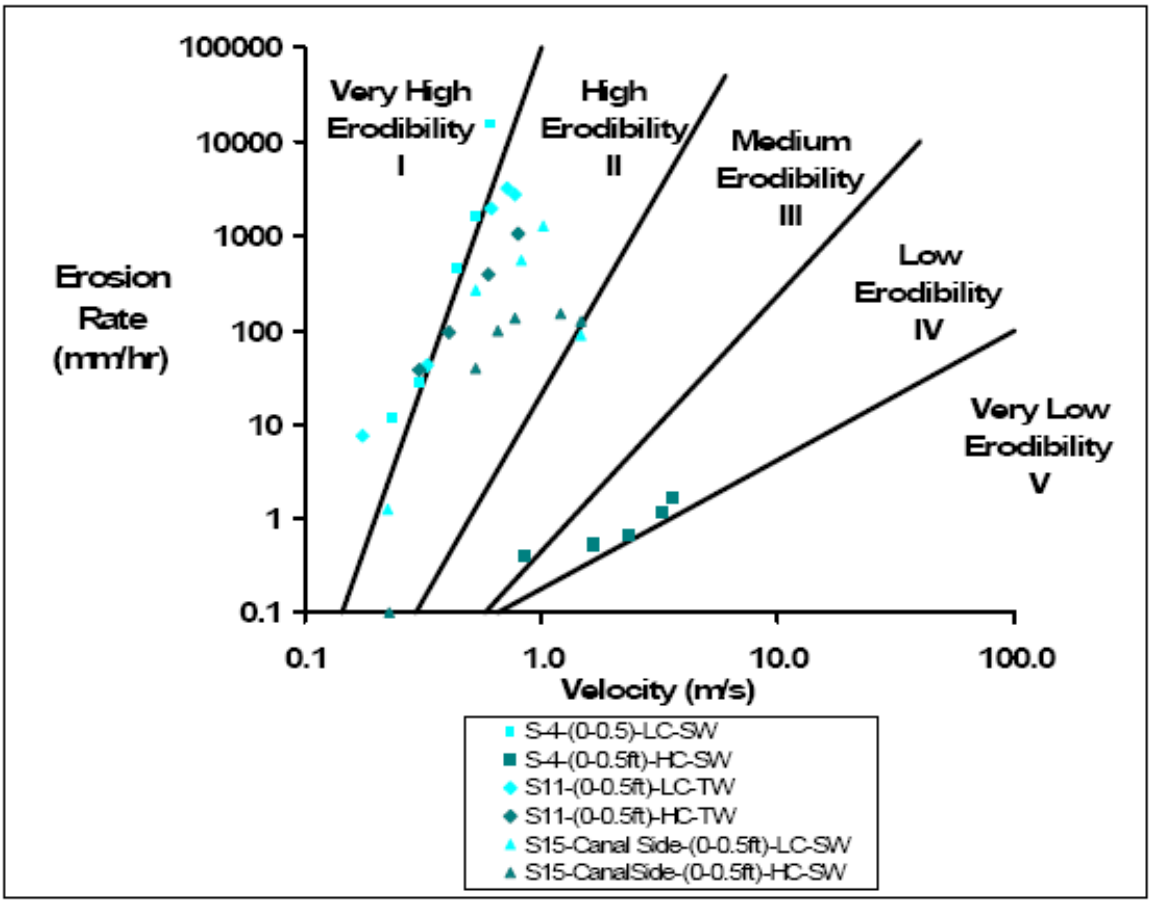


Figure 44. Influence of compaction on erodability (ILIT 2006, Figure 9.42)

iii. Results for Sample S-4

Sample S-4, described as clay-with-sand, lean clay, was collected from the levee along MRGO Reach 2, just south of Bayou Bienvenue. It was one of the samples for which both extreme levels of compaction were considered in the testing. Erodability results for the two states of compaction varied dramatically, which is not surprising for a sample comprised primarily of clay and fines (90%) that is subjected to vastly different degrees of compaction. The gross erosion rate data from the flume test for extreme high compaction indicate vertical erosion rates of between 1 and 2 mm/hr for velocities of approximately 3 to 4 m/sec. This is a very low value of erodability. For extreme low compaction, the trend in data points suggests a gross erosion rate that approaches 100,000 mm/hr (100 m/hr) for an imposed steady velocity of only 1 m/sec. These are extremely high rates of vertical erosion indicative of very soft sediments, unrealistically high. They are reflective of the extreme degree of under-compaction that was applied to the reconstituted sample. As is discussed earlier, computed average velocities reached 4 m/sec (13 ft/sec) and higher on the levee back side. Extrapolating the erosion rate data trend to higher velocity would yield even higher erosion values, ridiculously high values that are not reasonable. These unrealistic high values of erodability have severe

implications on the accuracy of any methods to predict levee response, if they are used for this purpose.

The gross erosion rates for the two states of extreme compaction differ by a factor of 100,000 for the two extreme compaction states. This is a very large difference, 5 orders of magnitude, i.e., completely different responses. With such a wide range of variability, accurately estimating erosion rates associated with the in-situ level of compaction and density is extremely uncertain. The very large difference renders results for the S-4 samples to be of no practical use as a measure of in situ sediment erodability. It also supports reasons cited previously why reconstituting and artificially compacting sediments is not good practice for erosion tests involving fine-grained and mixed sediments.

Because of bonds between small clay particles and other particles, cohesive sediments often erode in aggregates, or chunks, removed from the surface as fissures or cracks develop in the sediment surface under hydrodynamic loading. These types of aggregates are visible on the right hand side of the Figure 45 (from Bea 2008), which was collected near the location of sample S-4. The sample at S-4 was comprised of a high percentage of clay. Clays are very small particles. If the sample collected in the field is decimated into small clay particles prior to testing, bonds between particles are broken, and then the fine particles are subjected to currents in the erosion flume with light compaction they will be easily and rapidly eroded, behaving like very soft clay. This appears to have been the case in the testing done by the ILIT. When the samples were highly compacted and denser, they were much more highly resistant to erosion. Erosion of aggregates is generally a highly nonlinear process. Therefore it is absolutely critical to test using undisturbed samples, in order to preserve the natural properties and bonds between cohesive particles.

iv. Results for Samples S-5 and S-6

Samples S-5 and S-6 also were collected from the levee along MRGO Reach 2, in the general vicinity of Bayou Dupre. Levees in this general region were also heavily damaged. Sample S-5 was described as silt with clay (54% fines) subjected to light tamping in the sediment reconstitution process. Sample S-6 was described as sand with some clay (9% fines) subjected to extreme low compaction. Both samples were collected in the 0- to 0.5-ft depth-below-surface range. For a steady velocity of 1 m/sec, the gross erosion rate for Sample S-5 was about 1000 mm/hr (1m/hr). For Sample S-6, gross erosion rates at a velocity of 1 m/sec were about an order of magnitude higher, about 10,000 mm/hr (10 m/hr). Extreme high-compaction samples were apparently not analyzed at sites S-5 and S-6, severely limiting the usefulness of these results for estimating what the erosion rates might have been for the intact sediments.

Both the S-5 and S-6 samples only represent the upper 0.5 ft of the levee sediment column; therefore, no information about how erodability varied with depth is available at these two sites.



Figure 30: Close up photograph of soils on shoulder of breach on MR-GO EBSB at station 497+00 showing dredge spoil materials used in construction of the levee (Bea 2005). Bulk samples were taken of the soils from this breach shoulder and tested in the laboratory to determine the EBSB scour – erosion characteristics used in this study (Bea 2005).

Figure 45. Photograph showing cohesive sediment aggregates at bottom right of the photos (from Bea Declaration)

v. Results for Sample S-15

Four sediment samples were analyzed for site S-15, which was collected between the Michoud Canal and Pump Station OP-15, along the GIWW. Two samples were collected on the levee crown at site S-15, reconstituted in the laboratory, lightly tamped to an unspecified level, and then analyzed. Both samples are expected to be under-compacted (relative to what would have been the case for intact samples) based on the information provided about light tamping and its relation to the extreme low compaction method. One sample was collected in the 0-0.5 ft depth-below-surface range, and the other in the 0.5 to 1 ft range. The shallow depth of both samples precludes any information about erodability all through the levee, with depth below the initial surface. Both samples were classified as sand with some clay and with percent fines of 30%). Both show gross erosion rates of about 1000 mm/hr (1 m/hr) for a steady velocity of 1 m/sec.

Two samples collected at S-15 were from the waterway, or canal, side of the levee. These were compacted using both the extreme low and high levels. Results for the low-compacted canal-side sample are similar to those for the lightly tamped crown sample, gross erosion rates of about 1000 mm/hr (1 m/hr) at a steady velocity of 1 m/sec. Erosion rates for the extreme high compaction sample (values of approximately 0.1 m/hr

for current speed of 1 m/sec) were about an order of magnitude less than those for the extreme low compaction sample. It makes sense that the range of erosion rates, as a function of compaction state, for this sample is less than the range of results for sample S-4. The S-15 samples have a large percentage of sand. Density of sand is less subject to changes in compaction than sediment comprised primarily of clay and other fines. However, even a factor of 10 is considerable when considering the potential difference in levee erosion predictions that correspond to the two sets of results.

A trend toward an upper limit on the erosion rate for the extreme high-compaction sample is evident, a limit of about 100 mm/hr (0.1 m/hr). The presence of an upper erosion rate limit for the high-compaction sample is contrasted with results for the low-compaction sample where no upper limit was evident. This limit has great implications in assessing levee erodability at velocities higher than 1 m/sec, which would have been the case during much of the storm. Maximum velocities tested for these two samples were approximately 1 m/sec. The wide range of erodability results associated with the two degrees of compaction, and the presence of an upper limit for one level and not the other level, adds considerable uncertainty concerning actual erodability of the intact sediments at this site. Note that no severe levee degradation occurred at this site, a fact probably more related to hydrodynamic loading conditions (positive freeboard conditions) and not sediment properties.

The S-15 samples only represent the upper 0.5 ft or 1 ft of the levee sediment column; therefore, no information about how erodability varies with depth are available at this site.

vi. Results from Sample S-3

Three samples from site S-3 were collected in Shelby tubes, minimizing any adverse impacts on the in situ sediment characteristics. One sample was collected from boring site B1 in the depth zone of 2 to 4 ft and it was described as clay (classified as lean clay-fat clay). A second sample was collected from boring site B2 in the depth range of 0 to 2 ft and it was described as clay with some sand (classified as fat clay). A third sample was collected from boring B3 in the depth range of 0 to 1 ft and it was described as clay (classified as lean clay-fat clay). All samples were defined to have 90% fines; other properties varied (see Figure 42). All three samples were tested with salt water.

For Sample S3-B3-(0-1 ft), gross erosion rates were less than approximately 1 mm/hr (0.001 m/hr) for the range of velocities tested, up to several meters per second. Results indicate that surface sediments at this site were highly resistant to erosion. For the other surface sample, S3-B2-(0-2 ft), sediments are several times more erodable. Results for Sample S3-B3-(2-4 ft) also show these sediments to be highly resistant to erosion, with peak erosion rates of approximately 1 mm/hr for the range of velocities tested. All sediments at site S-3 (classified as either fat clay or lean clay-fat clay) were quite resistant to erosion. Results suggest that there is spatial variability in sediment characteristics and erodability, both horizontally and vertically within the levee at this site.

vii. Summary

The EFA flume used by the ILIT team is not suitable for replicating the oscillatory, unsteady, highly turbulent hydrodynamic regime that existing on both the front and back sides of levees along GIWW (east of Michoud Canal) and the MRGO Reach 2 levee.

The EFA flume provides estimates of gross erosion rates. However, gross erosion rates, alone, cannot be reliably used directly in estimates of levee erosion and degradation. They only tell part of the story. Many other important processes and factors must be considered.

Results from samples that were collected in Shelby tubes (which minimizes disturbance and maximizes retention of intact sediment properties) are much more reliable than results from the samples acquired by shovel, reconstituted, and then subjected to extreme levels of compaction (high and low).

Results of the erodability tests performed on the reconstituted samples subjected to artificial compaction are of practical no use. The degree of actual compaction in the intact sediments was lost in the sample acquisition and preparation process, so there is great uncertainty concerning the actual level of compaction (and therefore density and erodability) for the intact, in-situ sediments. These properties can not be reliably estimated using reconstituted samples.

Extremely large differences (several orders of magnitude) between erosion rates for the extreme low and extreme high compaction states render test results, analyses, and interpretation based on the results highly subjective and very uncertain.

Unbiased analysis must consider results for both the extreme low- and extreme high-compacted samples. Failure to do so will bias analysis and interpretation of results, and conclusions drawn based on the analysis.

Collection of samples only within the upper 4 ft of the levee sediment column (many samples collected in the top 1 ft only) biases test results to surface erodability and provides limited or no information on variation of erodability with depth well into the levee.

Lack of repeatability testing lessens confidence in the ILIT results.

e. Influence of Placement Method on Erodability

Several levee reaches in the region were relatively undamaged by Katrina. The south-facing levee of the St. Bernard polder was constructed with a clay cap over a sand core and the levees along the GIWW/MRGO Reach 1 were constructed with clayey soils trucked in from off-site borrow sources (IPET, 2007). Both of these reaches suffered only minor erosion damage during the storm, suggesting correlation between levee damage and sediment source, sediment properties, and/or construction method. The levee reaches that were most heavily damaged during Katrina were: the levee along MRGO Reach 2 between Bayou Bienvenue and Bayou Dupre (see Figures B-14 to B-18 in Appendix B), a reach immediately to the south of Bayou Dupre (see Figures B-11 to B-13), and the easternmost portion of the levee along the GIWW east of Pump Station OP-15 (see Figures B-27 to B-29). Each of these reaches was constructed using hydraulically placed sediments. This also might suggest a correlation between sediment delivery and placement method and levee erosion. From images in Appendix B, note that other stretches of these very same levees or adjacent levees which also were constructed of hydraulically-placed sediments were not nearly as degraded during the storm or were undamaged by it. Relatively undamaged stretches include the following: areas along the southernmost portion of levee along MRGO Reach 2 south of Bayou Dupre (see Figures B7 to B10, A48, A49, A50) and long stretches adjacent to the GIWW channel between Michoud Canal and Pump Station OP-15 (see Figures B32 to B33) and even an undamaged section between Bayou Bienvenue and Bayou Dupre (Figure A20). Isolated sections of undamaged levee are interspersed among sections that were totally destroyed, so placement method does not tell the whole story behind levee performance.

The degree of sediment compaction (both that which occurs naturally and that which is mechanically-created) also influences levee erodability through its influence on sediment density. Levee sediments compact naturally due to the weight of overlaying sediment. Levees also are artificially compacted during the construction process by heavy equipment. For levees constructed of hydraulically placed material, the levees were generally constructed by pumping sediments into a containment area between formed dikes, slowly mounding the sediments though pumping and natural consolidation and compaction; and then lastly, the uppermost portion of the levee was shaped with earth-moving equipment using sediment that was removed from adjacent areas of the hydraulically-placed mound. Intuitively it seems, the levees constructed of sediments which were truck-hauled to the site, and shaped, might have been subjected to greater mechanical compaction during the levee construction process than those formed from hydraulically-placed material. Hydraulic placement might also influence the cohesive bonds within the sediments, similar to an erosion process. These factors might explain some of the differences in levee response that were observed.

f. Influence of Sediment Heterogeneity on Erodability

Along the MRGO and GIWW levees, it is possible that different sediment fractions became segregated to some degree during the hydraulic placement process. Therefore, for levees formed with hydraulically placed sediments, including the shaped portions, it is possible that there were localized pockets of coarser, non-cohesive and more erodable sediments present. Data from the sediment cores examined by the IPET and the sediment sampling done by the ILIT both indicate the presence of isolated occurrences of sandy and silty sediments among the predominantly clay levees. One of the cores acquired along MRGO Reach 2 showed a thick surface stratum of silty sand. All other cores showed lean or fat clay at the surface.

Many of the photos in Appendix A show localized erosion, with none evident to either side, even in areas where there are severe breaches. This probably occurs at least in part because the sediments at one location were more erodable than those at neighboring locations. Minimizing non-homogeneity in both sediment properties and the degree of compaction is a challenge in forming any earthen levee, regardless of sediment source or delivery method. Sediment heterogeneity was a likely factor in levee response during Hurricane Katrina. In light of the severe hydrodynamic loading experienced along the MRGO Reach 2 levee, sediment that behaved as non-cohesive sediment would have been readily eroded. Some areas along MRGO Reach 2 comprised of fat clay were able to withstand extremely high loading without suffering significant damage; some were not.

g. Modes of Levee Erosion for Different Hydrodynamic Regimes

Photos in Appendix A show both wave-induced erosion on the front side, as well as erosion on the back side. A number of the photos are shown in sections below to illustrate certain key points. The reader should closely examine the entire set of photos to gain an appreciation for what was prevalent in terms of processes and responses, and how they relate to subsequent discussion regarding different flow situations and velocity regimes for each situation. There is much insight to be gained from looking at the entire set of photos, observing both what is seen and not seen in them. Some of the photos show various stages of erosion processes at work. Seeing the intermediate states of degradation shed considerable light on what was most important in the levee erosion and degradation process.

Earthen levees can be eroded by water having sufficiently high velocity. The rate at which an earthen levee will erode, and the degree to which it will erode, depends upon the hydrodynamic forces acting on the levee surface as well as its resistance to erosion. The erosive force is determined by the nature and magnitude of the water velocities and by the duration of time for which erosion-producing velocities are present. Duration is a key parameter in any coastal erosion phenomenon, such as coastal levee or sand beach/dune erosion by high waves and water levels. The degree of erosion depends on

the flow situation and the location on the levee where these conditions occur. Several flow situations or regimes are possible: 1) flow that moves tangentially along the exposed (front) face of the levee prior to overtopping, 2) combined oscillatory, accelerating, and decelerating wave orbital velocities and mean currents on the front face and crest, with or without wave breaking, 3) accelerated water on the protected side (back side) caused by intermittent overtopping that occurs with individual waves that pass over the levee crest and cascade down the back side (water can reach supercritical flow speeds), and 4) steady flow over the levee crest and down the back side that can reach supercritical flow speeds, with or without the presence of waves. The presence of waves will periodically increase velocities and accelerate the flow over the levee crest, causing the overflow to pulsate.

i. Front Side Erosion by Currents (No Waves)

Information from past studies of erosion produced by flow over a vegetated earthen surface provides some insight into the possible erosion caused by water that flowed along the levees due to the build-up of the storm surge, prior to overtopping, compared to other flow situations. Figure 46 shows results from the work of Hewlett et al (1987), in which the authors relate the velocity for the onset of earthen levee erosion/damage to the quality of vegetation cover and the duration of a particular velocity. The results were derived for situations involving steady flow over vegetated earthen channels; which is not exactly the situation on a sloping vegetated levee. Absent from the results of Hewlett et al. is any dependency of erosion threshold on sediment characteristics of the earthen substrate, which is known to be an important factor. Despite the limitations, the information is useful as a rough estimate for examining the potential for erosion of the levees due to currents flowing along the levee. Note that the vertical scale in Figure 46 is presented in metric units (multiply m/sec by 3.3 to convert to ft/sec).

Results from Hewlett et al (1987) indicate that for steady velocities of 1 m/sec (roughly 3.3 ft/sec) velocities would have to be present for about 50 hours to begin to cause erosion of an earthen surface with poor quality of grass cover. For normal and good grass cover, results suggest an earthen levee surface will not experience erosion for even a much longer duration when subjected to velocities of this magnitude. Since the brunt of a hurricane typically lasts less than 24 hours, this magnitude of current speed would not be expected to create a problem on earthen levees during hurricanes. Figure 46 suggests that velocity magnitudes of 2 m/sec (6.6 ft/sec) would have to be present for approximately 5 hours to begin to erode the earthen surface for poor grass cover, 15 to 20 hours for normal cover, and that this magnitude of velocity would not erode an earthen surface with good grass cover during a hurricane. The results suggest that velocities greater than 2.5 m/sec (8.2 ft/sec) for two hours and 3 m/sec (9.8 ft/sec) for one hour are likely to begin causing erosion on earthen levees with poor grass cover. Even for earthen levees with good grass cover, steady velocities of 4.5 m/sec (14.8) for 1 hour are expected to cause erosion. Results reflected in these figures illustrate the importance, and value, of good grass cover on an earthen levee. It is important to point out that these results do not consider levee sediment properties, which influence erodability.

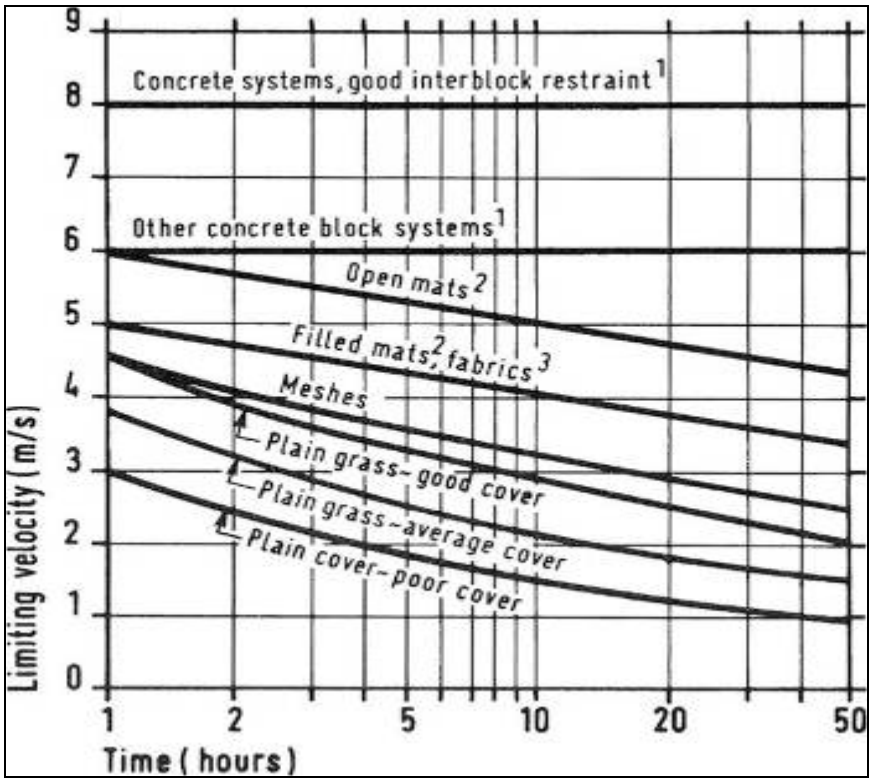


Figure 46. Onset of erosion/damage as a function of limiting velocity and duration (from Hewlett et al, 1987)

Computed velocities along levees adjacent to the MRGO Reach 2 and GIWW which eroded severely, associated with arrival of the storm surge, show maximum current speeds less than 2 ft/sec. In light of these current speeds and the information presented above for the onset of erosion of vegetated earthen surfaces, currents which flowed tangentially along the exposed (front) sides of the levees did not contribute to erosion of the levee in any significant way. Where current speeds were highest along the MRGO Reach 2, at the north and south ends of this levee reach, there was no levee erosion during Katrina; and where the currents speeds were lowest, between Bayou Bienvenue and Bayou Dupre, considerable levee degradation occurred. The strongest currents were computed in the vicinity of Paris Road Bridge. There was no record of any levee damage on the flood side of the levees at this location due to higher current speeds. The degree of levee damage is not correlated at all with the tangential surge-induced current speed along the levees.

ii. Front-Side Erosion by Wave Action

There were signatures of wave-induced erosion on the front side evident in photos taken following the storm of MRGO Reach 2 levees. Erosion on the front side manifested itself in two ways: 1) a band of relatively minor surface erosion that ran along the levee's front face which was prevalent and visible in many photos, and 2) isolated bench-cuts on the upper region of the front face, which were evident much less frequently.

Surficial Erosion Band

The prevalent signature, a band of surficial erosion on the levee front face, was caused by wave breaking on the levee front side slope. Whenever this erosion band is seen in Appendix A photos, it is present at nearly the same location on the levee face, above the levee toe and below the levee crest. Wave and water level conditions all along the MRGO Reach 2 levee were fairly uniform (see Figure 34). Along-levee uniformity in water levels and waves, the primary hydrodynamic loadings that cause erosion, and a rather uniform levee cross-section and front side slope, contribute to the erosion band being located at a similar position all along the levee. Based on model results, this zone reflects several hours of wave action and wave breaking on the front face at elevated water levels.

Figure 47 shows this erosion feature, in its prevailing location. The band is evident along the entire stretch of levee seen in this particular photo, as it is in many other photos. In some photos, the surface band was not evident; and in some photos, only traces of an erosion band were observed. The presence or absence of the band is most likely linked to quality of grass cover and sediment properties.



Figure 47. Example showing the surface erosion band (zone where grass is removed on the front side, of the levee (left side of the photo) with intact grass above it.

Sediments having poorer grass cover and/or more erodable sediments were more prone to this surficial erosion. Irregularity in extent and "patchiness" of the erosion band was related to local variability in quality of grass cover and sediment properties. Even where the grass was completely stripped away, which is seen in many photos representing long stretches of levee, the velocities experienced on the front side band were apparently not great enough to cause anything more than relatively minor surficial erosion on the front side.

Calculation of Wave-Induced Erosion

There is limited engineering guidance available at present for estimating wave-induced erosion on the front face of a grass-covered earthen levee. No reliable numerical model is presently available which properly treats all the important physics and factors, sediment type and strength, grass properties including root system structure, levee slope, irregular and unsteady hydrodynamic loading conditions (wave characteristics and type of breaking), and the various modes of erosion and transport. Consequently, predictive methods are based on erosion experiments conducted at prototype scale in large wave flumes.

Seijffert and Verheij (1998) provide valuable information for wave-induced erosion under wave conditions that are similar to those which existed along much of the MRGO Reach 2 levees during Katrina. They examined erosion of various clay levee test sections as a function of incident wave conditions, different sod (grass cover) and duration, all of which are important variables in determining the degree of levee erosion. Based on analysis of sediment cores in Table 4 that were acquired along the MRGO Reach 2, levee sediments were primarily comprised of clay, either lean or fat clay. Erosion signatures on the levee front face and the degree of erosion they observed by Seijffert and Verheij (1998) were similar to the signature and degree of erosion that occurred on the front side of the MRGO Reach 2 levee at many locations during Katrina.

Figure 48 shows erosion depth results from Seijffert and Verheij (1998). The figure shows depth of erosion as a function of duration, with erosion depths characterized for several different zones within the surf zone on the levee front face. Results illustrate several important points. First, the seaward extent of erosion Zone 1, the zone with the highest erosion, is located at a water depth corresponding to 0.5 times the incident significant wave height, which is well within the surf zone, or zone of wave breaking on the levee front face. Second, for the most energetic wave case they examined, the maximum vertical erosion observed in Zone 1 was only 70 mm, or less than 3 inches, after 18 hours of wave action. Finally, the data show that erosion depth is greatest in Zone 1, which spans a water depth range of 0.5*Hs to 0.3 *Hs; erosion in Zone 2 is about 50% of the magnitude of erosion in Zone 1; and erosion in Zone 3 is about 25% of the erosion in Zone 1. In other words the magnitude of erosion depth decreases in the landward direction, toward the position on the levee that corresponds to the elevation of the mean water surface.

Their observations are consistent with the character of the surface erosion band seen along much of the MRGO Reach 2 levee. The surface erosion band in Figure 47 is located further downslope from the levee crest on the front side, between the toe and the crest. There is intact grass cover visible above the erosion band. Many other photos in Appendix A show the same observation. Seijffert and Verheij (1998) presented no results for the swash zone, Zone 4; however, they note that erosion in the swash zone was less than erosion in the surf zone for the cases and conditions they examined. A number of photos in Appendix A show no erosion of the upper front side where the swash zone would have existed for the longest period of time.

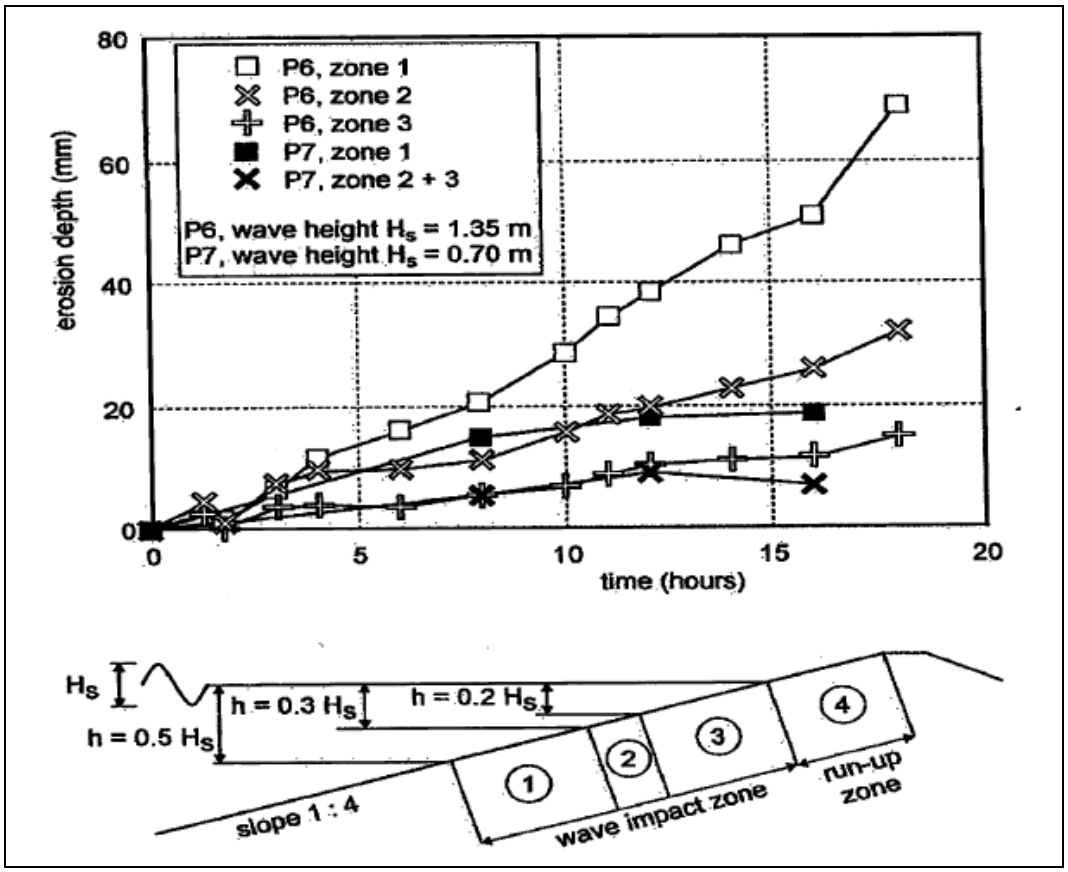


Figure 48. Results for wave-induced erosion of grass-covered clay levee (Seijffert and Verheij, 1998)

Seijffert and Verheij (1998) provided a relationship between vertical erosion rate, E, and the incident significant wave height, enabling calculation of vertical erosion rates for wave loadings during Katrina. The relationship expresses erosion rate as the product of a coefficient (which varies according to quality of grass cover) and the square of the incident significant wave height,

$$E = C_E * H_s^2 \qquad (1)$$

For good grass cover, they recommend coefficient values of 0.5 to 1 X 10^{-6};1.5 to 2.5 X 10^{-6} for average grass cover; and 2.5 to 3.5 X 10^{-6} for poor grass cover. Note that the incident wave height is specified in meters and the coefficient is expressed in $m^{-1}sec^{-1}$. In their erosion model, erosion is nonlinearly related to the incident wave height. Wave height and period for the P6 test condition they examined (wave height of 4.5 ft, wave period of 4.7 sec) is similar to but less energetic than the wave conditions along the MRGO Reach 2 levee (maximum height of 5 to 7 ft and corresponding period of 5 to 6 sec).

It is informative to make an estimate of the depth of erosion for a representative clay levee, using the method (Equation 1 above) of Seijffert and Verheij (1998). Table 5 lists hourly values of water level and incident significant wave height between 3:00 a.m. CDT and 3:00 p.m. CDT, on August 29, for a representative location between Bayou Bienvenue and Bayou Dupre, along with computed values of cumulative vertical erosion for three grades of grass cover (good, average, and poor), using Equation 1. Computed wave conditions did not vary much spatially along MRGO Reach 2, so these are considered representative values for the reach, and they provide a reasonable order of magnitude estimate for wave-induced vertical erosion.

Computed cumulative erosion values are quite small, 0.09, 0.4 and 0.5 ft (1, 4 and 6 inches) for good, average and poor grass covers respectively. These minor vertical erosion amounts are very consistent with the minor surficial wave-induced erosion that was observed along the front side of many areas of the grass-covered levees along MRGO Reach 2 (see photos in Appendix A). Results also suggest that for good grass cover, the front side vertical erosion would be very small. This is consistent with the observation that, along some of the levee sections, a surface erosion band was not evident.

Table 5. Temporal Variation in Surf Zone Conditions and Wave-Induced Vertical Erosion as a Function of Grass-cover Quality					
Time, CDT August 29	**Total Water Level (ft) NAVD88 2004.65**	**Significant Wave Height (ft)**	**Cumulative Erosion (ft) Good Grass Cover**	**Cumulative Erosion (ft) Average Grass Cover**	**Cumulative Erosion (ft) Poor Grass Cover**
3:00 a.m.	10.1	3	0.002	0.008	0.012
3:30 a.m.	10.7	3	0.004	0.016	0.024
4:00 a.m.	11.3	3.3	0.007	0.028	0.042
4:30 a.m.	12.1	3.6	0.011	0.044	0.066
5:00 a.m.	12.9	4.3	0.016	0.064	0.096
5:30 a.m.	13.9	4.6	0.022	0.088	0.13
6:00 a.m.	15.5	5.2	0.029	0.12	0.17
6:30 a.m.	16.8	5.9	0.039	0.16	0.23
7:00 a.m.	17.5	6.2	0.050	0.20	0.30
7:30 a.m.	17.5	6.6	0.062	0.25	0.37
8:00 a.m.	16.9	6.2	0.073	0.29	0.44
8:30 a.m.	15.9	4.9	0.080	0.32	0.48
9:00 a.m.	14.5	3.6	0.084	0.34	0.50
9:30 a.m.	13.1	3	0.086	0.34	0.52
10:00 a.m.	12.4	2	0.087	0.35	0.52
10:30 a.m.	12.7	2	0.088	0.35	0.53
11:00 a.m.	13.0	2	0.089	0.36	0.53

Wave-Induced Bench Cutting

Bench-cutting by wave action was the second type of erosion feature evident on the front side of the levees along MRGO Reach 2. Two small isolated bench-cuts are visible in the foreground of Figure 47. These features reflect deeper erosion than the surface erosion band discussed in the preceding section, but they reflect relatively minor erosion compared to backside head-cutting induced erosion features seen in the same photo. In Appendix A, a few photos show bench-cuts on the front side at a few isolated locations. They were not pervasive in extent along the levee like the surface erosion band. When the features are evident, their location is always higher on the levee front face, at or above the upper limit of the band of surface erosion. In light of their position, wave-induced bench-cutting was most likely caused by swash zone processes.

Seijffert and Verheij (1998) observed no significant erosion in the swash zone for grass-covered clay levees. One of the sediment cores acquired along Reach 2 showed a thick surface layer of silty sand. Because levees along Reach 2 were primarily comprised of lean and fat clays, and because the wave-induced bench-cuts were evident at relatively few isolated areas, the cuts were most likely formed in areas where wave up rush and down rush in the swash zone steadily worked on localized patches of highly erodable less cohesive sediment.

The most severe, deepest, wave-induced bench cuts were most likely formed later during the storm, once the storm reached its peak surge level. Computations show that wave heights increased steadily during the time the water level was rising rapidly toward its peak level. As the water level approached and reached its peak, it remained at or within 1 to 2 ft of the peak level for approximately 2.5 hours, 6:00 a.m. to 8:30 a.m. Duration of hydrodynamic loading is an important factor that influences the degree of erosion. This extended period of time at the highest water levels would have enabled the swash zone to be concentrated at the same location, high on the levee slope, for the longest period of time. These factors indicate that the deeper cuts formed later in the storm, and not earlier in the storm as the water level was rising on the levee front side at a much more rapid rate. As the water level rose rapidly, the swash zone moved steadily up the levee front face, not remaining in any one place for very long, until near the time of peak surge.

Isolated wave-induced bench cuts are evident at a few locations along Reach 2, but they are noticeably absent from most of the photos in Appendix A. In Figure 47 for example, front-side bench cut features are not evident anywhere else along the front face, even at locations along the levee where both surficial front side erosion and significant back side erosion occurred, and even where severe head cuts developed on the back side but did not advance to or through the levee crest. At these locations the sediments are clearly erodable enough to be removed by hydrodynamic conditions on the back side. Clearly in these instances the water level and breaking waves would have reached the upper portion of the levee front face wherever overtopping was occurring, with the potential to create bench-cuts on the front side. A long-continuous zone of deep front side erosion due to wave action, like the continuous surficial erosion band, which runs along the entire length of levee, is not evident. These same observations are seen in many of the photos. If wave-induced bench cutting were a prevailing feature along the levee system, one would expect it to be a prevalent feature on many more levee sections where back-side erosion occurred. That was not the case.

Also, if long expanses of levee experienced extensive erosion on the front side, not just in isolated pockets, one would expect to see significant amounts of sediment deposited at and seaward of the front side levee toe, transported there by the mean undertow velocity that existed in the surf zone on the front face. Evidence of widespread severe erosion of sediment from the levee front face and deposition of that sediment at or just beyond the toe is never seen in any of the photos in Appendix A. A few photos in Appendix A appear to indicate seaward transport of sediment; but in these cases, there is strong evidence of that the features were associated with water exiting the flooded polder following passage of the storm.

Figure 49 shows the only photo from the entire set of 50 in Appendix A in which many discrete bench-cuts were evident in one photo and where a pattern of front-side wave-induced bench-cutting was the prevalent erosion signature, in addition to the surface erosion band. The location of the bench cuts is at and above the upper edge of the surface erosion band. It is likely that these cuts were formed much later in the storm

and then perhaps continued to enlarge as the water levels dropped following the peak, thereby eroding areas lower on the levee and into the surface erosion zone. The features are isolated cuts, not a continuous zone of deep erosion seen along the entire levee reach seen in the photo. The discreteness and narrowness of the many cuts, or gullies, suggests the convergence of wave up rush into concentrated zones of down rush, a process that occurs in the swash zone on natural sandy beaches. This erosion process would be self-reinforcing, exacerbating erosion by forming an increasingly deeper cut which then concentrates down rushing water within the gully. This process would have continued as water levels dropped.

This site was examined more closely. Figure 50 shows the post-storm LIDAR data at this same location. The arrows in the figure clearly identify two of the larger cuts. These particular cuts are clearly recognizable in the photo and in the 3D topographic surface created from the LIDAR data. Figure 51 shows cross-sections cut through both the pre- and post-storm LIDAR elevation surfaces at a nearby location just to the south of the larger bench-cuts where no bench-cut feature is present. The location of these cross-sections is denoted as "Cross-section 1" in Figure 49. The crest elevation of the levee here is 19 to 19.5 ft, among the highest crest elevations found anywhere along the hurricane protection system.

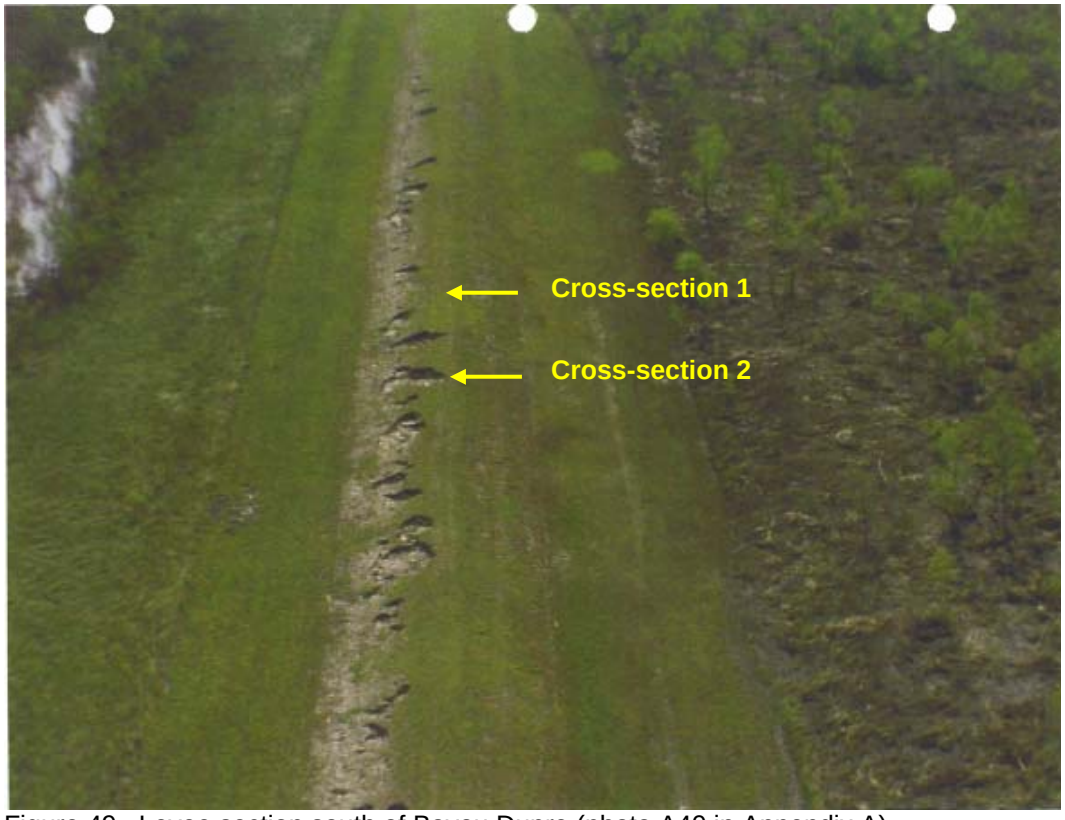


Figure 49. Levee section south of Bayou Dupre (photo A40 in Appendix A).

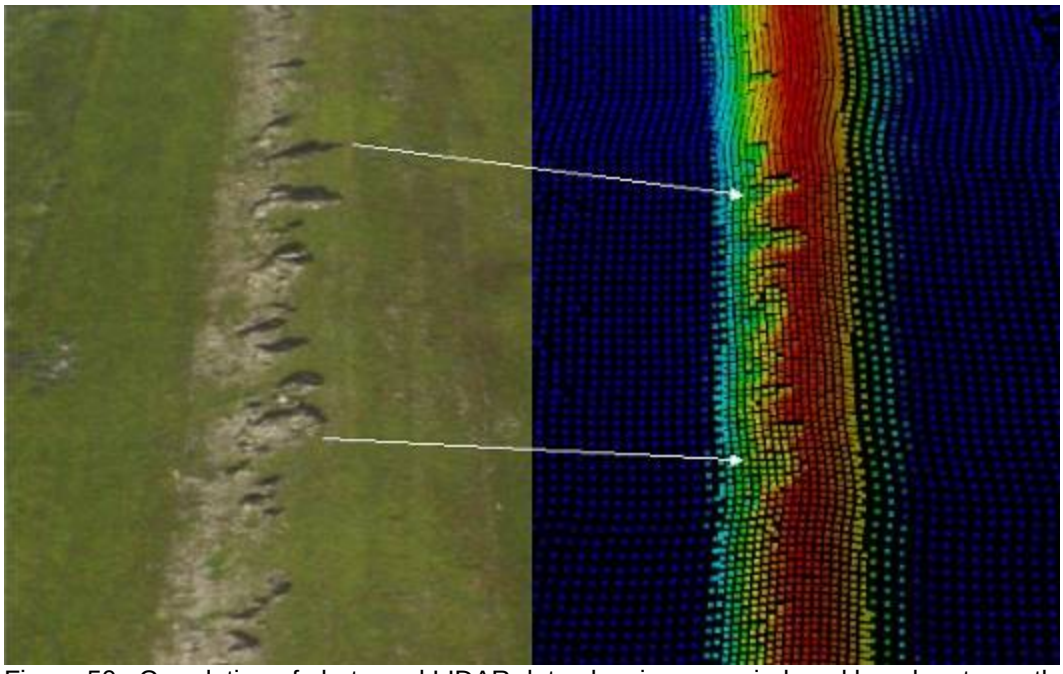


Figure 50. Correlation of photo and LIDAR data showing wave-induced bench cuts south of Bayou Dupre.

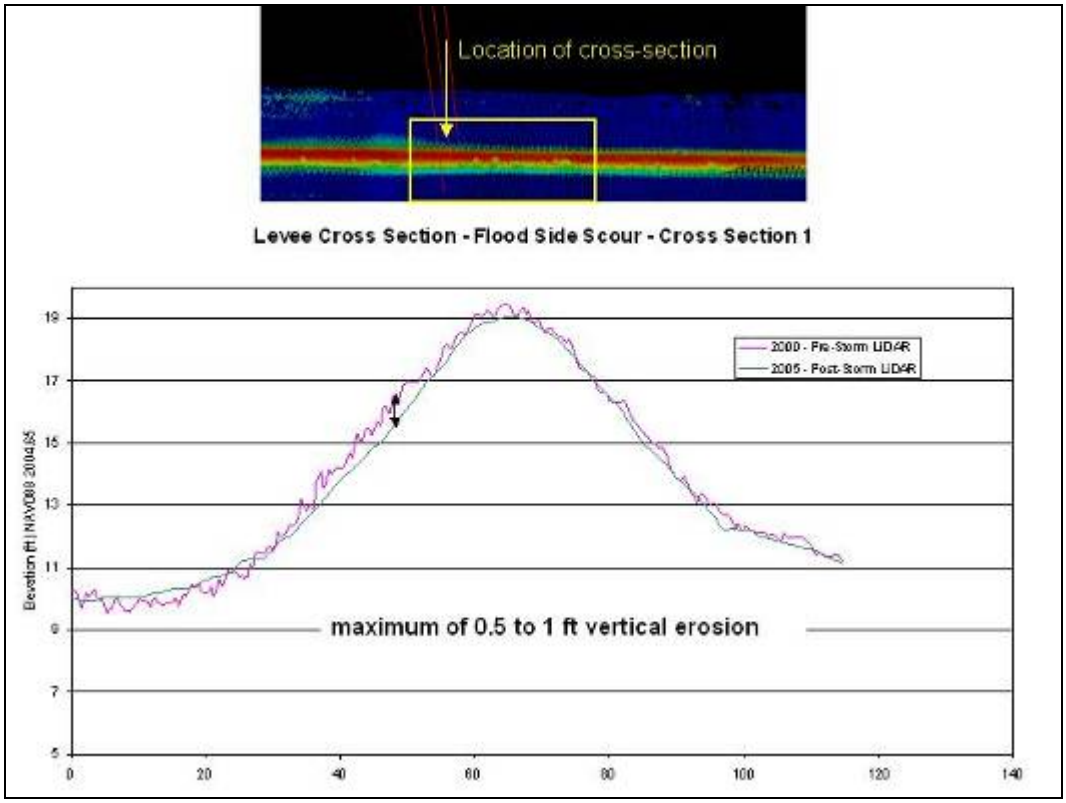


Figure 51. LIDAR data at a location without wave-induced bench cuts, Cross-section location 1.

Differences between pre- and post-storm levee elevation data show the degree of erosion associated with the surface erosion band. The amount of vertical erosion is generally greater than 0.5 ft, but is less than 1 ft. This magnitude of erosion is consistent with results of the analysis presented previously based using the methods proposed by Seijffert and Verheij (1998) to compute wave-induced erosion depth. The measured amount of vertical erosion might be slightly greater than results using the method of Seijffert and Verheij (1998) because the sediments might be more erodable than the clay levees they examined. This is still relatively minor erosion. The surface erosion band occurs within the surf zone on the levee face defined by the elevation range of 12 ft to 17 ft; the upper elevation of the surface erosion zone is less than the estimated total water level along most of the MRGO Reach 2, 17.5 to 18.3 ft, which is consistent with findings of Seijffert and Verheij (1998).

Figure 52 shows cross-sections taken through the pre- and post-storm LIDAR data at the center of one of the most severe wave-induced bench cuts. The location of the bench cut is denoted as "Cross-section 2" in Figure 49. The pre-storm elevation of the levee crest at this location also is 19 to 19.5 ft. Comparison of pre- and post-storm LIDAR data show the degree of vertical erosion in this cut, a maximum of 2 to 3 ft. Vertical erosion is less than 2 ft in most places. Erosion begins at an elevation of about +13 ft, and extends upward on the slope to the crest. Erosion is greatest at higher elevations, 18 to 18.5 ft, which are at or slightly above the peak water level.

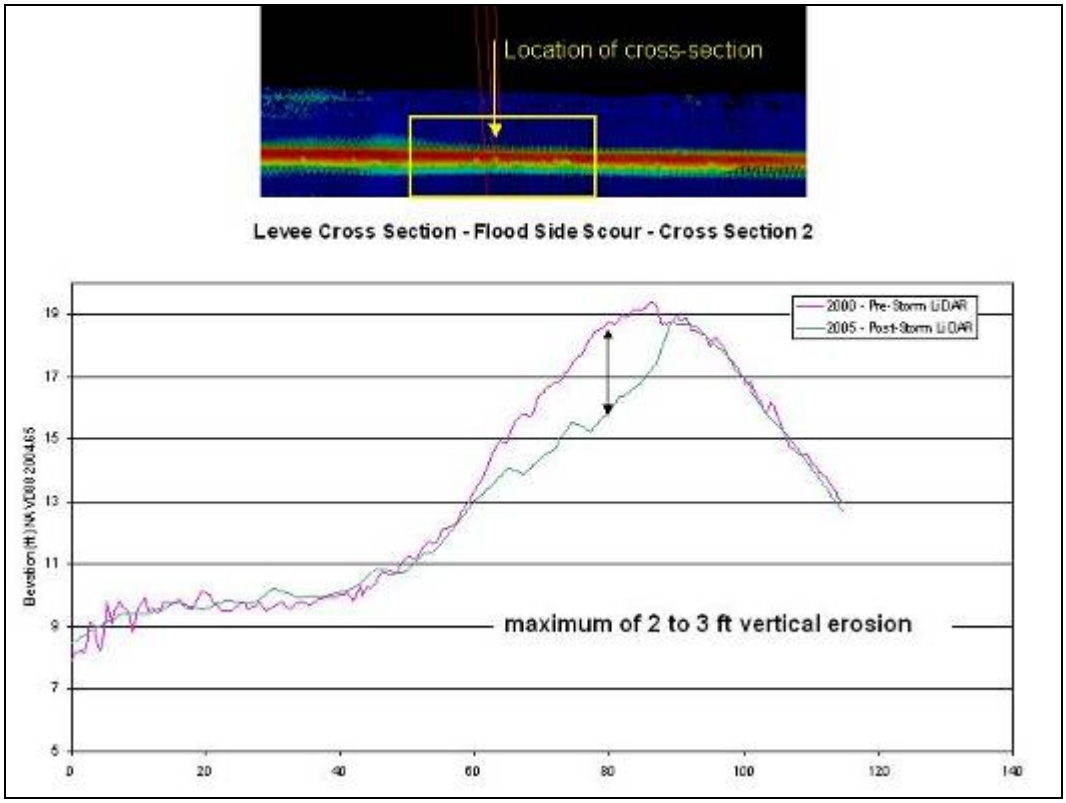


Figure 52. LIDAR data at location of the most severe wave-induced bench cut, Cross-section location 2

At this location, the cut extends through the levee crest; however, the crest elevation was degraded by only 0.5 to 1 ft. A few other cuts appear to extend through the crest to a similar degree; many do not. Horizontal erosion distances ranged from near zero, at an elevation of 13 ft, to a maximum of 15 ft at an elevation of approximately 17.5 ft. Note that for most of the bench-cuts along this length of levee, erosion is not as severe as it is at this particular cut.

In light of the very high levee crest elevation, and the positive freeboard condition at the time of peak surge (maximum water level 1 ft below the levee crest), the amount of wave-induced erosion on the front side would represent nearly a worst case from the perspectives of duration and concentration of wave energy on the front face. Erosion is very much dependent upon duration. Only minimal evidence of overtopping and backside erosion is evident at this location. Without much overtopping, dissipation of wave energy and erosion within the swash zone would be concentrated on the upper front levee face for the longest period of time and with the greatest intensity, maximizing the potential for swash zone erosion. Also note that the severe bench-cut did not significantly degrade the levee crest despite the long duration of time the hydrodynamic loadings must have been acting on and concentrated on this particular area of the front side.

Summary

There were two signatures of wave-induced erosion on the front side of levees along MRGO Reach 2: 1) a band of relatively minor surface erosion associated within the breaking wave zone, and 2) isolated bench cuts on the upper front face that are related to swash zone processes acting on pockets of more erodable non-cohesive sediments.

The band of minor surface erosion was prevalent. The surface erosion band extended uninterrupted along the entire stretch of levee in many of the photos shown in Appendix A.

In contrast, bench cuts were isolated features, very limited in occurrence, and of relatively small extent along the levee.

The MRGO Reach 2 levee was comprised primarily of clay and covered with grass. The observed position of the surface erosion band on the levee front face is very consistent with observations by Seijffert and Verheij (1998), who examined wave-induced erosion on the front side of grass-covered clay levees through large-scale testing.

The surface erosion band represented minor vertical erosion, 0.5 to 1 ft, in the case examined using LIDAR data. This magnitude of erosion is consistent with the small values of erosion depth computed using the method of Seijffert and Verheij (1998).

The surface erosion band was not evident at some locations. Where it was not present, grass cover and sediment resistance to erosion prevented waves from stripping away the sediments and removing the grass cover.

There was no continuous zone of severe wave-induced bench cutting evident on the levee front side in any photo; including none in photos that showed the levee crest intact and erosion on the back side.

There was no evidence of significant sediment accumulation at and seaward of the levee toe on the front side, which would have accompanied substantial front-side erosion caused by waves. Any such feature was noticeably absent from the photos.

The most severe wave-induced beach cuts formed later in the storm, at the highest levees, when the incident wave energy was greatest, had the longest duration to work on eroding sediments in the swash zone on the front side, and at locations where local patches of sediment were more erodable.

Only rarely was an isolated wave-induced bench cut through the levee crest evident where extensive backside erosion also was evident. This is consistent with a decrease in swash zone erosion as overtopping increases and with the occurrence of these features only at the highest levees.

Lower levees would have been subjected to more damaging overtopping before cuts on the front side could have had time to form into deep erosion features. Incident wave energy was less, earlier in the storm. The swash zone advanced steadily up the levee front face as surge levels rose; so the swash zone was not located at one place on the levee slope for very long. Only when the swash zone became concentrated at its highest point on the levee, and for the longest duration, were deeper wave-induced bench cuts able to form, and at localized patches of more erodable sediments.

As overtopping increased, the swash zone regime on the front side became less energetic; more waves advancing over the levee crest, fewer running back down the slope to interact with up rushing waves. The swash zone would have been most energetic for the longest period of time at the highest levees, for the highest water levels, and less energetic for lower water levels and for shorter durations of time earlier in the storm.

iii. Back Side Erosion by Wave Overtopping and Overflow

Head-Cutting Process

Earthen levees along MRGO Reach 2 were comprised of mostly cohesive sediment (lean and fat clay). Back side levee erosion due to wave overtopping and overflow occurred through a process called head-cutting. High velocities on the backside of the levee induced erosion of the levee surface due to high shear stresses. A rough irregular erosion feature or pocket developed. High speed flow down the back side flowed over the perturbation and created a more turbulent regime which exacerbated the

erosion. The growing perturbation and increasing turbulence built upon and reinforced itself creating a deeper head cut. The edge of the head cut nearest the levee crest became steep for cohesive sediments, flatter for less cohesive sediments. Cascading water falls over steep-faced head cuts creating an even more turbulent and highly erosive fluid regime. As erosion progressed, the head cut migrated in a direction opposite the flow, toward the levee crest. If head cutting persisted long enough, the cut eroded through the levee crest and the crest was lowered. As a breach formed through the levee, vertical erosion continued, as did lateral erosion of the levee on either side of the breach. This was the predominant mode of levee erosion and breaching that occurred along the MRGO Reach 2 levee during Katrina.

Figure 53 illustrates the hydrodynamic loading that caused head-cutting, for a levee along the north side of the GIWW/MRGO Reach 1 at the Paris Road Bridge (the bridge supports are seen in the frame). A wave crest cascading down the backside of the levee is evident. On the right hand third of the photo, a wave crest is cascading over a rather steep-faced head cut. Figure 54 is a photo taken at the same location following the storm. The frame shows the presence of a head cut on the backside of the levee. The formation of the head-cut follows an evolving process. On the left hand side of the frame, the head cut is not as advanced as it is on the right side of the frame where the water was cascading down the steep leading edge of the cut. Differences in the amount of erosion are attributed to difference in local sediment properties and erodability. On the right hand side of the frame, the head cut is more advanced, having proceeded further up the levee backside, approaching the levee crest. Where the head cut is most severe, the face of the leading edge of the cut nearest the levee crest is quite steep. Note that no front side erosion occurred at this location.



Figure 53. Overtopping of the northern levee at Paris Road Bridge.



Figure 54. Erosion formed by head-cutting of the northern levee at Paris Road Bridge.

Figure 55 from Appendix A is an excellent illustration of the various stages of head-cutting due to wave overtopping and overflow. In the upper third of the photo, there is a region on the levee back side where erosion of the surface has begun. Erosion is surficial in nature; no deep head-cuts are evident. Sediments eroded from the levee surface were deposited at the base of the levee. In the center of the photo there are several head-cuts in various stages of growth and advance toward the levee crest. The leading edge of the head-cuts is rather steep, which is characteristic of this mode of erosion for levees comprised of cohesive sediments. As the head-cut advanced toward the levee crest, it grew deeper; and as it did, more sediment was eroded and deposited at the base of the levee and inland. As water flowed through the head-cut the cut widened as the lateral edges were eroded. The increased flow transported sediment further landward and created fan shaped sediment deposits (overwash deposits) landward of the levee base.

The length and elongation of the sediment deposit in the landward direction increases with increasing current speed through the head-cut. This is nicely illustrated in the figure. Both the amount of sediment deposited in the backside and the degree of elongation of the deposit, are well-correlated with the size/maturity of the head-cut. The most severe of the head-cuts (the one in the foreground of Figure 55) advanced all the way through the levee crest. The cast shadows by the leading edges show just how steep the leading edge (the side toward the levee crest) is in the more advanced head-cuts.



Figure 55. Levee section south of Bayou Dupre

Fast-flowing water over this steep leading edge creates waterfalls, and cascading water, which generates extremely high velocities and very turbulent conditions, both of which exacerbate erosion of the earthen levee surface.

Levee Damage as a Function of Mean Overtopping Rate – Current Guidance

In current coastal engineering practice, for the situation involving an earthen coastal sea dike or levee that is exposed to wave action and overtopping, levee damage is related to the mean overtopping rate (mean in the sense of an average over many individual waves). As discussed earlier, if waves are present, overtopping, erosion and damage can occur while the surge level is below the crest of the levee. As the surge level rises and approaches the crest, the mean wave overtopping rate will increase. As the surge level rises above the crest of the levee or wall, and steady overflow begins, the rate of overtopping increases significantly. Increases in overtopping rate will increase erosion of, and damage to, an earthen levee.

Table IV-5-6 from USACE (2002), shown in Figure 56, reflects current USACE guidance which relates mean overtopping rate to levee damage. The table indicates that the start of damage to an earthen grass-covered sea dike (or levee) subjected to wave action begins when the mean overtopping rate is between 0.01 and 0.1 cfs/ft (cubic feet per sec per foot of levee crest length) in English units (approximately 0.001 and 0.01 cu

m/sec/m, or 1 and 10 liters/sec/meter, respectively, in metric units). These guidelines were developed based primarily on field experiences in Japan and Europe with damage to earthen levees subjected to wave action and overtopping/overflow conditions. USACE has adopted a lower threshold value of 0.001 cfs/ft (approximately 0.0001 cu m/sec/m or 0.1 liters/sec/meter) for poor quality earthen levees with poor quality grass cover in its most current levee certification guidance. Note that Figure 56 is in metric units. To convert from cu m/sec-m to cfs/ft, multiply rates by 10.8.

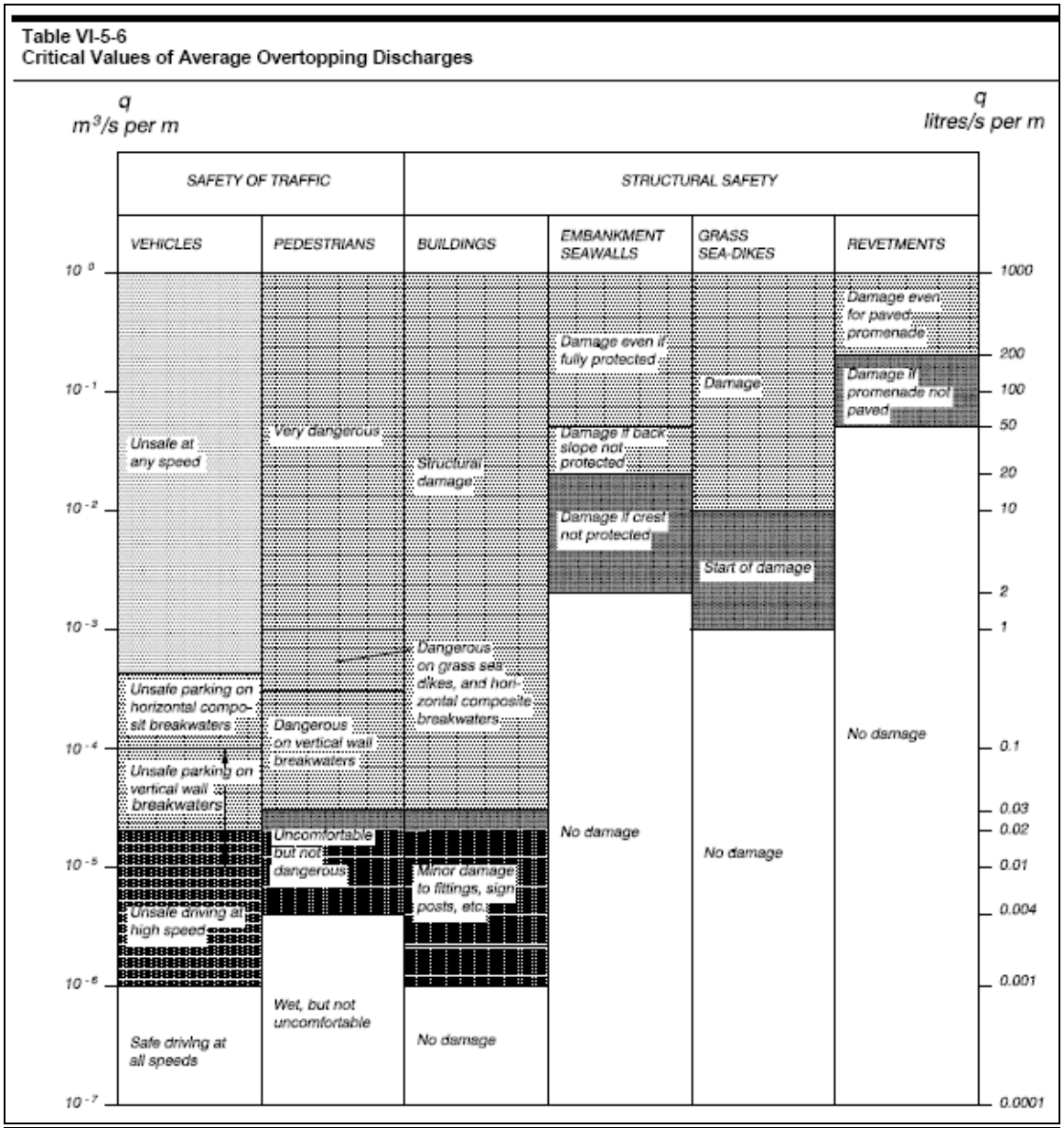


Figure 56. Threshold for damage as a function of mean overtopping rate

The USACE guidelines for thresholds-for-damage due to overtopping are consistent with threshold values adopted by the Technical Advisory Committee on Flood Defence in the Netherlands (TAW 1989 and TAW 2002). The TAW guidelines adopt these threshold values:

- 0.1 liters/s per m for sandy soil with a poor grass cover
- 1.0 liters/s per m for clayey soil with a reasonably good grass cover
- 10 liters/s per m for a clay covering and a grass cover according to the requirements for the outer slope or for a armored inner slope

In English units, these threshold values are equivalent to 0.0011, 0.011 and 0.11 cfs/ft, which are nearly the same as those cited in USACE (2002). The higher value, 10 liters/s/m (0.11 cfs/ft), is reserved for high quality clay levees that are well constructed and compacted, with very good turf conditions on the surface.

The overtopping manual recently developed by the European engineering community, Wave Overtopping of Sea Defences and Related Structures: Assessment Manual (EurOtop 2007) cites these threshold values:

- No damage if crest and rear slope are well protected 50-200 liters/sec/meter
- No damage to crest and rear face of grass covered embankment of clay 1-10 liters/sec/meter
- No damage to crest and rear face of embankment if not protected 0.1 liters/sec/meter

Based on guidance used by the USACE and the international engineering community, mean overtopping rates of 1 cfs/ft or greater are expected to produce damage even for high quality earthen levees. Overtopping rates of 1 cfs/ft exceed damage thresholds in current guidance by factors of 10 to 1000 depending on quality of the levee sediments and grass cover. Mean overtopping rates of 2 cfs/ft or greater are expected to produce damage even for armored levee crests and back sides (paved surfaces for example). Note that a value of 10 cfs/ft (approximately 1 cu m/sec/m) is the upper value in the damage scale shown in Figure 56.

Overtopping Rate Calculations – Implications for Levee Damage

Table 6 shows calculated mean overtopping rates for a series of points along the entire MRGO Reach 2 levee. Results shown in the table were computed using the COULWAVE Boussinesq-type numerical model (the same model applied by the IPET, 2006). This modeling work is described in greater detail in the expert report written by Resio (2008). Point 1 in the table is located at the confluence of the MRGO with the GIWW, north of Bayou Bienvenue; and point 21 is located at the southeastern corner of the MRGO Reach 2 levee. The points are evenly spaced so they provide a complete picture of conditions along the levee. For each location, the maximum total water level (including computed wave setup) is listed. The next three entries are levee crest heights, which are defined for each subsection of the levee represented by one of the 21 points. As

shown previously in this report, levee crest height varied considerably over relatively short distances; this variability was considered in the analysis. Three different crest heights are shown: an average of the lower 25% of the levee crest elevations, an average for the median 50%, and an average for the highest 25% of the levee crests. Next shown are maximum mean overtopping rates computed during the storm. Mean overtopping rates were computed for a series of 30-min time blocks during the storm. The maximum mean overtopping rate was the largest of the values computed for the entire set of 30-min blocks. The maximum rates closely correspond to the time of peak water level, which also closely corresponds to the time of peak wave height. Overtopping rate maximums are shown for each of the three levee crest heights. A weighted average rate, calculated using the maximum mean overtopping rates for each of the three levee crest heights, is listed. The weighted average is a gross indicator of maximum amount of overtopping that occurred along the levee reach represented by each of the 21 points.

It is important to note that these computations were made for the initial levee condition, not a degraded condition having a lower crest elevation. Degradation and lowering of crest height was prevalent at many locations. For a degraded levee crest, the mean overtopping rate would increase significantly.

Table 6. Along-Levee Variation of Maximum Mean Overtopping Rate

Point #	Maximum Total Water Level (ft)	Levee Crest Elevation (ft)			Overtopping Rate (cfs/ft)			
		Lower 25%	Median 50%	Higher 25%	Lower 25%	Median 50 %	Higher 25%	Weighted Average
1	16.8	11.0	15.3	16	39	4.9	2.1	12.6
2	17.3	17.6	18.0	18.5	1.2	0.7	0.2	0.7
3	17.5	14.0	16.5	17.7	17.9	3.8	1.7	6.8
4	17.6	15.5	16.4	17.0	8.2	4.4	2.5	4.9
5	17.9	15.5	16.2	17.0	9.3	6.3	3.0	6.2
6	18.0	15.7	16.5	17.3	9.1	5.7	2.8	5.8
7	17.8	15.4	15.7	16.0	10.2	8.9	7.6	8.9
8	18.0	15.0	16.2	17.0	13.4	7.4	4.0	8.0
9	18.0	15.0	16.6	18.4	13.2	5.5	1.4	6.4
10	18.3	14.0	17.0	19.0	25.0	4.5	1.0	8.8
11	18.2	17.5	18.0	18.5	2.8	2.2	1.5	2.2
12	18.1	17.0	17.7	18.4	4.0	2.3	1.4	2.5
13	18.2	17.1	17.6	18.1	3.9	2.4	1.8	2.6
14	18.3	17.5	18.0	19.0	2.6	2.0	0.9	1.9
15	18.2	17.6	17.9	18.4	2.4	2.0	1.5	2.0
16	18.2	14.0	16.8	18.3	24.9	5.4	1.6	9.3
17	18.2	17.3	17.8	18.6	3.0	2.1	1.2	2.1
18	18.1	18.2	18.5	18.8	1.6	1.2	0.9	1.2
19	17.8	17.8	18.3	18.8	1.7	1.1	0.6	1.1
20	17.7	14.5	17.0	18.0	14.4	2.5	1.3	5.2
21	17.5	17.0	17.3	17.5	2.3	1.9	1.7	1.9

Computed average maximum overtopping rates exceeded 1 cfs/ft at all points along the MRGO Reach 2 levee south of Bayou Bienvenue (point 2), without exception. This magnitude of overtopping is 10 times the guidance threshold for damage to high quality grass-covered clay levee, which has been adopted by the international engineering community. Overtopping of 1 cfs/ft is 100 to 1000 times the threshold for lesser quality levees adopted by the same engineering community. Average maximum overtopping rates that exceeded 1 cfs/ft are shown as either lighter or darker gray shaded cells in Table 6. Many sections of the levee were heavily damaged under these loadings, as shown in Figure 40, photos in Appendix A and in renderings of post-storm LIDAR data in Appendix B.

Examination of average maximum overtopping rates partially tells the story of levee degradation. Water tends to seek out low spots in the levee, so low spots are most vulnerable to breaching. Wave overtopping and overflow occurred at the low spots first, subjecting them to the greatest hydrodynamic loadings for the longest periods of time. For points south of Bayou Bienvenue, except for a few points at the southeastern end, for the lower 25% of levee crest heights, maximum mean overtopping rates ranged from 2 cfs/ft to 20 cfs/ft. The very large number of shaded gray cells in Table 6, especially the number of darker cells, shows just how pervasive and damaging the overflow and overtopping conditions were during Katrina along nearly the entire length of the MRGO Reach 2 levee, particularly the lower spots. Rates of 2 cfs/ft are capable of damaging armored and protected levees.

There are correlations between the degree of levee destruction that occurred along MRGO Reach 2, as seen in Figure 40, and the maximum overtopping rates shown in Table 6. For example, between Bayou Bienvenue and Bayou Dupre, maximum overtopping rates exceeded 2 cfs/ft at the lower levees throughout this reach. For points 4 through 8, maximum overtopping rates exceeded 2 cfs/ft for all three crest elevations. In general, levees in this area were lower than levees elsewhere along MRGO Reach 2 and this area was very heavily damaged. There is a high correlation between maximum overtopping rates and the degree of levee destruction that occurred along this reach. As another example, also seen in Figure 40, the lower third of the MRGO Reach 2 levee experienced fewer breaches and less overall levee degradation than the area between Bayou Bienvenue and Bayou Dupre. The lesser degree of degradation along the southern third of the levee correlates well with the generally lower overtopping rates seen in Table 6 for the lower third of the levee (the lower third of the points, 14 to 21).

Figure 57 shows data from Table 6 displayed in a different format. The total water level and levee crest elevation (or crest height) values were used to calculate freeboard values. Based on analysis presented in a previous section, freeboard is an important factor in levee response. Figure 57 shows the relationship between freeboard and mean overtopping rate, for conditions at the time of peak storm surge and waves. Peaks in water level and significant wave height occurred nearly at the same time. The figure shows mean overtopping rates associated with peak wave conditions when water levels were below the levee crest (positive freeboard values) and rates associated with

combined overflow and wave overtopping (negative freeboard values). The data fall along clear trend lines.

Erosion of the levee backside would have begun once mean overtopping rates exceeded the threshold for erosion and levee damage, 0.01 to 0.1 cfs/ft, depending upon local sediment properties and grass cover. This would have occurred when water levels were several feet below the crest height. It would have taken some time for the erosion and ensuing head-cutting to progress to the point where the levee crest was lowered. Therefore, a value of +1 ft freeboard (corresponding to overtopping rates of 0.5 to 1 cfs/ft) was recommended as the trigger which defined the point at which levee crest lowering began (a trigger of +1.5 ft was recommended for more highly erodable sediments). These triggers were applied in the breaching algorithms used in the inundation modeling within the St. Bernard polder, which is documented in the expert report of Fitzgerald (2008). At a freeboard of zero, mean overtopping rates approached potentially very damaging levels of 2 cfs/ft.

The relationship between mean overtopping rate and freeboard is linear until the mean water surface is 1 ft above the levee crest elevation (-1 ft freeboard). Beyond this loading condition, the slope of the trend line changes significantly; the overtopping rate increases much more as freeboard becomes more negative.

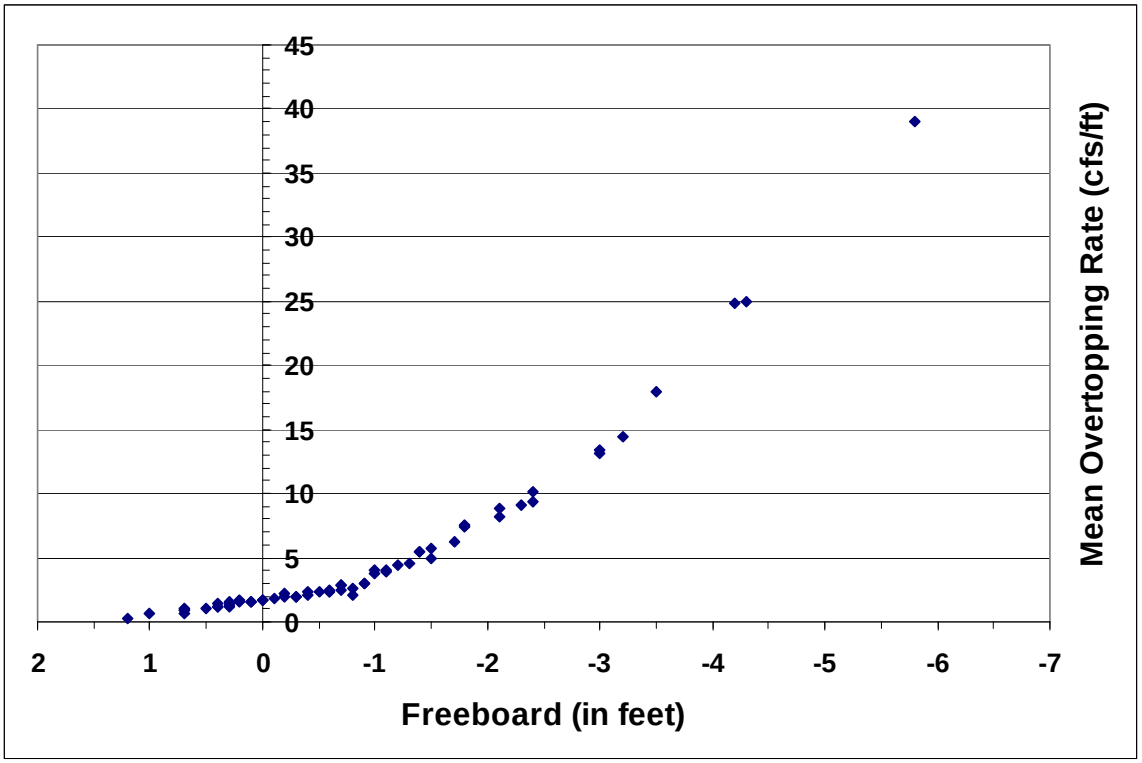


Figure 57. Mean overtopping rate as a function of freeboard, for peak wave conditions.

Using the broad-crested weir formula from classical hydraulics that excludes wave contributions to overtopping, where flow rate per unit length of weir is related to freeboard raised to the power of 1.5, mean overtopping rates at freeboards of -1 ft are computed to be 2.7 and 3 cfs/ft. These computations assume weir coefficients that range from 2.7 to 3.0, values that have been obtained experimentally on actual weirs. Computed values of overtopping rate are similar to those shown in Figure 57 using the COULWAVE model for a freeboard of -1 ft. This result indicates that once the mean water level exceeded levee crest elevation by 1 foot or more, the contribution of waves to mean overtopping rate became increasingly less important. Note that at a freeboard value of -1 ft, mean overtopping rates approached 3 cfs/ft.

Maximum total mean water levels along MRGO Reach 2 south of Bayou Bienvenue ranged from 17.5 to 18.3 feet. Wherever the levee crest elevation was 1 ft or more below these mean water levels, overflow conditions had great damage potential, aside from any wave effects. Inspection of Figure 40 shows such areas to be widespread.

Table 6 also provides perspective on locations where this was the case. Cells shaded light blue are those where the total mean water level was 1 ft or more above the levee crest elevation (shown under the three levee crest elevation columns). The large number of blue-shaded cells shows just how prevalent and damaging the effects of extreme water levels alone were, particularly between Bayou Dupre and Bayou Bienvenue and just to the south of Bayou Dupre. In these regions, levees were subjected to severe overflowing and damaging conditions, aside from any wave effects. At locations where freeboards were -2, -3 or -4 ft, overflow rates were more than 7.5, 14, and 22 cfs/ft, respectively, magnitudes that are off the damage scale in Figure 56.

Freeboard is influenced either by rising water level or by a degrading levee crest elevation. Along the MRGO Reach 2 and GIWW (east of Michoud Canal) levees that were damaged during Katrina, the levee crest was lowered by amounts ranging from 5 to 10 ft at many locations, leading to negative freeboards of -10 ft in places. For a freeboard value of -10 ft, the broad-crested weir equation indicates overtopping rates of 85 to 95 cfs/ft.

The relationship between freeboard and mean overtopping rate shows the reinforcing and exacerbating nature of damage caused by overtopping/overflow. Wave overtopping led to the onset of damage to the earthen levee. Then while transitioning to combined overflow and wave overtopping as rising water levels approached and then exceeded the levee crest, the degree of damage steadily increased. In response to increasing overflow rates the levee crest degraded further, which continued to increase the magnitude of overflow, which further damaged the levee at even greater rates. The interactive process, involving feedback between damaging levels of wave overtopping/overflow and levee degradation, reinforced itself once it began.

Figures 58a and 58b show the variation of mean overtopping rate with time for a few of the locations/levee conditions shown in Table 6. Data shown in Figures 58a and 58b were selected from conditions listed in Table 6 that corresponded to integer values of

levee crest elevation. Results are representative for the MRGO Reach 2 levee, in light of the similarity in water level and incident wave conditions that were experienced along the levee. Figure 58a shows results for lower levee crest heights of 11, 14 and 15 feet; Figure 58b shows results for higher crest heights of 16, 17, 18 and 19 ft. Conditions for the 11-ft levee crest are representative of conditions experienced at degraded levees, where degradation was on the order of 4 to 7 ft. Levees having crest elevations of 19 ft were among the highest levees in this region. The temporal variation in overtopping rate shows two peaks, as do the water level hydrographs shown previously. This pattern reflects the strong dependence of mean overtopping rate on water level (through its influence on freeboard). The existence of a second peak, which had a lower peak surge, is highly sensitive to the levee crest height.

The pair of figures illustrates a number of points. First, peak maximum mean overtopping rate is highly correlated to the duration of overtopping/overflow, the greater the rate the longer the duration. Second, even for the highest levees along MRGO Reach 2 (those having 19-ft crest heights) mean overtopping rates exceeded the threshold-for-damage guidance values of 0.01 to 0.1 cfs/ft for two hours, reaching maximum overtopping rates of 1 cfs/ft right at the time of peak water level. For levees with crest heights of 19 ft, overtopping rates exceeded 0.1 cfs/ft beginning at around 6:30 a.m., 30 minutes prior to the time of peak surge.

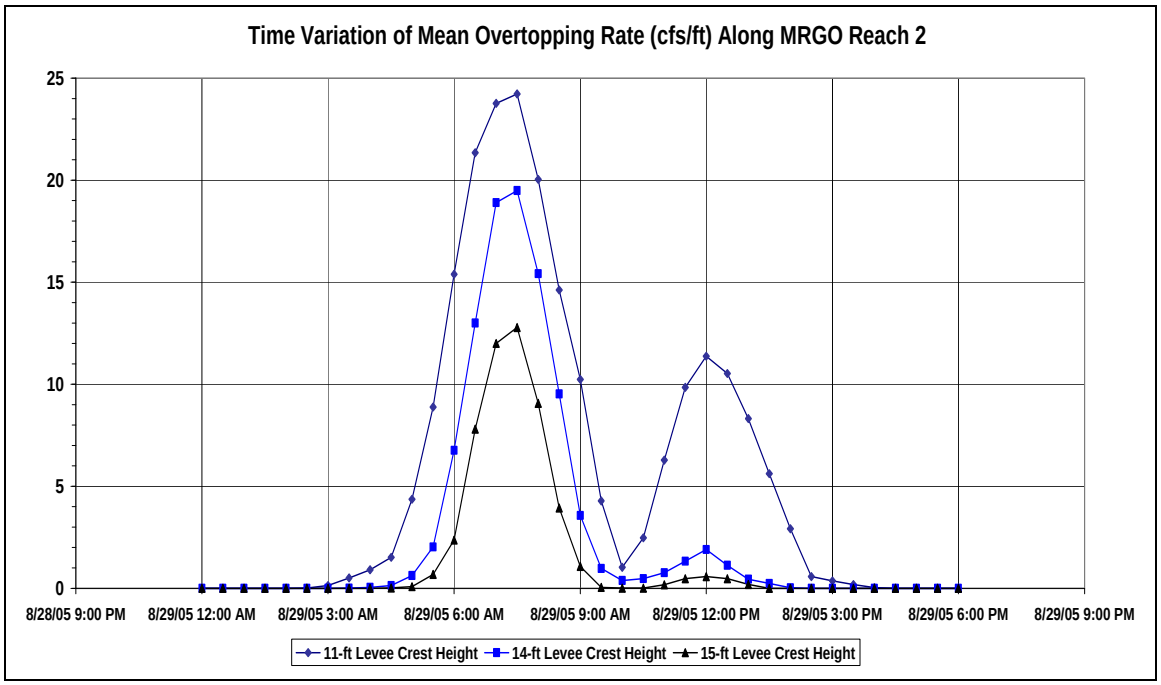


Figure 58a. Mean overtopping rate as a function of time along MRGO Reach 2

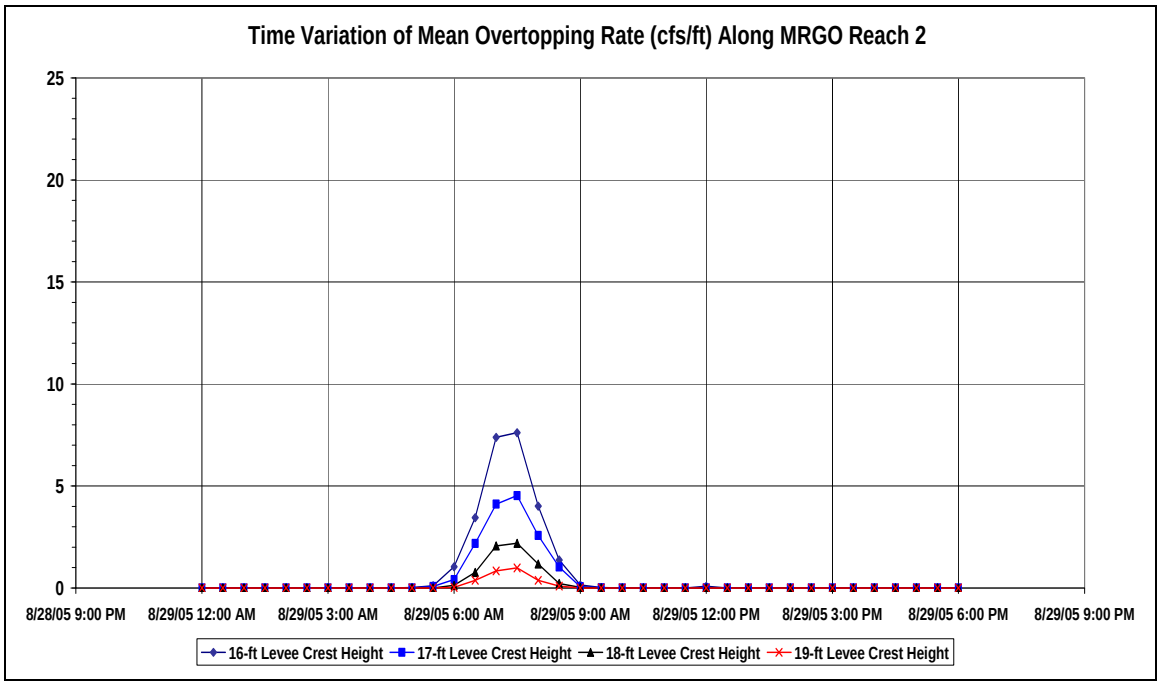


Figure 58b. Mean overtopping rate as a function of time along MRGO Reach 2

Third, the magnitude and duration of overtopping/overflow increased significantly as levee crest height decreased. There were many levees with crest elevations of 15 to 16 ft between Bayou Bienvenue and Bayou Dupre. For these crest heights, the overtopping rate exceeded 0.1 cfs/ft beginning at 5:00 to 5:30 a.m., several hours before the time of peak surge; and rates exceeded 1 cfs/ft beginning at 6:00 a.m., one hour before the time of peak surge. Overtopping rates exceeded a magnitude 1 cfs/ft for 2.5 to 4 hours. Where the levee crest height was 17 ft or less, mean overtopping rates exceeded 1 cfs/ft for more than 2 hrs, and rates exceeded 2 cfs/ft for 1.5 hours.

In places, levee crests were even lower than 15 ft. For a crest elevation of 14 ft, overtopping reached a level of 0.1 cfs/ft at 4:30 a.m., and a level of 1 cfs/ft shortly thereafter at 5:30 a.m., 1.5 to 2 hours before the time of peak surge. Overtopping rates exceeded 1 cfs/ft for approximately 5 hours. For a crest height of 11 ft, which would reflect a degraded levee condition, overtopping rates exceeded 1 cfs/ft for approximately 10 hours, and 2 cfs/ft for 8 hours.

For the energetic incident wave conditions created by Hurricane Katrina, mean overtopping rates approached 2 cfs/ft for freeboards of approximately zero, i.e., when the mean water level was right at the levee crest (see Figure 57). For 16-, 15-, 14-, and 11-ft crest heights, the magnitude of mean overtopping rate exceeded 2 cfs/ft for 2, 2.5, 3.5 and 8 hours, respectively. Even for a 17-ft crest height, mean overtopping rate exceeded 2 cfs/ft for 1.5 hrs. The durations of overflow at this magnitude provide perspective on just how long the levees were subjected to extremely damaging conditions, and then even more so as levee crests degraded and lowered.

Summary

In current USACE and international engineering guidance, the threshold-for-damage criteria for earthen levees and sea dikes that are subjected to overtopping is based on the mean overtopping rate, recognizing the dominant role of water passing over the levee and down the back side in determining damage.

All overtopping situations shown in Figure 58 (crest heights of up to 19 ft, the highest along MRGO Reach 2) exceeded threshold-for-damage values that are currently in use by the USACE and international coastal engineering communities for earthen levees (0.001 to 0.1 cfs/ft).

Mean overtopping rate is sensitive to the difference between water level and levee crest elevation (freeboard), which makes this a key parameter in levee and floodwall response (see Figure 57).

From a hydrodynamic loading perspective, waves can severely damage an earthen levee when the mean water surface is below the levee crest.

Levees along MRGO Reach 2 that had crest heights of 18 ft or less were subjected to maximum mean overtopping rates that exceeded 2 cfs/ft, the threshold-for-damage for armored paved levee slopes in current engineering guidance. The lower the levee crest, the longer the duration above 2 cfs/ft. For 17- 16-, 15-, 14-, and 11-ft crest heights, the mean overtopping rate exceeded 2 cfs/ft for 1.5, 2, 2.5, 3.5 and 8 hours, respectively.

In terms of overall regional levee response, calculations and observations suggest that those areas along MRGO Reach 2, which were subjected to averaged maximum mean overtopping rates of 2 to 2.5 cfs/ft or higher, were severely damaged. For about one third of the locations along MRGO Reach 2, lower spots in the levee experienced mean overtopping rates that exceeded 10 cfs/ft.

Overflow creates a self-reinforcing erosion situation, in which overflow and levee degradation feed upon each other once the erosion process is initiated. As the levee erodes and degrades, and the crest lowers in response to overflow, the magnitude of overflow increases which continues to further degrade the levee. The factors that would tend to slow or stop the process once it begins are a decrease in water level on the front side and/or an increase in water level on the back side such that water levels were similar.

h. Analysis of Eroded Sediment Volume

Wave-induced erosion on the front side created minor surficial erosion along much of the MRGO Reach 2 levee. This erosion feature was widespread but represented minor amounts of erosion. Isolated occurrences of wave-induced bench cuts on the front side also were evident but not prevalent in the Appendix A photos. If wave-induced

erosion on the front side was a dominant and prevalent process, then one would expect to see the levee in various stages of front side erosion, in areas where the levee crest was intact. Figures 59 through 62 show pre- and post-storm levee elevations along the centerline of the entire levee, front/back/total volume change at a resolution that enables identification of discrete breach locations, indicates those levee sections which remained intact (at the centerline), the degree of vertical erosion, and the eroded sill depths at breaches. Wall sections are designated with black triangles, which reflect the length of each wall section. In this set of four figures, erosion is denoted as negative (-) volume change and accretion or accumulation is denoted as a positive (+) change.

Figures 60 through 62 show areas where the pre- and post-storm crest elevation data parallel each other but are offset by some rather uniform amount. A rigorous effort was undertaken by the IPET to establish reliable vertical datums for the region, and to rectify pre- and post-storm LIDAR data sets to the same vertical datum, NAVD88 2004.65, based on known information regarding the surveys, benchmarks and vertical datums. The offset reflects an unresolved datum issue with one of both of the LIDAR data sets. Uncertainty remains over which data set is more accurate. The post-storm LIDAR data lie consistently below the pre-storm LIDAR data where the levee crest remained intact (intact levee crests were confirmed with visual inspection of photos in Appendix A and the graphical images in Appendix B that depict the levee surface).

Figure 63 shows pre- and post-storm cross-sections from an intact levee section; it clearly shows the presence of the offset. The offset biases volume change calculations, often appearing as a small amount of erosion on both the front and back sides that varies gradually along the levee, as seen in Figures 60 through 62.

In Figure 59, the levee crest remained intact at only a few isolated locations. At these intact locations, front- and back-side eroded volumes are quite small relative to eroded volumes at other locations. They reflect the influence of the elevation offset; alongshore uniformity in eroded volume also is an indicator. In light of variability in sediment properties and grass cover, one would expect to see alongshore variability in front side eroded volumes as is the case when both front and back sides are eroded. At the sections where the levee crest is intact, there is no large front side erosion of a magnitude that is comparable to magnitude of the front side erosion volume that occurs when the levee crest is degraded. There are no continuous areas where front side erosion is large and back side erosion is small.

Figures 60 and 61 both show many more levee sections which remained intact. Observations are the same. Where the levee crest remained intact, the front-side eroded volumes are small and uniform in magnitude along the levee; these are attributed to the elevation offset. There are no continuous areas where front side erosion is large and back side erosion is small. There are no “spikes” or other identifiable sections where there is significant front side erosion volume that one would expect to see if severe wave-induced bench cutting was present and widespread on the front side.

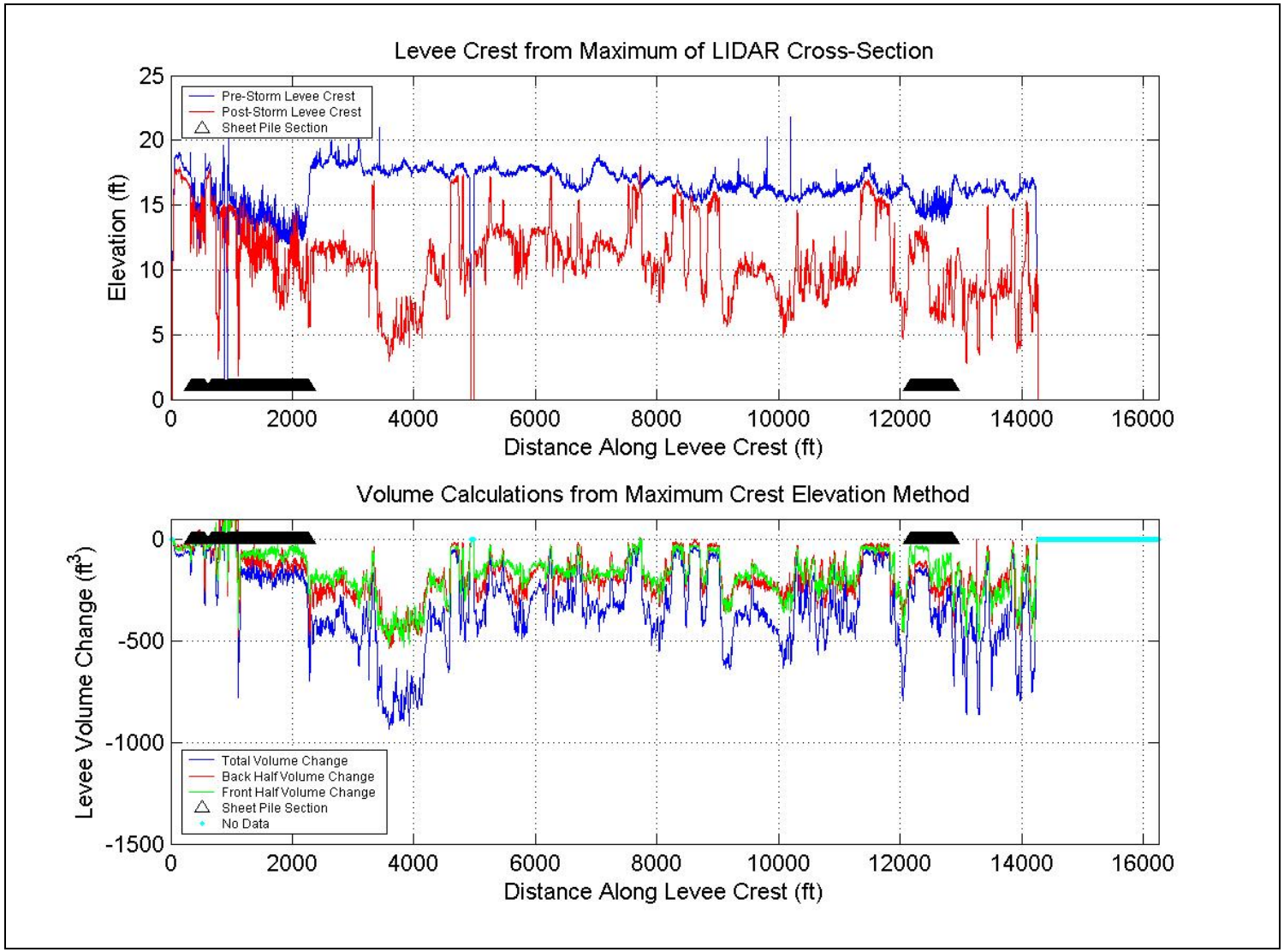


Figure 59. Along-levee variation in: pre-post storm levee centerline elevation, and front, back and total eroded

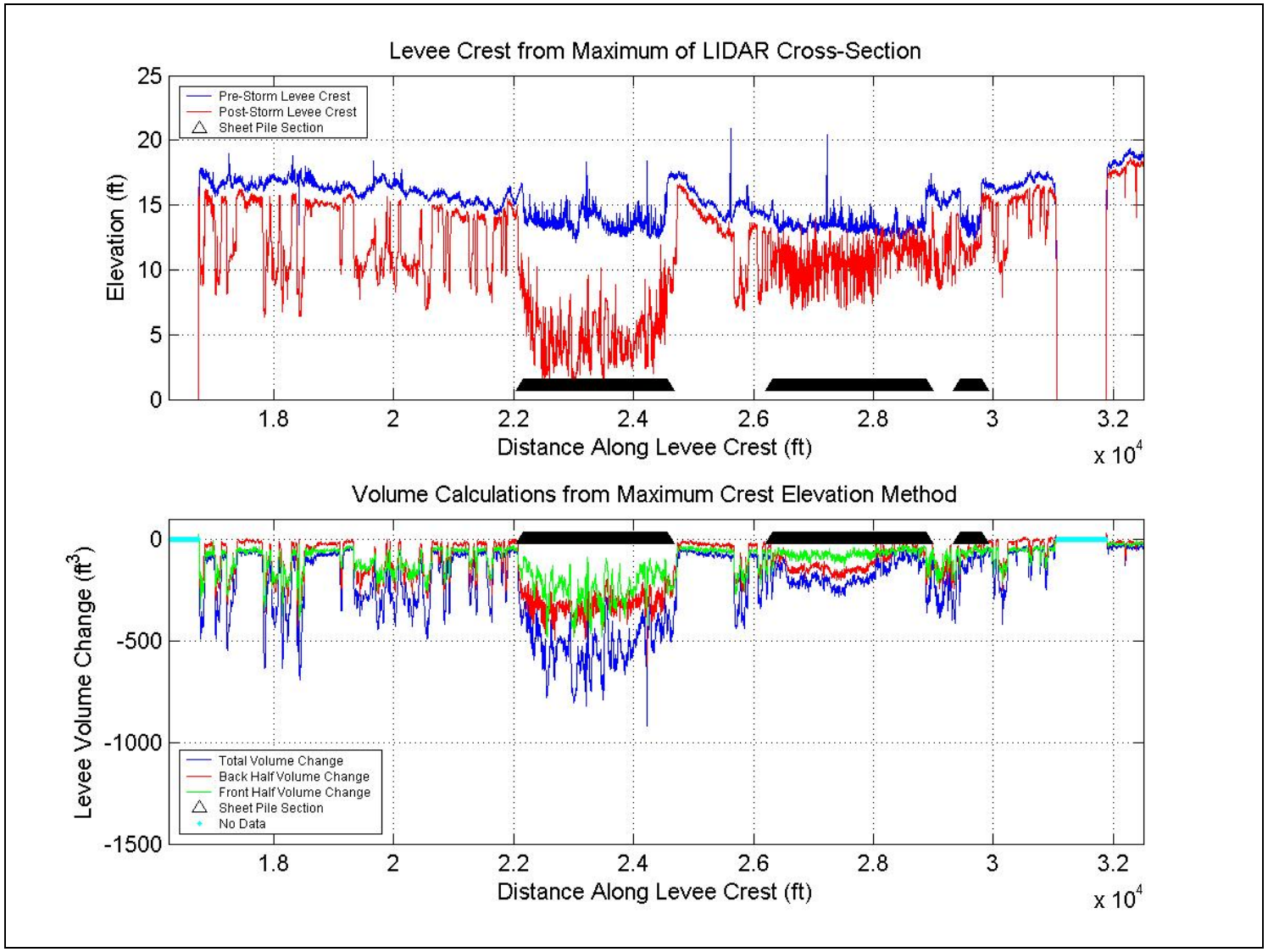


Figure 60. Along-levee variation in: pre-post storm levee centerline elevation, and front, back and total eroded volumes.

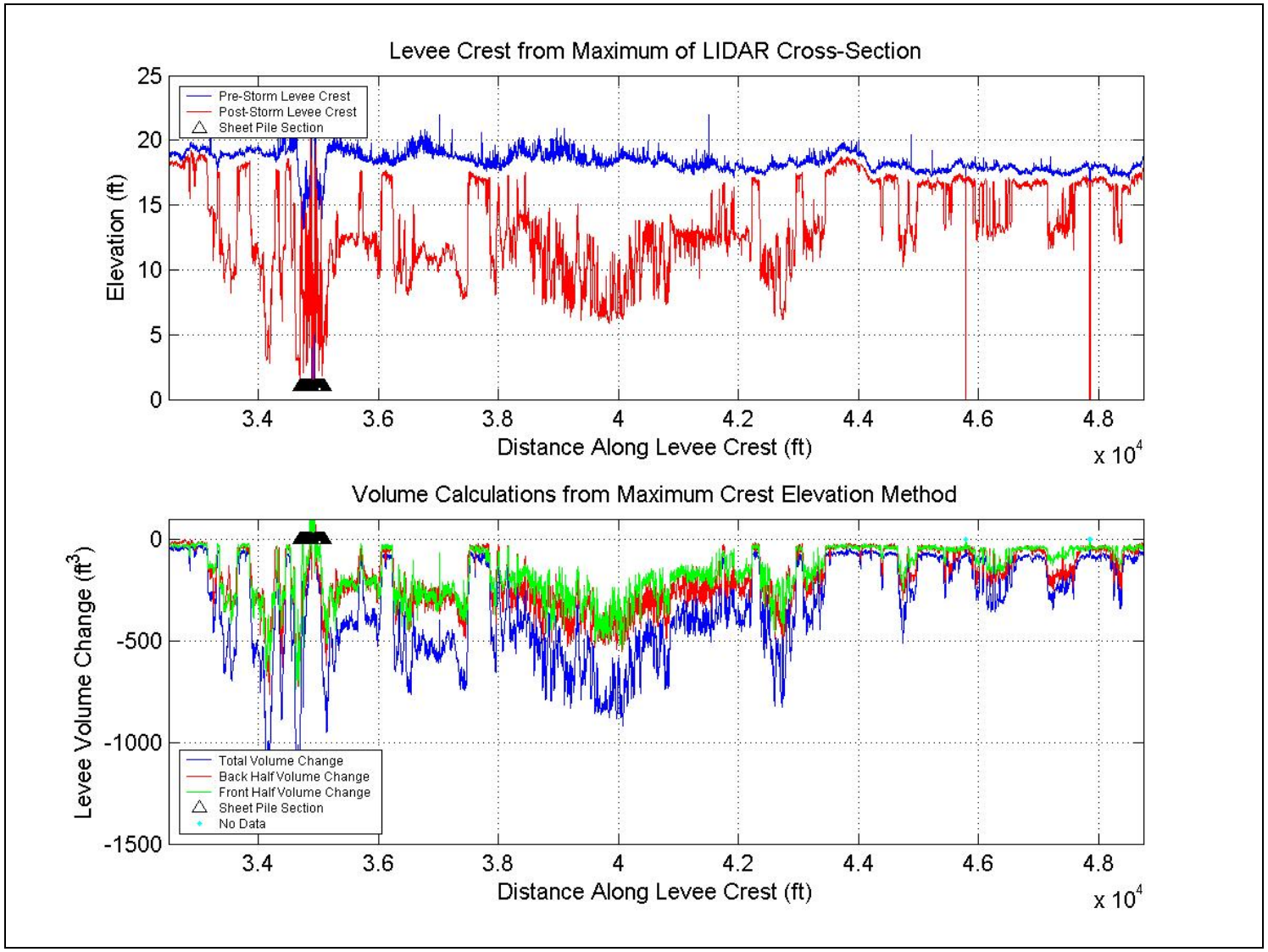


Figure 61. Along-levee variation in: pre-post storm levee centerline elevation, and front, back and total eroded volumes.

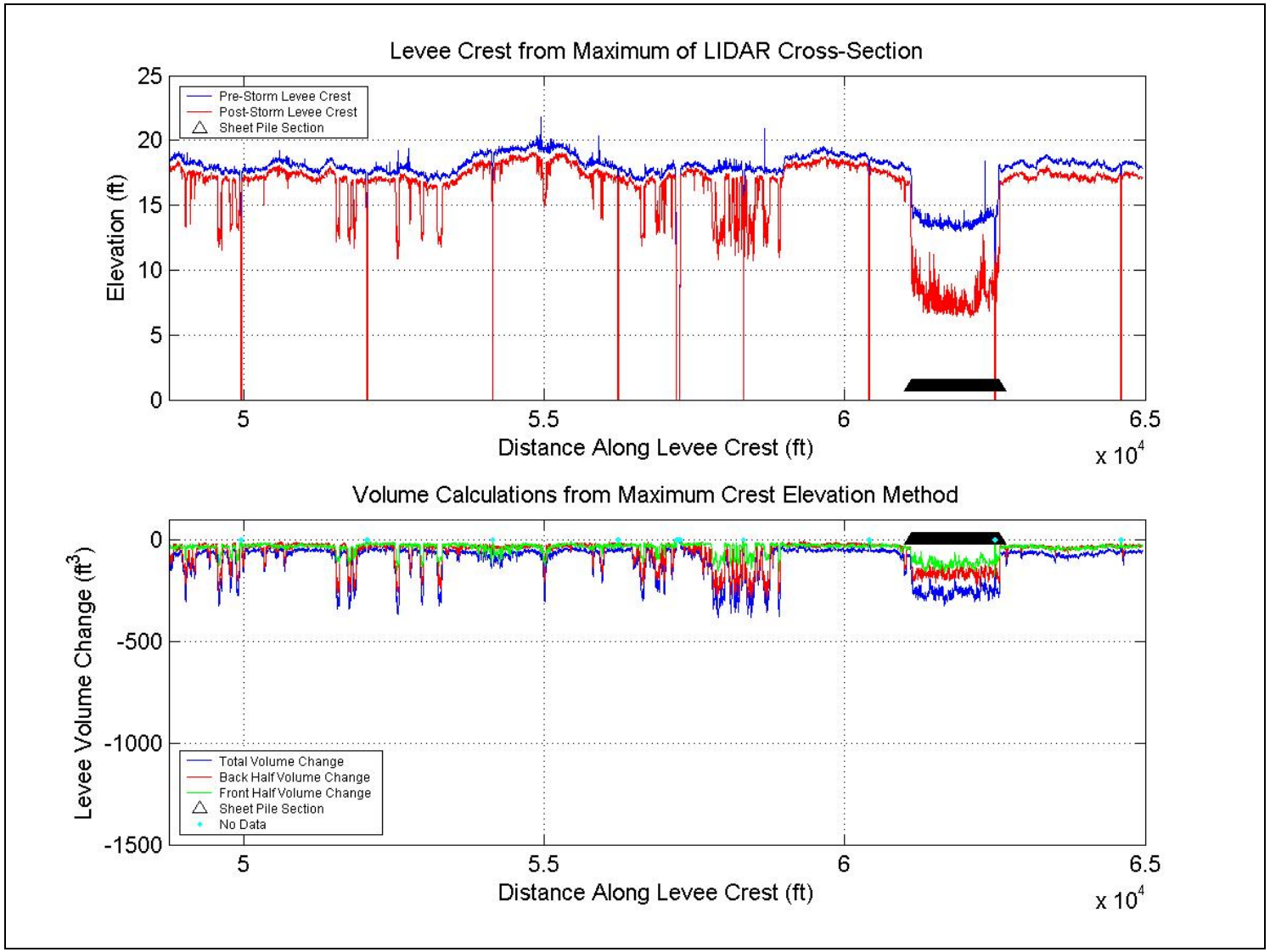


Figure 62. Along-levee variation in: pre-post storm levee centerline elevation, and front, back and total eroded volumes

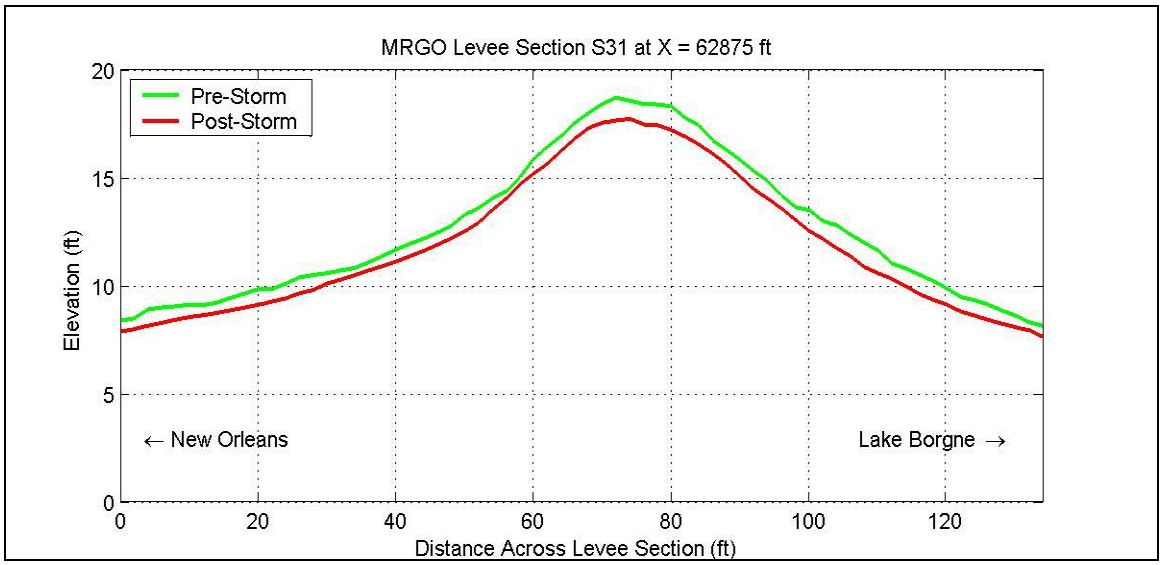


Figure 63. Pre- and post-storm profile showing vertical elevation offset

There is no evidence of any significant accumulation on the front side that might be associated with a large volume of sediment being eroded and deposited at the levee toe or along an adjacent area of intact levee. The only instances of significant accumulation are at Bayous Bienvenue and Dupre, both sites where significant water flowed out of the polder following passage of the storm and transported sediment seaward and caused sediment accumulation.

Figure 62 shows the southeastern 16,000 ft of the levee system. Much less breaching occurred in this region than along the other sections; much more of the levee crest remained intact. Despite the fact that there are breaches, what is notable is the fact that no significant erosion of the front side (no widespread front side erosion spikes), or accumulation, occurred where the levee crest stayed intact. Where the levee crest is intact, the front-side erosion signature is quite uniform and small in magnitude (an artifact of the elevation offset). There are no continuous areas where front side erosion is large and back side erosion is small.

In looking at the volume change data for the entire MRGO Reach 2 levee, there is no compelling evidence that wave-induced front side erosion was a dominant or prevalent factor in levee response. No significant erosion signatures or spikes were evident on the front side in instances when the levee crest was intact and backside eroded volume was small. At sections where the levee crest is intact, there is no large front side erosion of a magnitude that is comparable to magnitude of the front side erosion volume that occurs when the levee crest is degraded. This is particularly evident in Figure 62 where the opportunity for front side erosion was greatest over the longest stretch of levee. Along this reach there was the greatest potential for wave-induced front side erosion because of the longer duration for exposure to front-side wave loading before overtopping began as a consequence of the higher levee crest elevations in this region.

i. Primary Cause for Levee Erosion and Degradation - Rationale

i. Erosion Potential – Front Side Versus Back Side

A previous section of this report discussed the differences in maximum velocity between the front side, crest, and back side of the levees along MRGO Reach 2. The great differences between intermittent maximum velocities of 5 ft/sec on the front side versus the persistent mean velocities of 10, 13 and 25 ft/sec on the back side, for the 16-, 15- and 14-ft levee crest heights that were prevalent between Bayou Dupre and Bayou Bienvenue (see Figure 39), are indicative of the dominance of back-side erosion caused by overtopping/overflow compared to front side erosion caused by wave action. An often-used rule of thumb states that sediment transport is related to velocity raised to the third power (a measure of power in the flow field). Inherent to this rule is a nonlinear relationship between velocity and erosion. Applying this rough rule of thumb to these velocity differences (10/5, 13/5 and 25/5) indicates that erosion potential ("potential" because sediment properties and vegetation cover are also factors) on the levee back side is 8 to 125 times greater than erosion potential on the front side. Velocity differences and potential erosion differences are consistent with the dominance of backside erosion compared to front side erosion as evidenced in the Appendix A photos and Appendix B images of post-storm LIDAR data.

ii. Timing and Magnitude of Back Side and Front Side Erosion

Table 7 shows hydrodynamic loading conditions (water level excluding wave setup, significant wave height and mean wave setup) that are representative for the MRGO Reach 2 levee between Bayou Bienvenue and Bayou Dupre. The levee crest elevation is 15.4 ft, representative of many low spots along MRGO Reach 2. The berm just seaward of the levee toe is assumed to have an elevation of 9 ft. Both incident wave conditions (defined at a location in the MRGO channel) and depth-limited wave heights at the levee toe are shown. Mean overtopping rate was computed using the COULWAVE numerical model. Wave periods during this entire period of time were 4 to 6 sec, higher when wave heights were greatest. Potential for erosion was examined as a function of overtopping rate, using information discussed previously that relates mean overtopping rate to levee damage using current engineering guidance, or in the case of wave-induced erosion, it was calculated using the method of Seijffert and Verheij (1998) assuming average grass cover. The following narrative describes the likely hydrodynamic loading and erosion situation as it unfolded along MRGO Reach 2.

Table 7. Temporal Variation of Hydrodynamic Loading and Potential for Erosion Along the MRGO Reach 2 Levee						
Time, CDT August 29	**Water Level (ft) NAVD 2004.65**	**Incident Wave Height (ft)**	**Wave Height at Levee Toe (ft)**	**Mean Wave Set-up (ft)**	**Mean Overtopping Rate (cfs/ft)**	**Vertical Erosion (ft) Average Grass Cover**
3:00 a.m.	10.1	3	0.7	0.39	0	0.008
3:30 a.m.	10.7	3	1.0	0.39	0	0.016
4:00 a.m.	11.3	3.3	1.4	0.42	0	0.028
4:30 a.m.	12.1	3.6	1.9	0.44	0	0.044
5:00 a.m.	12.9	4.3	2.3	0.38	0.06	0.064
5:30 a.m.	13.9	4.6	2.9	0.31	0.24	0.088
6:00 a.m.	15.5	5.2	3.9	0.55	1.7	0.12
6:30 a.m.	16.8	5.9	4.7	0.48	6.0	0.16
7:00 a.m.	17.5	6.2	5.1	0.28	9.9	0.20
7:30 a.m.	17.5	6.6	5.1	0.3	10.2	0.25
8:00 a.m.	16.9	6.2	4.7	0.48	6.5	0.29
8:30 a.m.	15.9	4.9	4.1	0.56	2.0	0.32
9:00 a.m.	14.5	3.6	3.3	0.25	0.61	0.34
9:30 a.m.	13.1	3	2.5	0.18	0.03	0.34
10:00 a.m.	12.4	2	2	0.19	0	0.35
10:30 a.m.	12.7	2	2	0.13	0	0.35
11:00 a.m.	13.0	2	2	0.03	0	0.36

Between 3:00 a.m. and 4:00 a.m., water level rose from 10.1 ft to 11.3 ft. Rising water steadily flooded the berm seaward of the levee toe. At 4:00 a.m. water depth at the toe was 2.3 ft. The shallow water limited the amount of wave energy that reached the toe and the front face of the levee. Significant wave height at the toe was only 1.4 ft. For a significant wave height of 1.4 ft and periods of 4 to 6 sec, erosion pressure on the levee front face was quite small. Cumulative wave-induced erosion was negligible as seen in computed values. Front side velocities associated with this small amount of wave energy would not have created significant erosion on the levee sections comprised of lean and fat clay. For patches of sand a small amount of erosion might have occurred in response to this wave action.

At 5:00 a.m. the water level had risen to 12.9 ft, half way up the levee front face. Wave action was increasing; significant wave heights at the toe, reaching the levee face, were 2.3 ft. Wave energy reaching the levee face was still limited by the shallow water on the berm. Cumulative vertical erosion due to wave breaking on the cohesive sediment of the levee front face was small, less than 1 inch. Most importantly, at this point in time several hours before the peak surge, waves were beginning to run up the levee face and over the crest, where they were accelerated down the back side. Mean overtopping rates were 0.06 cfs/ft, at the threshold for damage to an earthen levee in current engineering guidance. At patches of more highly erodable sand, some erosion would have occurred in response to the wave action. A mean overtopping rate of 0.06 cfs/ft is 60 times the threshold for damage indicated in current engineering guidance (0.001 cfs/ft) for levees

comprised of poor quality materials. Therefore, sandy or silty sediment would already have begun to be stripped from the back side levee face at these overtopping rates.

At 5:30 a.m. water had risen to a level of 13.9 ft, within 1.5 ft of the levee crest. Wave action is steadily increasing, as the deeper water over the berm allows more of the incident wave energy to reach the levee face. Significant wave heights at the toe were 2.9 ft. At this point in time, more waves were running up and over the crest, and accelerating down the back side; and the number of waves propagating over the crest was steadily increasing as the water level increased. The swash zone was advancing up the front face with the rising water level, but becoming less energetic as more waves were running up and over the crest. The mean overtopping rate was 0.24 cfs/ft, a magnitude that exceeds the damage threshold in current guidance for a high quality, well compacted, clay levee with good grass cover. For levee sections comprised of cohesive clay, erosion on the back side was the dominant erosion mechanism at this point in time, and thereafter. Front side vertical erosion was negligible; cumulative erosion in the surface erosion band was on the order of 1 inch. More erosion of non-cohesive sediments on the front side would have occurred in response to the increased wave action; however the area of greatest erosion would have shifted to the back side. Severe head-cutting and degradation on the back side would have begun for levees with more erodable sediment at this rate of overtopping. Erosion on the back side was now the dominant erosion process, irrespective of sediment type. Once significant overtopping occurred, the velocity regime on the back side was greater than the velocity regime on the front side and it was more persistent and acted on the entire levee back side; so for any type of sediment, the erosion pressure on the back side was greater than erosion pressure on the front side. Back side erosion remained the dominant process once overtopping and overflow began, and it remained that way throughout the rest of the damaging part of the storm. Note that levee sections with lower crest elevations would have experienced this loading situation sooner.

At 6:00 a.m. the water level had risen to 15.5 ft, right at the levee crest. Water levels were rising very rapidly, at a rate of 2.5 to 3 ft/hr. Wave action was steadily increasing as well; significant wave heights at the toe of the levee front face were 3.9 ft. Some of the larger waves passing the toe were breaking on the front face. Some were breaking directly on the crest and some on the back side of the crest. Most waves advanced over the crest and down the back side. Steady overflow began, pulsating with the passage of each wave that propagated over the crest. Breaking waves on the front side continued to erode the clay in the surface erosion band; cumulative erosion was 1.5 inches at this time. This degree of erosion might have been sufficient to remove the grass in places. As a result of many more waves overtopping the levee crest, and the onset of steady overflow, mean overtopping rates increased dramatically, to 1.7 cfs/ft. For this magnitude of overtopping/overflow, many sections of levee were experiencing severe back side erosion, degradation and crest lowering. Head cutting would have been leading to severe breaching. The more erodable sediment degraded at faster rates compared to the more erosion-resistant sediment. Levee sections with lower crest elevations would have experienced this loading and degradation situation sooner.

At 6:30 a.m. the water level had risen to 16.8 ft, 1.4 ft above the levee crest, if the crest had not already been degraded to a lower elevation. Wave heights were increasing, and significant wave heights at the toe of the levee were 4.7 ft. Hydrodynamic loadings on the levee at this time would have been much like those seen in the video of the laboratory-scale tests. Considerable wave breaking directly on the crest and back side of the crest was occurring, dramatically exacerbating erosion of the crest and back side. Steady overflow was occurring, and pulsating with every wave. Each wave was passing over the crest and accelerating down the back side. At a freeboard value of -1.4 ft, massive overflow was occurring, at a rate of 6 cfs/ft. Severe degradation and breaching was taking place at erodable areas, with levee crest being lowered and breaches growing deeper and wider. And, the peak water level and wave conditions had yet to occur. Levee sections with lower crest elevations would have experienced these loading and degradation conditions sooner.

In the 7:00 to 7:30 time frame, storm surge reached its peak level of 17.5 feet, and wave conditions reached maximum values of approximately 5 ft at the toe. Mean overtopping rates reached levels of more than 10 cfs/ft, off the damage chart in Figure 56. Assuming that the levee crest would degrade to a crest elevation of 10 ft, mean overtopping rates of 40 cfs/ft would have occurred at this crest elevation.

To provide some perspective on the magnitudes of overflow being discussed here, 40 cfs/ft entering a square plot of land one acre in size behind the levee would inundate the area to a depth of 6 ft in only 30 seconds. In its degrading and degraded state, this magnitude of overtopping was occurring along miles of levee from Bayou Bienvenue to Bayou Dupre. At rates of 10 cfs/ft, 2 cfs/ft and 1 cfs/ft, the same area would fill to a depth of 6 ft in 2, 10 and 20 minutes, respectively.

The self-reinforcing process of levee destruction due to overflow, and increases in overflow created by a degrading levee crest, was in full force. This process occurred for hours as the levees continued to degrade. It continued until surge levels in Lake Borgne dropped below levels in the inundated St. Bernard polder, that afternoon.

This realistic scenario illustrates the dominance of overtopping and overflow in the degradation of the MRGO Reach 2 levee, and its subsequent role in flooding of the St. Bernard polder.

iii. Visual Evidence

If the severe levee degradation that was observed was predominantly caused by wave-induced front side erosion initiated lower on the levee face prior to overtopping, one would expect to see intermediate stages of the process along large stretches of levee captured in the photos, particularly those where extensive erosion is evident on the back side. Intermediate stages of extensive front-side erosion are never evident in these instances.

A noticeable observation was the very large number of photos that showed evidence of significant erosion on the back side, even significant head-cuts just up to the levee crest, but with absolutely no evidence at all of any significant front-side wave-induced erosion other than the surface erosion band. The band is often visible, but the surface erosion band does not reflect significant vertical or horizontal erosion. Figures 64, 65 and 66 from Appendix A show examples where the dominance of backside erosion is clearly evident. The surface erosion band is evident in each of the three photos. In Figure 66, considerable backside degradation has occurred, with relatively little evidence of significant erosion on the front side. The surface erosion band is less pronounced in Figure 66 compared to Figure 64. Despite the apparent increased resistance to erosion on the front side in Figure 66, the erosion on the backside is considerable and prevalent. Head-cuts in various stages of advance toward the levee crest are evident. The hydrodynamic loadings were certainly imposed on the front side prior to and during overtopping. The minor surface erosion band is clearly evident in some cases, but there are no occurrences of pervasive deeper bench-cuts on the front side.



Figure 64. Post-storm photo illustrating dominance of back side erosion compared to front side erosion.



Figure 65. Post-storm photo illustrating dominance of back side erosion compared to front side erosion.



Figure 66. Post-storm photo illustrating dominance of back side erosion compared to front side erosion.

On the back side, erosion signatures are much more severe and much more widespread. Note that the levee crest is intact, without loss of vegetation, along most of the levee in each photo, despite erosion on both front and/or back sides. These three figures, and many others in Appendix A, suggest that the minor surface erosion zone occurred on the front side; then overtopping and head-cutting occurred and dominated the process, often producing considerable back-side erosion like that shown in Figure 66. Head cutting eventually migrated to, and sometimes through, the zone of surface erosion on the front face. Several occurrences of this are seen in Figure 66.

The leading edge (closest to the front side) of the head-cuts that formed in the primarily clayey cohesive sediment levees along MRGO Reach 2 are very steep and slope downward from the front side toward the back side. Conversely, the leading edge (closest to the front side) on wave-induced bench cuts slopes upward from the front side toward the back side and the slope is less steep (see Figure 52). The dominant mode of erosion usually can be distinguished by the characteristics of the leading edge on the erosion feature. Figure 67 shows levee response dominated by advanced head cuts. The head cuts in the foreground illustrate the steep leading edges. The center region of the photo in Figure 67 illustrates the dominance of back-side erosion compared to front side erosion. Note the appearance of a minor wave-induced bench cut in the center of the photo, and its small size relative to the other erosion features visible in the photo. Head cuts on the back side are much more advanced and severe than front-side erosion at the very same location. Figure 68 illustrates many of the same points and it also shows clean leading-edge cuts right in the middle of the minor surface erosion band on the front side.

When significant wave-induced bench cutting is evident on the front side, it is seen near the upper part of the front levee face (for example, see center of Figure 67). The cuts are isolated, discrete pockets of erosion; they are relatively small in size. A few photos show isolated instances where severe wave-induced bench cuts on the front side extended into and through the levee crest, triggering overtopping. Figures 69 and 70 are examples.

Note that the bench cuts are isolated erosion features and are not widespread deep erosion zones that extend for great distances along the levee like the band of minor surface erosion. Also note that if sediments are erodable enough to lead to bench-cutting on the front side, then as soon as overtopping occurs and there is flow through the cut and down the backside, backside erosion of these same highly erodable sediments will quickly become the dominant erosion mechanism because of the much higher velocity regime on the backside compared to the front side.



Figure 67. Examples of advanced states of head-cut migration (of the leading edge) to and through the zone of wave-induced surface erosion on the levee front side.



Figure 68. Examples of advanced states of head-cut migration (of the leading edge) to and through the zone of wave-induced surface erosion on the levee front side.



Figure 69. Example of a front side wave-induced head-cut that extends into and through the levee crest. Cut lead to minor overtopping and overwash of sediment.



Figure 70. Example of a front side wave-induced head-cut that extends into and through the levee crest. Cut lead to minor overtopping and overwash of sediment.

As discussed previously, the most severe wave-induced bench cuts on the front side formed later in the storm, at higher elevations on the levee where the potential for front side erosion was maximized and overtopping was minimized. The two cuts shown in Figures 69 and 70 appear to fall into this category; neither cut lead to significant overtopping or an advanced stage of levee degradation. These two cuts are among the very few that are evident in the Appendix A photos; and they are among the most severe front-side cuts seen in any of the photos. These cuts occur at higher levees where there has been little damage due to overtopping or overflow.

If the wave-induced bench cutting mechanism was a predominant cause for levee erosion and degradation along the Reach 2, one would expect to see them much more often in the set of photos in Appendix A, in various stages of development, widespread and not isolated features. Their isolated occurrence suggests they are related to patches of highly non-cohesive sediments.

If front side wave-induced erosion was a dominant mode of erosion, one would expect to see deposits of sediment on the front side slope, at the levee toe, and seaward of the levee toe associated with sediment moved offshore due to wave breaking and undertow associated with breaking waves which would act to transport the sediment offshore. This was not evident in the volume change analysis discussed in a previous section. In the entire set of Appendix A photos, there were never significant sediment deposits evident on the front side of levees that did not appear to be features (erosion or depositional in origin) associated with return flow toward Lake Borgne, which exited the St. Bernard polder following passage of the storm. In the vast majority of photos, any significant sediment deposits were always observed on the backside, indicating that overtopping and transport of sediments landward was the dominant erosion and levee degradation process. None of the Figures 64 through 74 show any accumulation of sediment near or on the front side toe, or seaward of the surface erosion band, even in areas where considerable erosion and degradation of the levee has taken place. Each photo shows large fan-shaped sediment depositional features on the back side indicating the dominance of back side sediment erosion and transport, but no significant depositional features on the front side.

Figures 72 through 74 show no pronounced signature of wave-induced surface erosion band on the front side (only traces in Figure 73 and none in Figures 72 and 74). The grass and sediment properties at these sites were capable of resisting wave-induced erosion on the front side, but the back side suffered severe erosion and degradation. These three figures show the dominance of erosion on the back side due to overtopping/overflow compared to wave-induced front side erosion.



Figure 71. Example showing widespread levee crest degradation with no evidence of sediment deposited at the front side levee toe. Note large back side deposition.



Figure 72. Example showing levee crest degradation with no evidence of sediment deposited at the front side levee toe. Note extensive back side deposits.



Figure 73. Example showing widespread levee crest degradation with no evidence of sediment deposited at the front side levee toe. Note extensive back side deposits.



Figure 74. Example showing widespread levee crest degradation with no evidence of sediment deposited at the front side levee toe. Note extensive back side deposits.

Figure 72 shows evidence of water that flowed out following the storm through one of the more severe breach cuts, traces of a fan-shaped sediment deposit in the upper left hand side of the photo. Additional scour and erosion at the very lowest spots on the degraded MRGO Reach 2 levees occurred during outflow of water back toward Lake Borgne following passage of the hurricane. Once the storm center passed north of Lake Borgne, winds directions shifted rapidly, changing to directions blowing from the west. As this occurred water levels in Lake Borgne dropped. The combination of winds blowing from the west and decreasing water levels in Lake Borgne lead to flow toward the east, back out of the flooded St. Bernard polder. Flow would have sought out and been concentrated in the lowest spots on the degraded levee. As water levels steadily dropped, the out-flowing water would have been increasingly confined to the lowest elevations on the damaged levees, i.e., the most severe breaches. Less severe breaches probably did not capture much if any return flow, or if they did not for very long. Out-flowing water would have exacerbated erosion in the deepest cuts.

Figures 75 (foreground of the photo) and 76 (several places) show evidence of water flowing back out through several severe breaches. One signature is sediment deposits formed on the flood side of the levees directly seaward of the outflow channels (see trace signatures in Figure 72 and Figure 76). These are not locations where front side erosion was a dominant process. A second signature is the clean arc-shaped edges of the breach channels formed by exiting flow. Several outflow channels seen in Figures 75 and 76 have a nozzle-like shape to them and clean well-defined arc-shaped edges, which indicate exiting flow converging into a constricted channel, flow through the breach channel, and then expanding once flow exits the constricted channel. Sediment deposits in the left foreground of Figure 76 also show this pattern of expanding flow on the outboard side. Any overflow-induced head cuts on the flood side that were created initially by the storm appear to have been have been eroded and destroyed by the exiting flow. Head cuts are evident on the back side of the levee. These cuts were formed by the exiting water. Also note evidence of sediments deposited on the levee back side, opposite each of the major breach channels. These deposits were formed by overtopping/overflow and subsequent sediment overwash processes that occurred early during the peak of the storm, before flow exited the polder following the storm.



Figure 75. Example showing severe levee degradation with no evidence of sediment deposited at the front side toe (upper part of photo). Note extensive back side deposits.



Figure 76. Example showing signatures of water flow exiting the flooded St. Bernard polder though low spots on the degraded levee.

V. Erosion at Floodwalls

a. Overtopping Jet and Fluid Velocities

Another type of situation of levee degradation (and wall failure in places) was overtopping of a floodwall and erosion of the earthen surface on the backside. Figure 77 shows the computed speed of a plunging jet (for a steady overflow case, no waves) that would impact the earthen surface on the protected side as a function of height of the wall crest above the earthen surface on the protected side and the height of the surge level above the crest of the wall. The computations neglect the presence of wave action. The circle in the figure shows the range of conditions that were generally prevalent for floodwalls of the hurricane protection system and the degree of overtopping that occurred during Katrina, in the region of interest. In general the distance between wall crest and the ground surface on the backside was 6 ft, by design. Some available information showed differences of nearly 8 ft, and some showed differences less than 6 ft. Water velocities at impact associated with steady overflow from these elevations are expected to exceed 15 ft/sec, and between 25 and 30 ft/sec for greater fall distances.

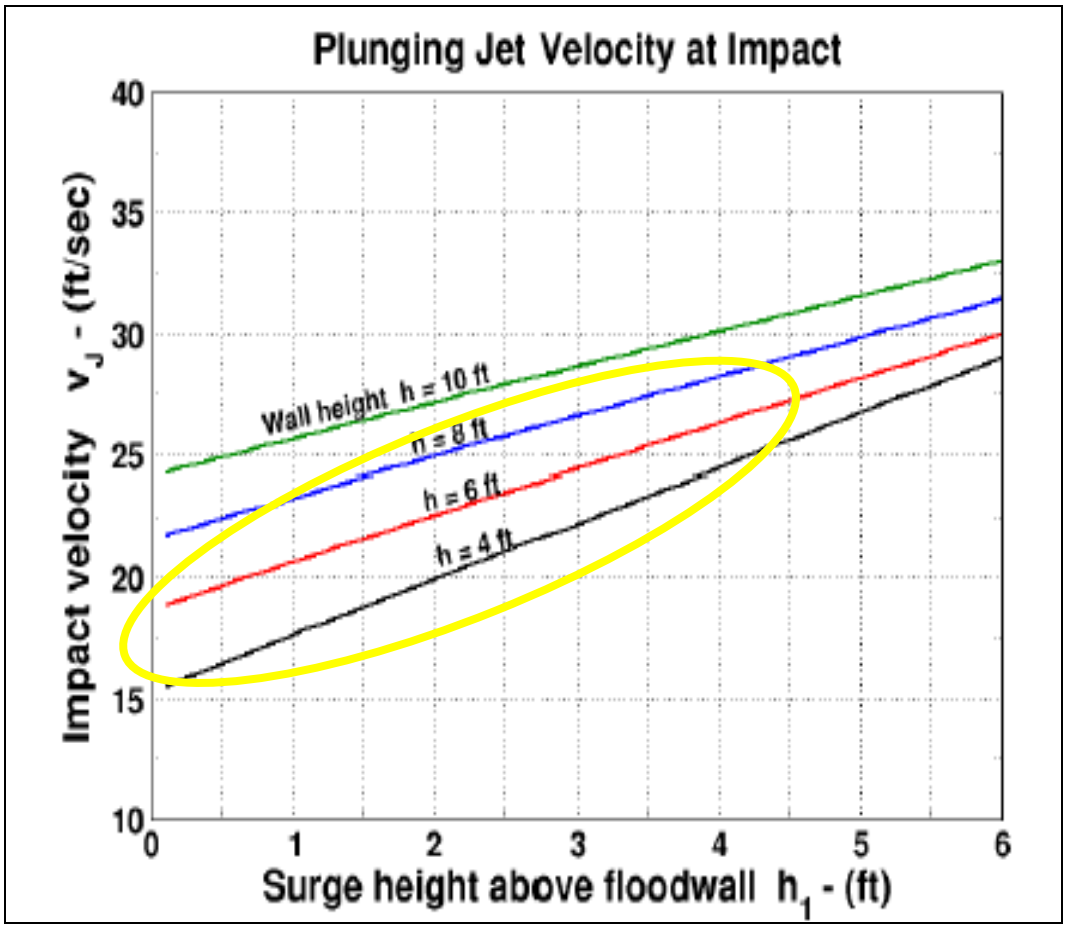


Figure 77. Impact velocity associated with steady overtopping of a floodwall, as a function of wall height and surge height above the wall

The overtopping jet tends to strike the earthen surface normal to a flat earthen surface, or nearly so, velocities produced by the jet have more erosion potential than comparable velocities that are directed parallel to a levee surface. The presence of waves can increase overtopping velocities and the speed of the jet which impacts the earthen surface during the passage of each wave. Waves can cause the point at which the overtopping jet impacts the ground to extend further from the wall; and the position where the overtopping jet impacts the ground surface migrates back and forth with each passing wave. The presence of waves can also change the angle at which the jet interacts with the levee surface.

b. Erosion Due to Overtopping

Figure 78 illustrates flow over a floodwall and plunging (in this case) of a jet that is directed into standing water on the protected side of the floodwall. The plunging jet penetrates the water and creates large eddies that erode material from the unprotected soil surface. The same mechanism will scour bed material when there is not standing water on the protected side of the floodwall. Eroded material is thrown into suspension and carried away by the turbulent flow. This scouring action removes material that may be providing critical lateral support on the protected side of the floodwall. Failure can occur due to scour if the remaining levee foundation adjacent to the wall cannot withstand either the shear/normal forces exerted by the jet or is insufficient to counterbalance the overturning moment exerted on the flood side of the floodwall by the elevated water and waves, if present.

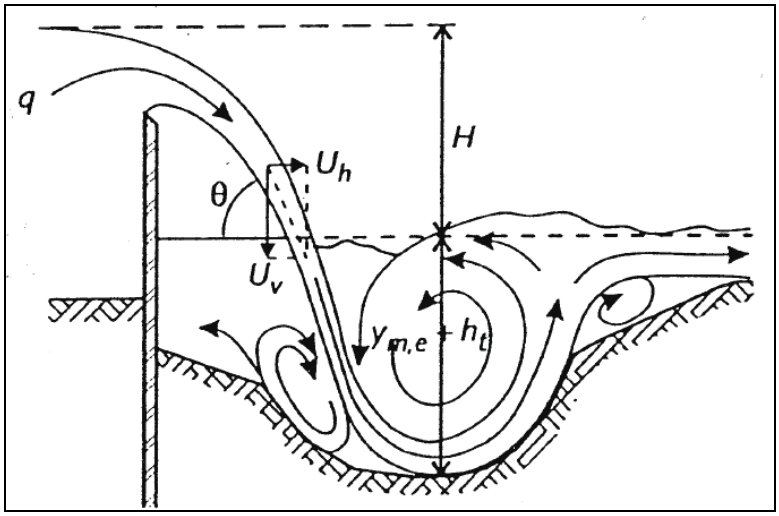


Figure 78. Scour hole formation by overtopping jet (from Hoffmans and Verheij 1997)

Total collapse of a floodwall section allows a large volume of water to flow into the protected region through the resulting breach, and this may cause adjacent wall sections to fail and enlarge the breach. Localized partial failure includes tilting of the floodwall so gaps open up between the dislodged section and adjacent undamaged floodwall. Provided the wall does not tilt farther, it still affords some degree of flood protection. However, the wall top elevation is decreased by tilting, and the overflowing water jet will be directed on foundation soil farther away from the wall that could increase the scour hole width. During Katrina, scour hole formation and wall failures of varying degrees occurred at numerous locations along the hurricane protection system. As the scour hole deepens, the fall distance of the overtopping jet increases, which can increase the velocity at impact and exacerbate the scour.

Figure 79 shows photos taken at several locations along the hurricane protection system of southeastern Louisiana following Hurricane Katrina. Figures 79a and 79b show scour hole formation at locations along the Inner Harbor Navigation Canal where waves were relatively small. The width of the scour hole is relatively small, compared to that seen in the other photos. If no waves are present, the overtopping jet can be sucked against the wall, restricting the scour hole to a short distance away from the wall. Figures 79c and 79d were from a wall section that was subjected to overtopping for several hours along the Gulf Intracoastal Waterway. Figures 79e and 79f show scour hole formation behind walls along the MRGO Reach 2 levee/wall system. The width of the scour hole is wider here than at the other locations, due to the greater influence of wave action. Figures 80 through 83 from Appendix A show stretches of overtopped wall, in varying states and stages of failure, which occurred along MRGO Reach 2. Note the very wide scour hole which forms on the back side along the entire length of overtopped wall due to the overtopping jet. Also note the severe buckling of the sheet pile wall as it became unstable, as well as the complete wall failures that lead to localized braches through the hurricane protection system. Figure 82 shows sheet pile walls at a breach, which are turned outward toward the MRGO. Floodwater which exited the inundated polder, following passage of the storm out of the region, turned the sheets outward.



Figure 79. Back side scour trenches along the Southeastern Louisiana hurricane protection system caused by overtopping and overflow during Hurricane Katrina.



Figure 80. Overtopped and partially failed sheet-pile wall just south of Bayou Bienvenue



Figure 81. Overtopped and completely failed sheet-pile wall south of Bayou Bienvenue

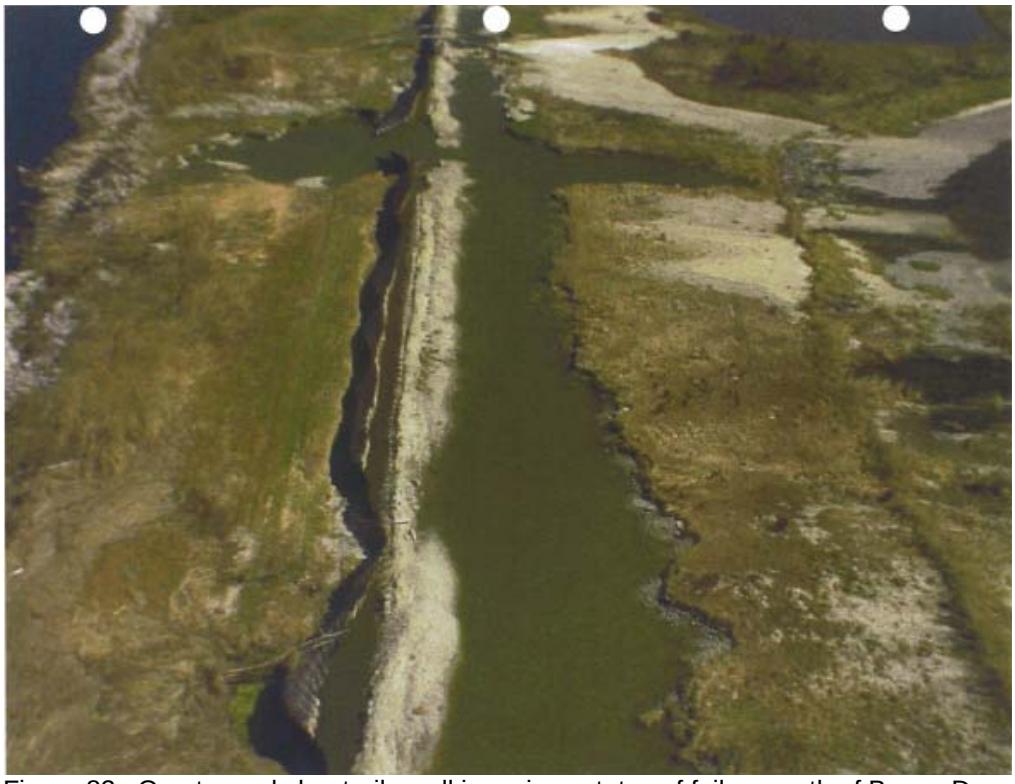


Figure 82. Overtopped sheet-pile wall in various states of failure north of Bayou Dupre



Figure 83. Overtopped and partially failed sheet-pile wall near southern end of levee along MRGO Reach 2

VI. Influence of the MRGO on the Critical Levee and Wall Breaches

a. Major Sources of Floodwater into the St. Bernard Polder

Hurricane Katrina produced unparalleled wave and storm surge conditions for the New Orleans vicinity. Katrina was a very large Category 3 storm (on the Saffir-Simpson wind intensity scale) when it passed the New Orleans area on the morning of 29 August 2005. Twenty-four hours earlier this storm had been the largest Category 5 and most intense storm on record (in terms of central pressure), within the northern Gulf of Mexico. Due east of the Mississippi River delta, a deepwater National Oceanic and Atmospheric Administration (NOAA) buoy recorded the highest significant wave height (55 ft) ever measured in the Gulf of Mexico. The large size of Katrina throughout its history, combined with the extreme waves generated during its most intense phase, enabled this storm to produce the largest storm surges (reliable observations up to 28 ft) that have ever been observed within the Gulf of Mexico, as determined from analyses of historical records. As another example of Katrina's strength in terms of storm surge, the previous highest high-water mark (HWM) from Hurricane Camille was 24.6 ft; Camille is the only Category 5 storm to make landfall in the Gulf of Mexico over the interval that records have been kept, approximately 150 years (IPET, 2006).

Along the exposed eastern side of the hurricane protection system surrounding the St. Bernard polder, the reach adjacent to the Mississippi River Gulf Outlet (referred to here as the MRGO Reach 2 levee), Katrina produced maximum storm surge levels of 17.5 to 18.3 ft which overwhelmed the levee and walls. These peak water levels exceeded, by nearly 5 ft, those for which this levee reach was designed. Design water levels were 12.9 to 13.4 ft. Wave conditions created by Katrina along this levee reach were characterized by significant wave heights of 6 to 7 ft and mean wave periods of 5 to 6 sec. These wave conditions were quite similar to those factored into the levee's design, wave heights of 6.6 to 7 ft and periods of 6.2 to 6.4 sec. But the extreme storm surge created by Katrina completely overwhelmed this reach of the levee/wall system, exceeding levee and wall crests by up to 4 ft in places. Within the Inner Harbor Navigation Canal (IHNC), Katrina generated maximum water levels of 14.3 to 15.4 ft, which exceeded the design water level of 13.5 ft by approximately 1 to 2 ft. Katrina's storm surge also overwhelmed this part of the hurricane protection system.

The video file provided by the Plaintiff's experts Kok et al. (2007), entitled "*St Bernard (24h in 1.36 min).avi*," is an animation of simulated interior flooding within the St. Bernard polder during Katrina, for levee and wall conditions as they existed at the time of the storm. The animation illustrates the most important aspects of the flooding and inundation process. While some details in the simulation made by Kok et al. (2007) are incorrect, the "big picture" is accurately portrayed.

One series of events occurred along the east side of the IHNC, wall failures which lead to two breaches (locations of both are shown in Figure 84) and entry of flood water

into the Lower 9th Ward. The north breach happened first, very early in the morning of August 29; the south breach happened several hours later. These events lead to substantial early flooding in the westernmost region of the polder. Flooding in the Lower 9th Ward could be generally characterized as early flooding due to water which entered through the IHNC breaches and more massive flooding later due to water that originated along the MRGO Reach 2.

This second, and most important, series of events were the severe levee erosion, degradation and subsequent widespread breaching that occurred between Bayou Bienvenue and Bayou Dupre, and south of Bayou Dupre (the many breach locations are shown in Figure 84). Levee degradation and breaching along the MRGO Reach 2 created a very large source of flood water which propagated across the Central Wetlands region between the hurricane protection system levees and the interior 40-Arpent levee which surrounded the heavily populated areas. This water eventually flowed over the 40-Arpent levee and flooded the entire Chalmette area including the Lower 9th Ward. This was, by far, the greatest source of flood water that entered the polder, greatly exceeding all other sources. The majority of this water came through breaches in the levee/wall system between Bayou Bienvenue and Bayou Dupre. This source of water led to massive and widespread inundation throughout the polder, reaching water surface elevations of 11ft NAVD88 2004.65 throughout the more heavily populated areas. These water levels created inundation of up to 17 ft in the lowest areas of the polder that were below sea level.

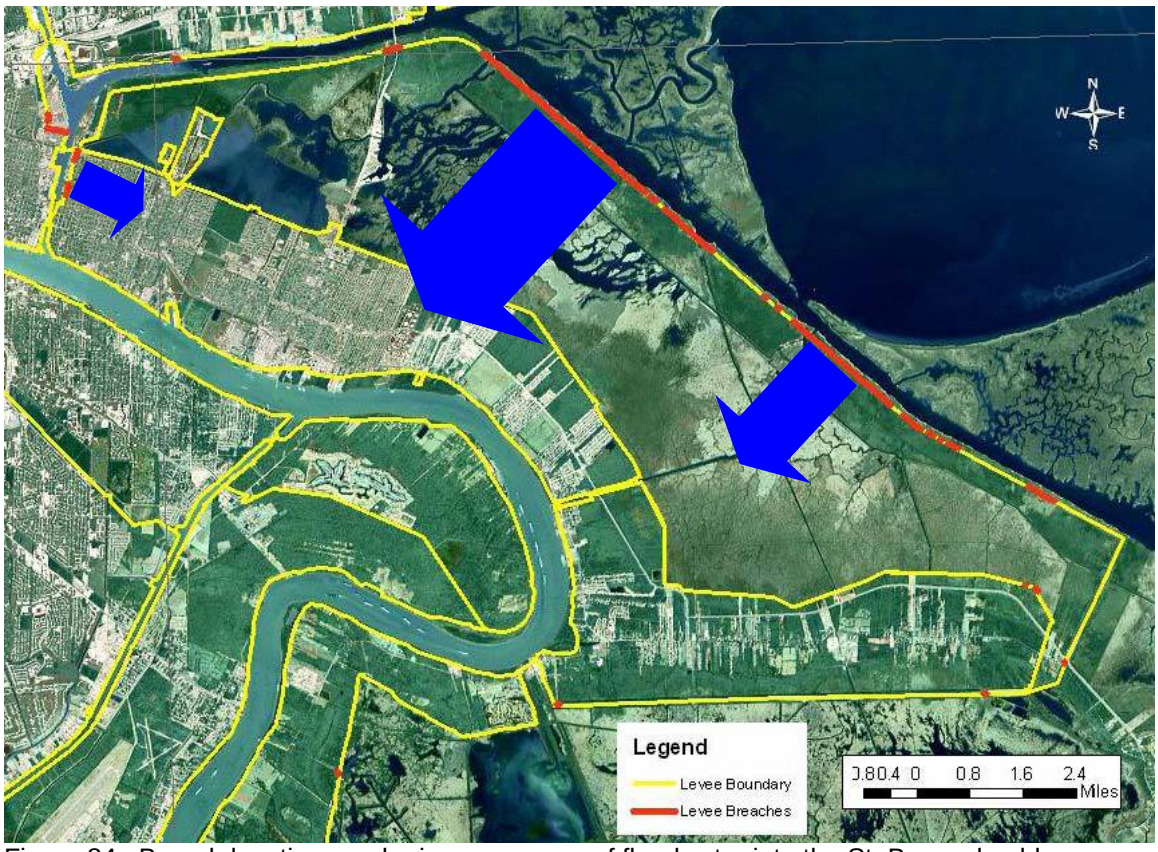


Figure 84. Breach locations and primary sources of floodwater into the St. Bernard polder

There were other sources of flood water which entered the St. Bernard polder around its periphery, and they are addressed in much greater detail in the interior inundation modeling that was done and is described in the expert report by Fitzgerald (2008); but these were less signficant sources of water compared to the major sources of water introduced by these two series of events.

The role of the MRGO was examined in terms of how it might have altered water levels, wave conditions, velocities and overtopping rates along key areas of the periphery of the St. Bernard polder, both along the MRGO Reach 2 levee and along the flood wall on the eastern side of the IHNC adjacent to the Lower 9th Ward. The analysis was done using numerical storm surge and wave models, applied to various hypothetical cases, to make the assessment of changes to hydrodynamic loading conditions. In light of changes to loadings, differences in damage to the levees and walls at the primary breach locations were examined, and inferences were drawn regarding how the MRGO might have influenced levee/wall responses at these critical locations. The following cases were examined in this report:

1) Case H1 (Base Case): occurrence of Katrina for the levee and MRGO channel and wetland conditions that existing at the time the hurricane struck on August 29, 2005.

2) Case H2: occurrence of Katrina for a hypothetical condition that assumes the MRGO navigation channel did not exist, wetlands were in their 2005 condition, with the LPV levees/walls at their pre-Katrina locations and actual elevations. This case was designed to examine any direct effect of the MRGO channel itself.

3) Case H3: occurrence of Katrina for a hypothetical condition that assumes the MRGO navigation channel did not exist, wetlands were in their pre-MRGO condition (1958), with the LPV levees/walls at their pre-Katrina locations and actual elevations. This case was designed to examine both the direct effects of the MRGO channel and effects of changes to wetlands that have occurred since MRGO construction.

4) Case H5: occurrence of Katrina for a hypothetical condition that assumes the MRGO navigation channel was at its authorized dimensions (eliminating effects of side bank erosion and changes to cross-sectional area that have occurred), wetlands were in their 2005 condition, with the LPV levees/walls at their pre-Katrina locations and actual elevations.

5) Case H6: occurrence of Katrina for a hypothetical condition that assumes the MRGO navigation channel was at its authorized dimensions (eliminating effects of side bank erosion and changes to cross-sectional area that have occurred), wetlands were in their pre-MRGO condition (1958), with the LPV levees/walls at their pre-Katrina locations and actual elevations.

b. Breaching of the MRGO Reach 2 Levees and Walls

Analysis of photographic evidence; analysis of core log data, levee response and estimated freeboard conditions at peak water levels; analysis of numerical modeling results and calculations; as well as insights regarding coastal processes, led to the conclusion that wave overtopping and overflow were the most important processes in the destruction of the levee along MRGO Reach 2. The degradation process was driven by initiation of surface erosion on the levee back side due to wave overtopping and then steady overflow, subsequent formation of severe back side head-cuts, migration of those head-cuts to and through the levee crest, forming breaches, and then deepening and widening of the breaches as more and more water flowed through and over them in a self-reinforcing process. Floodwalls along the levee also were damaged and breached due to severe overtopping and overflow, and by the very high velocities which eroded the levee surface on the back side. In addition to magnitude of loading associated with overtopping/overflow, the degree of damage also was influenced by the duration of loading, quality of grass cover and properties of sediment comprising the levee (i.e. resistance to erosion). While the levee along MRGO Reach 2 was comprised primarily of lean and fat clay, there were pockets of silty and sandy soils present at some of the locations where core samples were acquired.

Levee erosion on the backside due to wave-induced overtopping began early in the morning on August 29, 2005. Once the mean water surface rose to within 3 to 3.5 ft of the levee crest, wave-induced overtopping began and mean overtopping rates reached levels of 0.01 to 0.04 cfs/ft. Once overtopping rates exceeded values of 0.001 to 0.01 cfs/ft; levee sections comprised of poor quality sandy and silty sediment and/or poor grass cover began to erode on the back side in response to the overtopping. As water levels rose and wave energy increased, and overtopping rates exceeded 0.1 cfs/ft, erosion increased.

More severe erosion of the levee occurred as the mean water level rose to within 1 to 0.5 ft of the levee crest and overtopping rates approached 1 cfs/ft. Rates of 1 cfs/ft were very damaging for levee sections comprised of more highly erodable silty and sandy soils, damaging for levee sections comprised of lean clay, but perhaps not so for those sections that had very good grass cover and were comprised of the most highly erosion-resistant fat clays. As water levels reached the levee crest, overtopping rates reached very damaging levels, 2 cfs/ft; and steady overflow began shortly thereafter in addition to wave overtopping. As the surge rose higher and mean water levels exceeded levee crests by 1 ft, mean overtopping rates approached 3 cfs/ft. Available information indicates that lean clay levees were severely degraded and breached under this magnitude of loading. The only levees which survived overtopping rates on the order of 1 to 2 cfs/ft were those that were higher (which would have reduced the magnitude and duration of overtopping and overflow), had very good grass cover, and were comprised of highly erosion-resistant fat clay.

Figure 85 shows results from overtopping simulator tests conducted in the Netherlands for a bare levee surface comprised of good clay, being eroded in response to

simulated wave overtopping (see EurOtop, 2007). The high level of turbulence on the back side is apparent. Mean overtopping conditions of approximately 0.001, 0.01, 0.05 and finally 0.1 cfs/ft were imposed on the levee test section, for 6 hours each. Erosion damage started for the first condition (two erosion holes) and increased during the other overtopping conditions. After 6 hours of testing at a mean discharge of 0.1 cfs/ft, there were two large erosion holes, about 3 ft deep, 3 ft wide and 13 ft long. This situation was considered as "not too far from initial breaching" (EurOtop 2007). One can envision just how severe erosion would have been for a levee comprised of more erodable sandy or silty sediment under a loading of 0.1 cfs/ft, compared to the good clay at this field site. A mean overtopping rate of 0.1 cfs/ft is the threshold for damage to a high quality clay levee that has been adopted in current engineering guidance. Typical low spots along the MRGO Reach 2 levee during Katrina were subjected to mean overtopping rates in excess of 1 cfs/ft (10 times the amount used in this erosion test) for 3 hours, and they reached and exceeded 10 cfs in many places (these durations assume no levee degradation). In light of the amount of levee degradation and crest lowering that actually took place along MRGO Reach 2, overtopping rates exceeded 1 cfs/ft for up to 10 hours, until water levels in Lake Borgne dropped below those in the flooded polder.



Figure 85. Test to examine erosion of a bare clay levee in response to simulated wave overtopping.

Once overflow of the levee crest commenced a devastating feedback process began, in which lowering of the crest increased the amount of overflow, which then caused more erosion and degradation, additional lowering of the crest, and so on. Weighted-average maximum overtopping/overflow rates exceeded 5 cfs/ft along much of the levee between Bayou Bienvenue and Bayou Dupre (rates of 10 to 20 cfs occurred at the low spots), where levees were severely degraded. Data indicate that even more erosion-resistant fat clays deeper into the levee eroded under the action of these higher overflow rates, which reached 40 cfs/ft for levees whose crests were lowered to 11 ft. This self-reinforcing and self-perpetuating process lasted for hours, until water levels in Lake Borgne began to drop below those in the inundated St. Bernard polder, that afternoon. High overflow rates, and the resulting high-speed jets of water which impinged on the earthen surface on the back side, caused walls to buckle, rotate and fail, and split apart to form breaches in places. Figures 86 through 91 show the aftermath of this destructive process along MRGO Reach 2.



Figure 86. Reach of levee between Bayou Bienvenue and Bayou Dupre that was severely degraded and damaged in places due to wave overtopping and overflow.



Figure 87. Reach of levee between Bayou Bienvenue and Bayou Dupre that was severely degraded and damaged in places due to wave overtopping and overflow.



Figure 88. Reach of levee southeast of Bayou Dupre that was severely degraded and damaged due to wave overtopping and overflow.



Figure 89. Reach of levee southeast of Bayou Dupre that was severely degraded and damaged due to wave overtopping and overflow.



Figure 90. Reach of levee southeast of Bayou Dupre that was damaged due to wave overtopping and overflow.



Figure 91. Reach of levee southeast of Bayou Dupre that was damaged due to wave overtopping and overflow.

Previous analyses showed that the most important variable influencing overtopping/overflow and levee response was maximum mean water level, through its influence on freeboard. Analysis of overtopping/overflow rates as a function of freeboard, and current engineering guidance for the onset of damage to earthen levees, showed that when the mean water level rose 1 ft or more above the crest, levees were subjected to very damaging overflow conditions of 3 cfs/ft, irrespective of any wave effects. The presence of waves made the arrival of damaging overtopping conditions occur sooner, and waves increased overtopping rates up to the point where water level was 1 ft above the levee crest. At that point, overflow rate became dominated by the water level; and the contribution of waves became increasingly less important for water levels that were more than 1 ft above the levee crest.

In light of the prime importance of maximum mean water level on levee degradation and breaching, one very important issue is how the MRGO influenced the spatial distribution of maximum water level along the MRGO Reach 2 levee for the various cases. Figure 92 shows the variation in maximum total mean water level along the levee, for the Base Case, H1, and the other cases, H2, H3, H5 and H6. Maximum wave set-up right at the levee is included in these water levels. Complete removal of the MRGO channel (cases H2 and H3) had a very small effect on peak water levels along the entire MRGO Reach 2 levee. On average, maximum water levels were 0.2 to 0.3 ft less along MRGO Reach 2 for Cases H2 and H3, compared to the Base Case.

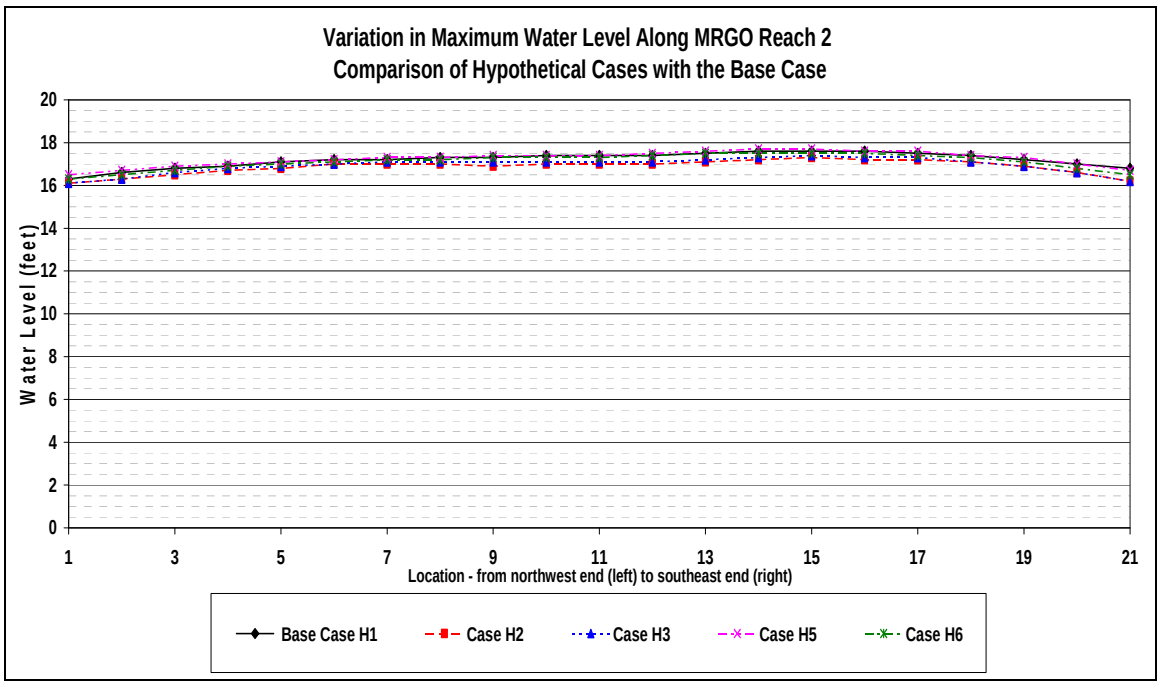


Figure 92. Along-levee variability in maximum mean water level for all cases

These results are consistent with previous findings of URS (2006) and IPET (2006) regarding the role of the Reach 2 channel on hurricane surge along this levee. Those two studies also concluded that Reach 2 of the MRGO channel had a very small effect on storm surge conditions along the MRGO Reach 2 levee of the St. Bernard polder during Katrina. To put these small water level changes in perspective, differences of 0.3 ft are less than 4 inches of change relative to a maximum storm surge that reached 17.5 to 18.3 ft along this levee (a change of less than 2%).

Comparing differences in maximum water levels for cases H2 (2005 wetland condition) and H3 (1958 wetland condition), differences are seen to be even smaller. The greatest differences are only 0.1 ft (changes of less than 1% of the peak water level). The storm surge built up against the MRGO Reach 2 levee primarily due to winds blowing from the east and east-northeast, driving water through Lake Borgne and over the inundated wetlands. The predominant momentum balance between wind shear stress and water surface slope within Lake Borgne shows this clearly, as do snap-shots of wind vectors and water surface elevations for the region (Figures 5 through 9). The small differences between H2 and H3 results indicate the negligible influence of differences in wetland condition on the storm surge and maximum water levels along the MRGO Reach 2 levee. The storm surge is a long wave. Frictional influence on its propagation and amplitude is relatively small at this location; and fictional effects of the wetland decreased as the storm surge rose. The regional storm surge created by Katrina was quite high, greatly exceeding the elevation of marsh vegetation in the Lake Borgne vicinity. For all these reasons, the wetland changes that occurred between 1958 and 2005, and changes in frictional influence associated with these wetland changes, had a negligible

effect on generation of the storm surge at this location during Katrina. The storm surge modeling for the various cases is described more completely in the expert report by Westerink (2008).

For Cases H5 and H6, in which the MRGO cross-section was modified from its actual pre-Katrina cross-section to its design cross-section, changes in maximum water level were negligible, 0.1 ft or less compared to the Base, south of Bayou Bienvenue. Results indicate that widening of the MRGO channel and changes to cross-sectional area that have occurred through time since its construction had very little effect on maximum water levels along the MRGO Reach 2 levee. The very small differences between cases H5 (2005 wetland condition) and H6 (1958 wetland condition) also indicate the negligible influence (0.1 ft or less) of wetland condition on maximum water levels along the MRGO Reach 2 levee.

Figure 93 provides perspective on how the different cases influenced the spatial variation in the very important parameter, freeboard (difference between the levee crest elevation and the maximum mean water surface elevation), along the MRGO Reach 2 levee. The figure shows the along-levee variation of both crest elevation (pre- and post-storm data) and maximum mean water surface elevation. Maximum mean water level for the Base Case, H1, is shown as a back solid line. The dashed black line is approximately 0.3 ft less, on average, than the line for the Base Case; this curve represents results for complete removal of the MRGO, cases H2 and H3. Results for Cases H5 and H6 are closer to the Base Case result.

Wherever the maximum water level equaled the levee crest elevation, damaging overtopping/overflow occurred (mean overtopping rates of 2 cfs/ft and greater). For cases H2 and H3, involving complete removal of the MRGO, there was a very small reduction in length of levee where the water level exceeded the levee crest. Between Bayou Bienvenue (located at a distance of zero) and Bayou Dupre (located at a distance of 34,000 ft), changes were negligible. This reach of levee was the lowest and most vulnerable to breaching along the MRGO Reach 2 levee. Figure 93 shows that overflow conditions along this critical reach were relatively unaffected by small changes in maximum mean water level. It was through this reach that the majority of flood water entered the St. Bernard polder.

In light of the negligible differences (0.1 ft or less) in maximum water level cited above for cases H5 and H6, relative to the Base Case, there was essentially no change in the length of levee for which overflow occurred, that can be attributed to the changes in MRGO cross-section that have occurred since its construction.

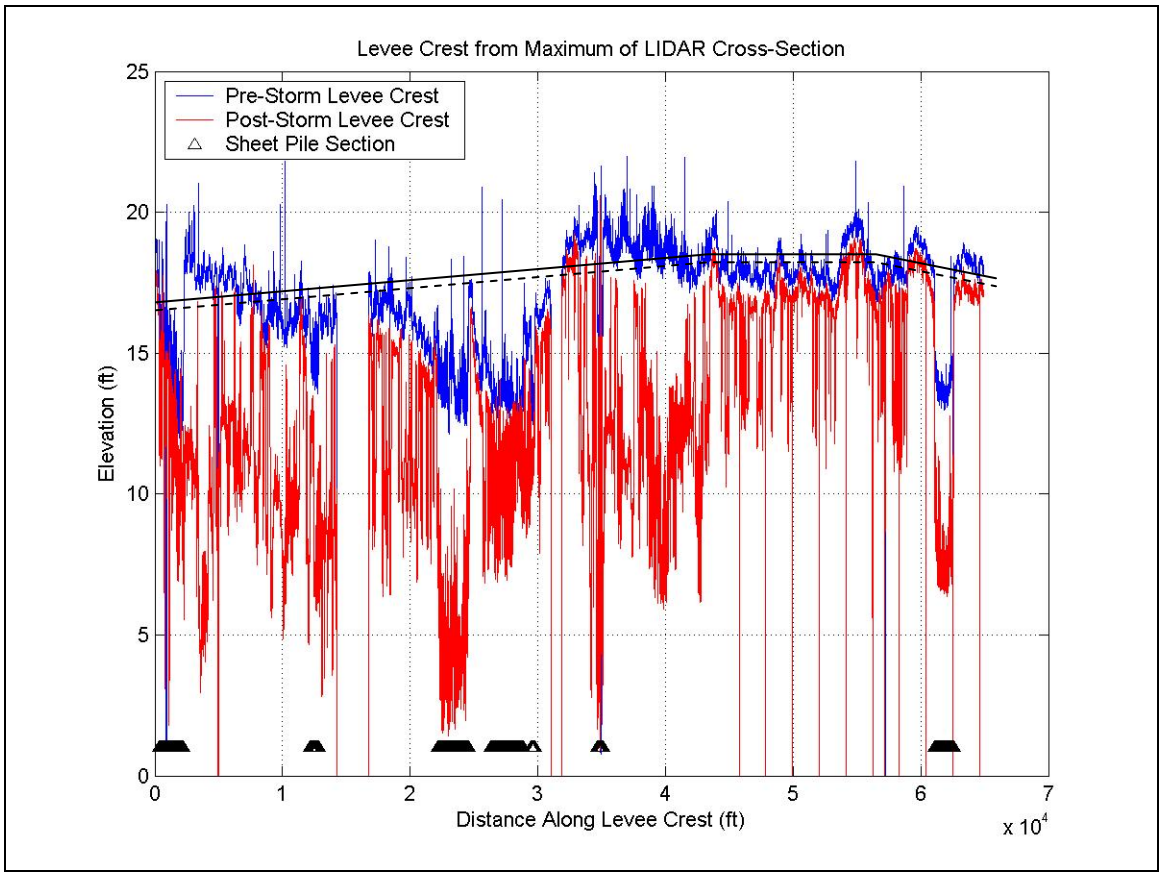


Figure 93. Freeboard conditions along MRGO Reach 2 levee, Base Case (solid black line) and Cases H2 and H3 (dashed black line)

A second issue with regard to water level is how the MRGO influenced the variation of water level with time. Both the magnitude (discussed above) and duration of high water levels are important factors in the hydrodynamic loading experienced by the MRGO Reach 2 levee, and in its subsequent erosion and degradation. Figures 94 (for Bayou Bienvenue), 95 (for Bayou Dupre) and 96 (for the southeastern end of MRGO Reach 2 levee) show differences in hydrograph shape for points that span this levee reach. Wave setup at the levee is neglected in these figures. In general, along MRGO Reach 2, that contribution of wave setup to the mean water level was 0.5 to 0.9 ft, 0.7 ft on average. Examination of differences in hydrograph shape at these three locations provides perspective on how the duration of high water levels was influenced by the MRGO along the entire length of the levee.

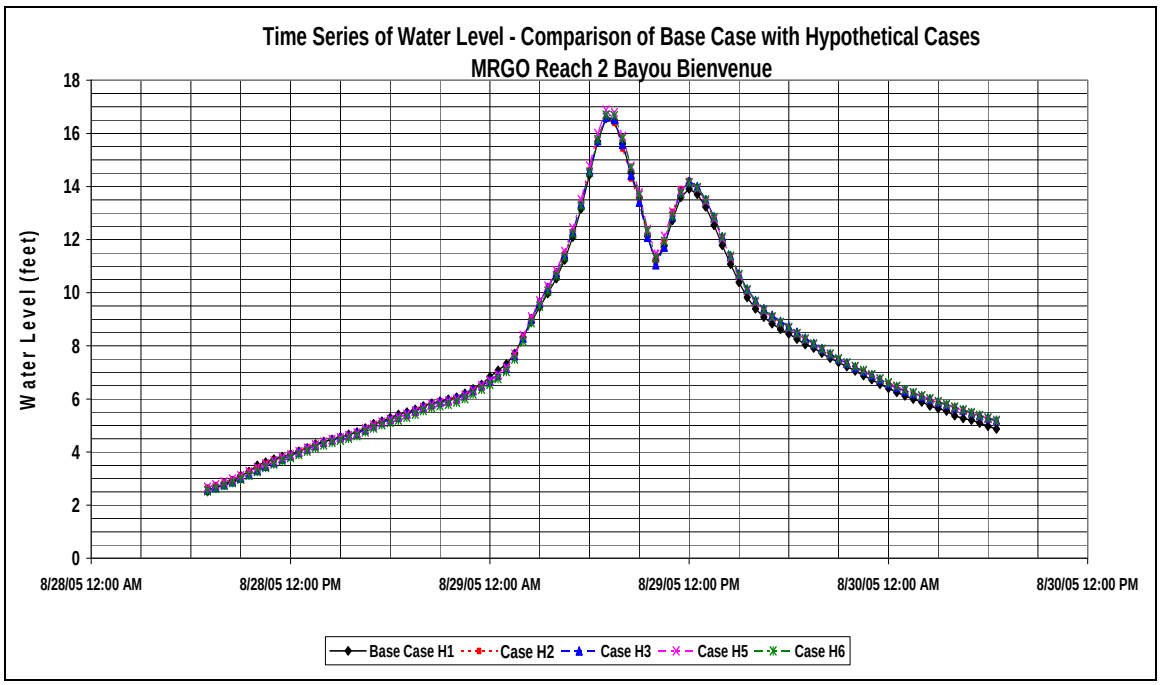


Figure 94. Comparison of temporal variation in water level for all cases, at Bayou Bienvenue

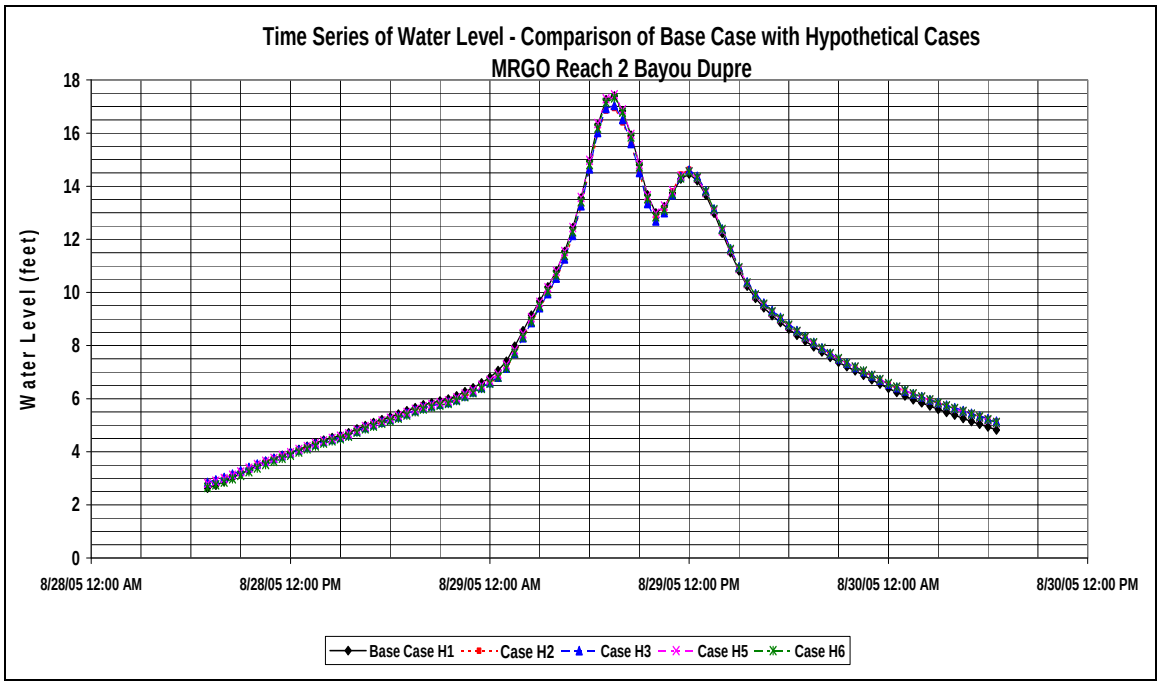


Figure 95. Comparison of temporal variation in water level for all cases, at Bayou Dupre

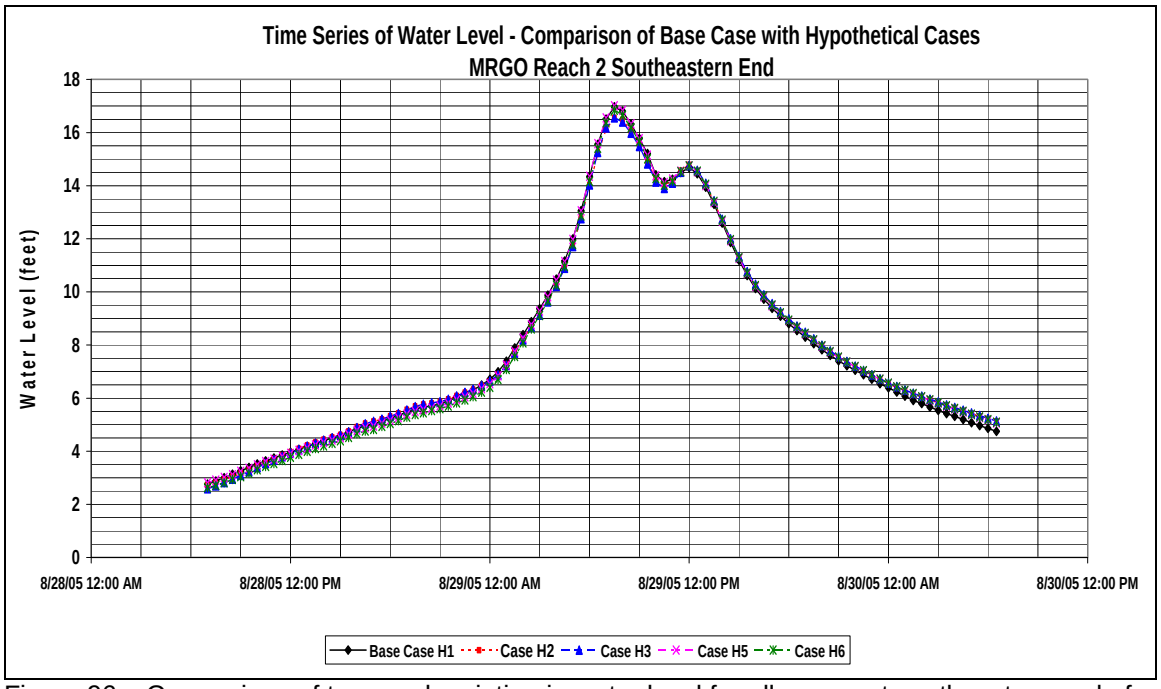


Figure 96. Comparison of temporal variation in water level for all cases, at southeastern end of the levee

The set of three figures shows that the MRGO had negligible influence on the storm surge hydrograph along the MRGO Reach 2 levee, particularly at the highest water levels. Overtopping of the levee between Bayou Bienvenue and Bayou Dupre first began at a water level of between 11 and 13 ft, for the very lowest spots on the levee. For water levels above 11 ft, differences among the various hypothetical cases, at any one point in time, were a few tenths of a foot (a few inches) at most. Differences in duration of time for which water level persisted above these elevated water levels were quite small, on the order of tens of minutes at most. Differences in hydrographs for the two wetland conditions (1958 and 2005) were small. Complete removal of the MRGO (cases H2 and H3) had negligible effect on hydrograph shape. Any effect of enlargement of the MRGO channel cross-section since its construction was negligible, in light of the very small differences between Cases H5 and H6, and the Base Case.

The amplitude of low-frequency (short-period) wind waves is influenced more by frictional dissipation over the wetlands than is the much lower frequency storm surge (long wave). Local incident wave conditions are also influenced more by changes to local depth associated with some of the cases in the vicinity of the channel. Changes to incident wave conditions are discussed in more detail in the expert report by Resio (2008). Figure 97 shows the variation of maximum significant wave height along the MRGO Reach 2 levee for all cases. Wave heights are generally higher between Bayou Bienvenue and Bayou Dupre for the Base Case, and for all the cases. Differences between the Base Case and the other cases are less in this region. Differences between the Base Case and the other cases are greater south of Bayou Dupre, in the area along the MRGO Reach 2 levee where the least amount of water entered the polder. The pattern of along-levee variation is unchanged in

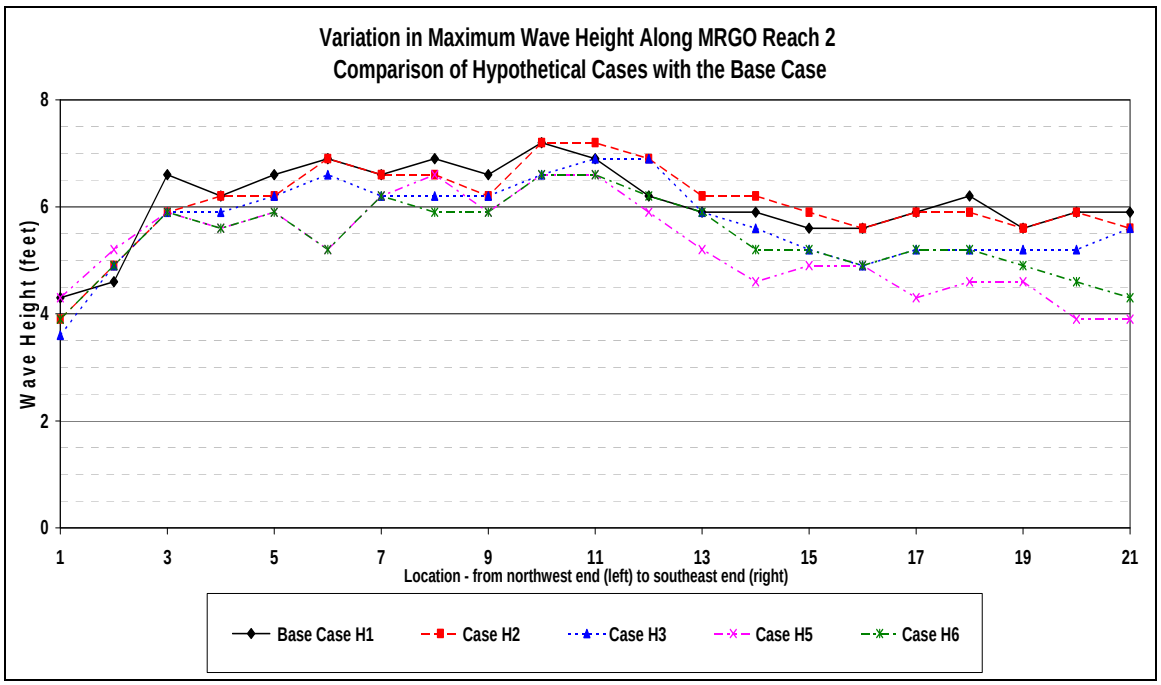


Figure 97. Comparison of along-levee variability in maximum significant wave height, for Base Case and all Cases

any of the cases, compared to the Base Case. For conditions involving complete removal of the MRGO, differences in significant wave height are 0.5 to 1 ft (5 to 15 %), compared to the Base Case, in the critical Bayou Dupre to Bayou Bienvenue reach. The effect of the changing the MRGO channel cross-section on incident wave heights, reflected cases H5 and H6, is greatest south of Bayou Dupre. Differences of 1 to 2 ft, reductions of 15 to 30%, occurred in this region. In the critical reach from Bayou Dupre to Bayou Bienvenue, differences were generally less than 1 ft (reductions of less than 15%).

The most important issue is how the MRGO influenced overtopping/overflow and back side velocity conditions along the MRGO Reach 2 levee. Overtopping and overflow, and high water velocity on the levee back side, were the primary causes for levee erosion and degradation, and damage to floodwalls. Extreme water levels were the most important factor that influenced overtopping/overflow, and back side velocities, through their influence on freeboard. As shown in Figure 93, maximum water levels were high enough, relative to levee/wall crest elevations, to induce persistent overflow along significant lengths of this levee, especially the critical section between Bayou Bienvenue and Bayou Dupre. Waves were also a contributor to overtopping and increased velocities on the back sides of the levees.

Figures 98 and 99 show the along-levee variation of two different measures of mean overtopping rate, for the series of locations that span the MRGO Reach 2 levee, for all cases. Calculation of overtopping rates and velocities at the levees are described in greater detail in the expert report by Resio (2008). Figure 98 shows along-levee variation in the weighted-average of the maximum mean overtopping rate for each location (i.e., an

average which considers variability in levee crest elevation). This measure represents an average maximum mean overtopping rate for the entire levee reach represented by each location. Figure 99 shows the variation in the maximum mean overtopping rate; this measure reflects the maximum mean overtopping rate computed for the lower 25% of the levee crest heights for each location. It reflects maximum mean overtopping rates for the lowest spots in the levee represented by each location, where breaches would tend to form first.

Overtopping/overflow rates for the Base Case, H1, were discussed in greater detail in a previous section. This section focuses on differences between the Base Case and cases H2, H3, H5 and H6. Recall that, in general, the magnitude of the maximum mean overtopping rate is highly correlated with the duration of overtopping, i.e. the higher the magnitude the longer the duration of overtopping, and the greater the levee erosion and damage. Therefore, these two figures provide good indicators of changes to levee damage, attributable to the MRGO, subject to quality of grass cover and properties of the levee soil at a particular location.

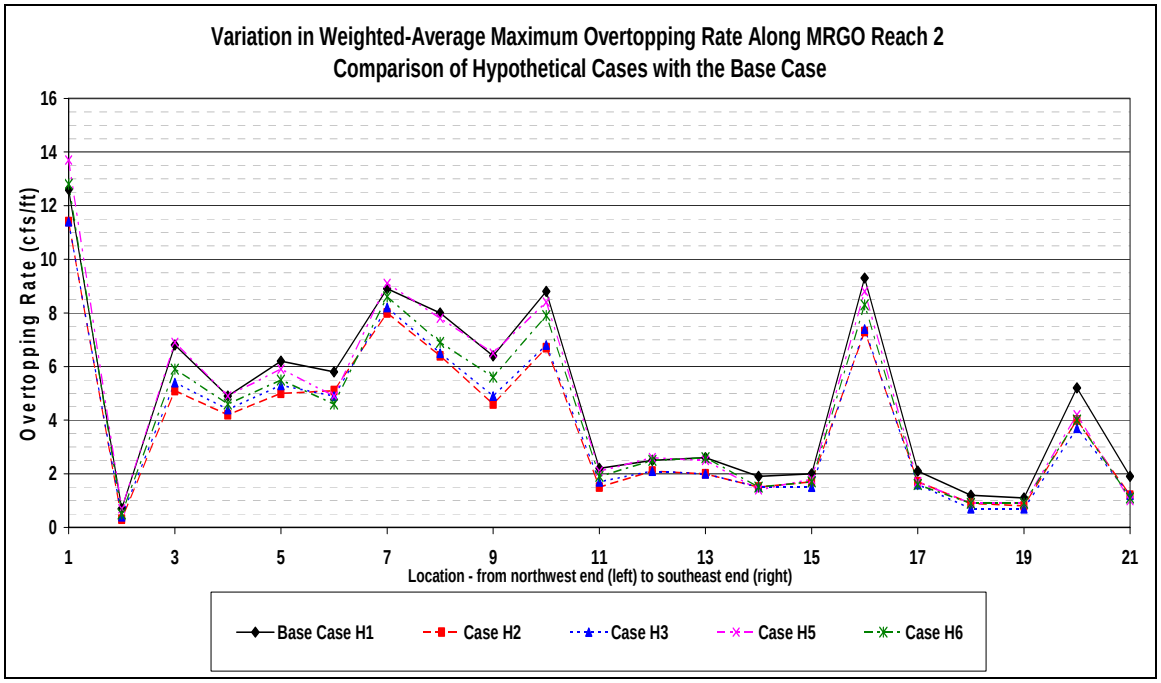


Figure 98. Along-levee variation in the weighted-average, maximum mean overtopping rate for all cases.

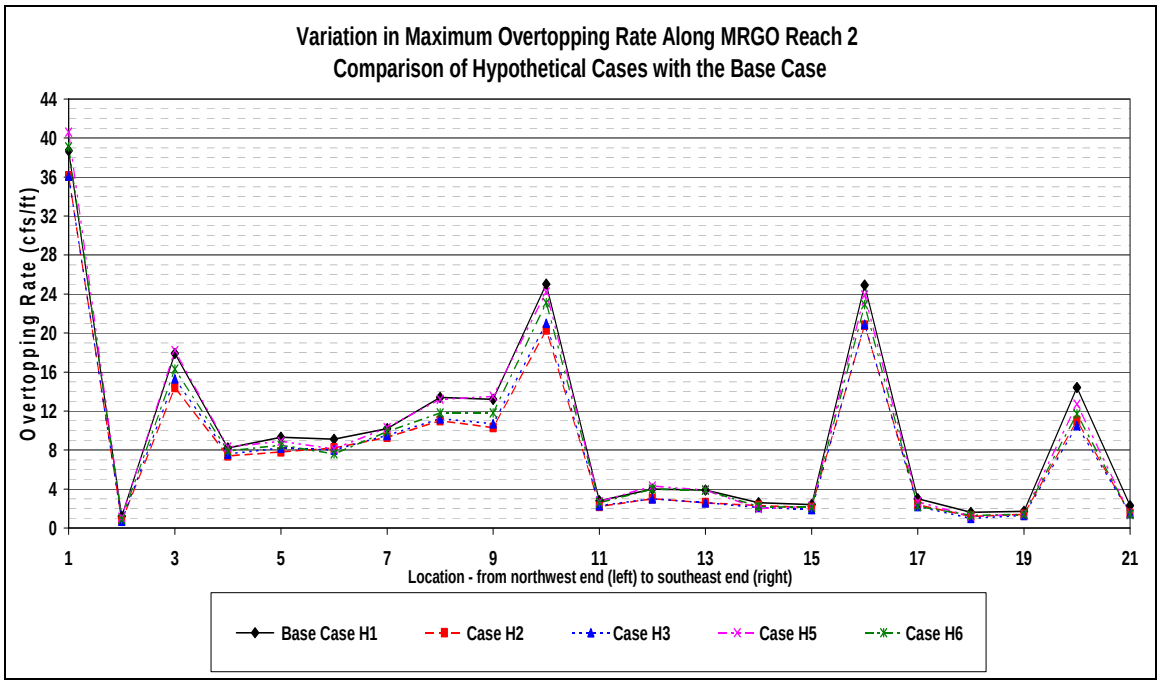


Figure 99. Along-levee variation in the maximum mean overtopping rate for all cases.

For each of the hypothetical cases examined, H2, H3, H5 and H6, reductions in weighted-average maximum mean overtopping rates and maximum mean overtopping rates for the lowest spots in each section were generally less than 30%, compared to overtopping rates for the Base Case, and 5 to 20% in the critical reach between Bayou Dupre and Bayou Bienvenue. The reductions in overtopping rates are consistent with the small changes in maximum water level and the magnitude of differences in maximum significant wave height among the cases, relative to the Base Case.

Most importantly, however, for each of the cases, H2, H3, H5 and H6, the weighted-average maximum mean overtopping rates and the maximum mean rates for the lowest spots in the levee exceeded 1 cfs/ft and approached 2 cfs/ft nearly everywhere along the MRGO Reach 2 levee. Mean overtopping rates of 1 to 2 cfs/ft would have been very damaging for levee sections comprised of highly erodable silty and sandy soils, and damaging for clay levees except those with the highest crest elevations, comprised of most highly erosion-resistant fat clays, and with very good grass cover. Along the critical reach from Bayou Bienvenue to Bayou Dupre, where the levees were lowest, for each case, H2, H3, H5 and H6, weighted-average maximum mean overtopping rates exceeded 4 cfs/ft (8 cfs/ft in places) and maximum overtopping rates exceeded 7 cfs/ft (12 cfs/ft in places). For these overtopping rates, this critical reach still would have experienced widespread and severe levee destruction and enabled a massive amount of flood water to enter the St. Bernard polder through this region, for each of the hypothetical cases. For each of the cases, the small reductions in maximum mean overtopping rate would not have been great enough to prevent breaching at low spots along other sections of levee. Neither complete removal of the MRGO, nor changes to wetland condition that have occurred since 1958, nor reduction of the MRGO cross-section to authorized dimensions

would have significantly altered the magnitude of overtopping and overflow that produced the severe levee and floodwall destruction which occurred along the MRGO Reach 2 levee.

Figure 100 shows differences, among all the cases, in the temporal variation of mean overtopping rate for a typical levee between Bayou Bienvenue and Bayou Dupre. The levee crest height is 15.4 ft at this location; the site is approximately at the mid-point between the two Bayous. Changes to the peak overtopping levels are small, less than 1 cfs/ft. A difference of 1 cfs/ft represents a 10 % reduction in peak values which were approximately 10 cfs/ft for the Base Case. Most importantly, the peak overtopping rates for all the hypothetical cases are still approximately 100 times the thresholds-for-damage in current engineering guidance for quality clay levees with good grass cover, and 10,000 times the threshold-for-damage for poorer quality levees. As levees with this initial crest height degraded, overflow rates increased to 20 to 40 cfs/ft. Differences are greatest, albeit small ones, for Cases H2 and H3, which also showed the greatest differences in maximum mean water level. This result illustrates the strong dependency of overtopping/overflow rates on mean water level. Changes to the durations of overtopping rate above values of the damaging levels of 1 and 2 cfs/ft, and greater, are small for each of the hypothetical cases. Overall, the MRGO had only a small influence on the temporal variation in damaging mean overtopping rates, not enough to significantly change levee and floodwall response along MRGO Reach 2.

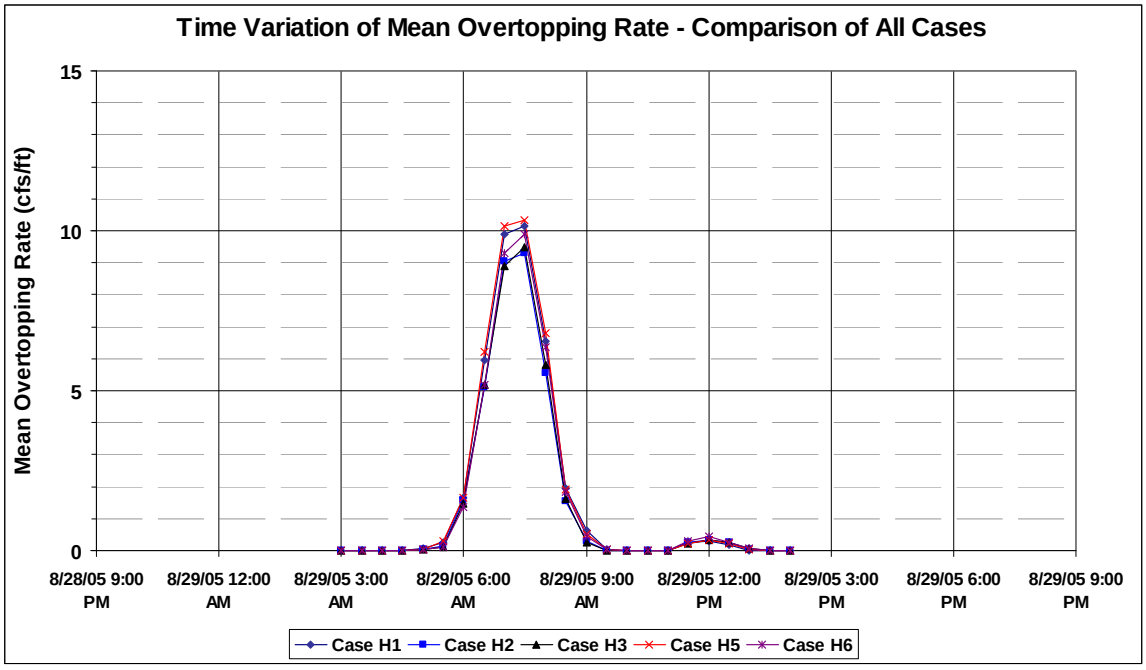


Figure 100. Temporal variation of mean overtopping rate for all cases, typical low levee between Bayou Bienvenue and Bayou Dupre

Figure 101 shows along-levee variation in the cube of velocity on the levee back side, for the lowest 25% of the levee crests, at each of the twenty-one locations along the MRGO Reach 2 levee. Low spots in the levee and walls, reflected by the lower 25% of crest heights, were subjected to high overtopping and overflow for the longest durations. Therefore, breaches formed in the lowest spots first, and they grew deeper and wider as they evolved in response to increasing rates of overtopping and overflow. Computation of velocities and hydrodynamic loadings on the levees are discussed in greater detail in the expert report by Resio (2008). Note that the vertical axis in the figure uses a logarithmic scale. The cube of velocity is a simple rule-of-thumb indicator for erosion potential that is often used for non-cohesive sediments; it reflects the non-linear relationship between erosion and velocity. The figure provides an indicator of changes to erosion potential at the lowest spots along the MROG Reach 2 levee. A velocity-cubed value of 1000 (ft/sec)**3 indicates a mean back side velocity of 10 ft/sec; a value of 125 (ft/sec)**3 indicates a mean back side velocity of 5 ft/sec. Velocity-cubed values exceeded 8,000 in places, indicating velocities that exceed 20 ft/sec.

Between Bayous Dupre and Bienvenue, erosion potential is much greater than at other locations. Erosion potential at a few locations at the southern end of the levee is an order of magnitude, or more, lower. In general, erosion potential decreases from north to south, with some fluctuations in erosion potential at particularly low spots in the levee. The variation of erosion potential along the levee is generally consistent with the degree of levee degradation and frequency of breaching evident in Figure 93, even though this measure of erosion potential does not consider soil properties or grass cover.

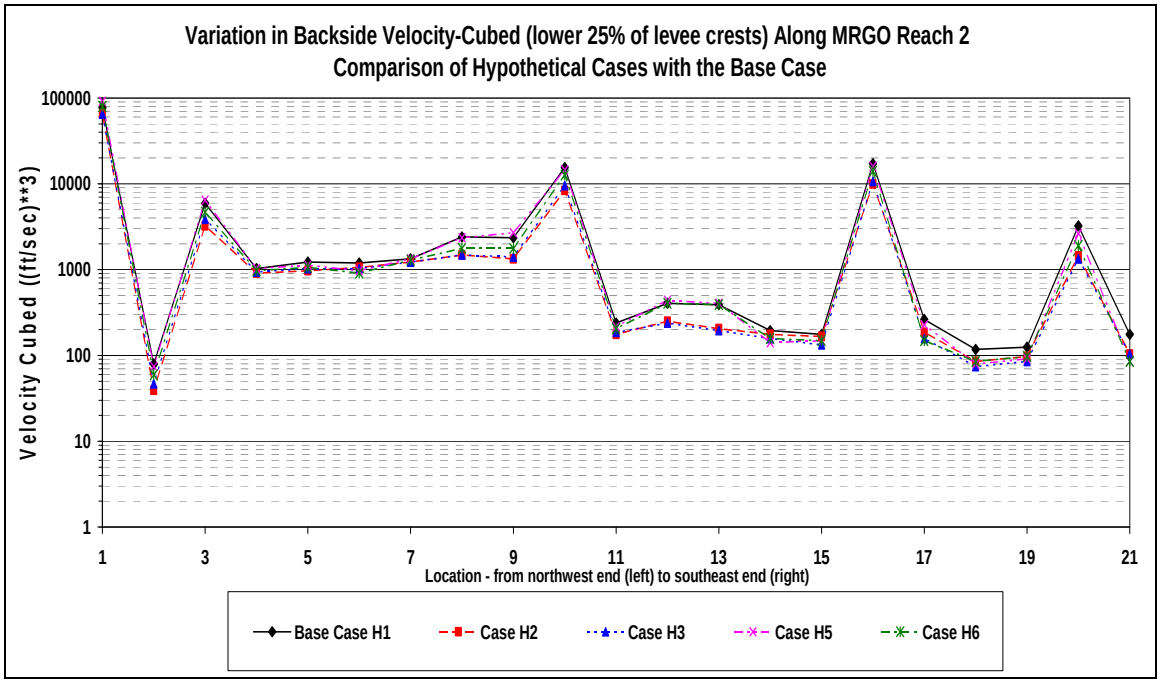


Figure 101. Along-levee variation in back side velocity-cubed, an indicator of erosion potential, for all cases

This correlation demonstrates the strong role of overtopping, overflow, and back-side velocities in levee and floodwall response.

What is most important are the very small differences in erosion potential at the levee low spots for each of the hypothetical cases, H2, H3, H5 and H6, relative to the Base Case. This is consistent with results discussed for levee overtopping/overflow rates and their relation to levee damage. Neither complete removal of the MRGO, nor changes to wetland condition that have occurred since 1958, nor reduction of the MRGO cross-section to authorized dimensions, significantly altered the levee and floodwall destruction which occurred along the MRGO Reach 2 levee, particularly in the critical reach between Bayou Dupre and Bayou Bienvenue.

c. IHNC Breaches (East Side)

Two breaches of the floodwall system occurred south of Florida Avenue Bridge along the east side of the IHNC. Both were sources of flood water into the Lower 9th Ward, as was steady overflow over the unbreached walls everywhere along the east side of the IHNC. Figure 102 shows the locations of both breaches. The photograph was taken looking toward the south. The smaller northern breach, approximately 250 ft in length, is seen in the foreground; and the larger southern breach, approximately 850 ft in length, is seen in the far field. The Florida Avenue Bridge is in the foreground on the right hand side. The Mississippi River is seen in the background along the top of the photo. The Claiborne Ave. Bridge is visible in the background, just south of the south breach; and the IHNC Lock (narrow waterway seen at the top center of the photo) is seen between the Claiborne Ave. Bridge and the Mississippi River.

Both wall crest elevation and water level at the site of these breaches were critical in determining the timing of breach formation. Crest elevations of nearby unfailed walls were 12 to 12.5 ft (a value of 12.3 ft was adopted here and in the inundation modeling work documented in Fitzgerald, 2008). The water level hydrograph, that was developed based on staff gage readings by the IHNC Lockmaster (see Figure 3), provided the most accurate information on the variation of water level though time in the vicinity of the two breaches. The maximum water level recorded at the Lock was 14.3 ft NAVD88 2004.65.

i. North Breach

Based on all available information considered by the IPET (2007), the breach formed before 4:30 a.m. CDT as a result of foundation failure. The conclusion reached by the IPET is that the breach at this site formed prior to overtopping or overflowing conditions. The north breach was the primary source of the early inundation within the Lower 9th Ward.



Figure 102. Oblique view of the two breaches into the Lower 9th Ward of the St. Bernard polder

Figure 103 shows observed water level data for the St. Bernard Polder (Chalmette and the Lower 9th Ward), which are based upon stopped clock data and eyewitness observations (the figure is from IPET 2006). The time of north breach formation is best estimated by the time required to fill the Lower 9th Ward section of the St. Bernard polder to observed elevations, +2 ft NAVD88 2004.65, at 5:15 a.m. It would have taken some time to fill the Lower 9th Ward basin to an elevation of +2 ft, the lowest parts of the polder were at elevations of – 6 ft. CivilTech Engineering (2008) reported several additional eyewitness accounts, accounts that were not part of the work of IPET (2006). One of these accounts was of a loud noise after 3:00 a.m. This noise might have been associated with failure of the wall at the north breach site. CivilTech Engineering (2008) also reported observations of accumulating flood water that led them to adopt 4:00 a.m. CDT as the time of north breach failure. The interior inudation modeling documented in the expert report by Fitgerald (2008) indicates that the time of the north breach was between 3:30 and 4:00 a.m. At 3:00 a.m., the water level in the IHNC was 8.1 ft; at 3:30 a.m. it was between 8.5 and 9 ft; at 4:00 a.m. it was 9.3 ft; and at 4:30 it was estimated to be 9.7 ft. Assuming that the breach occured between 3:30 and 4:00 a.m., the water level at this time was approximately 9 ft.

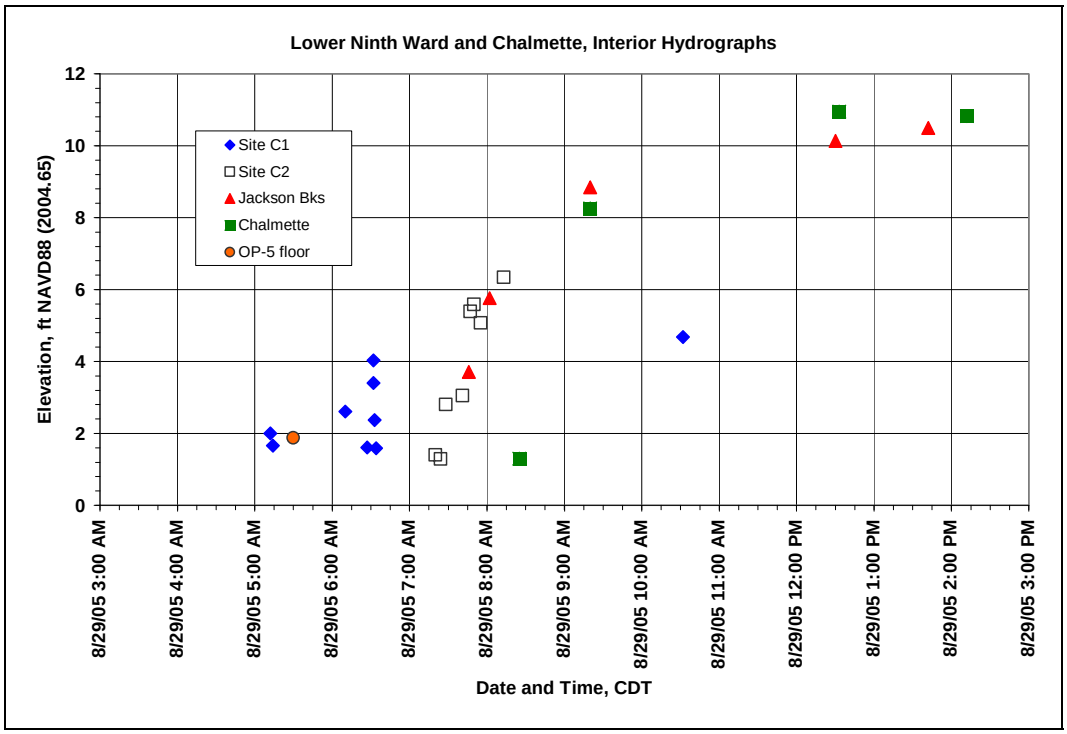


Figure 103. Chalmette and Lower Ninth Ward hydrographs (from IPET 2006).

The hypothetical cases were examined to see how they would have influenced occurrence of the north breach, i.e., did the peak water level reach a water level of 9 ft which would have triggered the north breach? Results from the SL15 ADCIRC modeling of all cases were considered; this modeling work is described in greater detail in the expert report of Westerink (2008). Estimated peak water levels from the SL15 ADCIRC simulation, for the Base Case and the hypothetical cases, H2, H3, H5 and H6, are shown in Table 8. Results are shown for several locations, Bayou Bienvenue, GIWW/MRGO Reach 1 at Paris Road Bridge, confluence of IHNC and GIWW/MRGO Reach 1, and at the IHNC Lock. Note that all water levels computed with the ADCIRC SL15 model were scaled upward using the same scaling factors that were discussed previously (1.12 along MRGO Reach 2, 1.08 at Paris Road Bridge, and 1.04 at the IHNC Lock. Upward scaling was done to account for a small regional low bias that was evident in the model results, based upon comparisons with excellent high water marks. All water levels are referenced to the NAVD88 2004.65 vertical datum.

It was shown and discussed in a previous section that Reach 2 of the MRGO had very little influence on water levels along the MRGO Reach 2 levee (changes of only several tenths of a foot). As is also shown in Table 8, removal of the MRGO in Cases H2 and H3, and reductions in MRGO cross-section assocaited with Cases H5 and H6, and changes to wetland condition that have occurred since 1958 reflected in Cases H3 and H6, had a small influence on maximum water level conditions at Bayou Bievenue, near the entrance to GIWW/MRGO Reach 1. Differences were 0.2 ft or less for all the hypothetical cases, which is approximately 1 % of the maximum water level of 16.8 ft.

Table 8. Effect of MRGO on Maximum Mean Water Levels – Estimated from ADCIRC SL15 Model Results				
Case	**Water Level at Bayou Bienvenue (ft)**	**Water Level at Paris Road Bridge (ft)**	**Water Level at GIWW/IHNC Confluence (ft)**	**Water Level at IHNC Lock (ft)**
Base Case H1	16.8	15.5	15.0	14.3
Case H2	16.6	15.2	11.0	10.5
Case H3	16.6	15.3	11.0	10.5
Case H5	16.9	15.9	14.5	14.0
Case H6	16.7	15.7	14.5	13.9

A similar result was found by de Wit et al (2008) for their cases 2C and 3 at Bayou Bienvenue involving complete removal of the MRGO and reduction in MRGO cross-section, respectively.

Changes for the hypothetical cases were slightly greater in GIWW/MRGO Reach 1 near Paris Road Bridge. For Cases H2 and H3, maximum water levels were 0.3 and 0.2 ft less, respectively, than maximum water levels for the Base Case. For Cases H5 and H6, maximum water levels were actually greater, by 0.4 and 0.2 ft, respectively, compared to the Base Case. In general, effects of the MRGO are quite small east of Paris Road Bridge. Changes were less than 0.4 ft for all the hypothetical cases, which is less than 3% of the observed maximum water level of 15.5 ft.

More significant differences between the Base Case and Cases H2 and H3 are evident in the IHNC. For cases with the MRGO removed, with just the GIWW channel present, surge propagation into the GIWW/MRGO Reach 1 is slowed and the amplitude is reduced due to the smaller water depth and cross-sectional area associated with the GIWW channel cross-section which was present at the time the MRGO was constructed and due to increased frictional resistance along the channel. A decrease in water level through the GIWW/MRGO Reach 1 was found by de Wit et al (2008) for their similar case, 2C. ADCIRC SL15 results for Cases H2 and H3 show an appreciable reduction in peak water level at the confluence of IHNC and GIWW/MRGO Reach 1 and at the IHNC Lock, differences of several feet. For Cases H5 and H6, changes to water levels at the confluence and the IHNC Lock are much smaller, reductions of 0.3 to 0.5 ft.

A primary feature of the observed hydrograph at the IHNC Lock was not simulated with the SL15 model, a single peak. The ADCIRC SL15 model predicted a double peak in the hydrograph at the IHNC Lock, not the single peak that was recorded there. Reasons for the discrepancy were discussed previously. One key factor in the predicted result with ADICRC SL15 was the model underprediction of peak water level along the south shoreline of Lake Pontchatrain, at the entrance to the IHNC, by 3 ft. Computed maximum water levels at this location were 9ft. The observed peak water level at the Lake Pontchartrain entrance to the IHNC was approximately 11.8 ft, based on a number of excellent high water marks acquired at the entrance (11.9, 11.8, 11.9, 11.8, 12.1 and 11.7 ft from IPET (2006)). In light of this discrepancy between computed and

observed peak water levels, the measured high water marks at the entrance were used to estimate peak water levels in the IHNC for Cases H2 and H3.

At the time peak water levels were being experienced at the Lake Pontchartrain entrance to the IHNC, at 9:00 a.m. CDT, wind was blowing from directions just west of north (see Figure 10), nearly in line with the main axis, or alignment, of the IHNC. The peak surge occurred at the IHNC Lock during Katrina (14.3 ft) at this time, 9:00 a.m. Storm surge along the south shore of Lake Pontchartrain was primarily being driven at this point in time by a momentum balance in the lake, a balance between wind stress and water surface slope that is clearly evident in Figure 10. Wind stress would have been acting to establish that same momentum balance within the IHNC, subject to conditions at the western end of GIWW/MRGO Reach 1. An estimate of the peak water level at the IHNC Lock, driven by the wind stress, can be made by extrapolating the water surface slope in Figure 10 to the site of the IHNC Lock, starting with a value of 11.8 ft at the shoreline of Lake Pontchartrain. An estimate of the peak water level at the IHNC Lock derived in this way is 13.5 ft. Water levels in the IHNC are influenced by conditions both in Lake Pontchartrain and Lake Borgne. The water level at the confluence of GIWW/MRGO Reach 1 with the IHNC also would have been influenced by the water level at the western entrance to this channel at the same time, which was approximately 13.6 ft at Bayou Bienvenue, estimated from ADCIRC model results. The actual peak water level in the IHNC near the site of the north and south breaches would have been approximately 13.5 ft for Cases H2 and H3 using this reconstruction method.

Kok et al (2008) and de Wit et al (2008) report that the water level at the breach site was 4.4 m (14.4 ft) for their ideal scenario (Scenario 2C) which removes the MRGO completely. Their scenario 2C is similar to Case H3 in that the MRGO is completely removed from the model simulations. Their results show a 1-ft decrease in peak water level from Paris Road Bridge to the confluence of GIWW/MRGO Reach 1 with the IHNC, and then a 0.3-ft increase from the confluence to the IHNC Lock. Note that in their modeling they force the peak water level at the Lake Pontchartrain boundary to be 12 ft, matching the observed high water marks. In this way they avoided relying on a model prediction of the water level along the south shore of Lake Pontchartrain to drive conditions within the IHNC.

De Wit et al (2008) computed a peak water level of 16.3 at Paris Road Bridge for their Base Case which is 0.8 ft higher than the two excellent high water marks of 15.5 ft that were acquired near this location. Assuming that their water level estimates are high by 5% at Paris Road Bridge, and using their computed changes in peak water level from Paris Road Bridge to the confluence of GIWW/MRGO Reach 1, and from there to the IHNC Lock, an estimate of peak water level at the IHNC Lock of 13.8 ft is derived using this reconstruction method.

A third method is just to use the Kok et al (2008) and de Wit (2008) value of 14.4 ft for peak water level at the IHNC Lock.

Regardless of which reconstruction method is used, the estimate of 13.5 ft based on water surface gradients computed with the ADCIRC SL15 model and measured high water marks, or the estimates of 13.8 ft or 14.4 ft based on the work by Kok et al (2008) and de Wit et al (2008), the same conclusion is reached. Peak water levels for Cases H2 and H3, with the MRGO completely removed, were high enough in either case to trigger the north breach, which occurred at a water level of slightly less than 9 ft. The same is true for cases H5 and H6, for which peak water levels at the IHNC Lock were estimated to be 14.0 and 13.9 ft, respectively. The MRGO had no influence on the occurrence of the north breach.

ii. South Breach

Figure 104 shows a photo from the site of the south breach. An irregular deep scour trough is evident on the back side of the wall, indicating overtopping/overflow prior to wall failure. The steel sheet-pile wall has been pushed to the east of its original past the scour hole, is lying down (at left side of the photo). The the original location is seen at the right hand side of the photo, at the edge of the repaired berm.

Figure 105 shows a photo taken between the north and south breaches. A scour trough is evident on the back side of the wall, and the wall appears to be leaning in the foreground, a beginning stage of rotational failure. The dimensions of the scour troughs shown in the two figures, and differences in the degree of scour trench irregularity at the two sites, suggest that the soil was highly erodable on the back side of the wall at the south breach site, compared to the site shown in Figure 105. The duration of scour by overflow at the south breach site (it only lasted until the wall failed) would have been less than the duration at the site of Figure 105, where the wall did not fail. This also suggests that the soil on the back side at the south breach site was highly erodable. The soil at the site shown in Figure 105 was more erosion-resistant. It is likely that once overflow began at the south breach site, the wall failed rather quickly. Data presented in IPET (2007) indicated that there was not a large mass of earth behind this floodwall.

Water level at the IHNC Lock reached 12.3 ft at 7:00 a.m. CDT (see Figure 3). At this time, water flowed over the low spots along this section of wall, assuming a wall elevation of 12 to 12.5 ft. Stopped clock data (Figure 103) showed a very rapid rate of water level rise in the Lower 9th Ward beginning in the 7:15 a.m. to 7:45 a.m. time frame. This rapid rise was apparently created by the south breach. The timing of the rapid rate of water level rise suggests that the south breach formed rapidly, on the order of 15 to 30 minutes, after overflow commenced.



Figure 104. Floodwall failure at the southern breach into the Lower Ninth Ward

Cases H2 and H3 were examined to see how they would have influenced occurrence of the south breach, i.e., did the peak water level reach a water level of 12 to 12.5 ft which would have led to overflow and triggered the south breach? The analysis above showed that peak water levels would have been 13.5 to 14.4 ft at the IHNC breach sites for Cases H2 and H3. For either case, overflow would have occurred at the south breach site. Results in de Wit et al (2008) indicate that the water level would have stayed above the wall crest elevation for 1.5 to 2 hours. This would have been enough time to create the south breach, which occurred rapidly once overflow commenced. Therefore, the conclusion is reached that the south breach would have occurred for either case H2 or H3, i.e. with the MRGO removed and for either wetland condition (1958 or 2005).



Figure 105. Scour hole formation on the back side of the floodwall, just north of the site of the southern breach into the Lower Ninth Ward

For cases H5 and H6, with the MRGO in at its authorized dimentions, for wetland conditions in 2005 and 1958, respectively, estimated maximum water levels at the IHNC breach sites were 13.9 and 14 ft, and the hydrograph shape was nearly the same as that for the Base Case, H1. Therefore, for both cases H5 and H6, the south breach would have occurred. Enlargement of the MRGO cross-section since its construction did not influence the occurrence of the south breach. De Wit et al (2008) report a maximum water level of 16.7 ft at the IHNC Lock for their case 3, in which the MRGO is at its authorized dimensions.

Appendix A: Oblique Photos - MRGO Reach 2 Levees and Floodwalls

This series of oblique aerial photos was taken of the MRGO Reach 2 levee following Hurricane Katrina. Photos were taken during a north-to-south flight inspection along the levee, so the MRGO navigation channel is always on the left hand side of the photos. An interpretation of what is evident in each photo is provided.

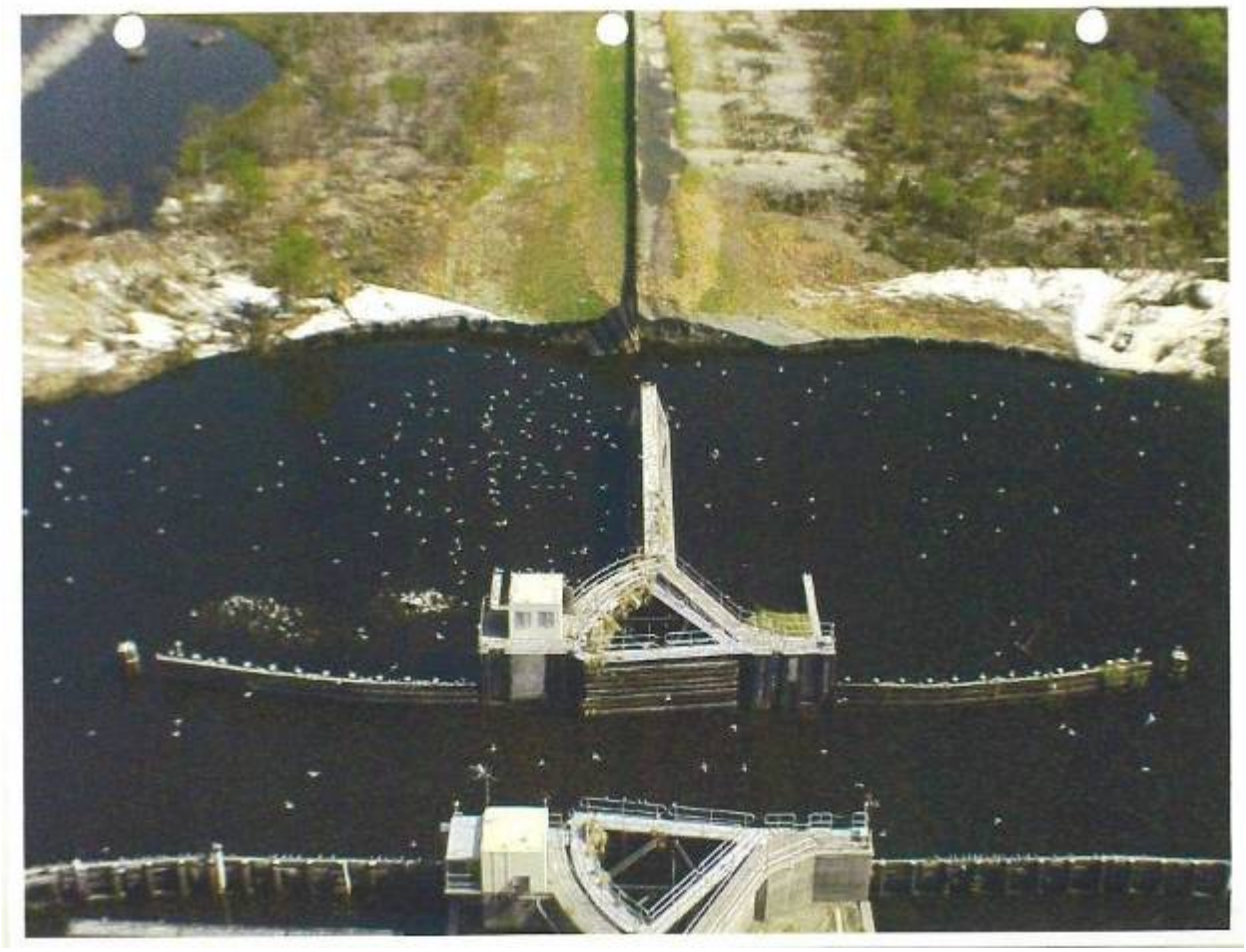


Figure A1. Bayou Bienvenue Gate Structure. Breaching and flanking of flood wall at transition from concrete wall to steel sheet-pile wall. Sediment deposits evident on both sides of the breach, indicating flow both into and out of the polder. Scour trench on the protected (back) side caused by overtopping of the steel sheet-pile wall in the adjacent levee. Deposits of sediment washed out from the scour trench are evident on the back side. No indication of significant erosion on the front (exposed) side of the levee face.



Figure A2. Embedded steel sheet-pile wall in the levee. Wall buckling is evident at a section in upper part of the photo. Wide scour trench caused by overtopping on the backside of the wall. Deposits of sediment washed out from the scour trench are evident on the back side. Some traces of surface erosion due to waves on exposed side along the wall are evident; isolated occurrence of heavier surface erosion near top of photos suggests more erodable sediments there. Much greater erosion signature and levee degradation on the back side due to overtopping compared to wave-induced erosion on the front side.



Figure A3. Embedded steel sheet-pile wall in the levee. Wall rotated and buckled. Wide scour trench on the protected side caused by overtopping. Large deposits of sediment washed out from the scour trench reflect considerable scour. Some slight erosion evident higher up on the levee face in front of the wall, probably due to wave action. Much greater erosion and degradation on the back side due to overtopping compared to degree of wave-induced erosion on the front side. Wall appears to be breached at top of photo.



Figure A4. Severely degraded levee. Evidence of overtopping indicated by overwash sediment deposits on back side. Channel present just to south (top edge) of the barge. Backside elongated sediment deposit suggests high overflow. Traces of deposited sediment at front of the channel mouth also suggest outflowing water. Channel likley fomed on outflow. Lowest spots on the degraded levee likely served as outflow channels for water exiting the polder following storm's passage. Situation in lower half of photo is less clear.



Figure A5. Severely degraded levee; entire levee gone in foreground; crest gone in background. Evidence of overtopping indicated by numerous overwash sediment deposits on back side. In upper portion of photo, degradation is dominated by headcutting with traces of surface erosion higher up on the levee front face. Lower half of photo is less clear. Significant sediment deposts on back side indicating overtopping. Cleanness of curved erosion line at southern edge of this breached area suggests a flow line marking edge of a channelized region of exiting water.



Figure A6. Rotational wall failure and breaching induced by overtopping and scour trench formation. Localized extremely wide scour trench probably induced by rotating wall sending overtopping jet further landward. Narrower scour trench evident along upright wall sections to either side. At top of photo, failure at transition from wall to levee is evident. Length of fan-shaped sediment deposits are evidence of strong flow through the breach. Surface erosion and loss of vegetation on front side evident higher up on the levee near base of the wall, due to breaking wave action. Erosion and degradation is dominated by overtopping processes.



Figure A7. Levee entirely eroded in many places. Evidence of overtopping and strong landward flows indicated by numerous elongated overwash sediment deposits on back side, some reaching considerable distances from the levee. Back-side head-cutting evident in center of the photo, as are several small wave-induced bench-cuts lower on the front face. Hour-glass shaped channel in the foreground and sediment fans on front side indicate channelized exiting water; head-cut evident on back side of this channel likley due to flow exiting the polder. Evidence of channelized exiting flow (channel and/or sedimetn deposits on the front side) also seen at two other locations.



Figure A8. Levee cross section in foreground is intact; no loss of crest elevation. Some traces of surface erosion evident on the front face, including beginning stages of front side bench cutting probably due to wave action, but no significant erosion of bench cuts into or through the levee crest. Overwash sediment deposits on the backside are evident at the top of the photo; they extend for considerable distances behind the most advanced breaches indicating high flows through the breach. Head-cutting associated with overtopping appears to be the dominant erosion mode; several stages are evident in the center of the photo, including advanced states that have cut completely through the levee crest.



Figure A9. Intermittent areas of severe levee degradation and loss of the crest, separated by fully intact cross-sections. Head-cut has migrated completely through the crest and well into the front levee face in numerous places. Elongated sediment overwash deposits on the backside are pronounced and they reflect high flow through the breaches. Also, there is no evidence of significant wave-induced erosion anywhere else on the front face.



Figure A10. Most of the levee is intact. Vegetation appears to be healthier and denser. Breach in center of the photo due to head-cutting; head cut has migrated completely through the crest and well into the front levee face. Overwashed sediment deposits on the backside are evident and they extend considerable distances. Head-cutting associated with overtopping appears to be the dominant erosion mode. Slight traces (an along-levee band) of wave-induced erosion higher up on the levee face are evident. No significant erosion due to waves on the front side in areas where head-cuts are not present.



Figure A11. Most of the levee crest degraded. Deep scour holes evident near the base of the levee on backside, probably due to high turbulence where flow regime changes from supercritical to subcritical near base of the levee. Traces of wave-induced erosion are evident on the levee front face. Predominant erosion signature induced by back-side head-cutting. Head cuts have migrated completely through the crest and well into the front levee face. Overwash sediment deposits on the backside are evident and they extend considerable distances indicating very high water velocities due to overtopping on the backside.



Figure A12. Levee crest is degraded in places; intact along much of this reach. Scour holes evident near the base of the levee on backside. Predominant erosion signature induced by head-cutting on the back side. Several stages of head-cutting are evident; head cut has migrated completely through the crest and well into the front levee face in places. Overwash sediment deposits on the backside are evident. Only traces of wave-induced erosion are evident on the levee front face at the intact sections, at the center of the photo, where there is extensive erosion on the back side. Erosion prevalent on back side at base of levee at this location.

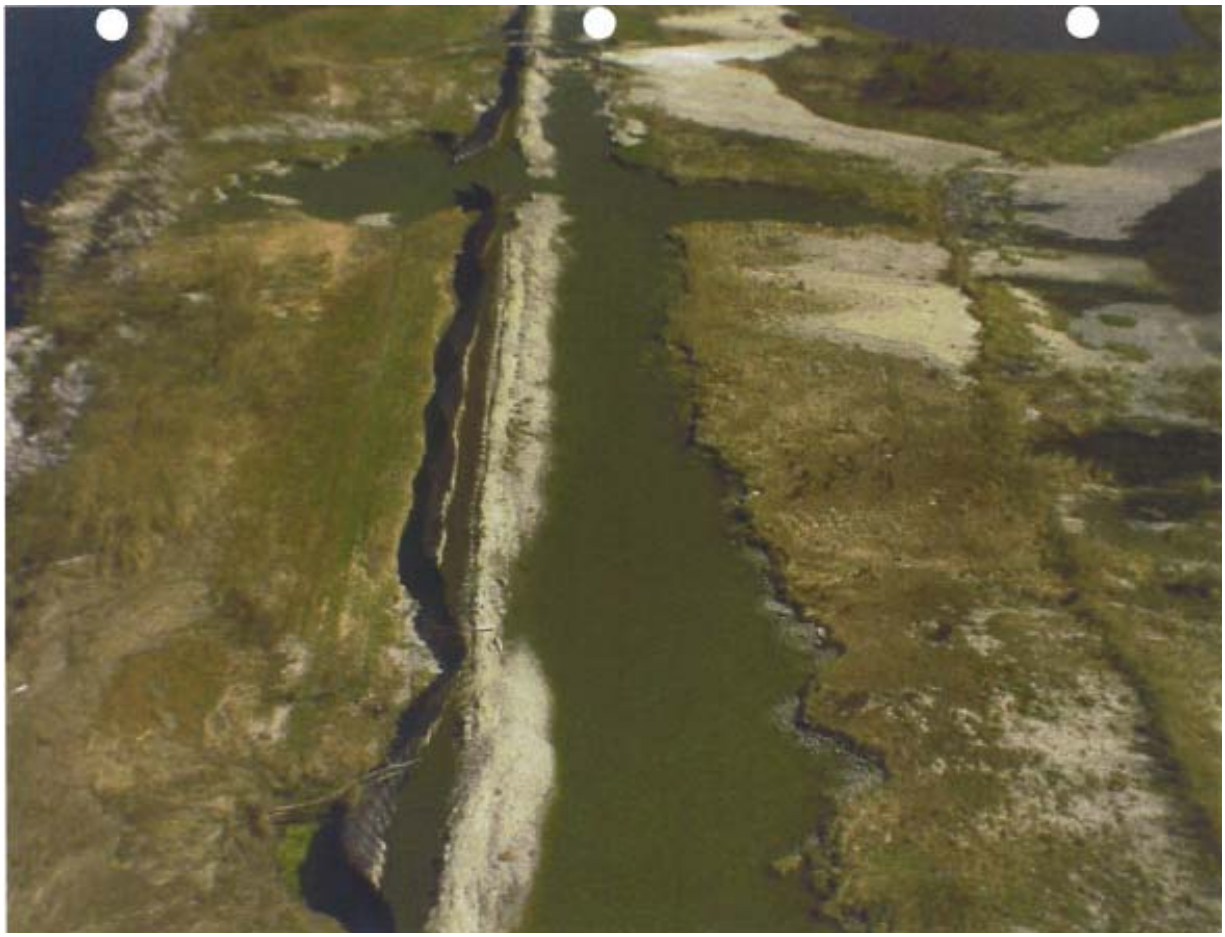


Figure A13. Severe failure and buckling of steel sheet pile wall embedded in the levee. Two scour trenches evident; a narrow straight trench close to the wall perhaps indicating early overflow with low wave action and much wider more irregular trench. Larger trench seems too wide for overtopping-induced scour; may be due to water flowing along the wall to exit the through breach after the storm. Breach through the wall is seen in the background. Wider trench on back side could have been formed initially due to wave overtopping and steady overflow and widened after wall rotated and failed, then widened later with exiting flow moving toward the breach. Evidence of flow in both directions through the breach (indicated by sediment deposits on both sides).



Figure A14. Levee crest degraded in a few places; intact elsewhere. Scour trench evident on backside of the floodwall in the background, with evidence of sediments carried away out of the trench and deposited further landward. Scour at transition from wall to levee. No significant erosion on the front side away from areas where head-cutting is evident. No along-levee band of wave-induced surface erosion is evident on the front face, only traces. Predominant erosion signature induced by head-cutting. Overwash sediment deposits on the backside are evident behind the levee and floodwall. Surface erosion at the levee base on the backside is evident.



Figure A15. Sheet pile wall embedded in levee. Wide irregular scour trench due to overtopping evident on the backside along the entire length of wall, with evidence of considerable amount of sediment eroded and carried away out of the trench and deposited further landward. No erosion on the front side, except traces in the foreground. Predominant erosion signature induced by overtopping.



Figure A16. Most of the levee crest degraded. Deep scour holes evident in the degraded levee, probably due to high turbulence and high speed flows though the head-cuts and breaches. Traces of surface wave-induced erosion on the levee front face in the foreground, but not in the upper half of the photo. Predominant erosion signature induced by overtopping and head-cutting. Several stages of head cutting are evident; head cut has migrated completely through the crest and well into the front levee face along much of this levee reach. Overwash sediment deposits on the backside are evident. No evidence of sediment deposition on the front side.



Figure A17. Short sheet pile wall embedded in levee. Wide scour trench due to overtopping evident on the backside along the entire length of wall, with evidence of sediments carried away out of the trench and deposited further landward. Erosion due to flow concentration is evident at transitions from wall to levee at both ends of the wall. Traces of wave-induced erosion evident on the front side, as are a few small erosion benches in the foreground (they do not extend to or through the levee crest). No along-levee band of wave-induced surface erosion is evident on the front face, only traces. Erosion caused by overtopping is predominant.



Figure A18. Levee crest in foreground is degraded; mostly intact elsewhere. Overwash sediment deposits on the backside are evident behind the levee. Predominant erosion signature induced by overtopping and backside head-cutting. Upper part of the photo shows isolated locations were front-side bench cutting occurred high on the levee face and might have led to overtopping and overwash of sediment. In middle of the photo there is a backside head cut evident near the levee crest, in an early stage of formation, which could also lead to the type of cut seen at one of the other two locations. Minor front side erosion is seen at the toe of the front-side. No clear along-levee band of wave-induced surface erosion. Erosion at base of levee is evident on the back side.



Figure A19. Levee crest intact throughout this reach, except at one spot where back-side head cut is near levee centerline. Predominant erosion signature induced by backside head-cutting. Only early stages are evident. Overwash sediment deposit evident at the more advanced head cut. Traces of erosion on front and back sides near the base of the levee and on front face are evident. No evidence of significant erosion on the front side, even in areas where back-side head-cuts are evident. Overtopping at this location appears to be less, or levees here are highly resistant to erosion.



Figure A20. Levee crest is intact throughout this reach. Traces of erosion on backside near the base of the levee are evident. Evidence of minor wave-induced surface erosion band on the levee front face is evident. Overtopping at this location appears to be minimal, or levees are highly resistant to erosion.



Figure A21. Levee crest mostly intact, except at a few locations. Severe levee degradation is evident at top of photo. Some traces of erosion on the backside near the base of the levee. Traces of wave-induced surface erosion are seen on front face. Erosion signature is dominated by isolated bench-cutting (wave induced) higher up on the front levee face near the crest, without evidence of strong back-side head-cutting or overwash. Most severe front side bench has progressed through the levee crest, and some sediment is deposited on the backside due to overtopping. Overtopping at this location appears to be minimal, or levees highly resistant to erosion.



Figure A22. Levee crest is completely degraded in center of the photo; intact to either side. Vegetation cover on the levee faces appears dense where the levee remains. Only a few traces of erosion on the front side anywhere else. Predominant erosion signature is head-cutting that has reached an advanced stage with a deep channel scoured through the levee. Overwash sediment deposits on the backside are evident behind the levee and breach channel. At the deep scour hole located on the levee front side, there is evidence of exiting water (fan-shaped deposit of sediment caused by water exiting from the polder).



Figure A23. Bayou Dupre Gate Structure. Section of the flood wall failed. Flanking and breaching of the flood wall at the transition from wall to levee. Deep scour hole formed on back side of the transition erosion Sediment fan on the back side evident at breach. Levee in foreground completely degraded. Surficial erosion on the levee front face is evident in the foreground, as is the vertical face of a head cut that has advanced completely though the levee crest to the surface wave erosion zone.



Figure A24. Bayou Dupre Gate Structure. Flanking and breaching of the flood wall at the transition from concrete wall to levee. Deep scour hole formed on back side of the transition erosion Sediment fan evident behind the breach. Levees in the background completely degraded. On front side, no evidence of wave-induced erosion seaward of the head-cuts or accumulation of sediment on the front side of the levee.



Figure A25. Predominant erosion signature is advanced stages of head-cutting on the backside due to overtopping and overwash of sediment. Where the levee is severely degraded, erosion pattern shows sharp nearly vertical leading edge of head-cuts which have advanced completely through the levee crest to and through the band of wave-induced surface erosion on the front side. The sharpness and prevalence of this leading edge does not suggest that this degree of degradation is initiated as wave-induced erosion that starts at the base of this surface erosion zone and works toward the crest. There is evidence of small front side erosion bench that has not cut through the crest; however, there is even more extensive backside erosion by head-cutting at this same location.



Figure A26. Levee crest is intact except at one spot. Predominant erosion signature is backside head-cutting. Early stages that have not advanced back through the levee crest are evident, as is a more advanced cut which has. Overwash sediment deposits evident behind the larger head-cuts. Slight wave-induced erosion on the front face is evident, in a band along the levee. No significant evidence of front-side erosion in several areas where back-side head-cutting is evident. Slight erosion is evident at the backside base of the levee. Overtopping at this location appears to be less, or levees highly resistant to erosion.



Figure A27. Levee crest is intact, except at two locations. Predominant erosion signature is backside head-cutting induced by overtopping. Early stages of backside surface erosion and cuts that have not advanced back through the levee crest are evident. Advanced head-cuts are also seen. Overwash sediment deposits evident behind the larger head-cuts. Band of slight surface erosion is evident on the front face. No evidence of bench cuts higher up on the front face in areas where early stages of backside head-cutting are evident, or anywhere else. Slight erosion is evident at the levee base on the backside.



Figure A28 Intact levee crest interrupted by severe levee degradation and breaching. Predominant erosion signature is head-cutting induced by overtopping. Sharp leading edge of head-cut has advanced completely through the levee crest to and through the front-side band of wave-induced surface erosion. Early stages of backside surface erosion and head-cutting are evident along much of the levee. Overwash sediment deposits evident behind advanced head-cuts. No significant wave-induced erosion in areas where head-cutting is not evident. Slight erosion is evident at the levee base on the backside. No evidence of sediment deposition on the front side.



Figure A29. Excellent example showing various stages of backside head-cutting and advance toward the levee crest, eventually cutting through the crest in the foreground and into the front-side zone of wave-induced surface erosion. Predominant erosion signature is head-cutting induced by overtopping and overwash sediment deposits on the backside. Overwash deposits evident behind the more advanced head-cuts; their inland extent, elongation and size correlate well with size of the head-cut. No front-side wave-induced erosion through the levee crest is evident in any area where the backside head-cut has not advanced through the crest. The entire area shows signs of erosion on the backside, and little erosion on the front side. Minor front side cuts are evident near bottom of the photo; surface erosion band is evident on the front side.



Figure A30. Levee crest degraded at many locations. Predominant erosion signature is head-cutting induced by overtopping. Overwash sediment deposits evident behind the more advanced head cuts. Continuous band of wave-induced surface erosion on the front face is evident. All major head-cuts have reached a similar state of advance through the levee crest and into the surface erosion band on the front side. Head-cuts in earlier stages of development are evident. No wave-induced erosion to or through the crest is evident in areas where head-cutting has not eroded the levee crest or in areas where the head-cutting is in an early stage of formation.



Figure A31. Levee crest is intact, except in the background. Photo is an excellent example of early stages of backside surface erosion and head-cut formation caused by overtopping. Predominant erosion signature is backside erosion and head-cutting. Also present is wave-induced surface erosion zone all along the levee front face. No evidence of severe front-side bench cutting. At one location in the foreground, a small bench formed higher on levee front face. Bu the levee crest is intact here. No significant wave-induced erosion into or through the levee crest from the front side is evident anywhere, particularly where erosion and overwash of sediment on the backside due to overtopping is evident.



Figure A32. Levee crest degraded at many locations in this reach. All major head-cuts have reached a similar state of advance through the levee crest; less advanced toward the top of the photo. Clear steeper leading edge along the head-cut is visible. Predominant erosion signature is head-cutting induced by overtopping. Large overwash sediment deposits evident behind the head-cuts. Surficial wave-induced erosion on the front face is evident all along the levee. No significant wave-induced erosion of the levee crest is evident in areas where head-cutting has not eroded to or through the levee crest or in areas where the head-cuts are forming on the backside.



Figure A33. Levee crest is intact except at locations at top of the photo. This is an excellent example of early stages of backside surface erosion and head-cut development, and some later stages. Predominant erosion signature is minor surficial wave-induced erosion of the levee surface on the front side and more substantial head-cutting induced by overtopping on the backside. No significant wave-induced erosion of the levee crest on the front side is evident in areas where head-cutting has not eroded to the levee crest or in areas where the head-cutting is in an early stage of formation.



Figure A34. Levee crest is intact except at a few locations. Predominant erosion signature is head-cutting induced by overtopping; several stages are evident. Overwash sediment deposits evident behind the more advanced head-cuts. Band of surficial wave-induced erosion on the front face is evident all along the levee. No wave-induced erosion up to or through of the levee crest is evident in areas where head-cutting has not eroded the levee crest. Traces of erosion seen near toe of levee on both front and back sides



Figure A35 Predominant erosion signature is minor wave-induced erosion of the levee surface on the front side and more substantial head-cutting induced by overtopping on the backside. Excellent example of early stages of backside erosion and head-cut development. More advanced cut completely through the levee crest and into the zone of wave-induced surface erosion on the front side is seen in foreground. The band of surficial erosion reaches a similar elevation and no higher toward the crest; this is seen in many other photos. No significant wave-induced erosion of the levee crest is evident in areas where head cutting has not advanced into the crest.



Figure A36 Example of early stages of backside head-cut development, and some later stages where cut is through the crest. Predominant erosion signature is minor wave-induced erosion of the levee surface on the front side and more substantial head-cutting induced by overtopping on the backside. No significant wave-induced erosion of the levee crest is evident in areas where head-cutting has not eroded to the levee crest or in areas where the head-cutting is in an early stage of formation. The band of surficial erosion reaches a similar elevation and no higher toward the crest, unlike head cuts on the back side which vary in distance from the crest.



Figure A37. Levee crest is intact throughout this reach. This is another excellent example of early stages of head-cut development. Predominant erosion signature is minor surficial wave-induced erosion of the levee surface on the front side and more substantial head-cutting induced by overtopping on the backside. No significant wave-induced erosion of the levee crest is evident in areas where head-cutting has not eroded to the levee crest or in areas where the head-cutting is in an early stage of formation. The band of surficial erosion reaches a similar elevation and no higher toward the crest, unlike head-cuts on the back side which vary in distance from the crest.



Figure A38 Levee crest mostly intact, except at two locations. Example of early stage of head-cut development, and some later stages where cut is through the crest. Predominant erosion signature is minor surfical wave-induced erosion of the levee surface on the front side, only traces in places, and more substantial head-cutting induced by overtopping on the backside. Large overwash deposits on back side behind advanced head-cuts. No significant wave-induced erosion of the levee crest is evident in any areas where head-cutting has not eroded to the levee crest or in areas where the head-cutting is in an early stage of formation. No evidence of sediment deposition on the levee front side.



Figure A39 Levee crest intact throughout this reach, except in the foreground. This is another example of early stages of head-cut development, and a later stage (foreground) where the cut extends through the crest. Predominant erosion signature is minor wave-induced erosion of the levee surface on the front side and more substantial head-cutting induced by overtopping on the backside. Larger overwash sediment deposits evident behind the more advanced head-cuts. No significant wave-induced erosion of the levee crest is evident in areas where head-cutting has not eroded to the levee crest or in areas where the head-cutting is in an early stage of formation.



Figure A40. There is a prevalent pattern of surface erosion on the front side and bench-cutting due to wave action, without much evidence of overtopping. Two of the bench cuts extend just through the center of the crest. Crest elevations here were high, about 19 to 19.5 ft. Overtopping is minimized at this high crest elevation, so wave action is concentrated on the front face for the longest possible duration. Photo suggests how far wave-induced bench-cuts on the front side could develop in the absence of overtopping sufficient enough to cause head-cutting at this location. No severe front side levee degradation is evident.



Figure A41. Levee crest is intact throughout this reach except at one location. Some localized surficial wave-induced erosion and bench cutting evident on front side. Bench-cutting high on the profile has completely cut through the levee crest at a high elevation to induce the overtopping which then led to much more rapid erosion by head-cutting associated with overtopping. Sediment overwash deposit on backside due to overtopping; do sediment deposition evident on the front side. Overtopping and overflow appear to have been minimal along this reach, except at this one location. No severe front side levee degradation is evident outside the isolated localized bench-cut.



Figure A42. Levee crest is intact except at two locations. Traces of localized surficial wave-induced erosion are evident on the front side in places. Head-cutting formed by overtopping at these two locations. Head-cutting has advanced just through the levee crest. At both locations bench-cutting due to breaking waves is not evident on the front side. Traces of erosion are evident on the levee backside near the base. Overtopping and overflow appears to have been minimal along this reach.



Figure A43 Levee crest degraded at a number of locations. Different stages of head-cut advance toward the front side and through the levee crest are evident, some very advanced. Steep leading edge on head-cuts is pronounced. Predominant erosion signature is head-cutting induced by overtopping. Large overwash sediment deposits evident behind each of the head-cuts. Band of surficial breaking wave-induced erosion on the front face is evident, lower on the levee face. No wave-induced erosion of the levee crest is evident in areas where head cutting has not eroded through the levee crest. No evidence of sediment being deposited on front face or toe of the levee.



Figure A44. Levee crest is intact, except at top of photo. This is another excellent example of early stages of head-cut development. Predominant erosion signature is minor surficial wave-induced erosion in a band along the levee surface on the front side and more substantial head-cutting induced by overtopping on the backside. No significant wave-induced erosion of the levee crest is evident in areas where head-cutting has not eroded to the levee crest or in areas where the head-cutting is in an early stage of formation. No severe erosion initiated from lower edge of surface erosion zone on the front face; no deposition of sediment on the levee front face.



Figure A45. Levee crest severely degraded along this reach. Different stages of head-cut advance toward the front side and through the levee crest are evident, many are very advanced. Steep leading edge along head-cut is evident. Predominant erosion signature is head-cutting induced by overtopping. Large overwash sediment deposits evident behind each of the head-cuts. No evidence of even surface erosion on the front face or levee crest. Vegetation appears to be dense, apparently enough to resist wave-induced erosion on the front face but not enough to resist overtopping forces. Note the debris (water-borne) that appears to have been blown into the area. No evidence of sediment deposition on the levee front side or at the front side toe.



Figure A46. Levee crest is intact except for one location. Several small over-topping-induced head-cuts visible, including some very narrow ones. Traces of front-side local scour are visible. No continuous band of wave-induced surface erosion. No significant wave-induced erosion of the levee crest is evident in areas where head-cutting has not eroded to the levee crest or in areas where the head-cutting is in an early stage of formation. Wide deep scour trench due to overtopping evident on the backside along the entire length of wall.



Figure A47. Rotational failure and buckling of the sheet pile wall. Wide irregular scour trench due to overtopping evident on the backside along the entire length of wall, with evidence of sediments carried away out of the trench and deposited further landward. Some traces of surficial erosion induced by wave action on the front side. Predominant erosion signature induced by overtopping, not front side erosion due to waves.



Figure A48. Levee crest is intact throughout this reach. Some localized wave-induced erosion evident at one isolated location. There are a few pockets of early stages of head-cut development evident on the backside. Predominant erosion signature is minor head-cutting induced by overtopping on the backside. Overwash sediment deposit evident behind the more advanced head-cut. Overtopping and overflow appears to have been minimal along this reach. No band of surficial wave-induced erosion along the front face is seen.



Figure A49. Levee is crest intact, except at one localized erosion area. Some traces of erosion caused by overtopping are evident on the back side. Traces of the band of surficial wave-induced erosion are seen along the front face. Overtopping appears to have been less along this reach.



Figure A50. Figure shows southeastern end of the MRGO Reach 2 levee. Levee crest is intact. Several small over-topping-induced head-cuts are visible. Predominant erosion signature is traces of wave-induced erosion of the levee on the front side and localized head-cutting due to overtopping on the back side. Surface erosion is evident at base of levee on the front side.

Appendix B: 3D Renderings of Post-Storm Levee Condition Based on LIDAR Data

This series of images shows color-shaded contours of levee elevation along the southern St. Bernard Parish the MRGO Reach 2 and hurricane protection levees, derived from the post-storm LIDAR data. Levee and wall crest elevations along the hurricane protection system in each image are cited, as is information about the peak water level and potential for overtopping during Katrina.

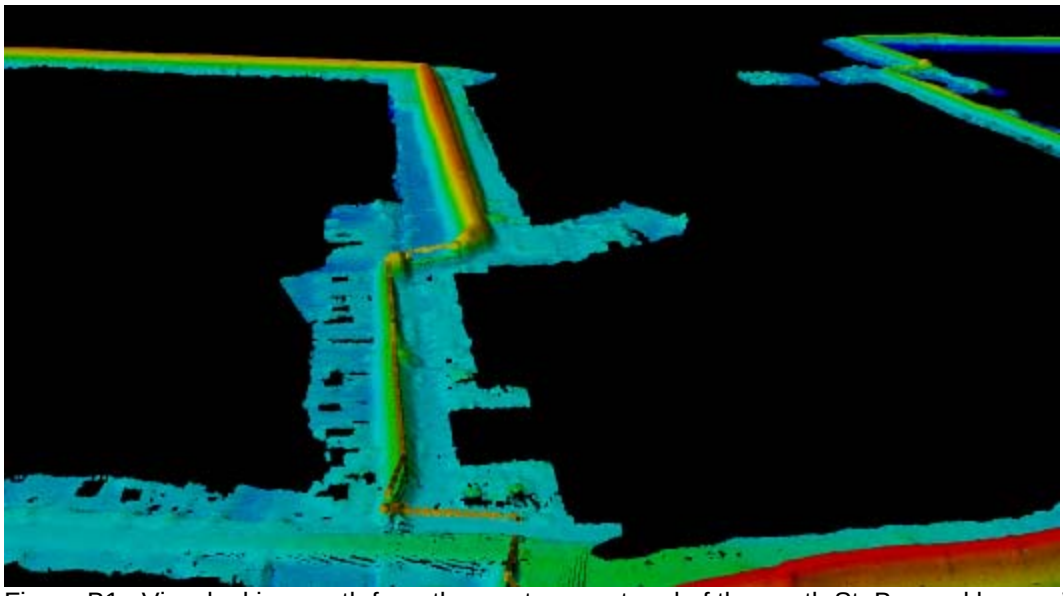


Figure B1. View looking south from the westernmost end of the south St. Bernard levee. Wall length is 1670 ft with crests of 12.5 to13 ft in many locations; most less than 13.5 ft; all lower than 14 ft. An excellent-rated high water mark acquired at this location indicated a peak water level of 11 ft, several feet less than the wall and levee crest elevations. Sheltered area from wave action, so overtopping was unlikely.

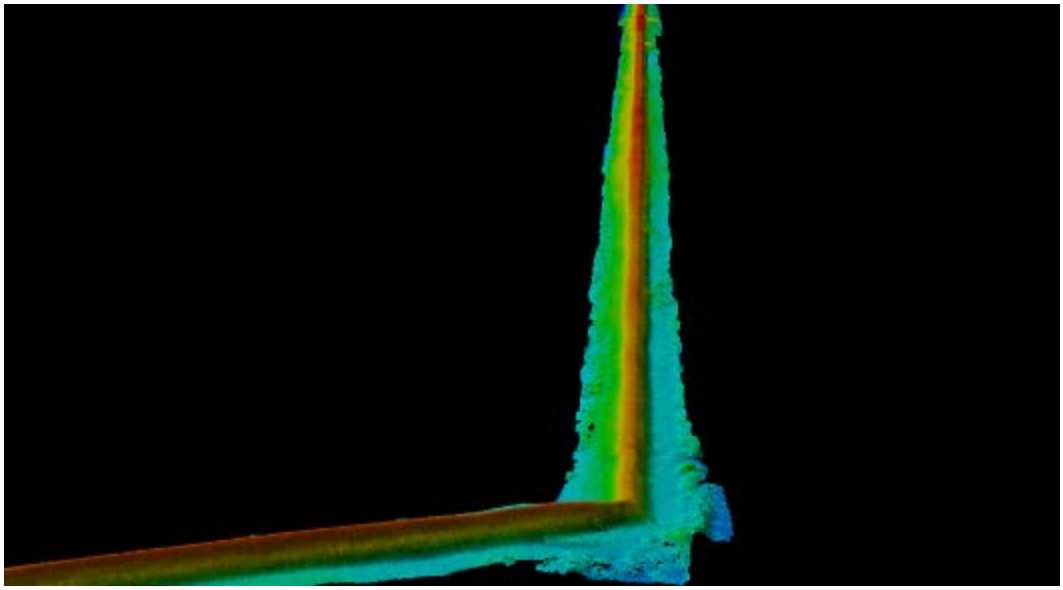


Figure B2. View looking east along the southern St. Bernard levee. Note low spot at the corner; levee crest elevations here are approximately 14 to 14.5 ft. Peak water level here was about 11 ft so wave overtopping here was unlikely. The higher spots along this levee are approximately 18 ft (red-colored sections). Peak water levels along this region increased from west to east, and were probably 12 to 13 ft in this region. Wave overtopping might have occurred at the low spots; no steady overflow at these water levels.

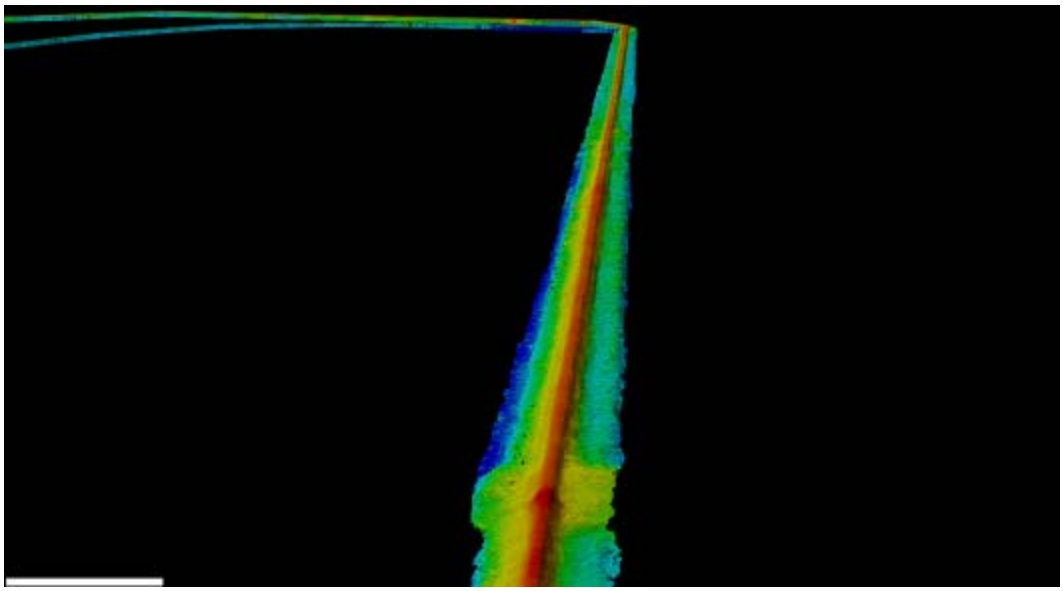


Figure B3. View looking east along the southern St. Bernard levee. Just to the west of the Creedmore structure levees crests ranged from 15 to 15.5 ft; elsewhere between the Creedmore and Caernarvon, elevations were generally16.5 to 18 ft. Peak water levels along this reach are estimated to be 12 to 14.5 ft. Some wave overtopping might have occurred at lowest spots; no steady overflow. East of Creedmore, elevations were 14 to 15 ft, gradually rising to 17 ft at the eastern end. Peak water levels along this region increased from west to east, and are estimated to be 14 to 16.5 ft in this region. Steady overflow and wave overtopping expected, of shorter duration due to sharper peak in hydrograph shape.

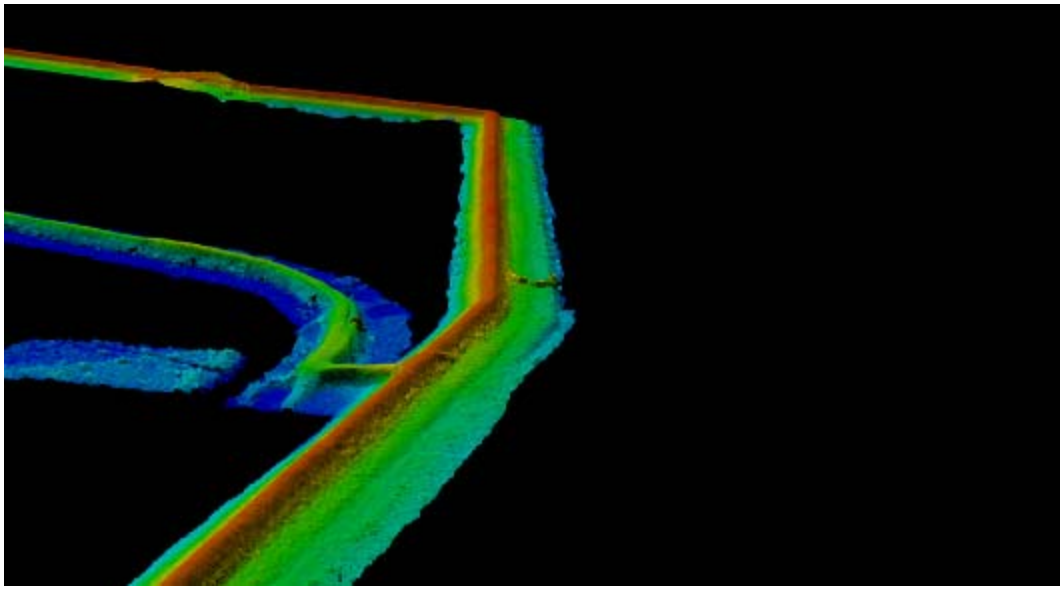


Figure B4. View looking east. The lower 40-Arpent levee is visible on the left. West of the juncture with the 40-Arpent levee, most crest elevations were 16 to 17 ft. To the east of the juncture, crest elevations were greater than 16.5 ft but less than 17 ft in most places. Peak water levels would have been around 16 to 16.5 ft; so wave overtopping, and perhaps steady overflow at isolated locations, expected in this region.

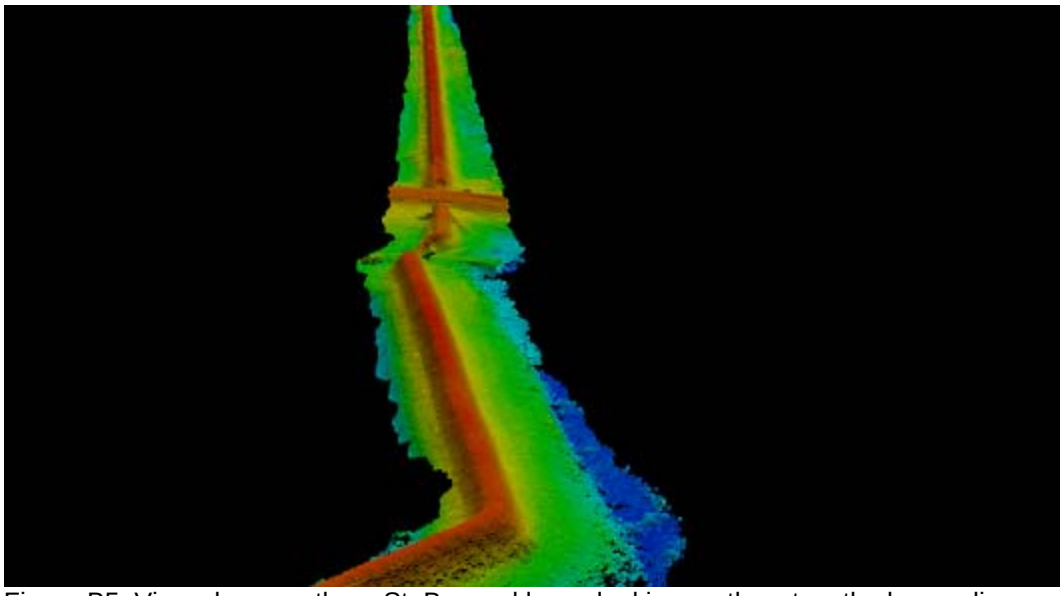


Figure B5. View along southern St. Bernard levee looking northeast as the levee alignment changes. The low spots on the 120-ft long wall in the center of the image are 15 to 15.5 ft; most 16.5 to 17 ft. Low spots on the levee on either side of the roadway are 13.5 and 14.5 ft. Peak water levels were around 17 ft, so steady overflow and wave overtopping expected in this region.

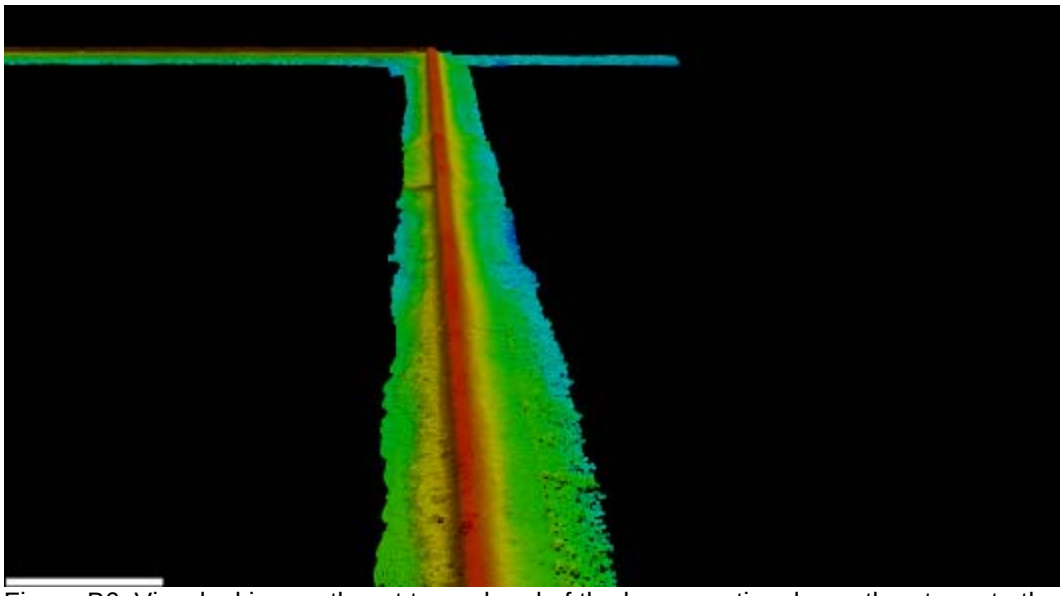


Figure B6. View looking northeast toward end of the levee section; levee then turns to the northwest along MRGO Reach 2. This is a relatively high stretch of levee. Low spots on the levee had crest elevations between 18 and 18.5 ft; most had elevations between 18.5 and 19 ft, and the highest posts exceeded 19 ft. For peak water levels of 17 to 17.5 ft, wave overtopping would be expected in this region, but no steady overflow.

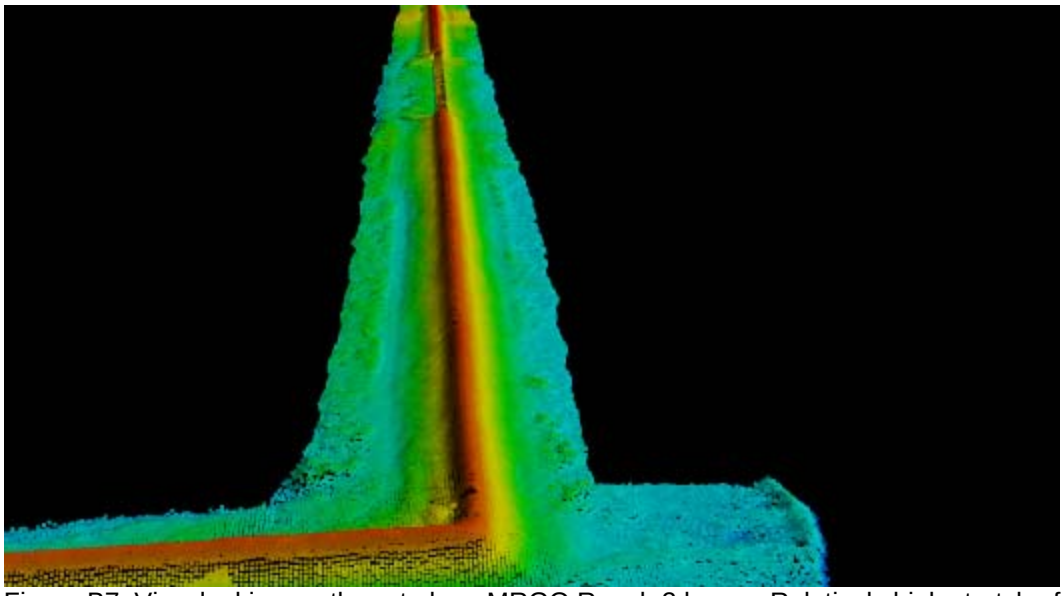


Figure B7. View looking northwest along MRGO Reach 2 levee. Relatively high stretch of levee in foreground. All crest elevations exceed 18 ft; most exceeded 18.5 ft. All were less than 19 ft. 1390-ft floodwall seen in the background. Low spots on the wall were 13.5 ft; most crests were 13.5 to 14.5 ft; highest were about 15.5 ft. For peak water levels of 17.5 ft, wave overtopping of levees would be expected, but no steady overflow over the levees. Some minor backside levee erosion (dark spot) evident at the corner. At the wall, steady overflow and wave overtopping would have persisted for several hours.

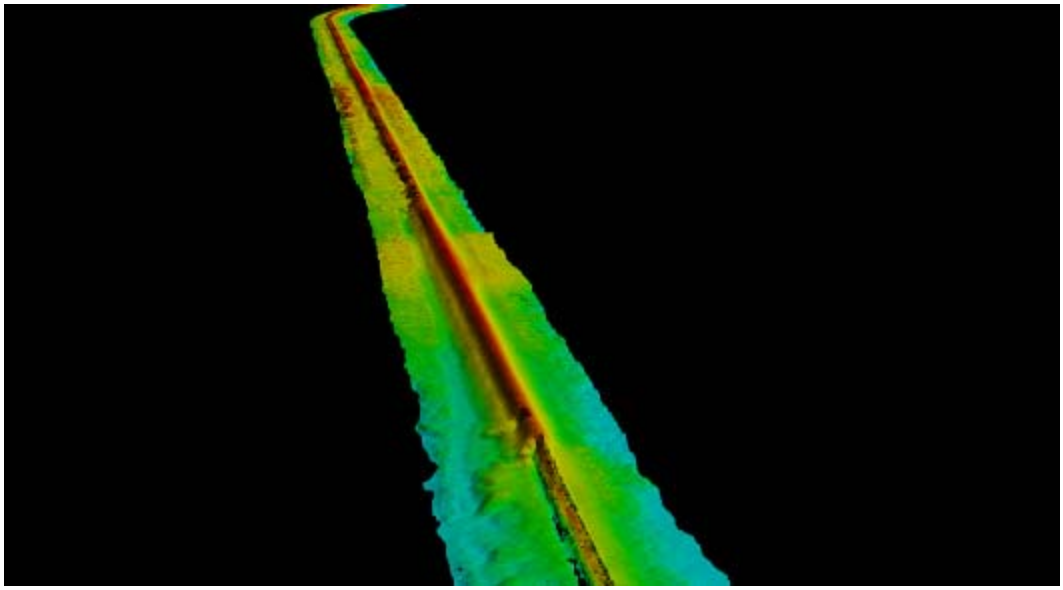


Figure B8. View looking northwest from the floodwall toward the bend in the levee just south of Bayou Dupre. High parts of the levee just north of the wall exceeded 19 ft; most were greater than 18.5 ft; all were greater than 18 ft. Further to the north in the more heavily eroded region, all elevations exceeded 17 ft; some low spots of 17 to 17.5 ft; most crest elevations exceeded 18 ft. For peak water levels of 17.5 ft, wave overtopping would be expected; steady overflow in places. Levee crest is generally intact; with some degradation of the crest in places.

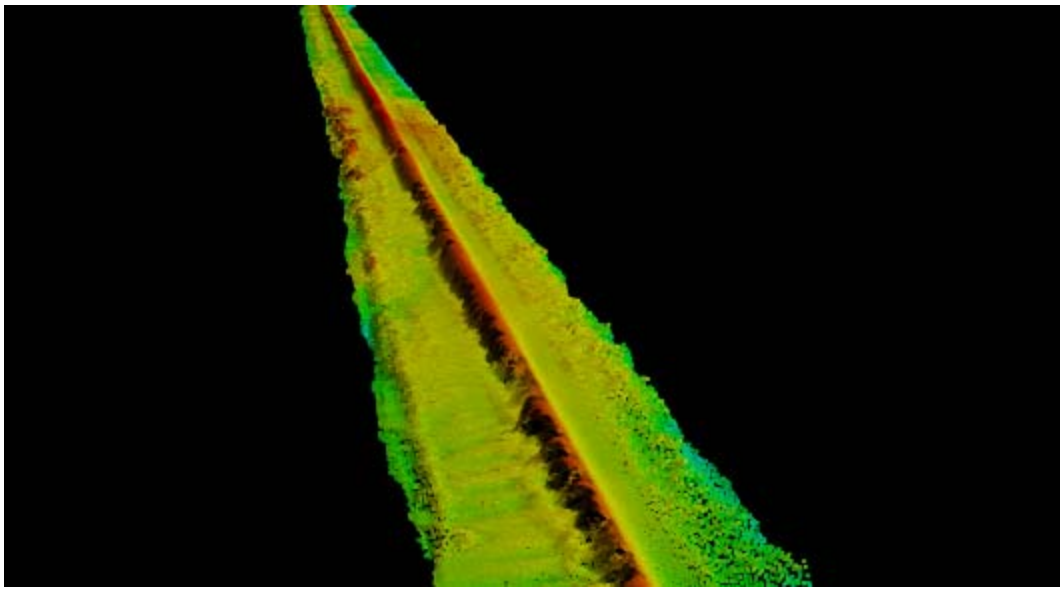


Figure B9. View looking northwest from the floodwall toward the bend in the levee, which is just south of Bayou Dupre. Levee crest is degraded in places. All levee crest elevations less than 19 ft. There were a few low spots with crest elevations between 17 and 17.5 ft; most were greater than 18 ft. For peak water levels of 17.5 ft, wave overtopping would be expected; steady overflow in places.

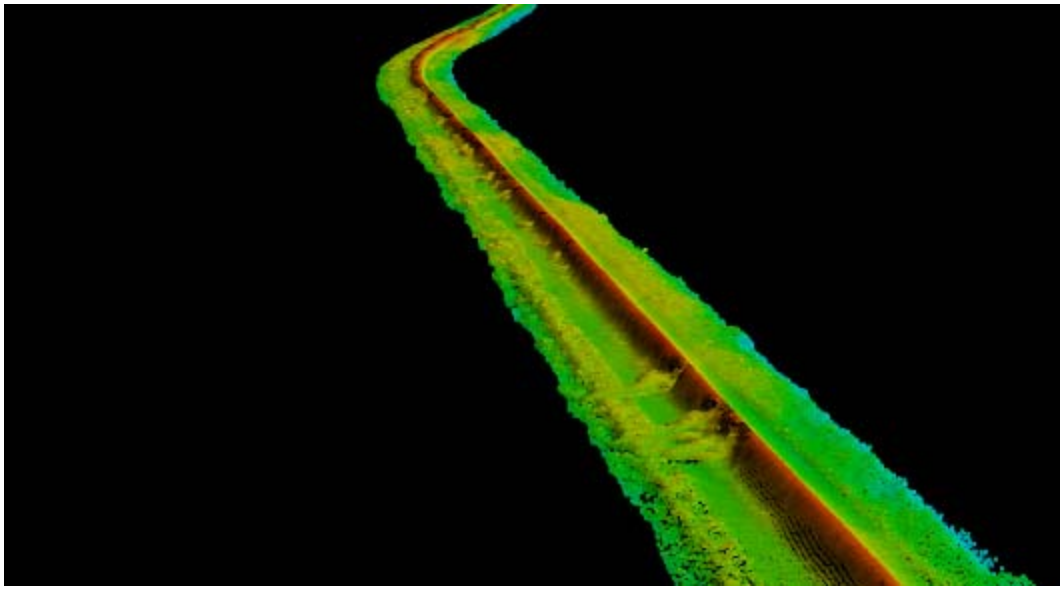


Figure B10. View looking northwest from the floodwall toward the bend in the levee, which is just south of Bayou Dupre. crest is generally intact, except in a few places. All levee crest elevations less than 19 ft. There were a few low spots with crest elevations between 17 and 17.5 ft; many exceeded 18. For peak water level of 17.5 ft, wave overtopping would be expected; steady overflow in places.

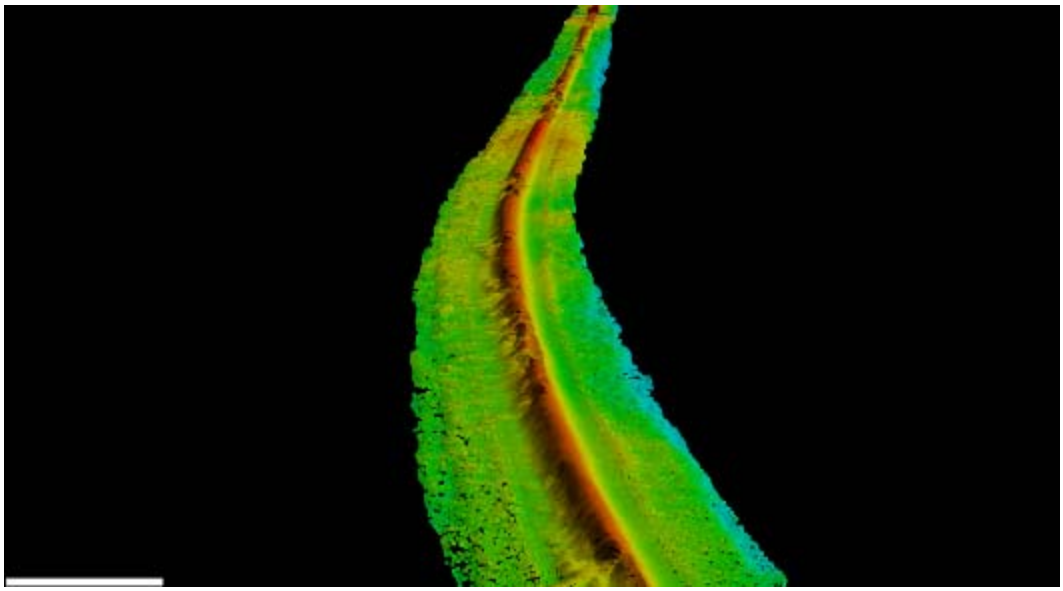


Figure B11. View of the bend in the levee just south of Bayou Dupre. Considerable levee degradation in places. Nearly all levee crest elevations exceed 17.5 ft; many exceeded 18 ft. Peak water levels were 17.5 ft, so wave overtopping would be expected, and localized overflow.

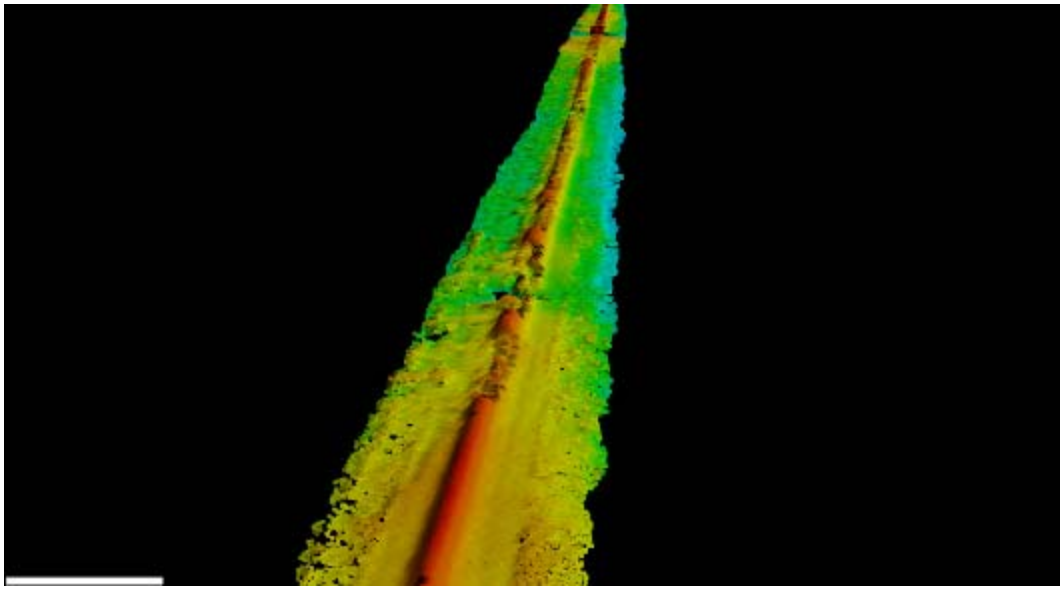


Figure B12. View looking northwest toward Bay Dupre (visible far in the background). Along the undamaged section of levee in the foreground, crest elevations exceed 19 ft. In the heavily eroded section just to the north of the high levee, most crest elevations exceeded 17.5 ft; most exceeded 18 ft; and many exceeded 18.5 ft. For peak water levels of 17.5 ft, wave overtopping would be expected, steady overflow in places.

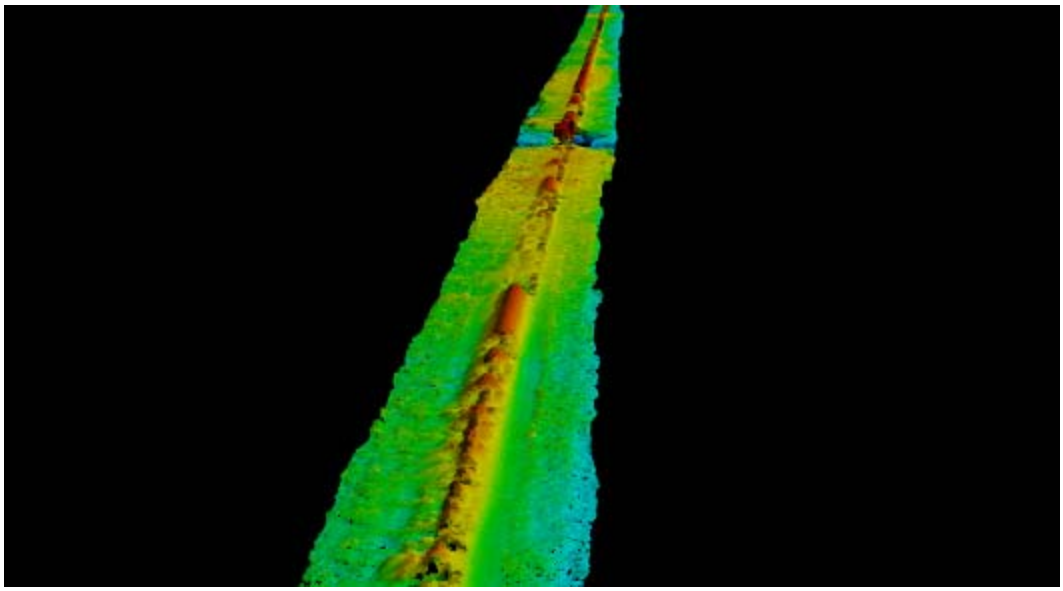


Figure B13. View looking northwest toward Bay Dupre (approach channel visible in the image). In this heavily eroded region, most crest elevations exceeded 18 ft; some exceeded 19 ft. For peak water levels of 17.5 ft, wave overtopping would be expected; perhaps overflow in places.

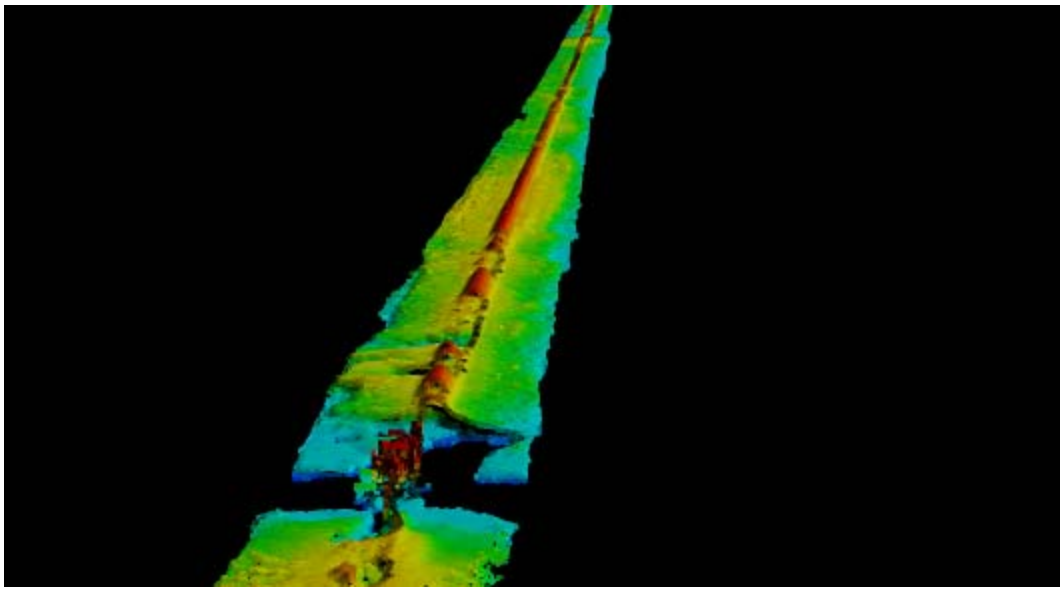


Figure B14. View looking northwest from Bay Dupre. A few low spots in this region had crest elevations of 18 to 18.5 ft; most greater than 18.5 ft. For peak water levels of 17.5 ft, wave overtopping would be expected; perhaps overflow in places.

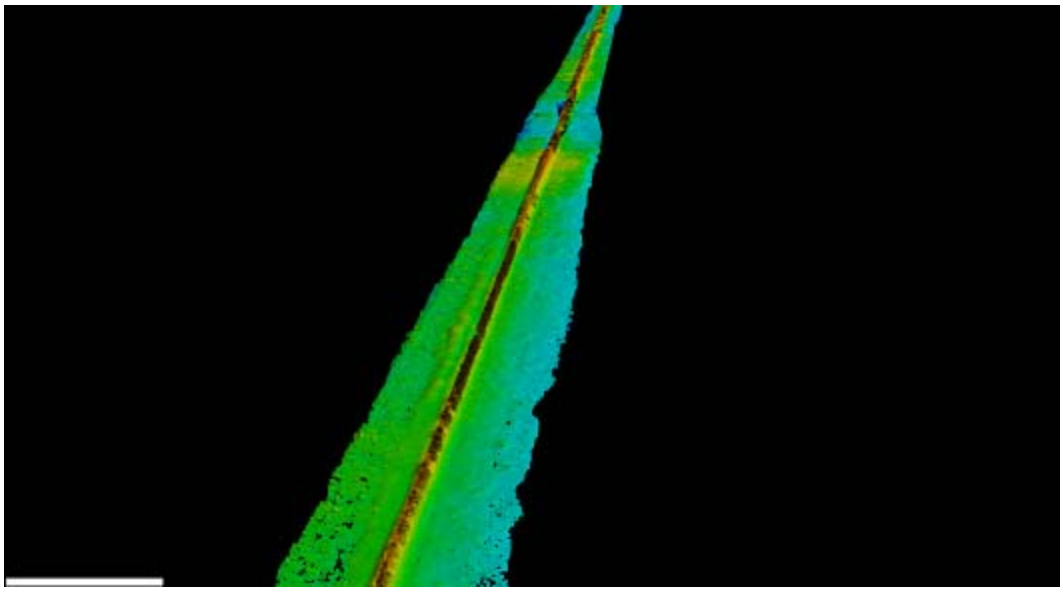


Figure B15. View looking northwest toward Bayou Bienvenue. This region was generally 1 to 1.5 ft lower than the levees to the south. Crest elevations here were 17.5 ft or less; many areas had crests of 16 to 17.5 ft. Wall elevations were low too. For peak water levels of 17.5 ft, large sections of this levee were heavily overtopped by steady overflow and wave overtopping. Same conditions persisted at the lowest wall sections for quite a few hours.

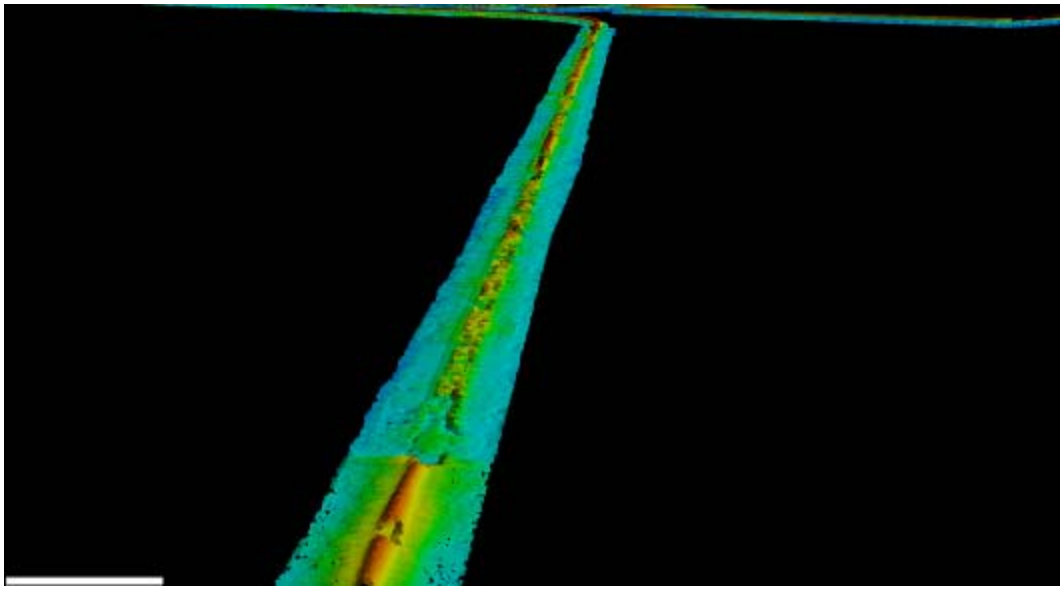


Figure B16. View looking northwest toward Bayou Bienvenue. Levee along New Orleans East visible in the background. Crest elevations here were 17.5 ft or less. Significant stretches had crests of 15.5 to 16.5 ft; the lowest had crests of 15 ft. Wall elevations were low too. For peak water level of 17.5 ft, large sections of this levee were heavily overtopped by steady overflow and wave overtopping. Same persisted at the lowest wall sections for quite a few hours.

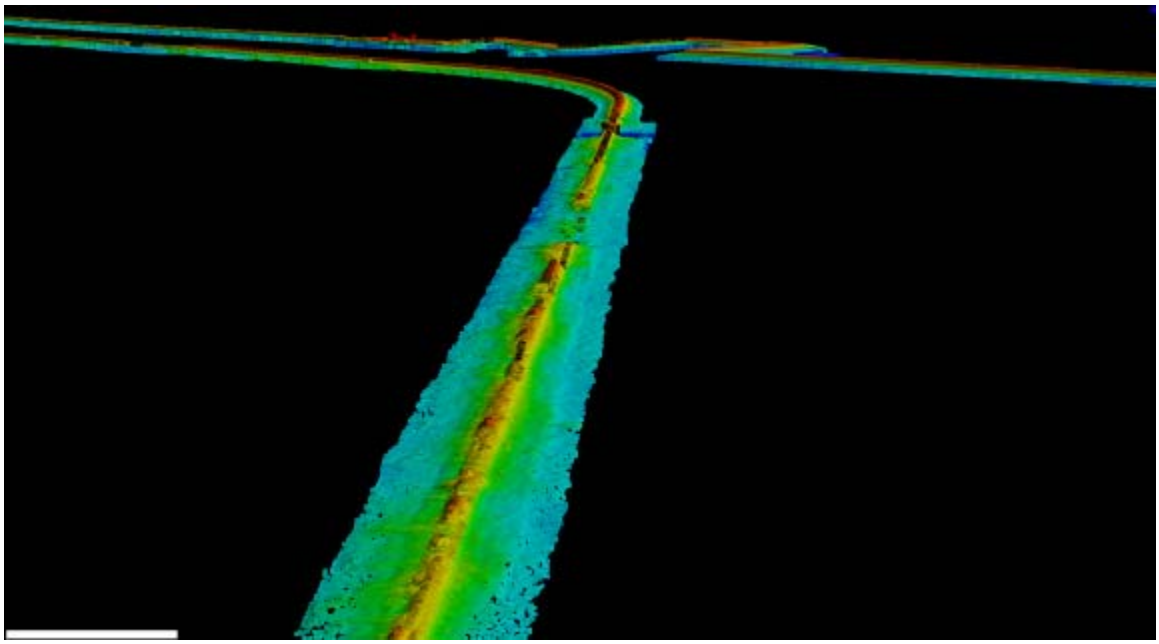


Figure B17. View looking northwest toward Bayou Bienvenue (background). Crest elevations here were 17.5 ft or less. Significant stretches had crests of 15 to 16.5 ft. Wall elevations were low too. Closer to Bayou Bienvenue, levees generally had crest elevations of around 17 to 17.5 ft, with spots as low as 16.5 ft. For peak water level of 17.5 ft, large sections of this levee were heavily overtopped with combined steady overflow and wave overtopping. Steady flow over the lowest wall sections persisted for hours.

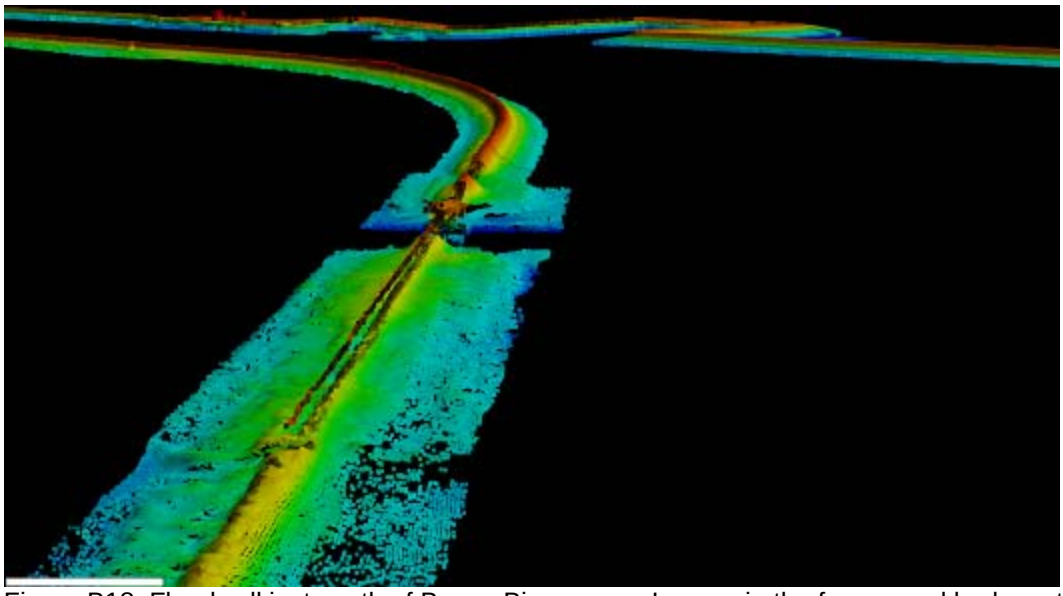


Figure B18. Floodwall just south of Bayou Bienvenue. Levees in the foreground had crests less than 17.5 ft. For peak water level of 17.5 ft, this section of levee was overtopped by wave action and steady overflow in places. Steady flow over the wall section and lower levees persisted for quite a few hours.

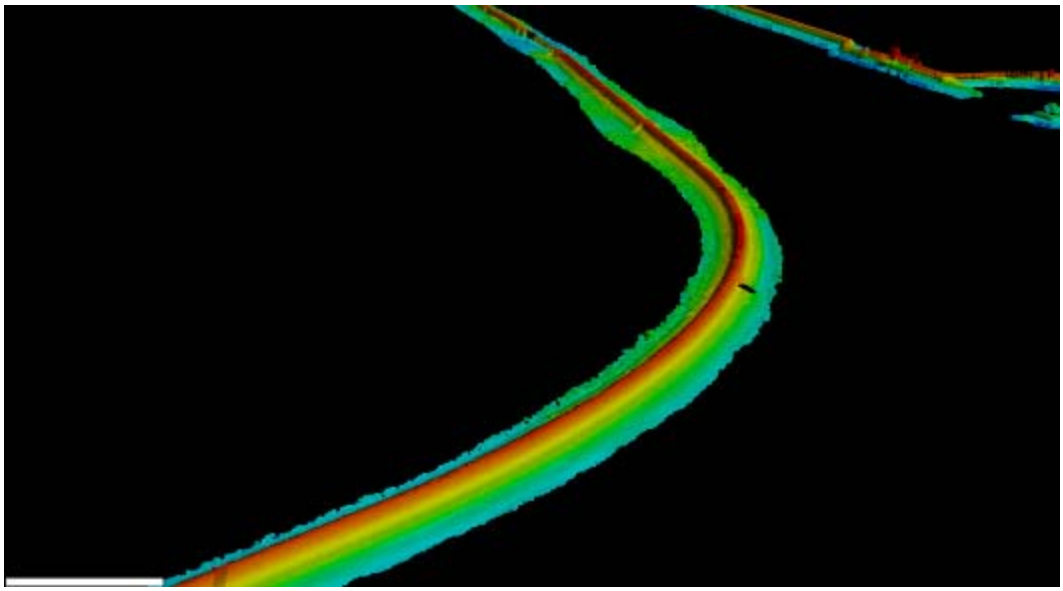


Figure B19. Junction of GIWW and MRGO waterways. Crest elevations along this levee bend exceed 18 ft in most places. Peak water levels near Paris Road Bridge (at the top of the image were 15.5 ft). Levels would be decreasing from 17.5 to 15.5 ft along this bend. Some wave overtopping of this levee section might have occurred; but no steady overflow.

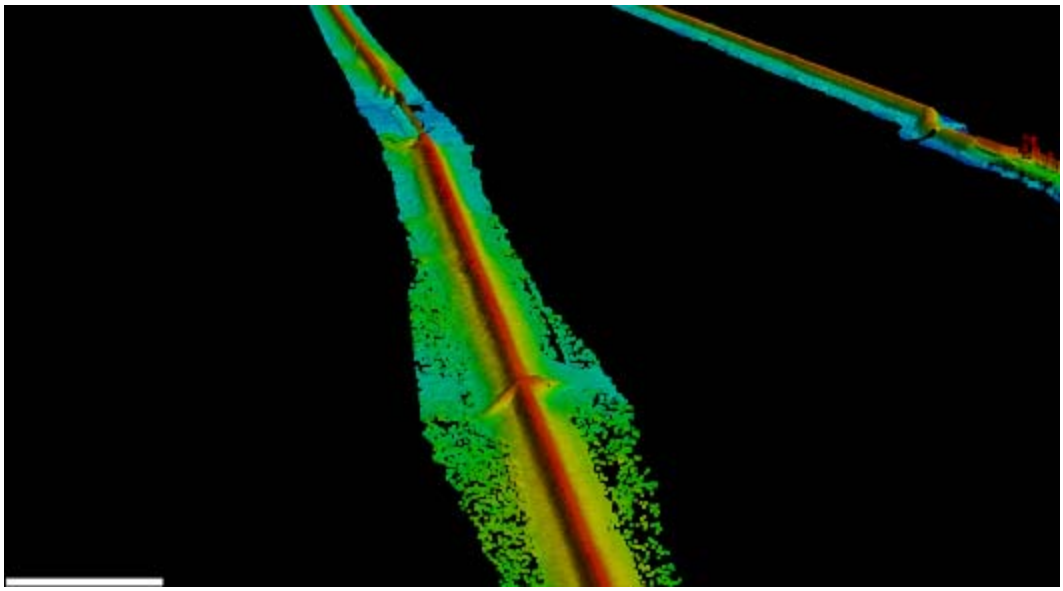


Figure B20. Crest elevations along this levee bend were 17.5 to 18.5 ft. Peak water levels near Paris Road Bridge (at the top of the image were 15.5 ft). Overtopping of the levee unlikely here.

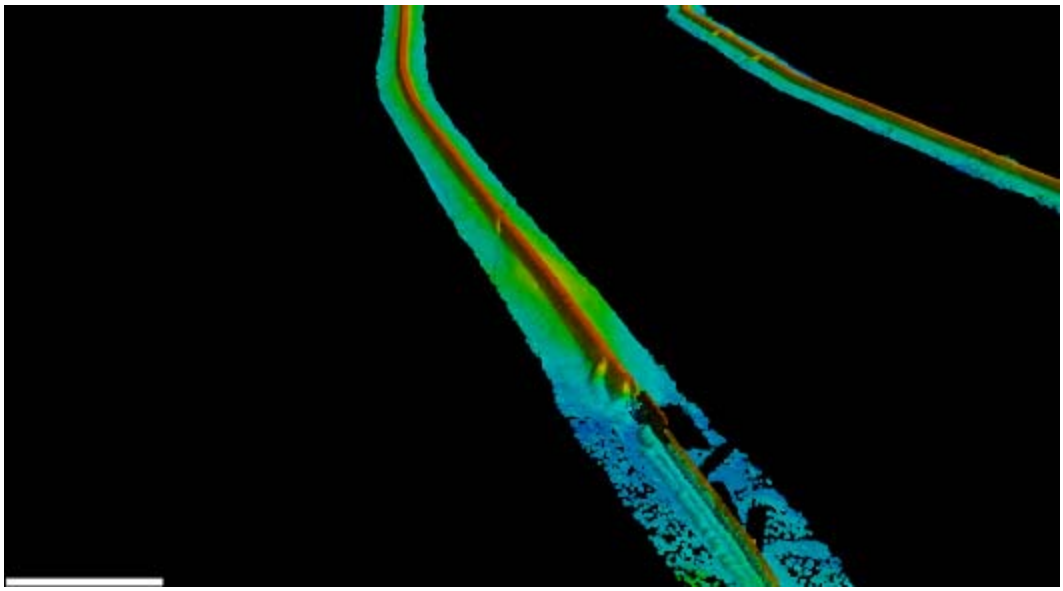


Figure B21. View looking west along GIWW/MRGO Reach 1 at Parish Road Bridge. Crest elevations of the wall were less than 13.5 ft, 11.5 ft at the lowest points. For peak water level of 15.5 ft, steady overflow over the wall expected for several hours. Levees immediately to the west had crest elevations from 16 to 17 ft. Perhaps some wave overtopping likely, with steady overflow possible in isolated locations.

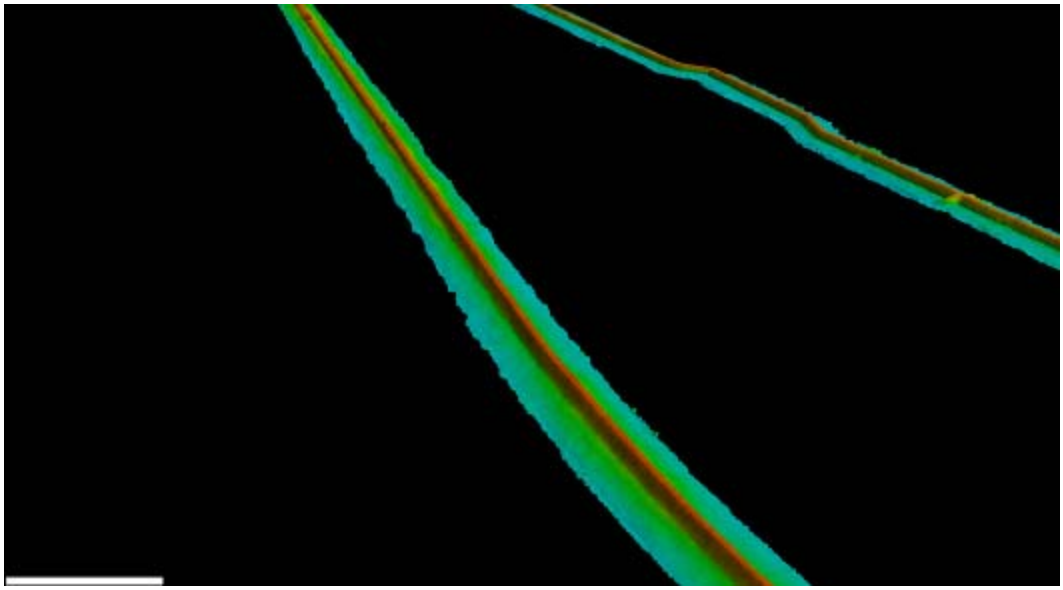


Figure B22. View looking west along GIWW/MRGO Reach 1. Levees had crest elevations from 15.5 to 16.5 ft, less than 15 ft in isolated areas. Wave overtopping expected, with some steady overflow at the lowest spots.

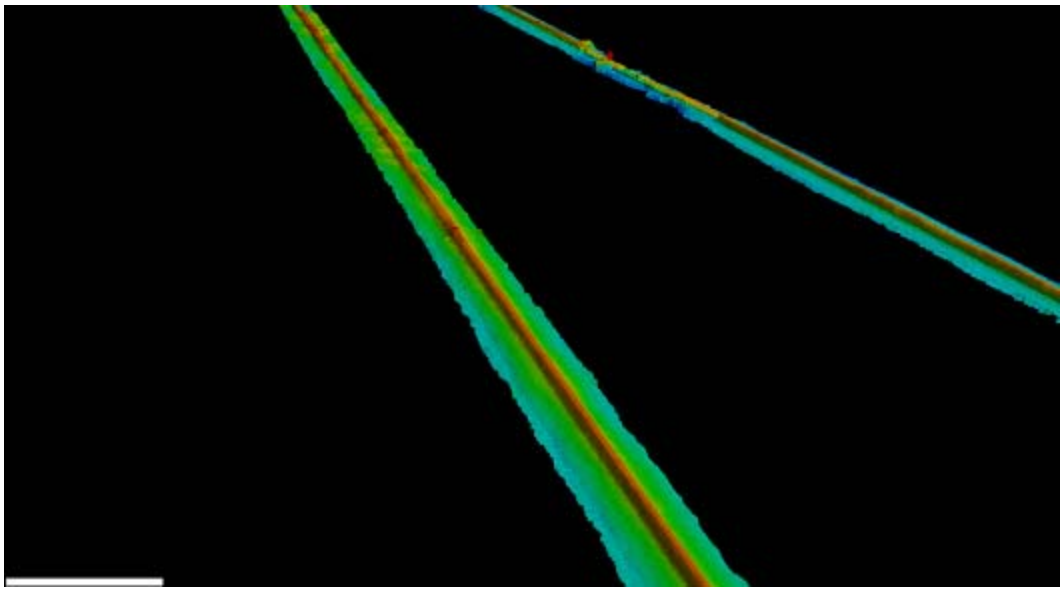


Figure B23. View looking west along GIWW/MRGO Reach 1. Levees had crest elevations from 15 to 16.5 ft. For peak water level of 15.5 ft, wave overtopping expected, and steady overflow at the lowest spots.

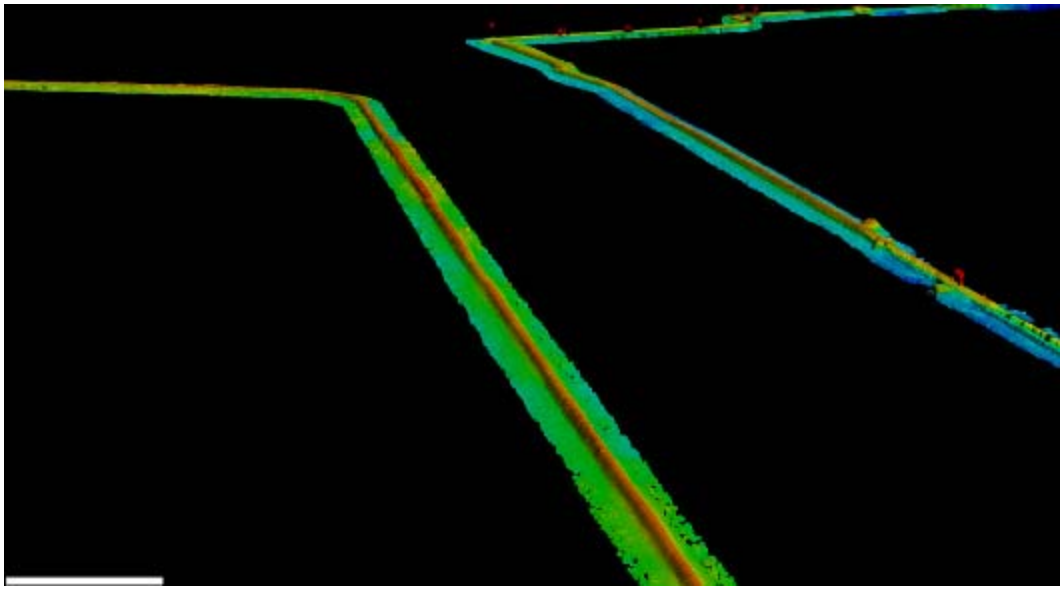


Figure B24. View looking west along GIWW/MRGO Reach 1, junction with IHNC in the background. Levees at and east of the bend had crest elevations from 14 to 17 ft. For peak water level of 15.4, wave overtopping expected with steady overflow in places.

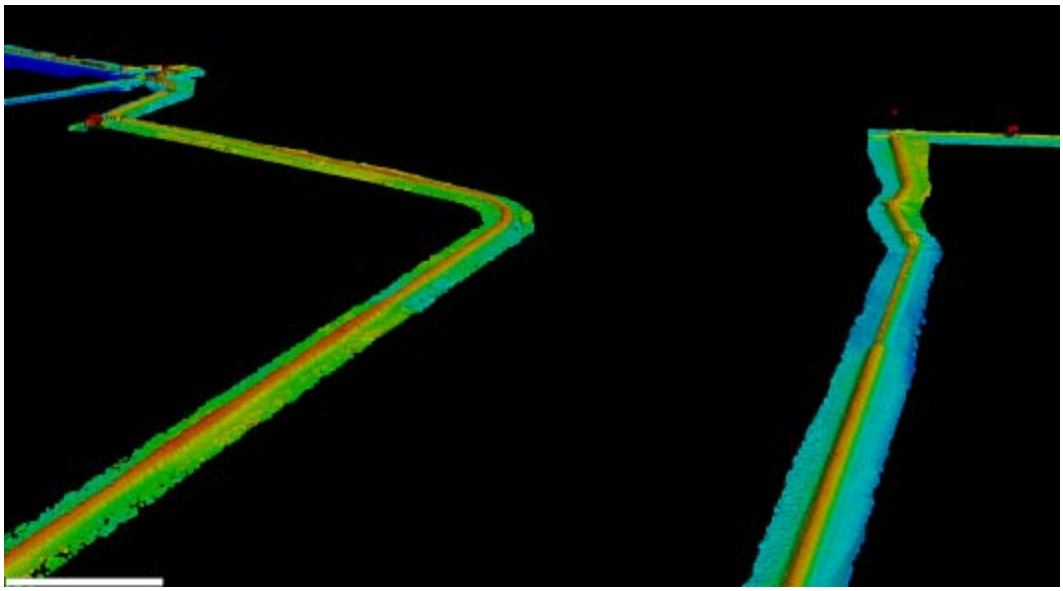


Figure B25. View looking west toward GIWW/MRGO Reach 1 junction with IHNC. At low spots on levees adjacent to the IHNC, crest elevations were 13.5 to 14 ft in places, 14 to 14.5 ft in many places, and much of the levee had crests of 14.5 to 15 ft. For peak water level of 15.4 ft, widespread steady overflow expected. For the walls north of Florida Avenue, some low spots had crest elevations of 12 ft, a number were 12.5 to 13 ft, many were 13 to 13.5 ft, and nearly all were less than 14.5 ft. For peak water level of 15.2 ft, widespread steady overflow expected for several hours in places.

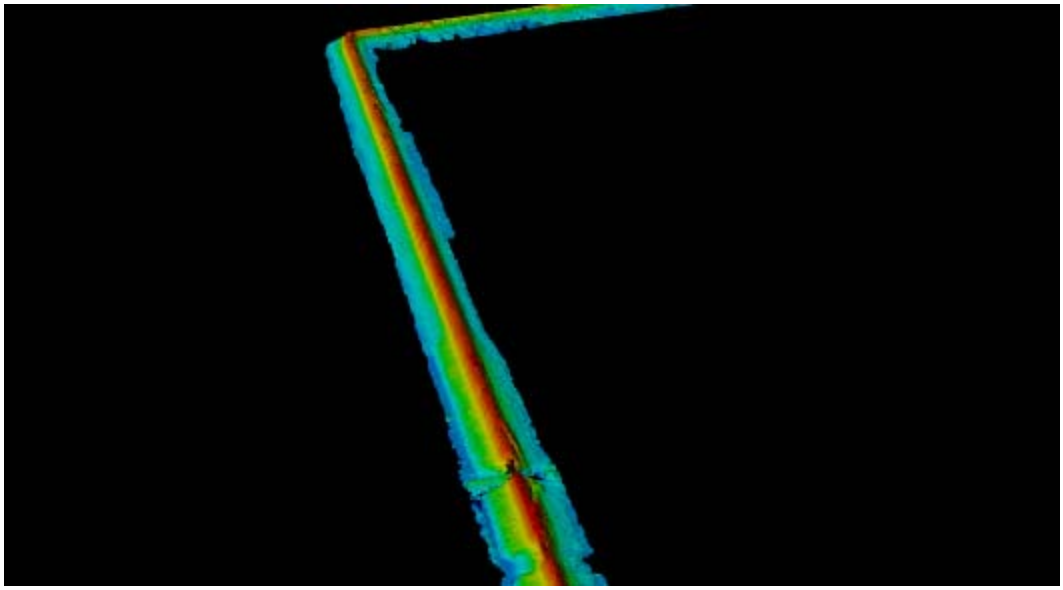


Figure B26. View looking south toward the southeastern most corner of the New Orleans East levee (Southpoint to GIWW reach). CSX rail line crossing of the levee seen in the foreground.

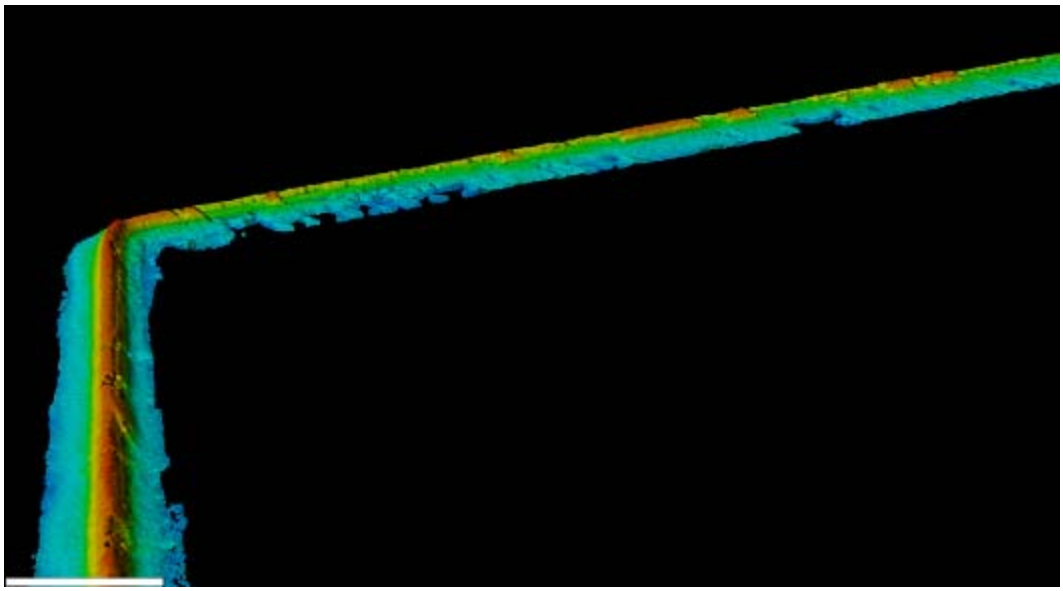


Figure B27. View looking south toward the southeastern most corner of the New Orleans East back levee (Southpoint to GIWW reach). GIWW runs along the levee at the top. Results of overtopping evident along both levees. Levee completely degraded in many places.

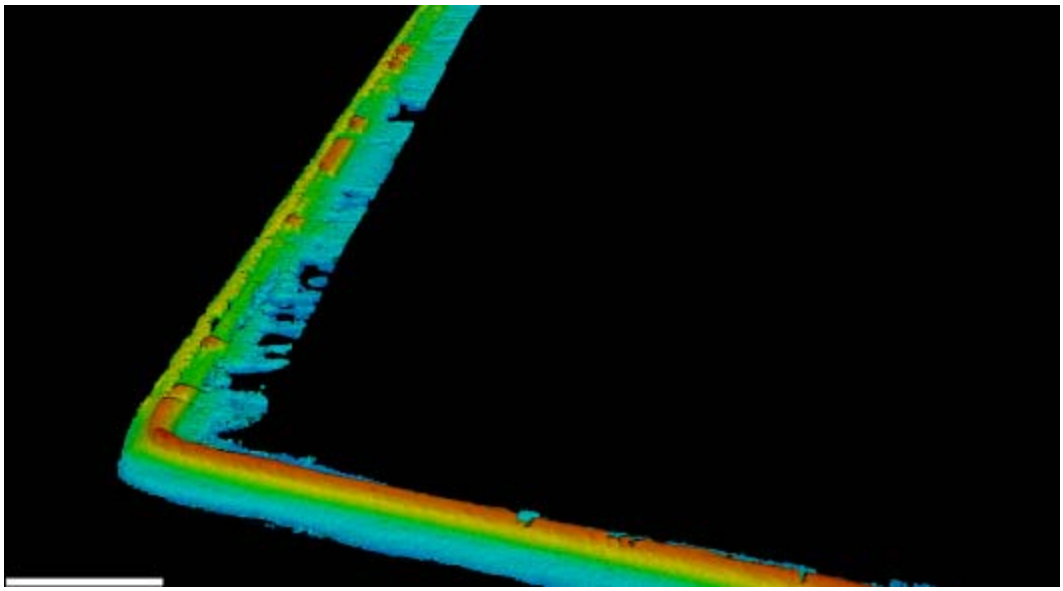


Figure B28. View looking east along the GIWW and New Orleans East back levee. Levee crest elevations at low spots were 15.5 to 16 ft. Most crests less than 16 ft in this region. For peak water level of 15.7 ft, wave overtopping expected, with steady overflow in places. Levee completely degraded in many places.

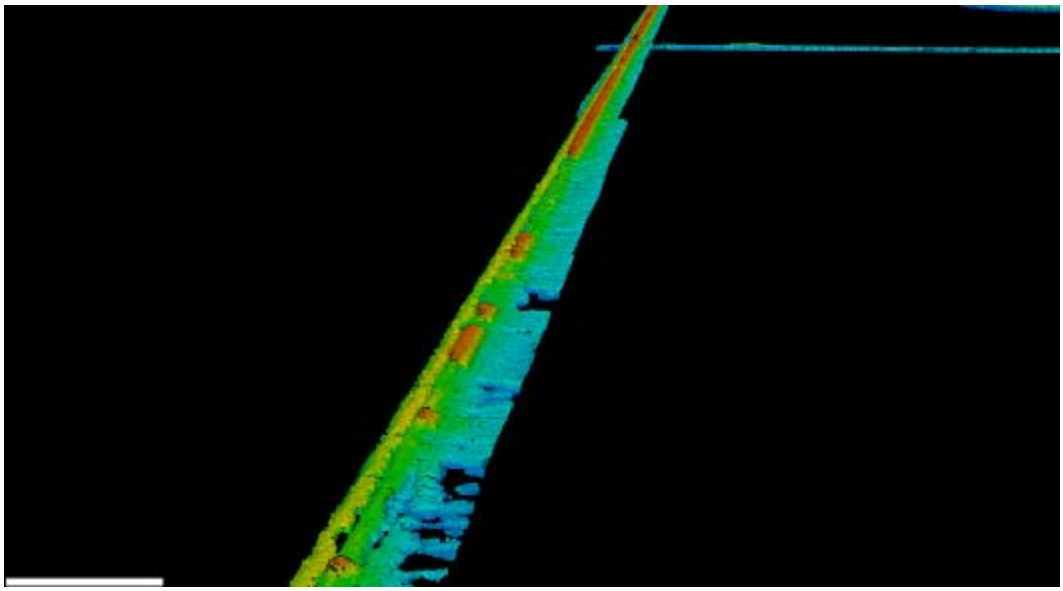


Figure B29. View looking east along the GIWW and New Orleans East levee. Maxent Levee in background. Levee crest elevations at low spots were 16 to 16.5 ft; many 16.5 to 17 ft, all less than 17.5 ft. For peak water level of 15.7 ft, wave overtopping expected. Levee completely degraded in many places

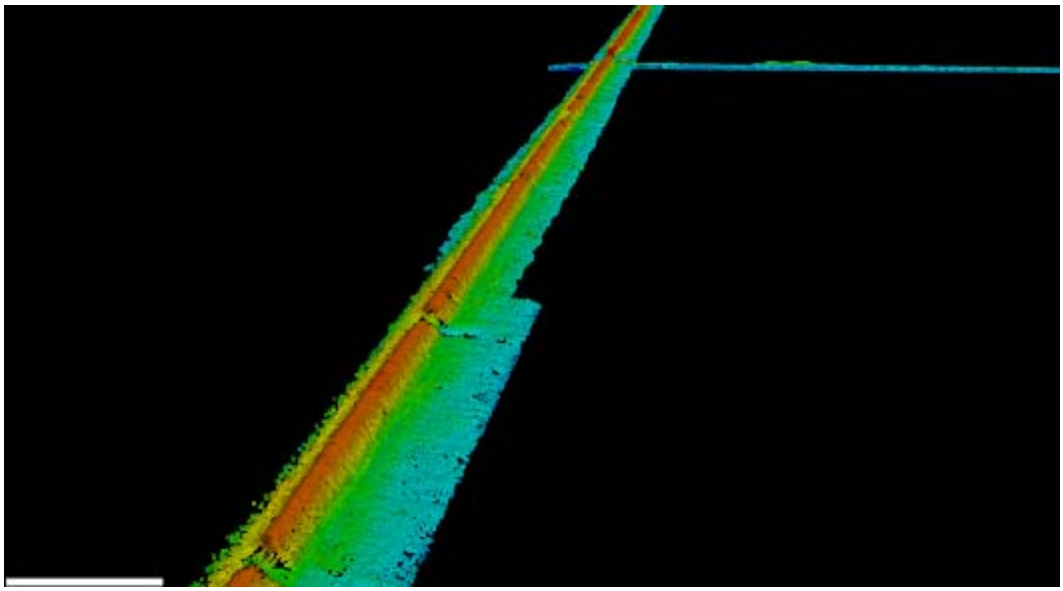


Figure B30. View looking east along the GIWW and New Orleans East levee. Maxent Levee in the background. Levee crest elevations at low spots were 16 to 16.5 ft; many crests 16.5 to 17 ft; most less than 17 and all less that 17.5 ft. For peak water level of 15.7 ft, wave overtopping expected. Levee fairly intact, except in several places.

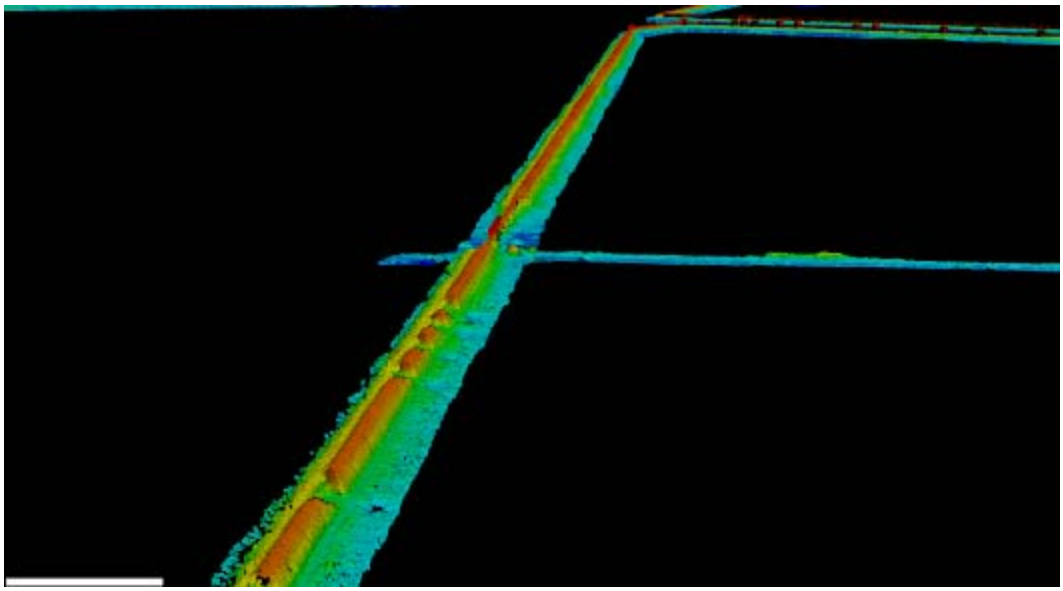


Figure B31. View looking east along the GIWW and New Orleans East levee. Maxent Levee in center; Michoud Canal in the background. Levee crest elevations at low spots were 16 to 16.5 ft; many crests 16.5 to 17 ft; all less than 17.5 ft. For peak water level of 15.6 ft, wave overtopping expected. Levee severely degraded in places. Pump Station OP-15 visible in the center of the image.

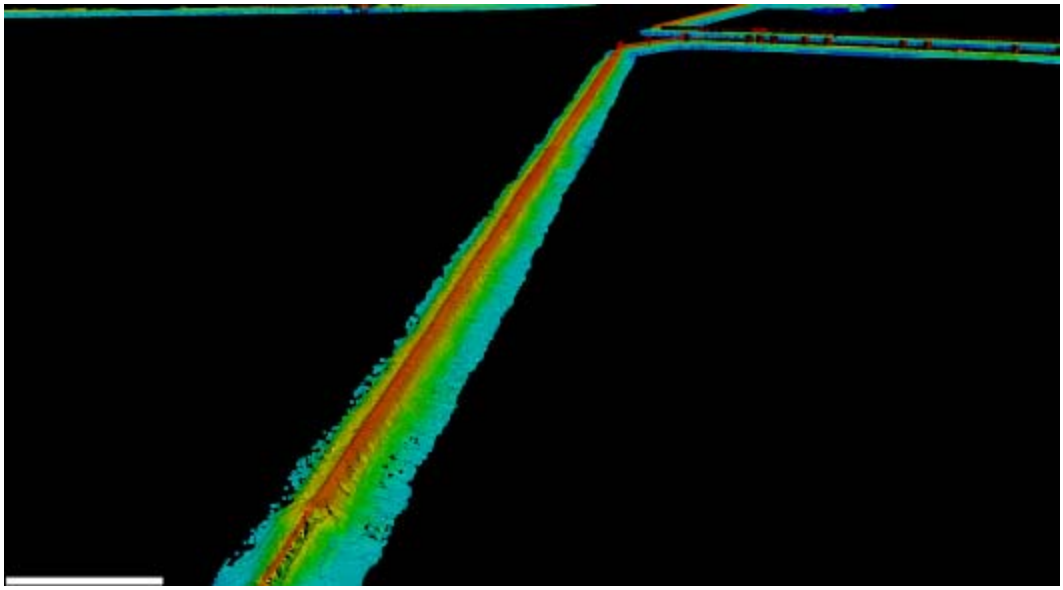


Figure B32. View looking east along the GIWW and New Orleans East levee. Wall at Pump Station OP-15 in the foreground. Michoud Canal in the background. Levee crest elevations at lowest spots were 16.5 to 17 ft; many crests between 17 and 17.5 ft; most greater than 18 ft. For peak water level of 15.6 ft, wave overtopping expected. Levee intact. Isolated rotational failure of sheet pile wall at Pump Station OP-15.

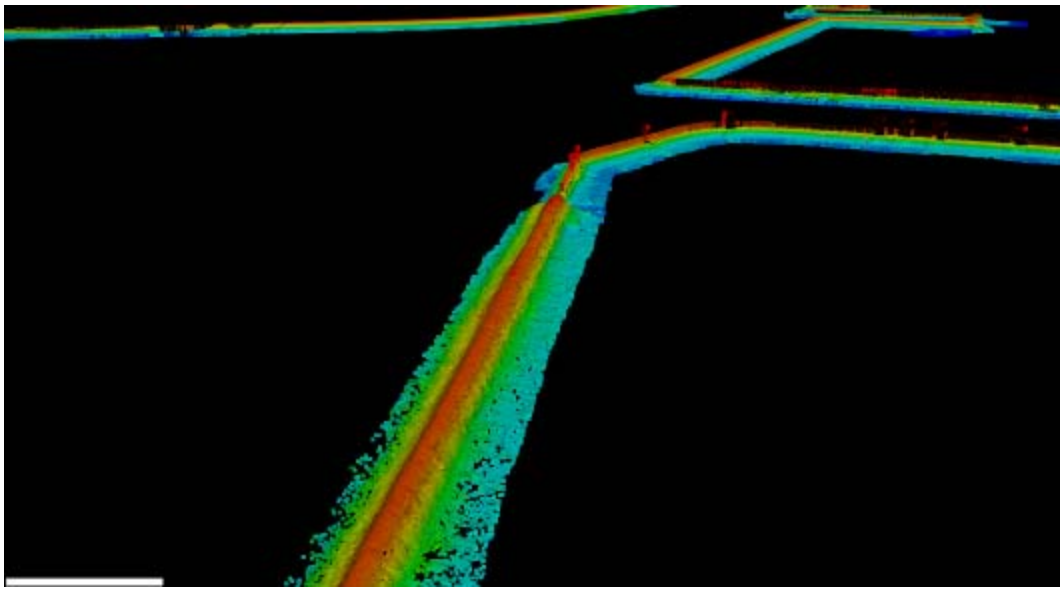


Figure B33. View looking east toward Michoud Canal along the GIWW and New Orleans East levee. Levee crest elevations at lowest spots were 17 to 17.5 ft; many crests between 17.5 ft and 18 ft. For peak water level of 15.6 ft, wave overtopping expected. Levee intact along this reach. Small breach in sheet pile wall at Air Products Plant.

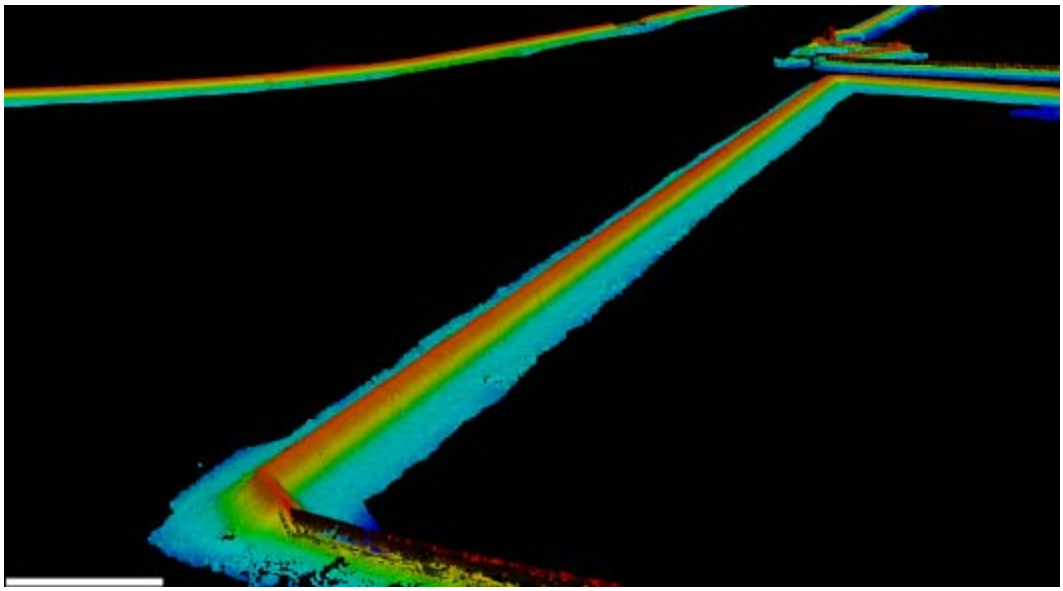


Figure B34. View looking east between Michoud Canal and Michoud Slip along the GIWW and New Orleans East levee. Levee crest elevations at lowest spots were 16 to 16.5 ft; most 16 to 17 ft. For peak water level of 15.6 ft, some wave overtopping expected in this region. Levee intact along this reach.

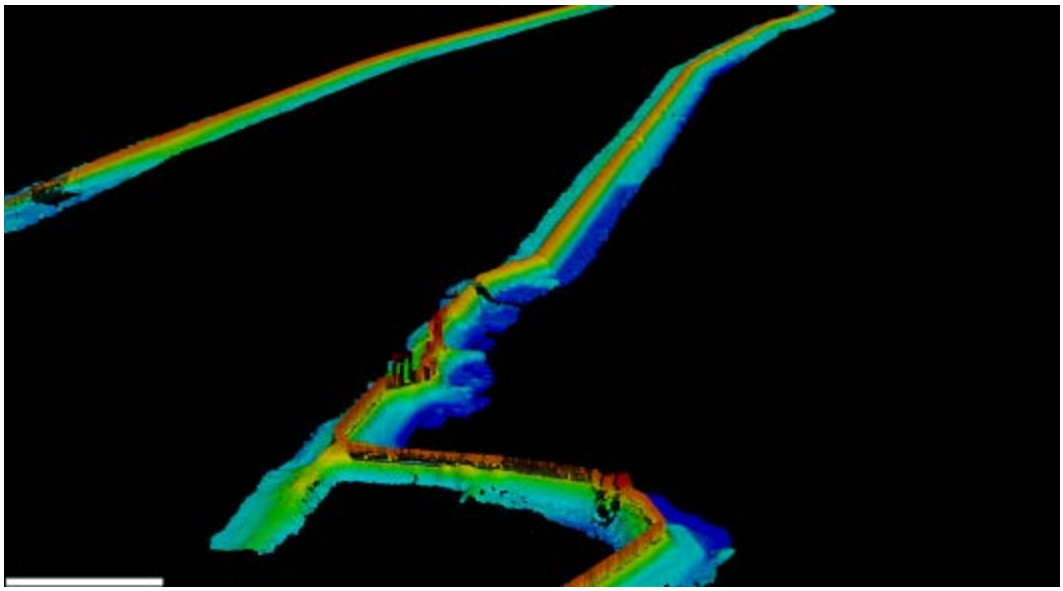


Figure B35. View looking east from Michoud Slip along the GIWW and New Orleans East levee. Wall crests elevations in the Slip were around 16.5 ft (no steady overflow expected). For levees west of Paris Road Bridge (west of the Slip), crest elevations were 14.5 to 15 ft (13.5 to 14.5 in low spots); many less than 15.5 ft. For peak water level of 15.5 ft, widespread steady overflow expected, persisting for several hours in places. Levee intact along this reach.

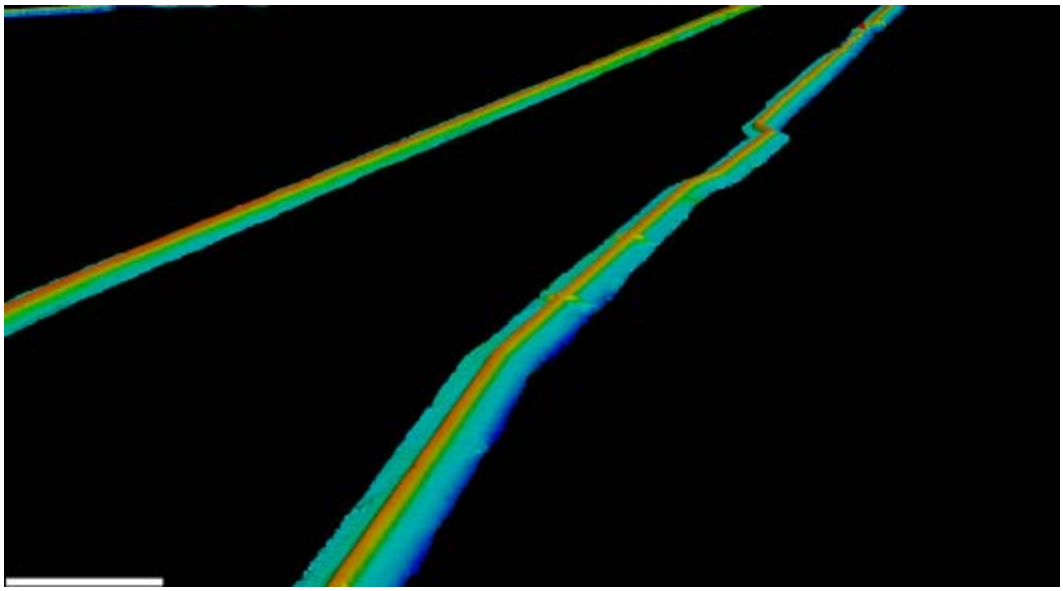


Figure B36. View looking east along the GIWW and New Orleans East levee. East of the jog in the levee, crest elevations in low spots were 14.5 to 15 ft; many less than 15.5 ft. For peak water level of 15.5 ft, widespread steady overflow expected, persisting for several hours in places. Levee intact along this reach.

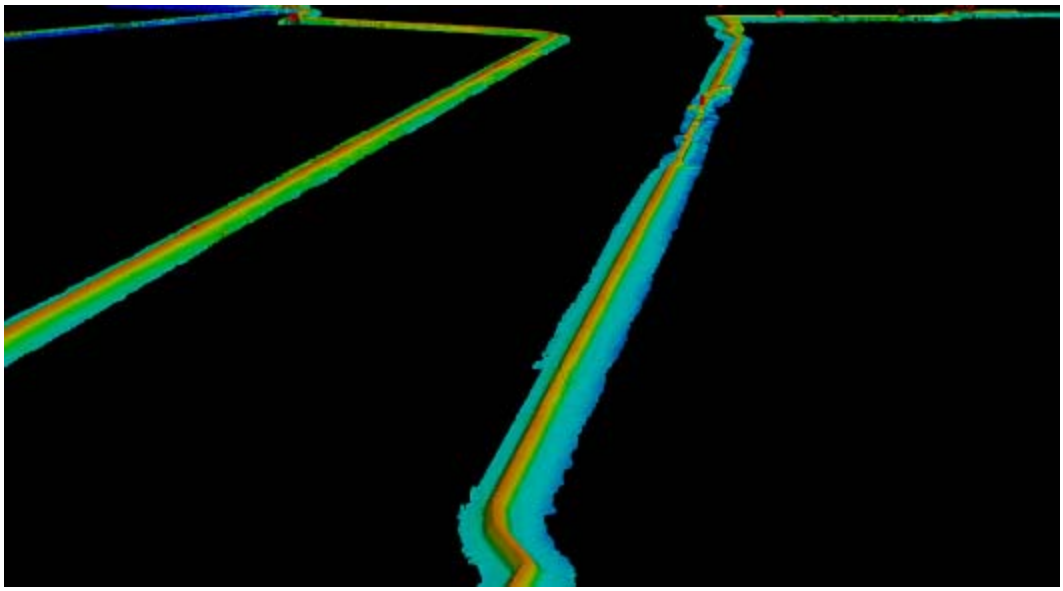


Figure B37. View looking east along the GIWW and New Orleans East levee. Floodwall at Bulk Loading Facility is visible. Crest elevations along the levee were 14.5 to 15 ft (low spots 14 to 14.5 ft); many less than 15.5 ft. For peak water level of 15.5 ft, widespread steady overflow expected for several hours. Levee intact along this reach.

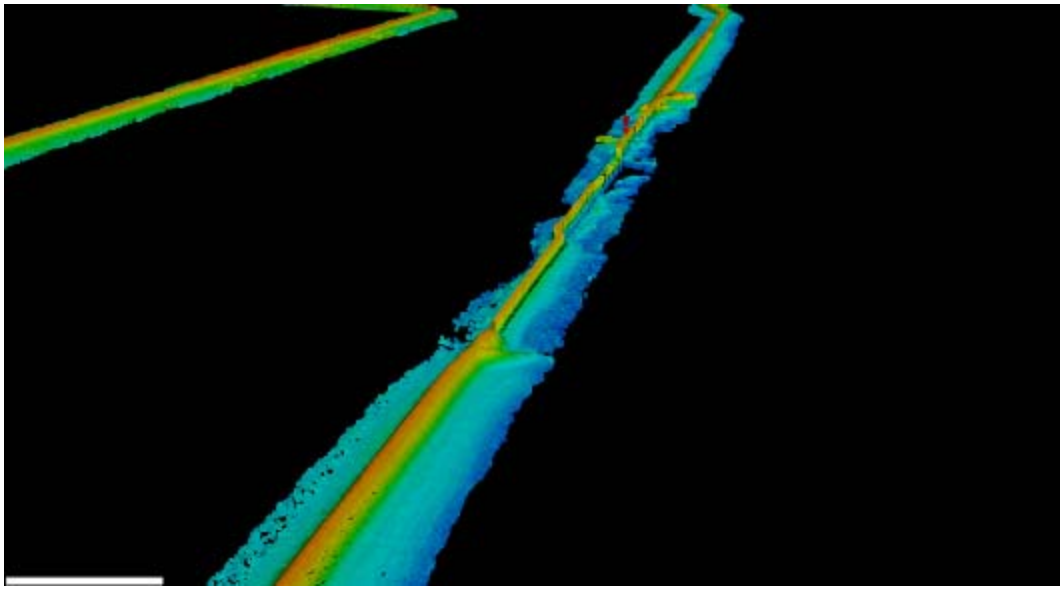


Figure B38. View looking east along the GIWW and New Orleans East levee at Bulk Loading Facility. Levee crest elevations immediately east of the wall were 13 to 14 ft. Crest elevations on the wall at the Bulk Loading Facility were about 14 ft. For peak water level of 15.4 ft, widespread steady overflow expected for several hours.

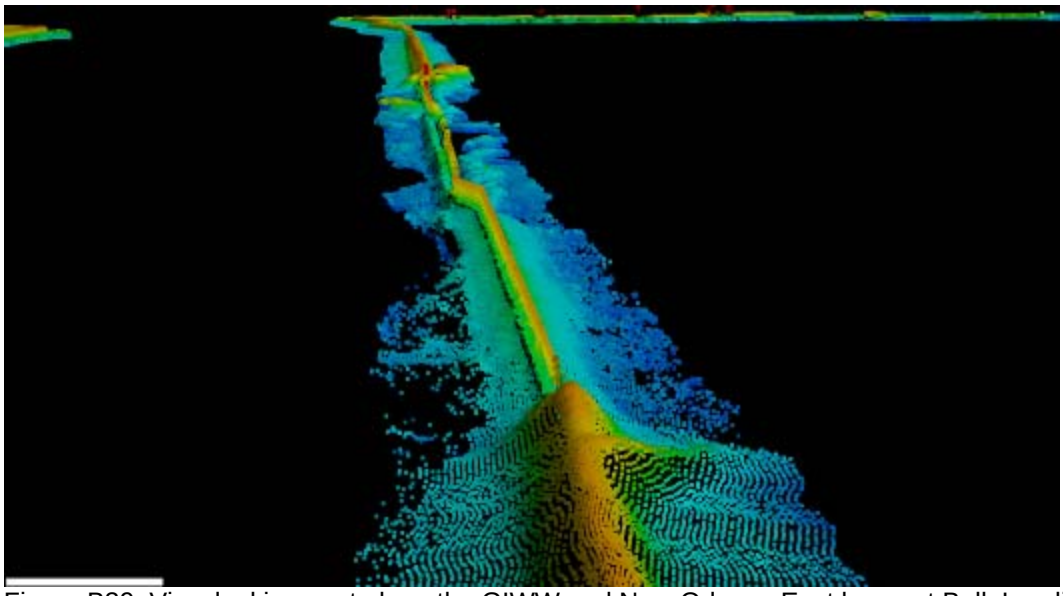


Figure B39. View looking east along the GIWW and New Orleans East levee at Bulk Loading Facility. Levee crest elevations immediately east of the wall were 13 to 14 ft. Crest elevations on the wall at the Bulk Loading Facility were about 14 ft. For peak water level of 15.4 ft, widespread steady overflow expected for several hours.

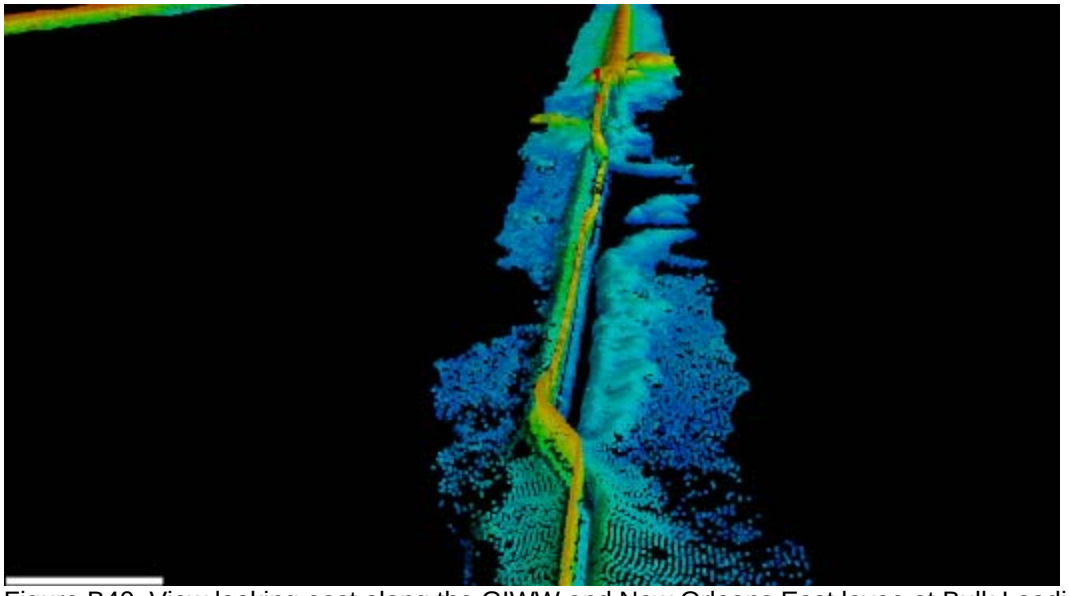


Figure B40. View looking east along the GIWW and New Orleans East levee at Bulk Loading Facility. Crest elevations on the wall at the Bulk Loading Facility were about 14 ft. For peak water level of 15.4 ft, widespread steady overflow expected for several hours. A section of wall rotated and failed, lowering the wall crest elevation. Scour trench evident as is failed wall section

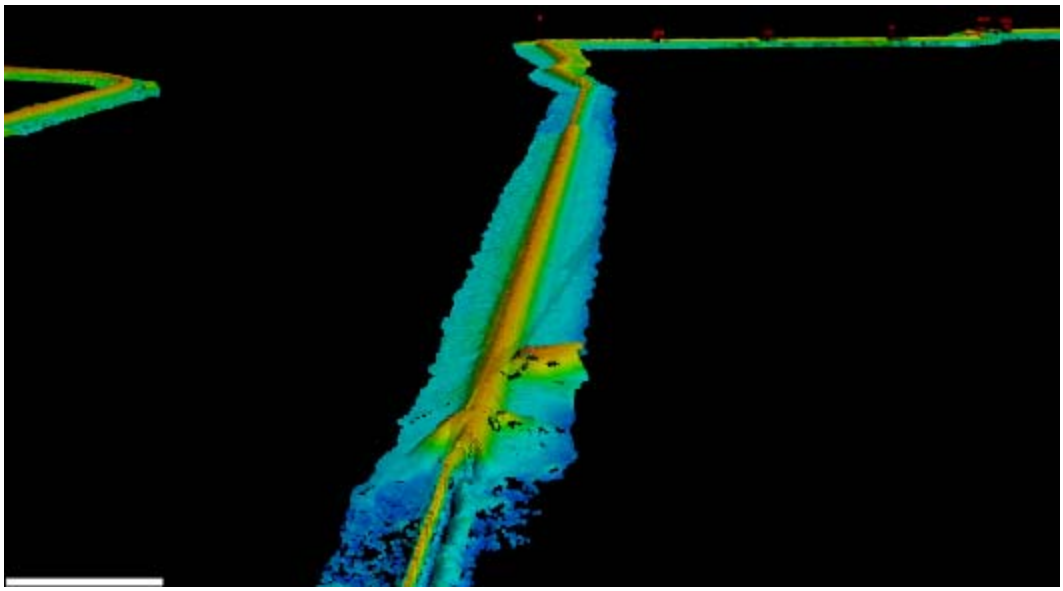


Figure B41. View looking east along the GIWW and New Orleans East levee between the Bulk Loading Facility and the IHNC. Levee crest elevations were approximately 14 to 14.5 ft (13.5 ft to 14 ft in low spots). For peak water level of 15.4 ft, widespread steady overflow expected for several hours.

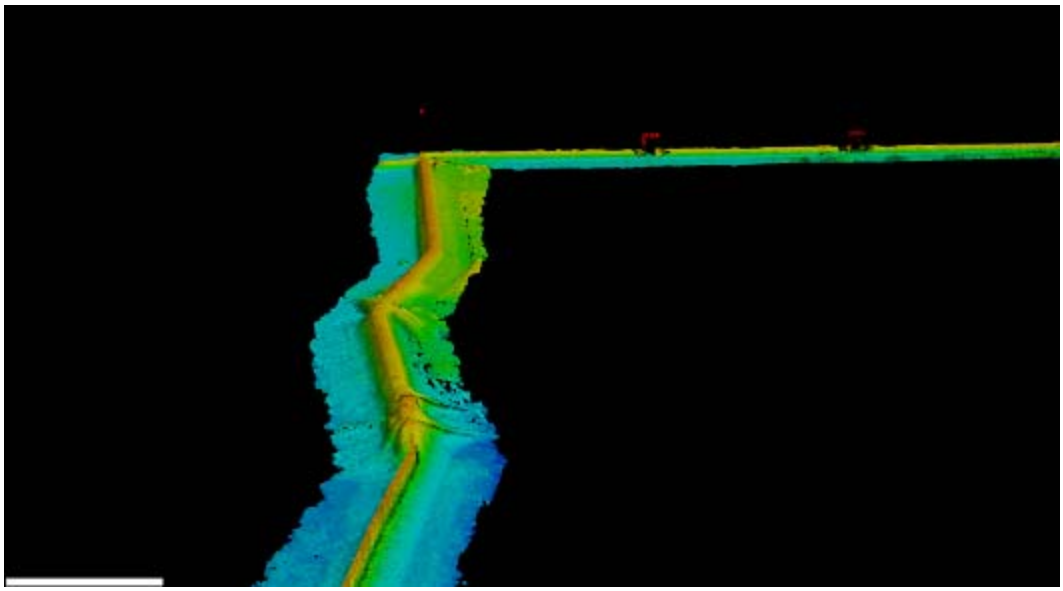


Figure B42. View looking east along the GIWW and New Orleans East levee toward the IHNC. Wall crest elevation was about 14 ft. Levee crest elevations were approximately 13 to 14 ft. For peak water level of 15.4 ft, widespread steady overflow expected for several hours. Levee generally intact in this region. Around the corner in the background, along the IHNC up to the I-10 overpass, crest elevations of levees/floodwalls/gates were 11.5 to 13.5 ft. For peak water level of 14.3 to 15.4 ft, widespread steady overflow expected for several hours.

APPENDIX C: Aerial Photos and Analysis of Pre- and Post-Storm LIDAR Data by Surfbreak Engineering Sciences, Inc.

William R. Dally, Ph.D., P.E.
Surfbreak Engineering Sciences, Inc.
315 North Lakemont Avenue, Suite A
Winter Park, FL 32792 U.S.A.

DRAFT (12/13/06)

Preliminary Attempt to Correlate MRGO Levee Performance During Hurricane Katrina with Levee Soil Properties

Methods

This facet of investigation of the damage to the earthen levee along the Mississippi River Gulf Outlet (MRGO) inflicted by Hurricane Katrina is primarily based on two sources/types of data: 1) LIDAR surveys performed of the levee region in 2000 and 2005 (i.e. before and immediately after the storm), and 2) soil cores of the levee obtained in 1985, 1991, and 2001. The immediate objective is to seek correlation, if any exists, between the spatial variation in the type & degree of damage suffered by the levee and the properties of the soil used in its construction.

The techniques used to reduce and to render the LIDAR data for making damage assessments, as well as to supplement the analysis with rectified, post-storm aerial photography, are described in an initial draft report entitled, "Mississippi River Gulf Outlet: Hurricane Katrina Damage Analysis Using High-Resolution LIDAR & Aerial Photos," dated October 17, 2006. In that study, the twelve-mile-length of the MRGO levee was divided into 33 sections (00-32), each nominally 2,000 ft in length, and detailed assessments of topographic change, levee crest reduction, and volume change were made for each section. This report, and the supporting graphics developed from the LIDAR data and photography, has been supplied on disk to CHL.

Since completion of the preliminary damage analysis report, logs from eight soil cores, taken along the location of the levee crest, were obtained from a CHL draft report entitled, "New Orleans East and St. Bernard Parish Levee Performance Report," dated

November 23, 2006. Based upon figures in the CHL report, the cores were then located in relation to the coordinate system used in the previous damage analysis. These locations are presented in Figure 1. [Although inquires have been made, copies of the original core logs and supporting documentation have not yet been obtained from the Corps, and consequently the figures in the CHL report were relied upon.]

With the core locations established, the eight appropriate levee sections were selected from the LIDAR & photography (03, 06, 09, 11, 12, 14, 30, and 31) and used to quantify the damage in the vicinity of each of the eight cores. These eight sections and the associated core logs are provided at the end of this report. Cross-sections of the levee at the core locations (derived from the LIDAR data), both before and after the storm, are also provided. In examining these profiles, it is noted that there is a concern with the veracity of the LIDAR data in that some of the profiles show almost uniform offset (erosion) between the two surveys. This issue is as yet unresolved.

Using the levee cross-sections, the location of the pre-storm levee crest and the subsequent elevation of the eroded profile at that location were established. Each of these 'eroded crest elevations' is indicated on the associated core log provided at the end of the report. It is noted that the LIDAR data and levee profiles are referenced to NAVD 88-2004.65, whereas the cores are referenced to 1929 NGVD. To convert the levee elevation from NAVD to NGVD, 1.7 ft was added to the NAVD elevation (see page II-59 of the IPET report), and the result drawn on the core log in each figure, referenced to NGVD.

Findings & Discussion

Cores 1, 2, 3, 4, 6, and 7 had been taken at locations that were subsequently heavily damaged during Katrina, whereas cores 5 and 8 were from locations that suffered relatively little damage. Also, cores 4, 6, and 7 were from locations where the levee was topped by a sheet pile wall whose crest elevation was typically 2-4 ft less than the adjacent, wholly earthen structure.

The levee material at the locations of cores 5 and 8 is almost exclusively fat clay of medium strength, which is the strongest soil sampled in any of the cores. As a first reaction, this would seem to indicate a correlation between this soil and the survivability of the levee. However, it is essential to note that every core from the heavily damaged sections also contained layers of fat clay of medium strength, which were eroded through during the storm. Without additional core information (particularly new cores from the surviving levee sections) and additional analysis, it is unwise at this juncture to conclude that simply using medium-strength fat clays in the construction of new levees is the key to ensuring their survival in the next major storm. Other observations and comments follow:

- Of the eight core locations, 1 & 8 had the highest pre-storm levee crest elevation (~17.5 ft NAVD88-2004.65). Location 1 was heavily damaged, whereas location 8 was intact. The significant difference in performance at the two locations must therefore be attributed to a difference in 1) storm surge elevation, 2) wave properties at the levee, and/or 3) levee material. Because location 1 is near the confluence of the GIWW and MRGO levees and location 8 is nearly 10 miles away, and recognizing the geometric/physical complexity of the adjacent areas of Lake Borgne, a significant difference in surge elevation and/or wave attack is possible. However, it is noted that the high water marks provided in the IPET report near location 1 are nearly identical to those at a location six miles beyond location 8 (i.e. ~18.3 ft NAVD), but that near location 6 (ref. Figure 1), the high water marks were significantly higher (~ 21.4 ft NAVD) albeit of lesser quality.

- Location 2 (which failed) and location 5 (which remained intact) also had similar pre-storm crest elevations (~15 ft NAVD), but were only 2.2 miles apart, and therefore probably experienced similar surge elevations. However, the pre-storm elevation of the polder ‘floor’ at location 5 was nominally 10 ft NAVD, and only 6.5 ft NAVD at location 2, meaning that the erosive down rush on the backside of the levee at 2 was likely greater than at 5. To the contrary, as indicated in the photography, location 2 was fronted by significantly more ‘protective’ marsh than

location 5, and yet location 5 faired much better. Although the details of the hydraulic conditions at these two locations remain uncertain, the levee at location 5 did contain significantly more medium fat clay in its upper layers than it did at location 2.

- All profiles from the heavily damaged sections indicate that failure was initiated by erosion of the backside of the levee. The final state of damage is asymmetric, with more erosion taking place on the New Orleans side of the levee. There is no evidence of failure from front-side erosion or from piping.

- In section 30, where core 7 was located, it is clear that the damage to the levee was caused by overtopping of the sheet pile wall. This wall appears to have had a pre-storm crest elevation nominally 4 ft lower than the adjacent, wholly earthen levee to the north, which survived.

Recommendations

It is certain that additional study is needed before many of the questions raised in this preliminary effort to understand the MRGO levee performance can be answered with confidence. This additional study must include a carefully designed, well-executed, field campaign to collect additional data. Specific needs include:

1. A thorough check for all existing information available on the pre-storm soil properties of the MRGO levee. Has anything been missed?

2. The critical need is for more soil cores and erosion tests from the sections of levee that survived Katrina. Cores taken even in rebuilt sections will be valuable in checking and in building confidence in the pre-storm core information that is available in these levee sections.

3. Accurate, GPS-based survey of the levee crest and the polder floor is needed to check the veracity of the LIDAR data and to resolve the apparent offset issue. Again, data collected along the sections of levee that survived Katrina will be particularly useful.

4. Detailed review of the most recent ADCIRC, STWAVE, and COULWAVE results for the MRGO region, which utilized the high-resolution grids developed by/for the Risk Assessment Group. Wave transformation through the fronting marsh along MRGO is a potentially important issue for which no field data, and little numerical experience, exists.

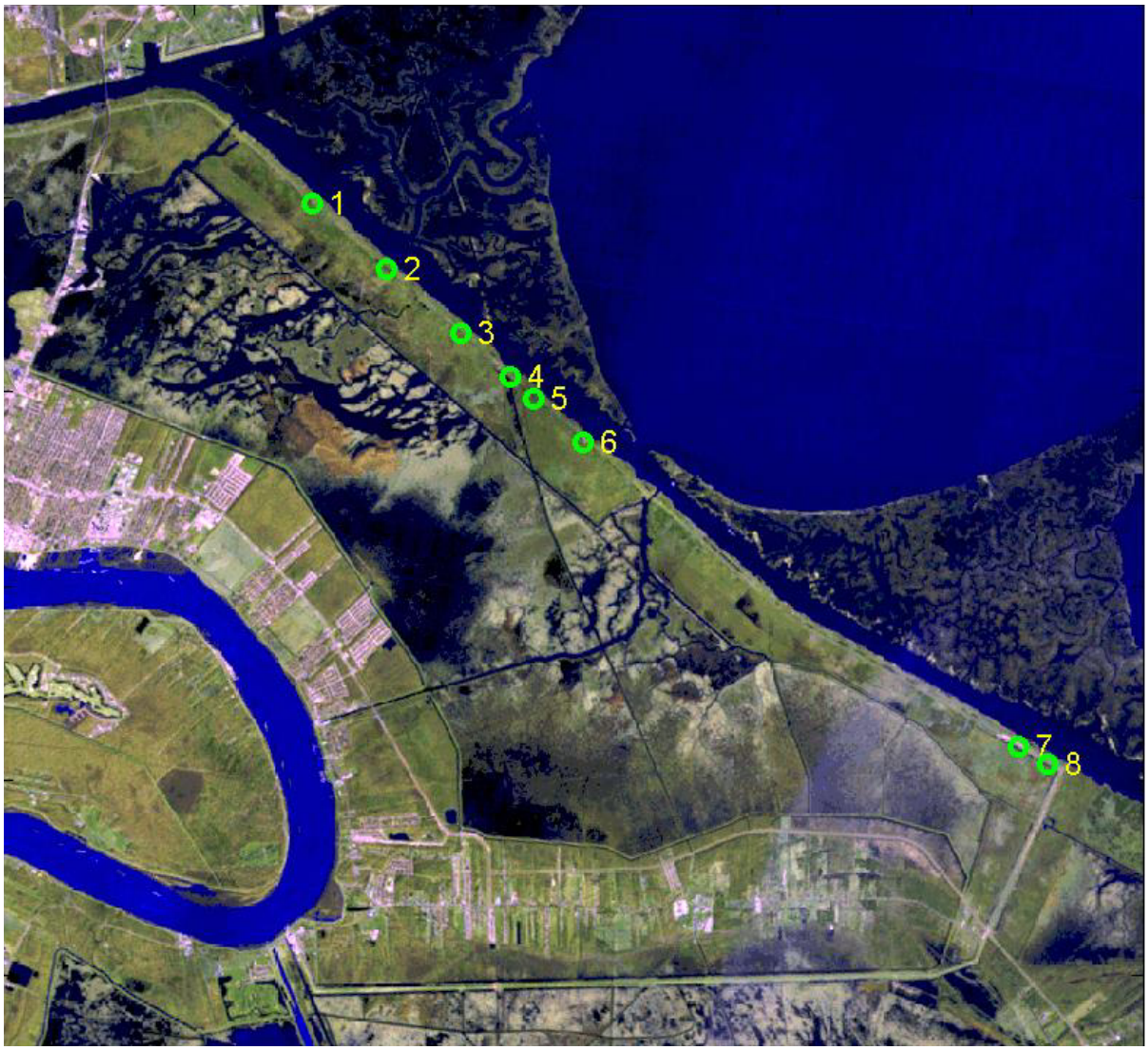
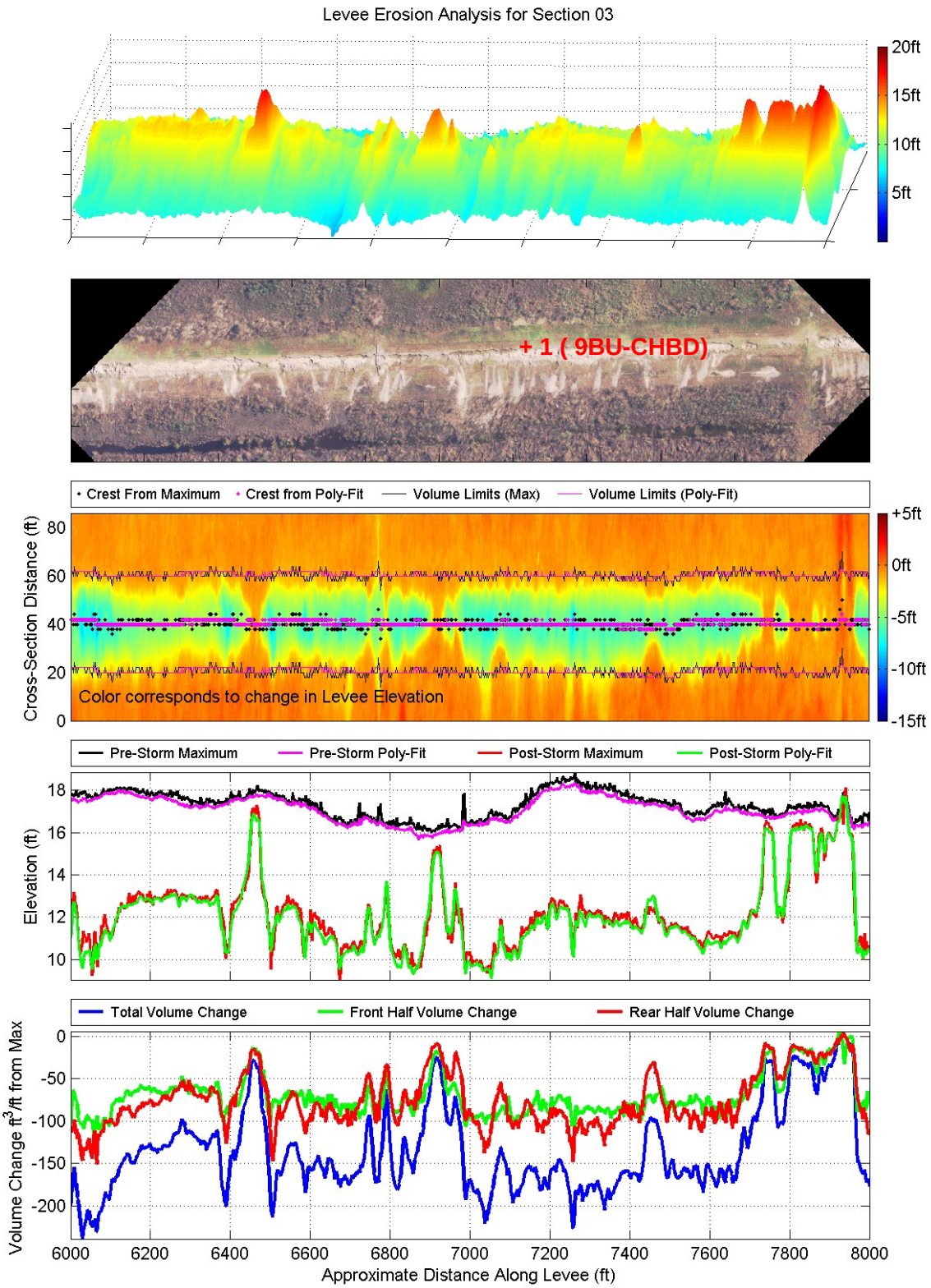
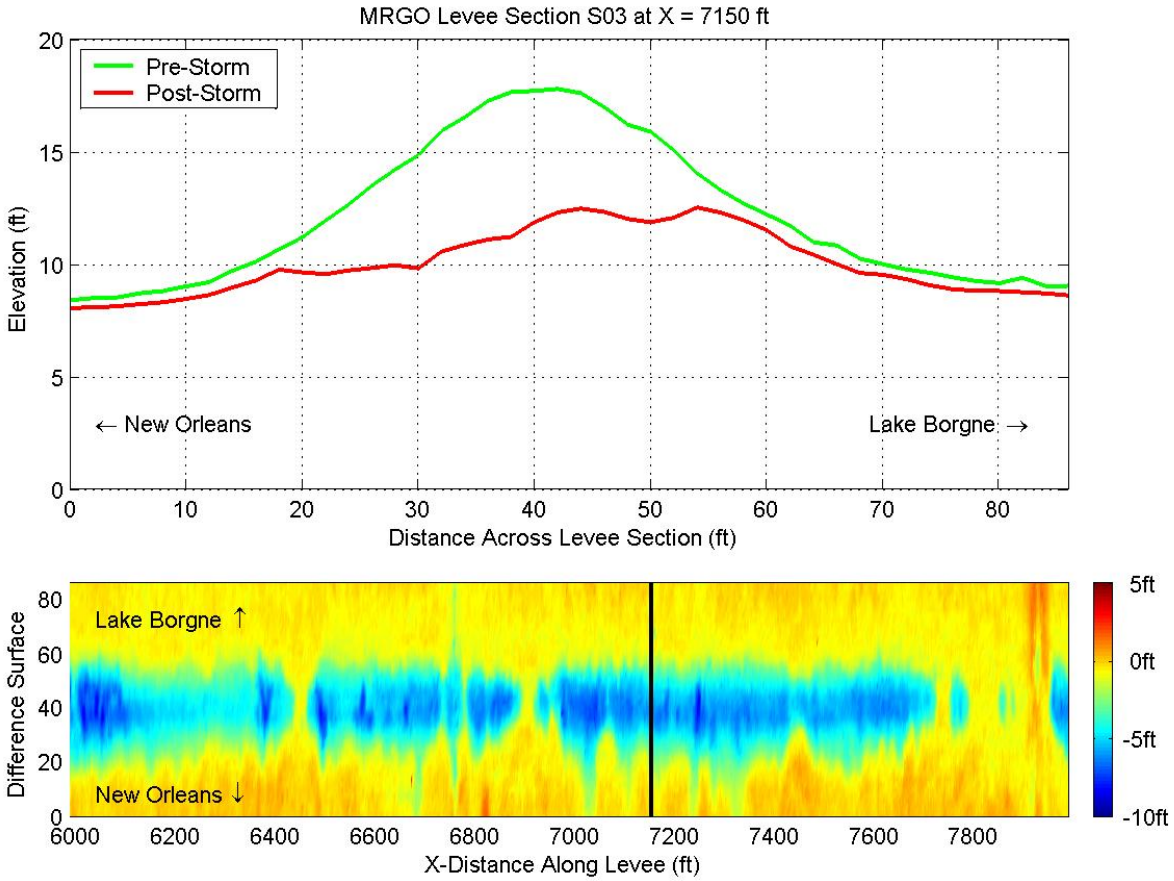


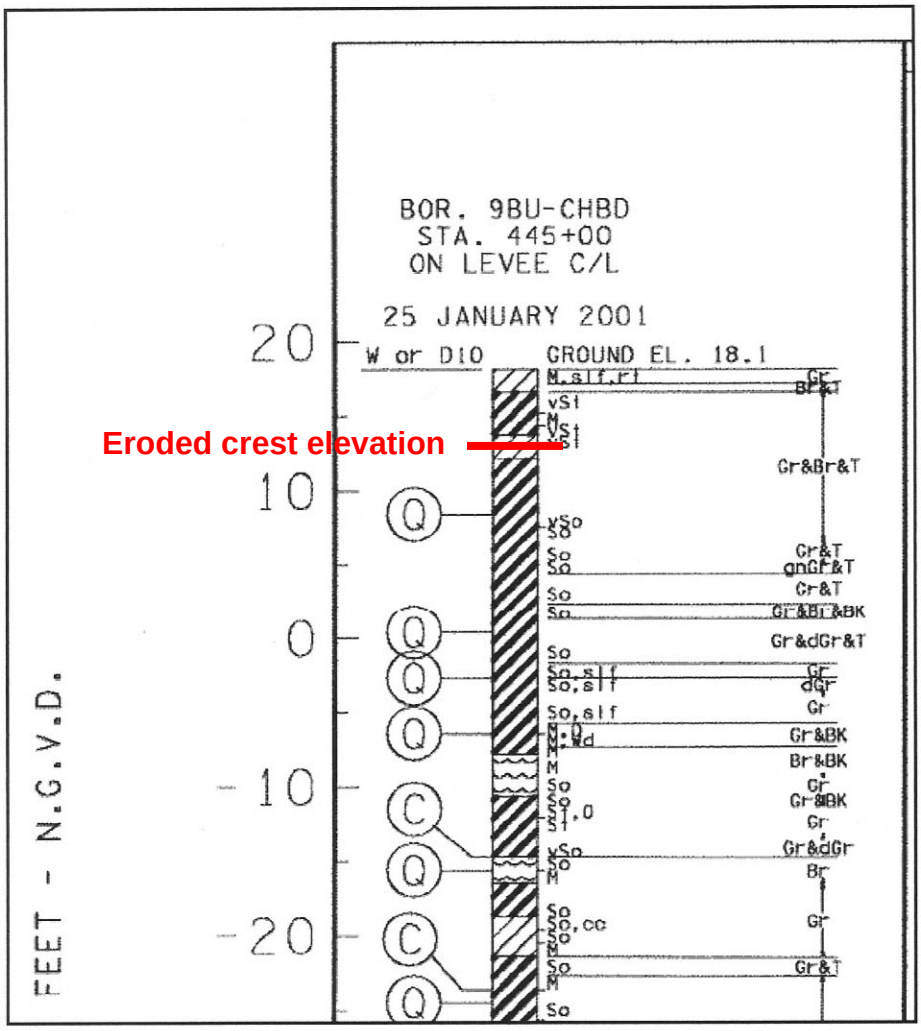
Figure 1 - Approximate location of the available core information for the MRGO levee.



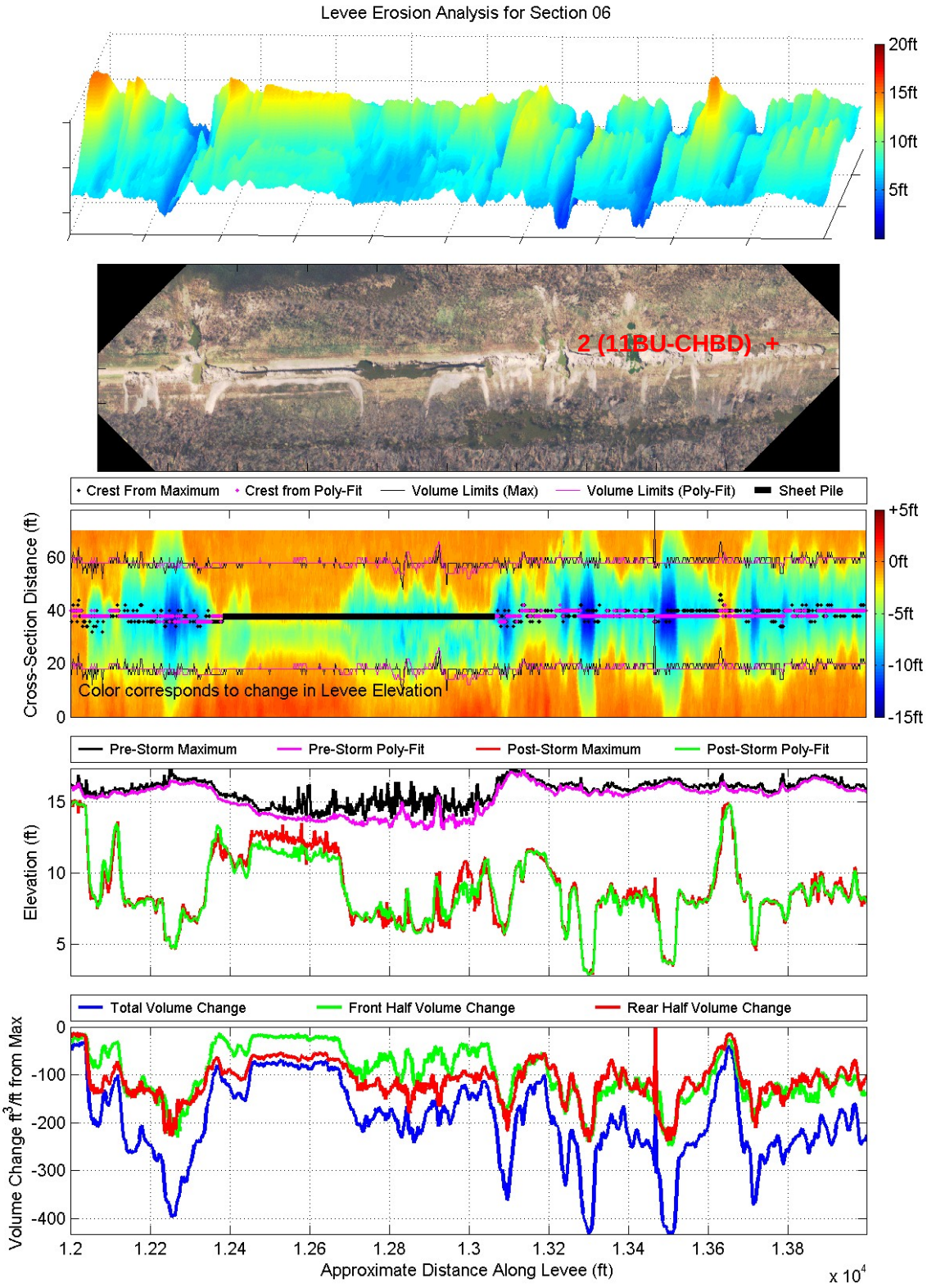
Damage assessment in Section 03, containing Location 1.



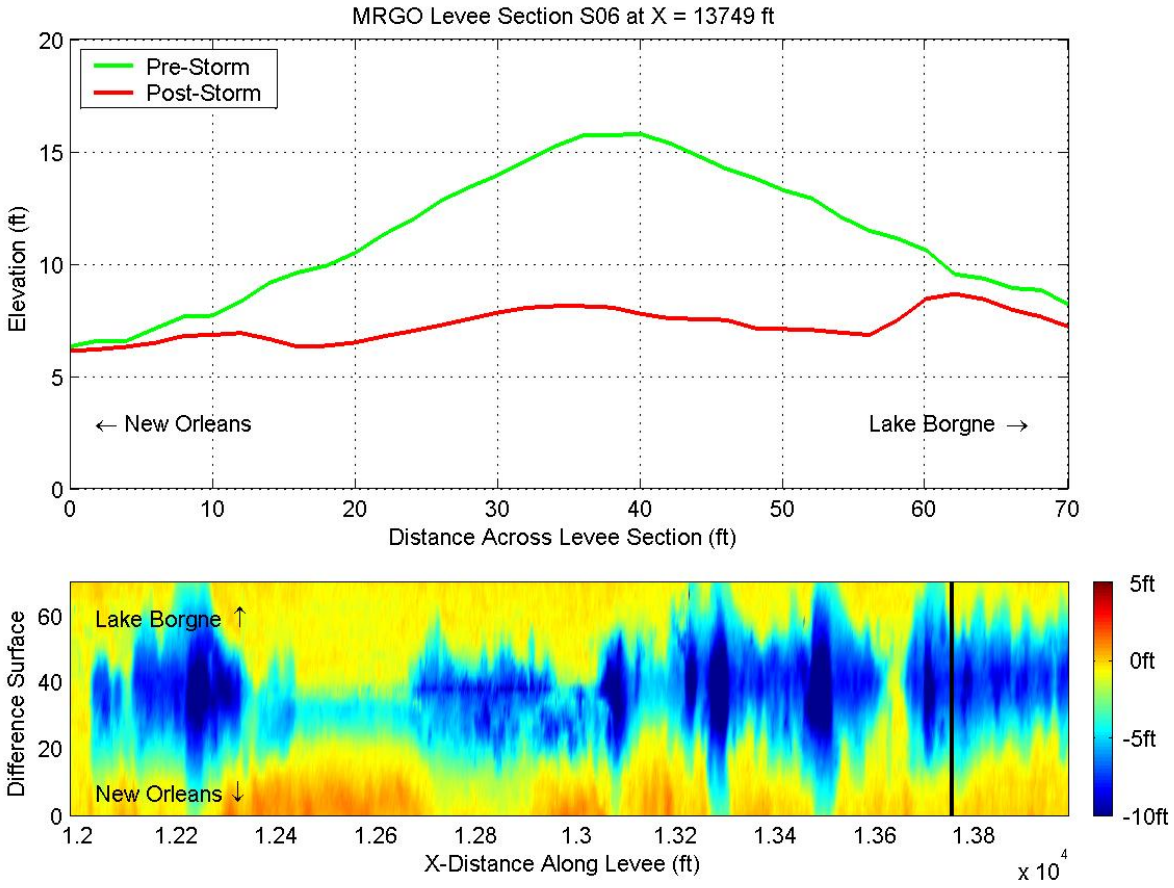
Levee cross-sections at Location 1.



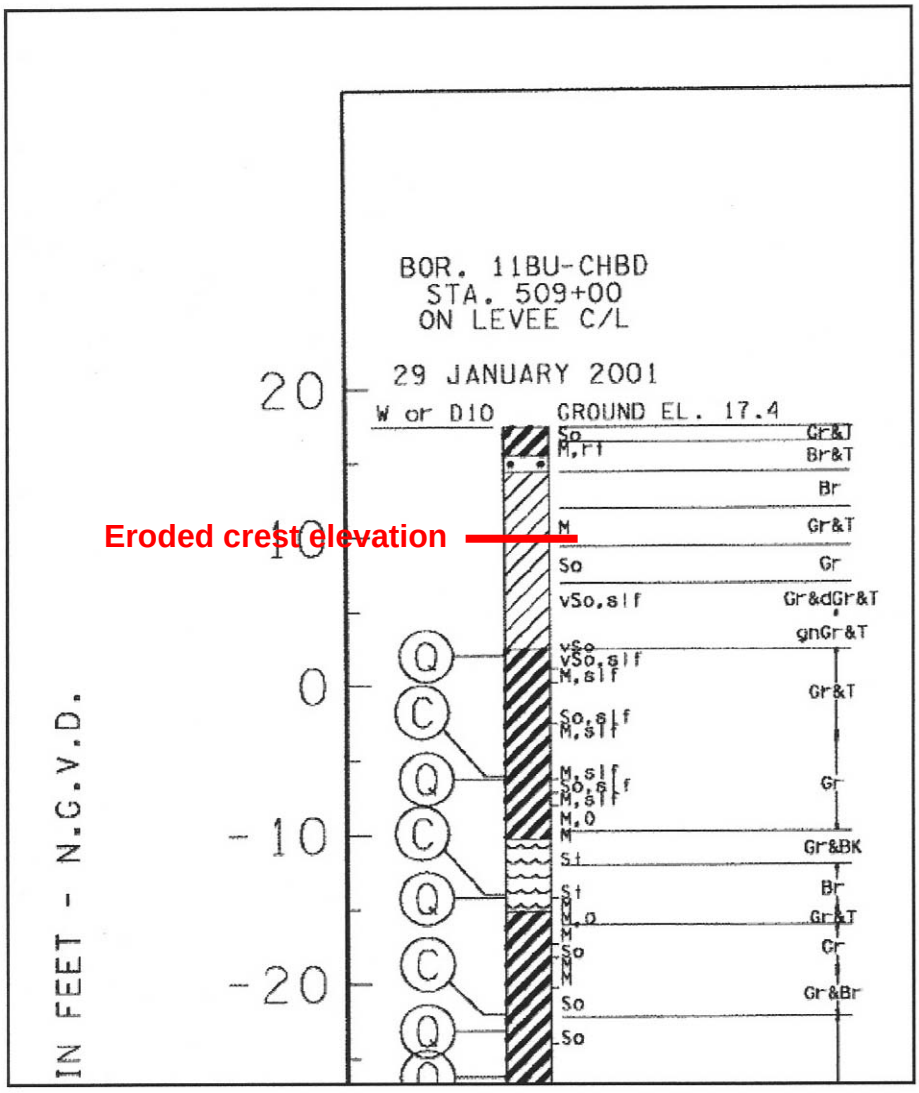
Core from Location 1.



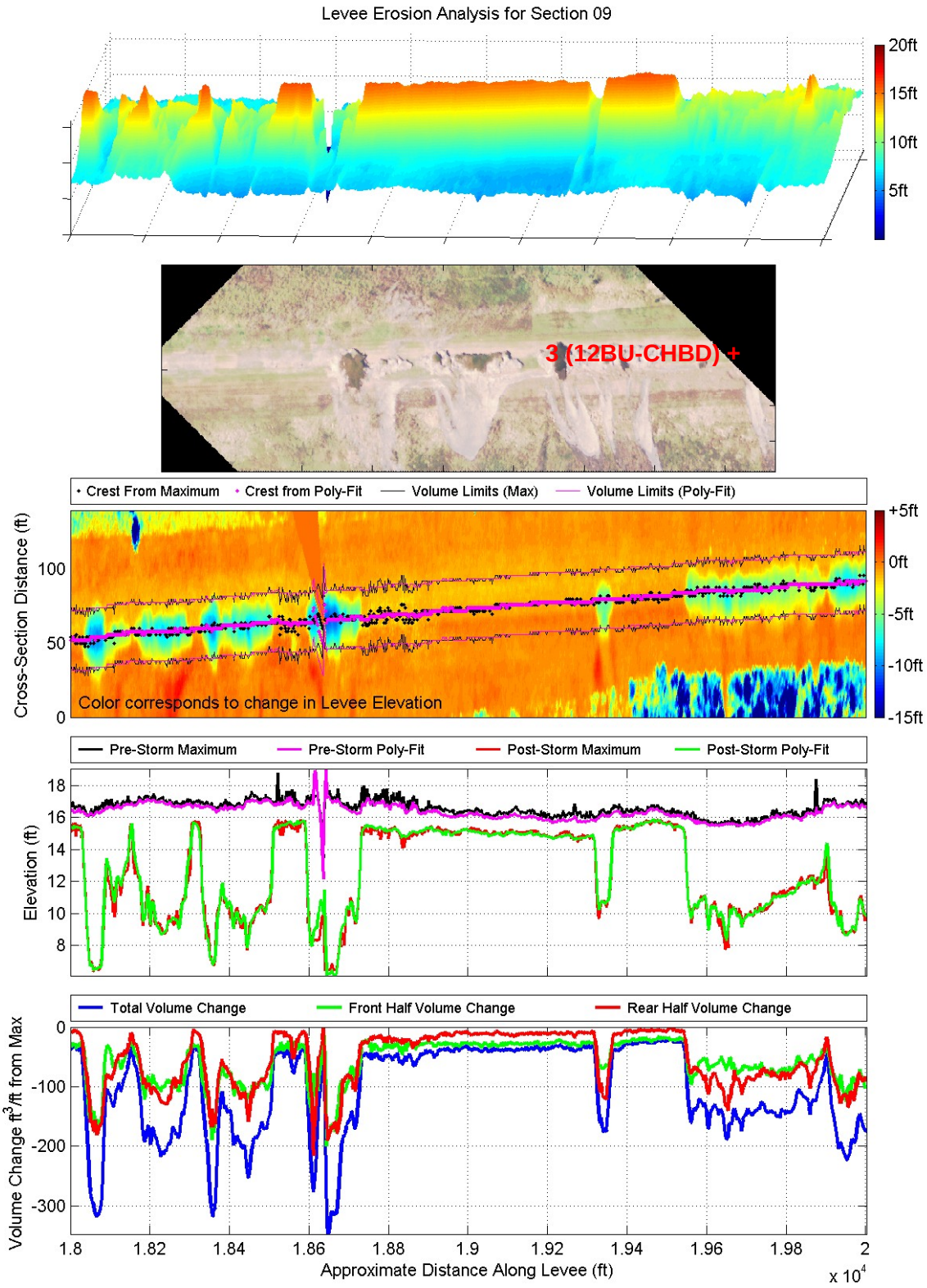
Damage assessment in Section 06, containing Location 2.



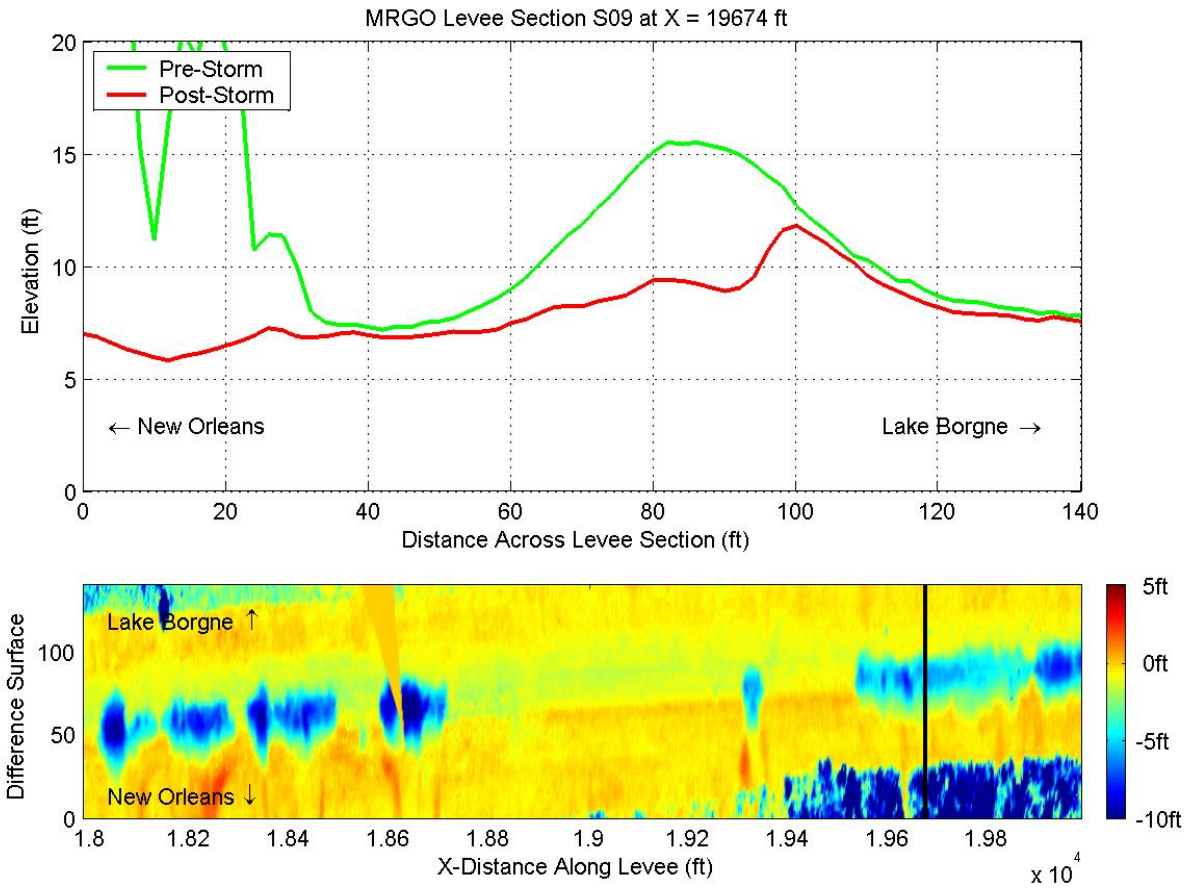
Levee cross-sections at Location 2.



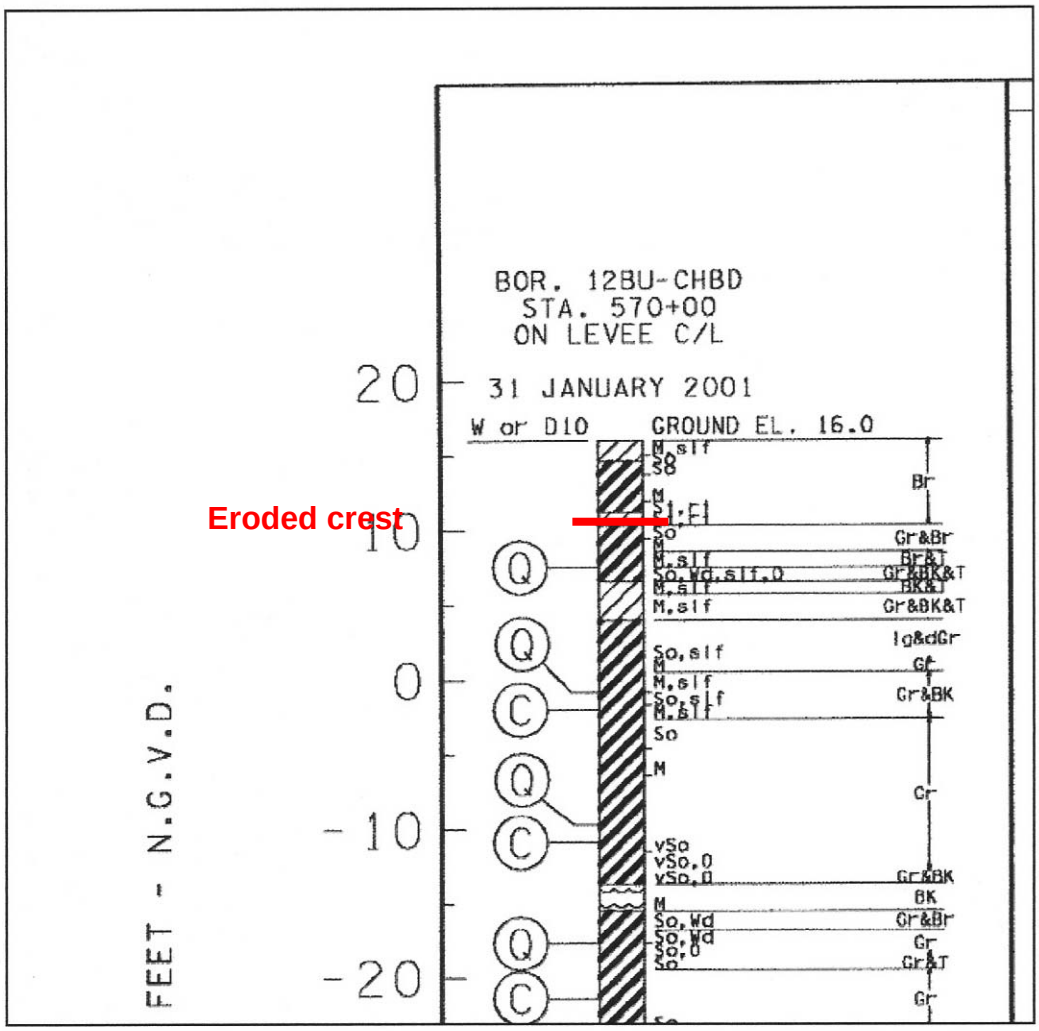
Core from Location 2.



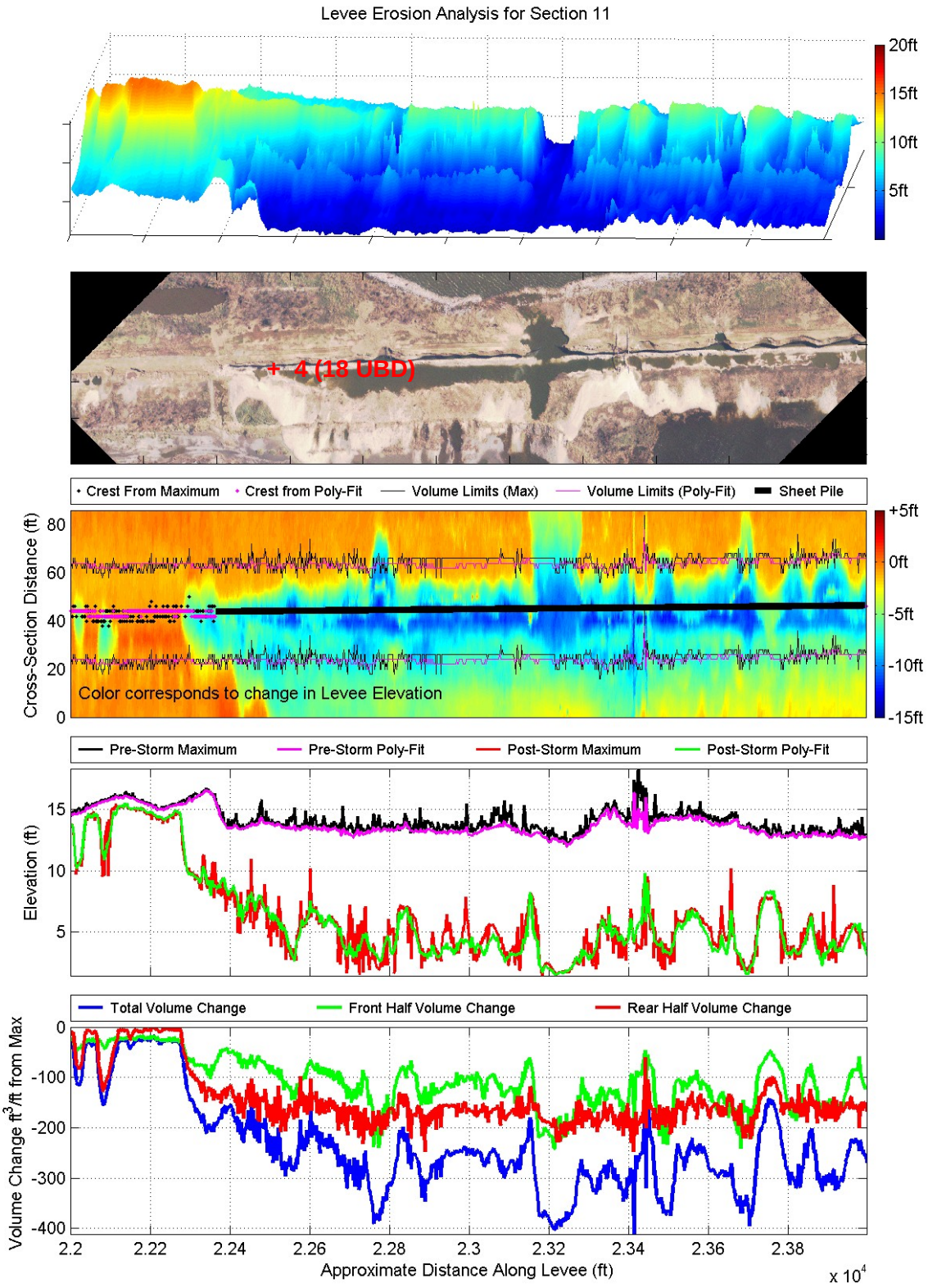
Damage assessment in Section 09, containing Location 3.



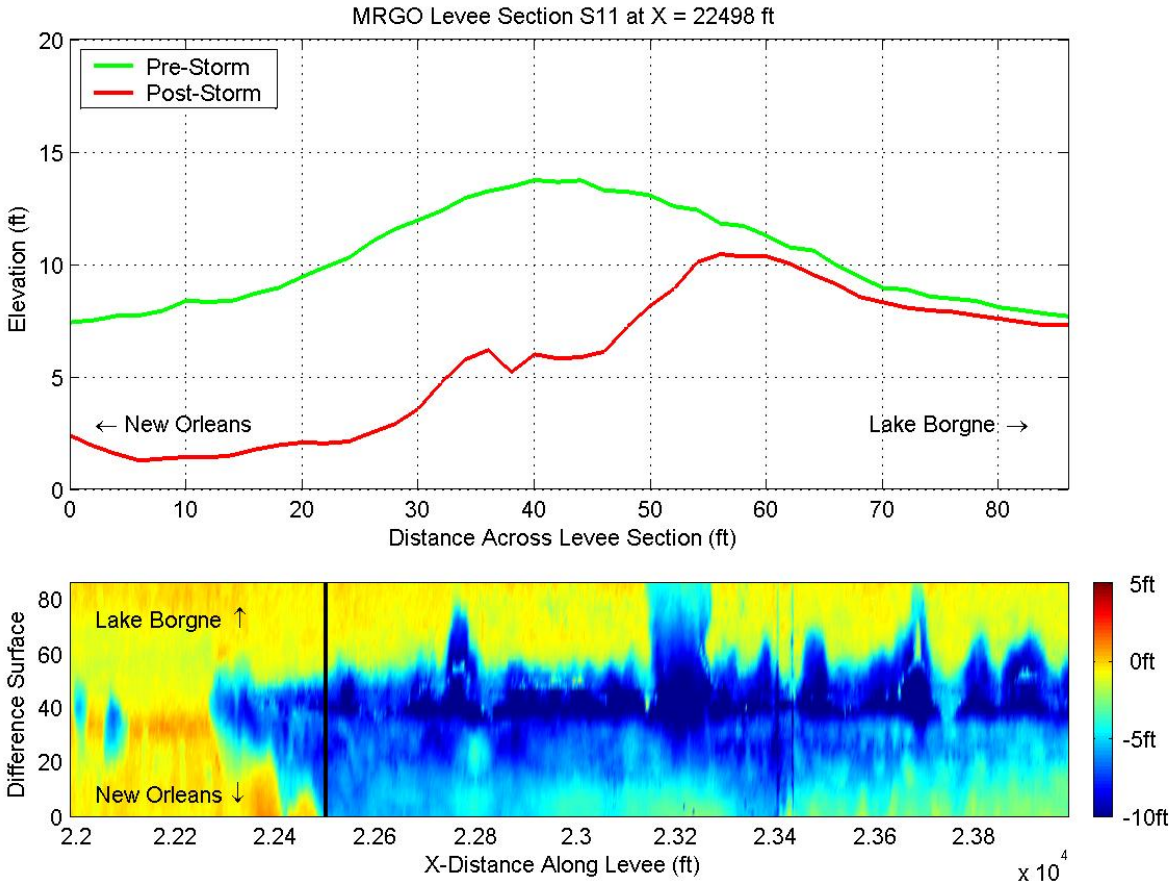
Levee cross-sections at Location 3.



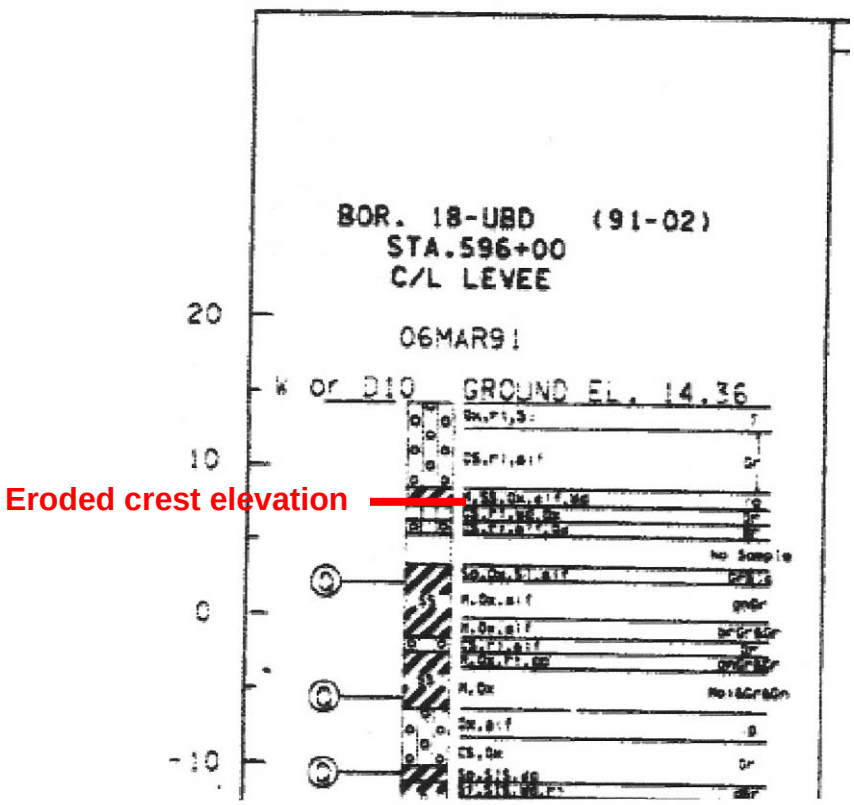
Core from Location 3.



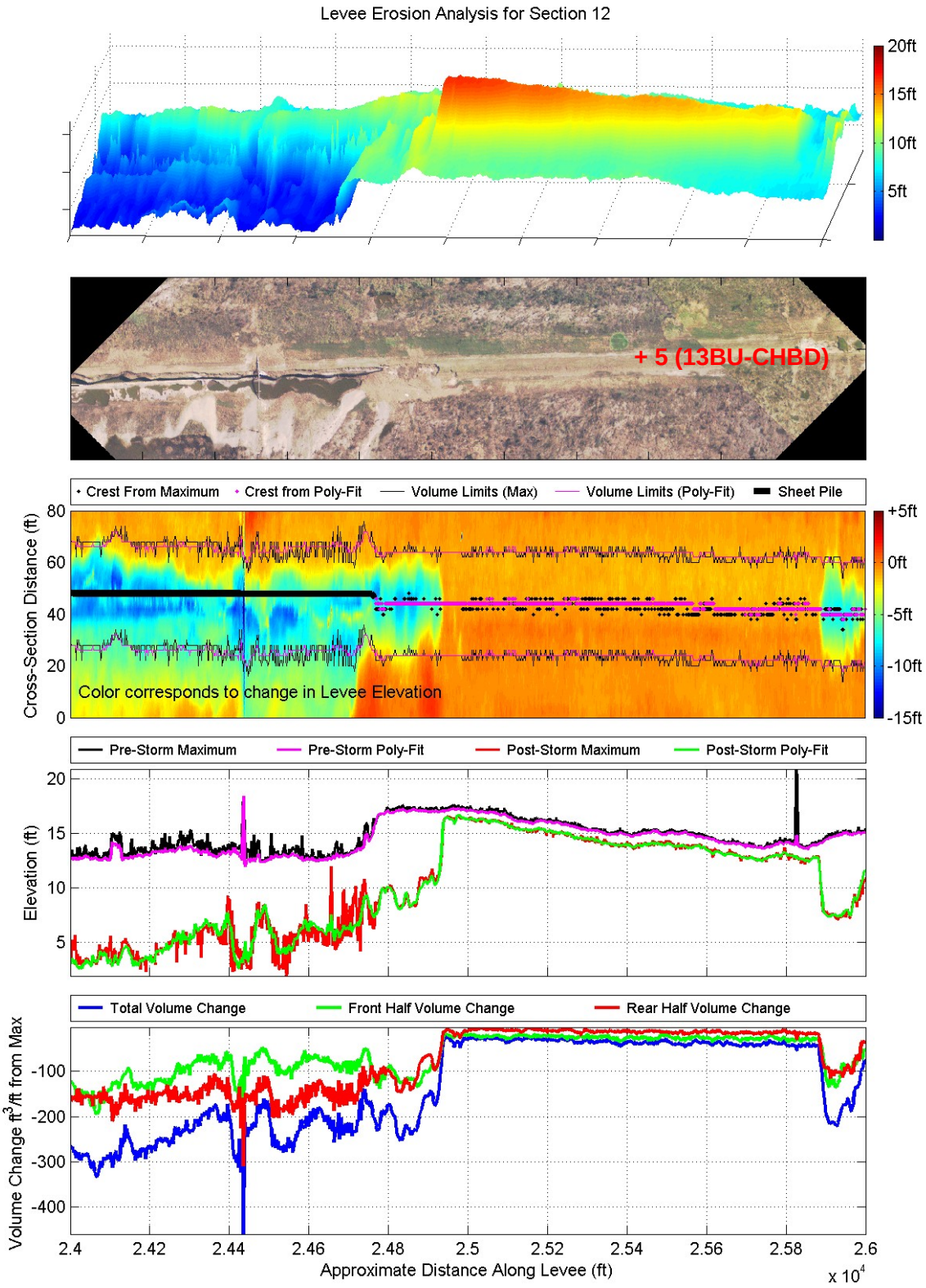
Damage assessment in Section 11, containing Location 4.



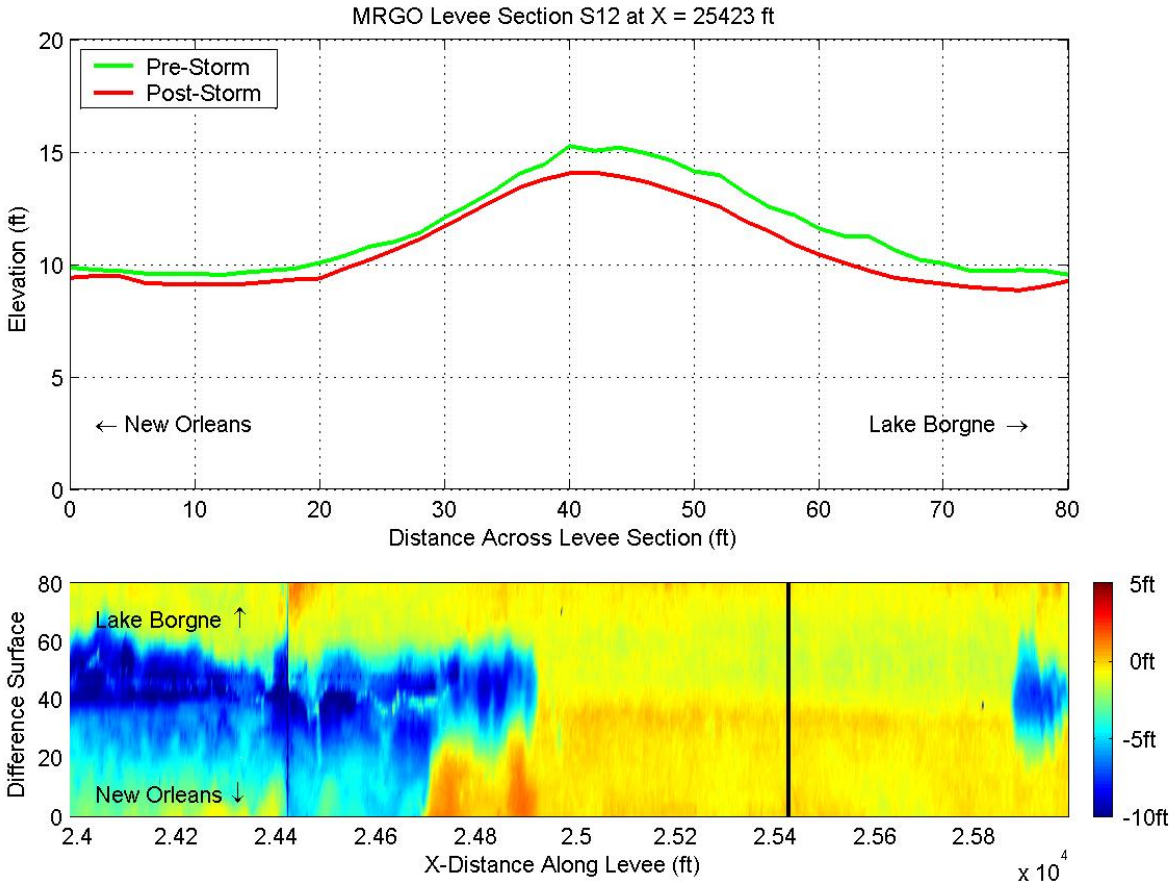
Levee cross-sections at Location 4.



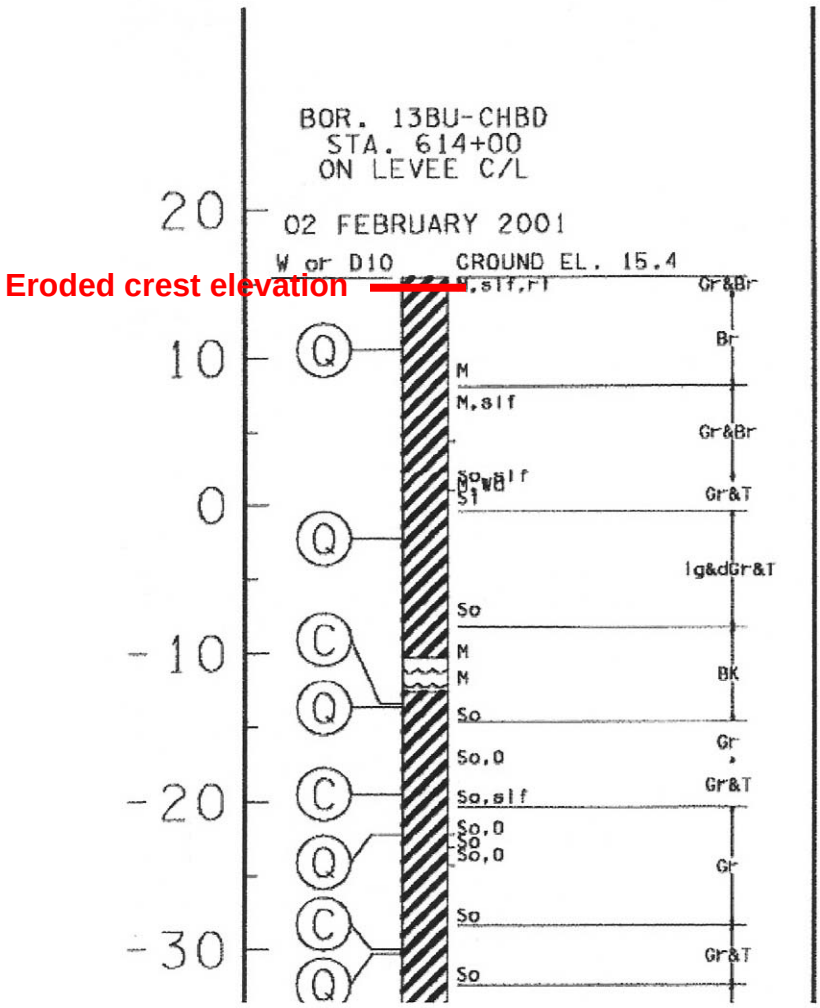
Core from Location 4.



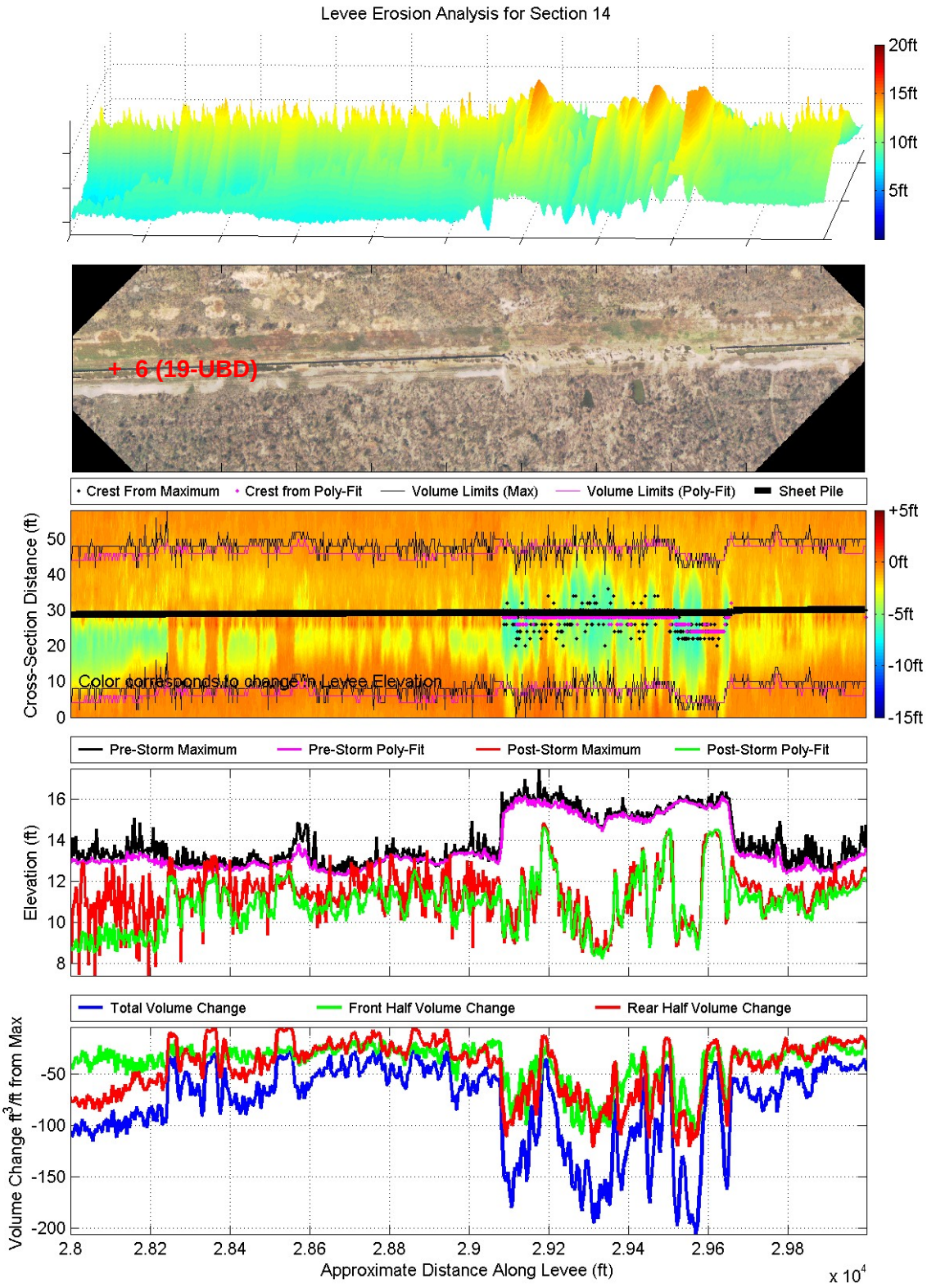
Damage assessment in Section 12, containing Location 5.



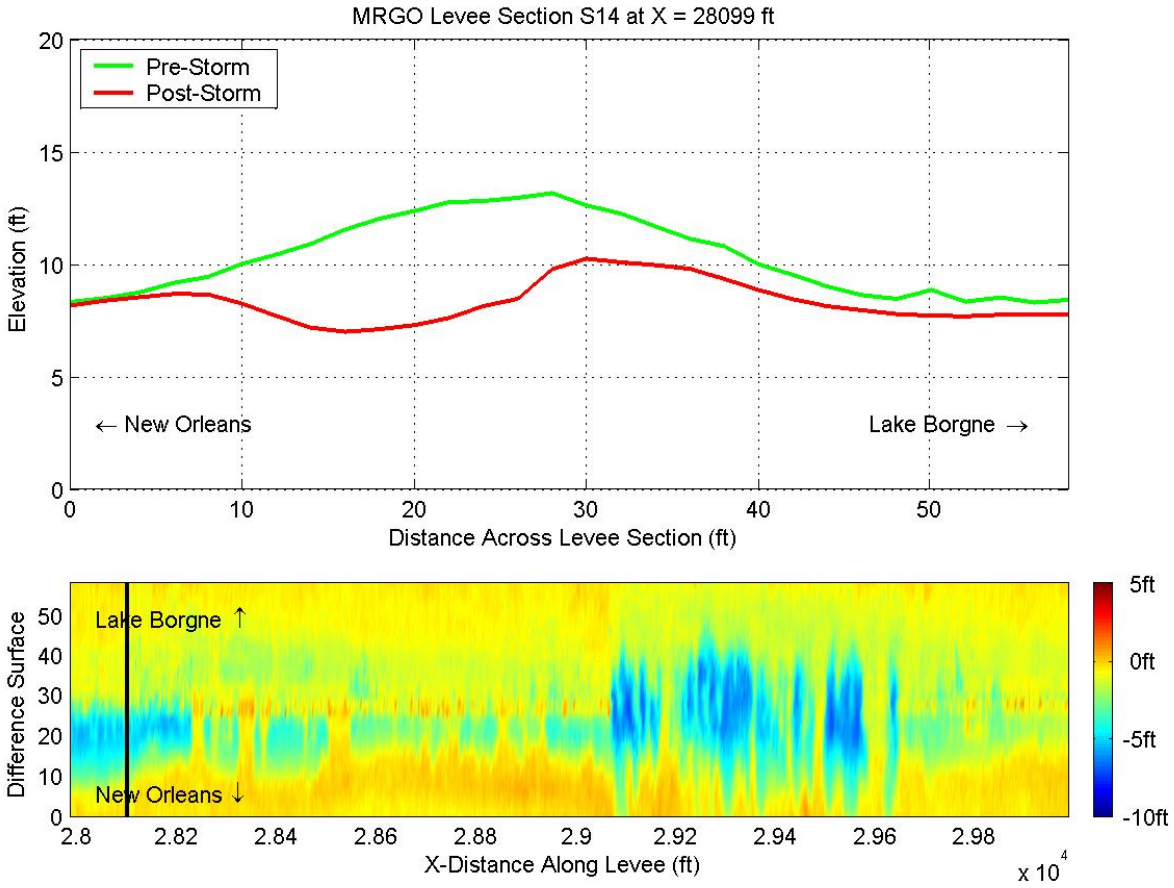
Levee cross-sections at Location 5.



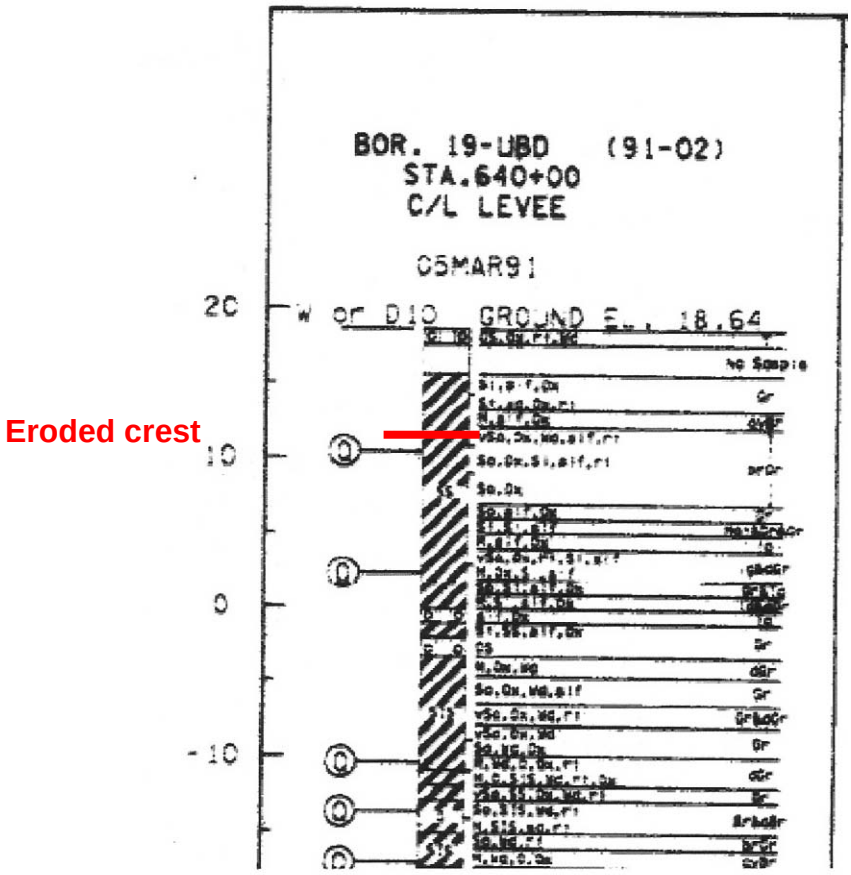
Core from Location 5.



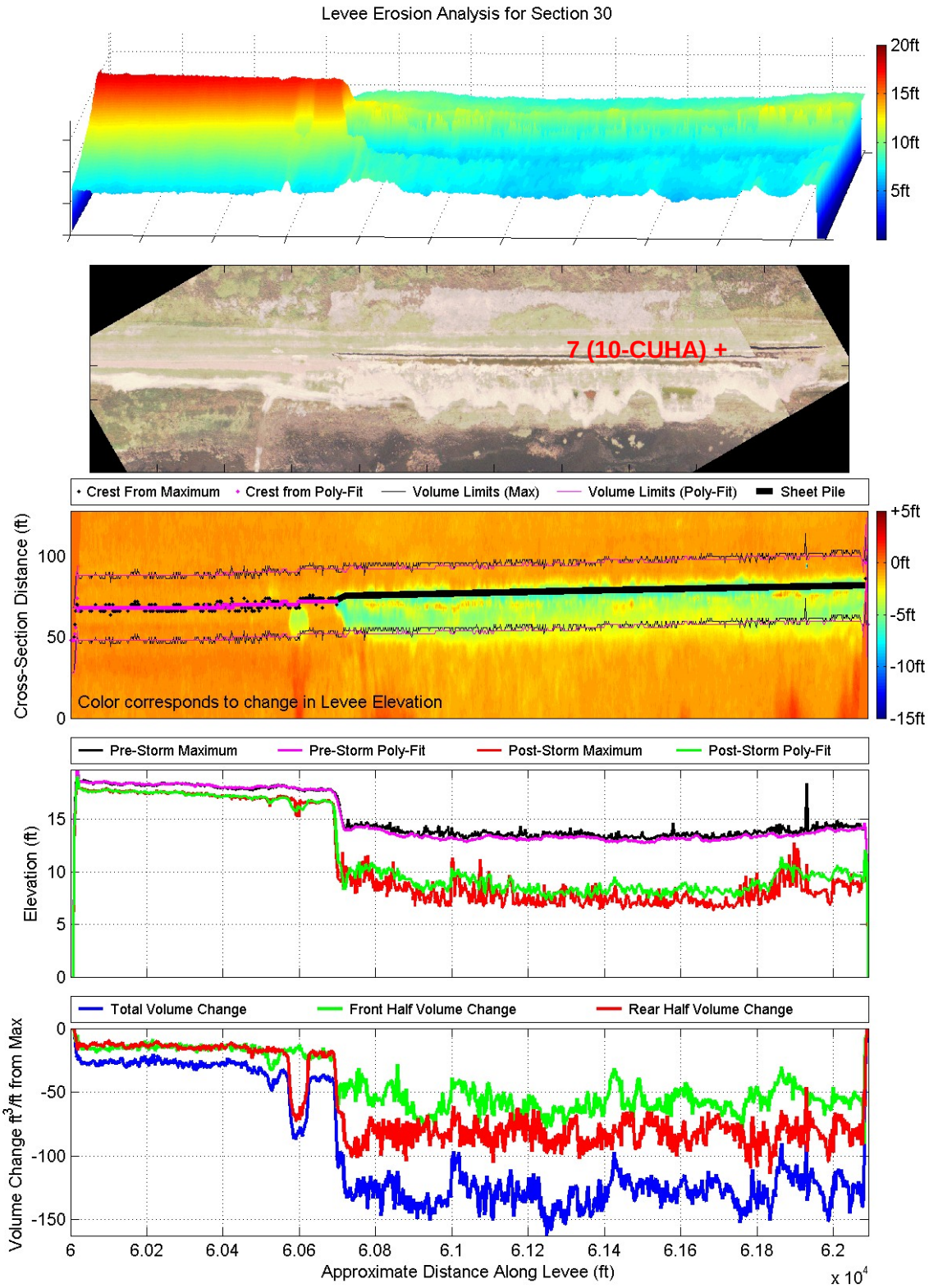
Damage assessment in Section 14, containing Location 6.



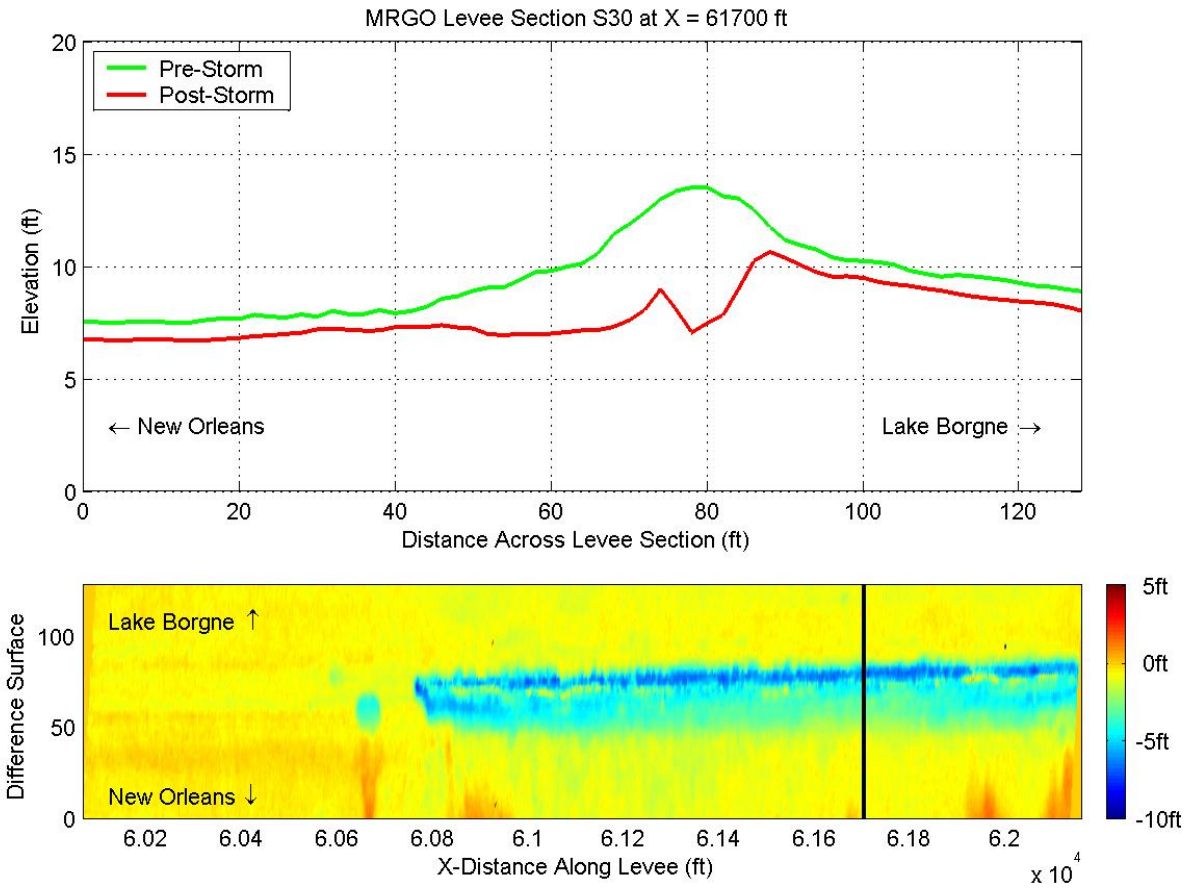
Levee cross-sections at Location 6.



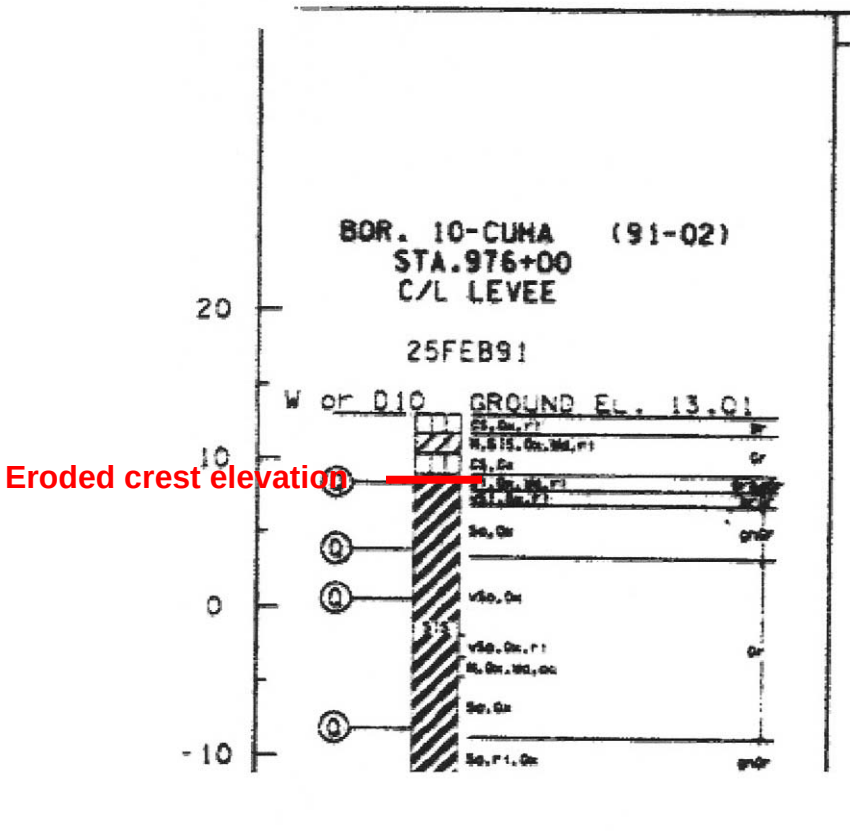
Core from Location 6.



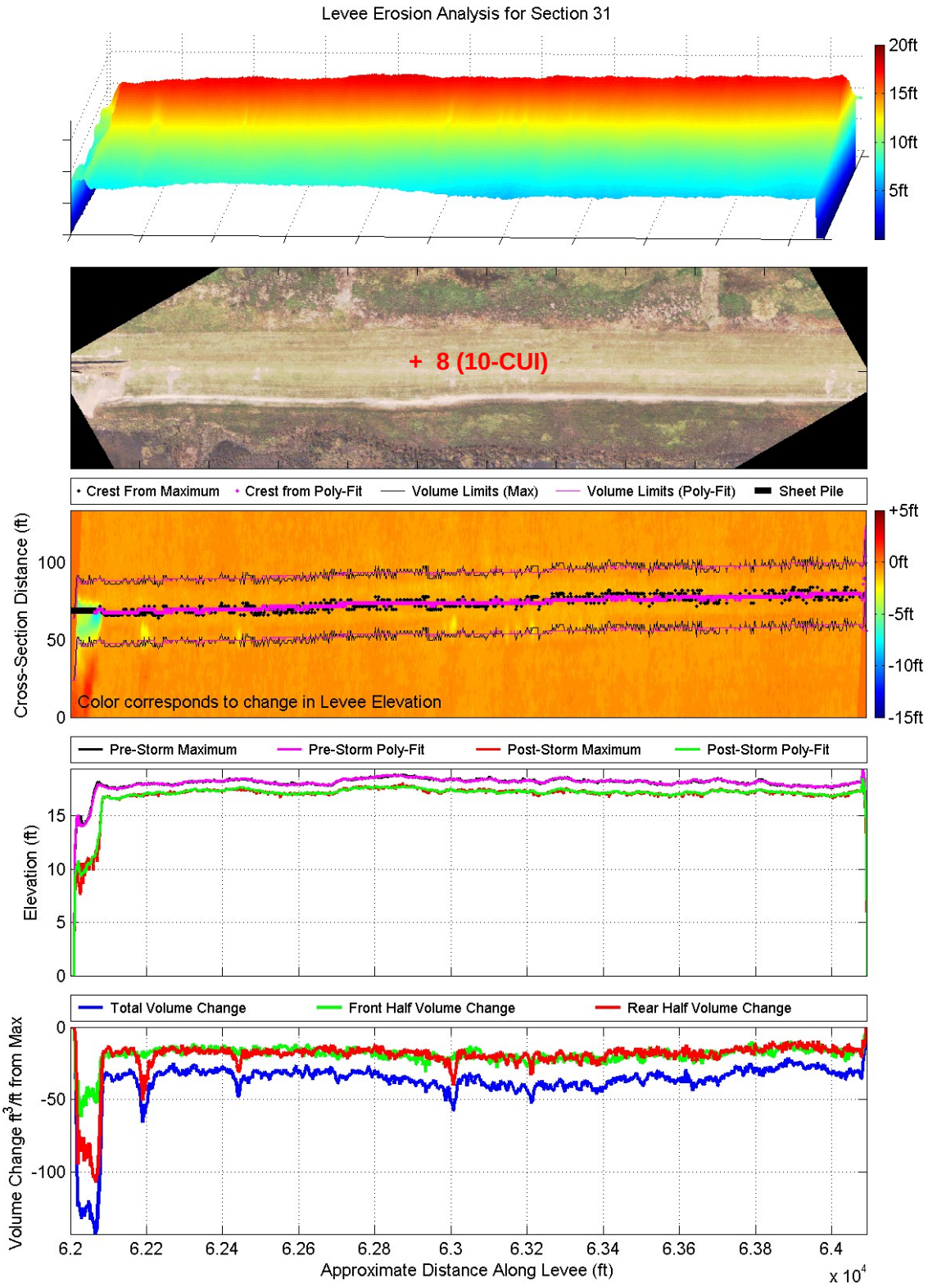
Damage assessment in Section 30, containing Location 7.



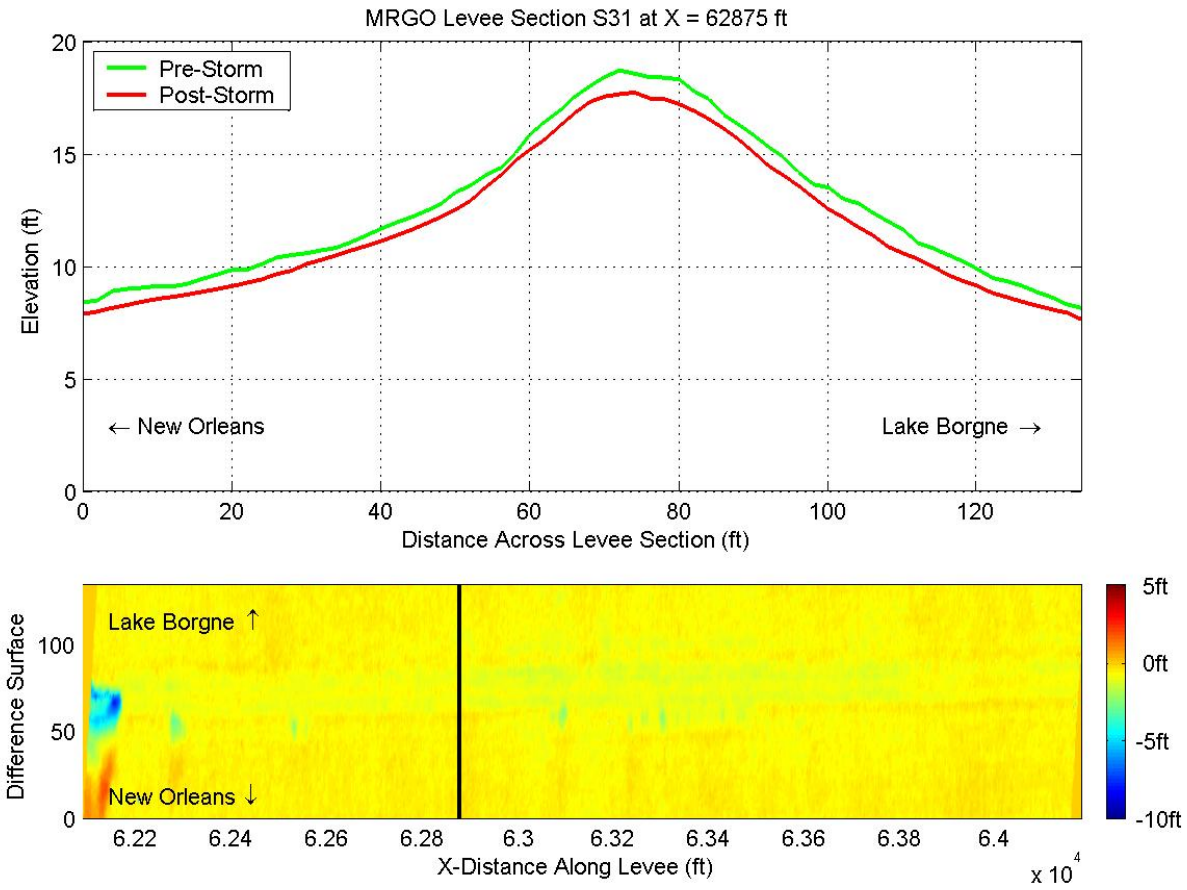
Levee cross-sections at Location 7.



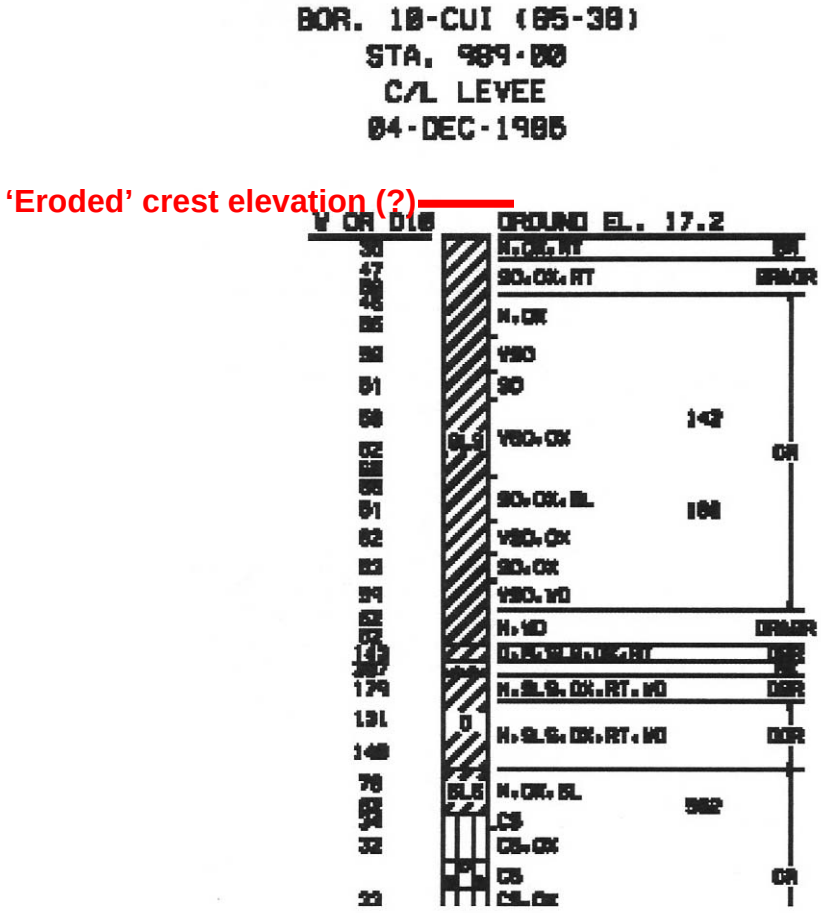
Core from Location 7.



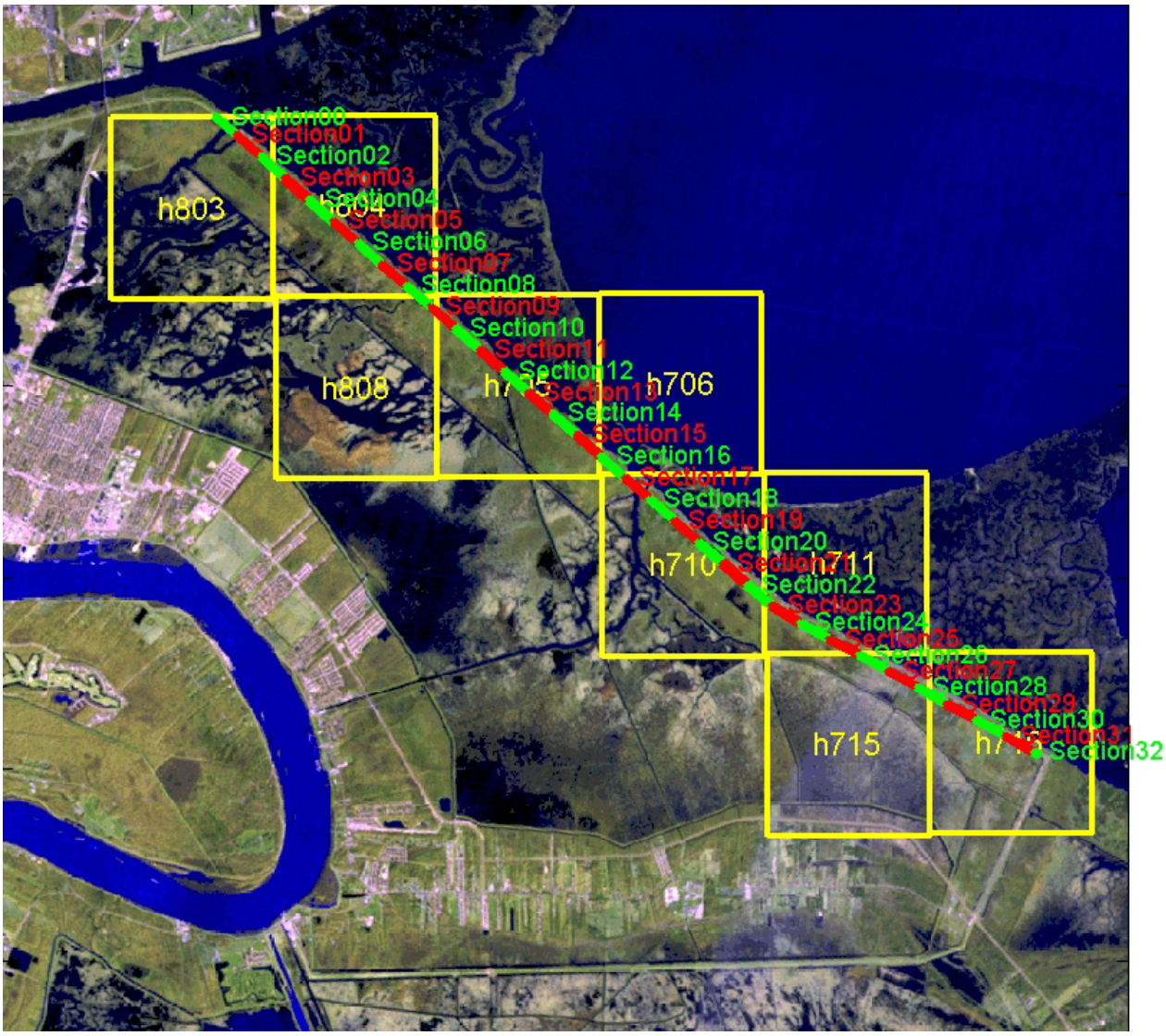
Damage assessment in Section 31, containing Location 8.



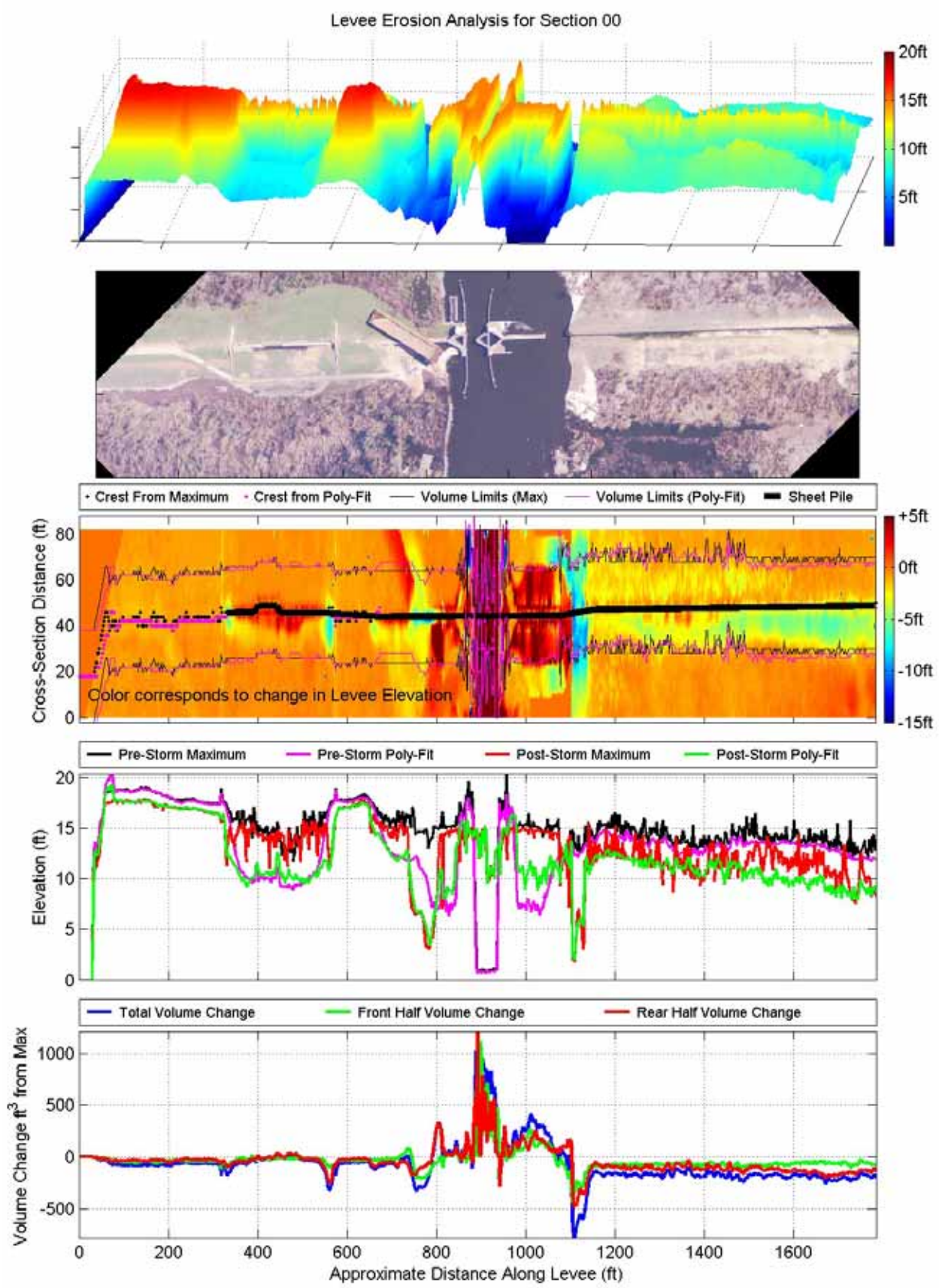
Levee cross-sections at Location 8.

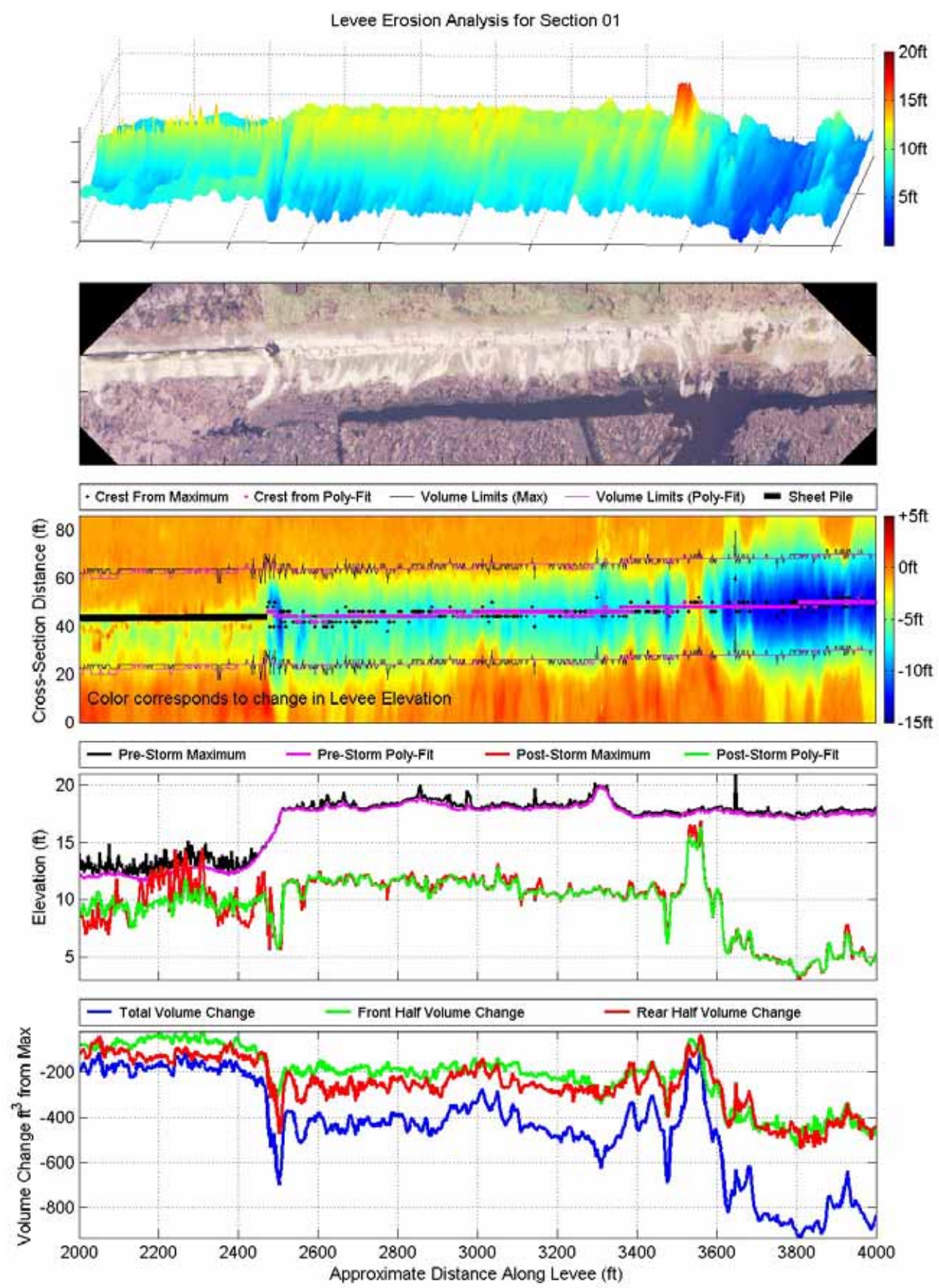


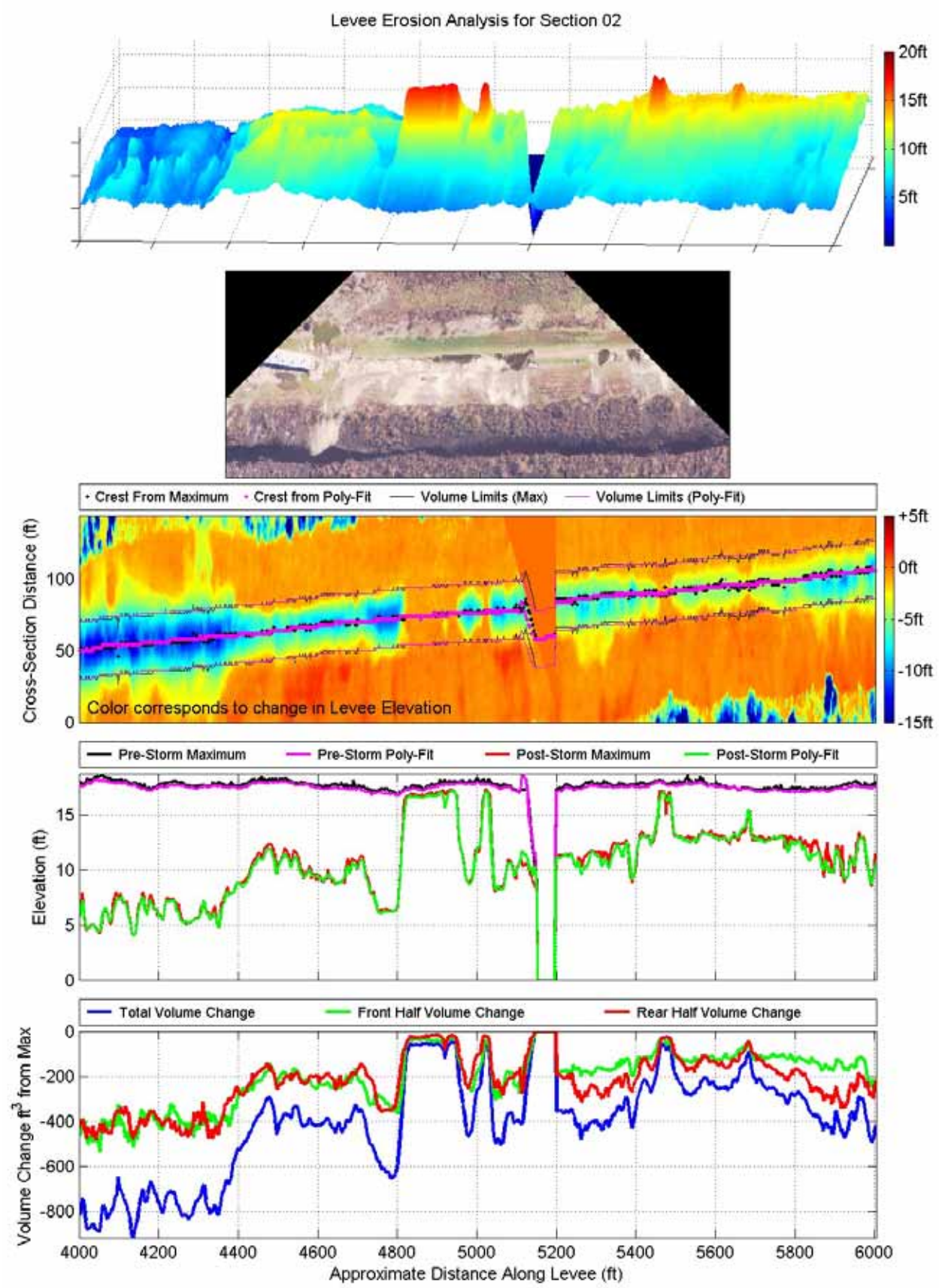
Core from Location 8.



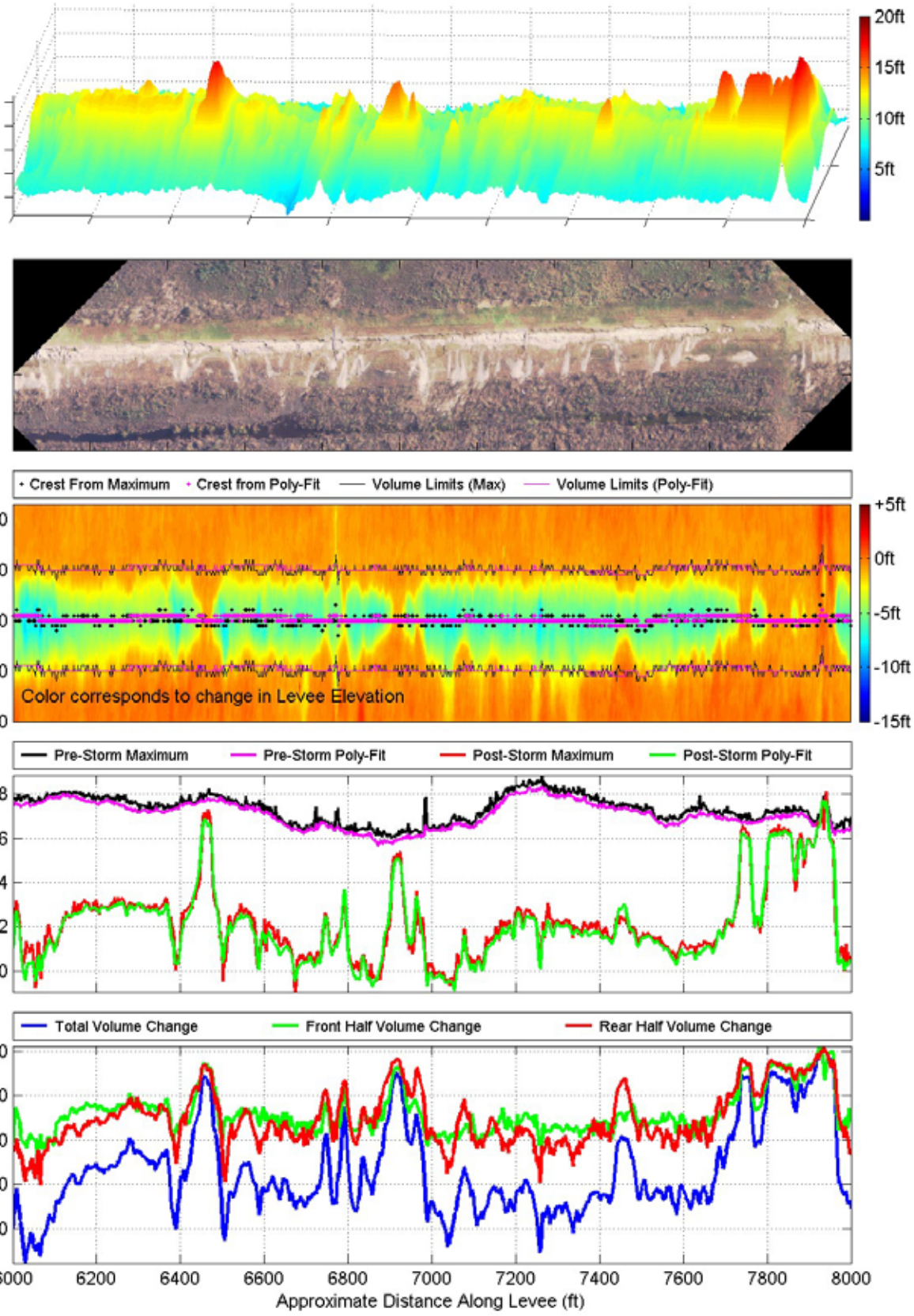
MRGO Levee sub-section locations.

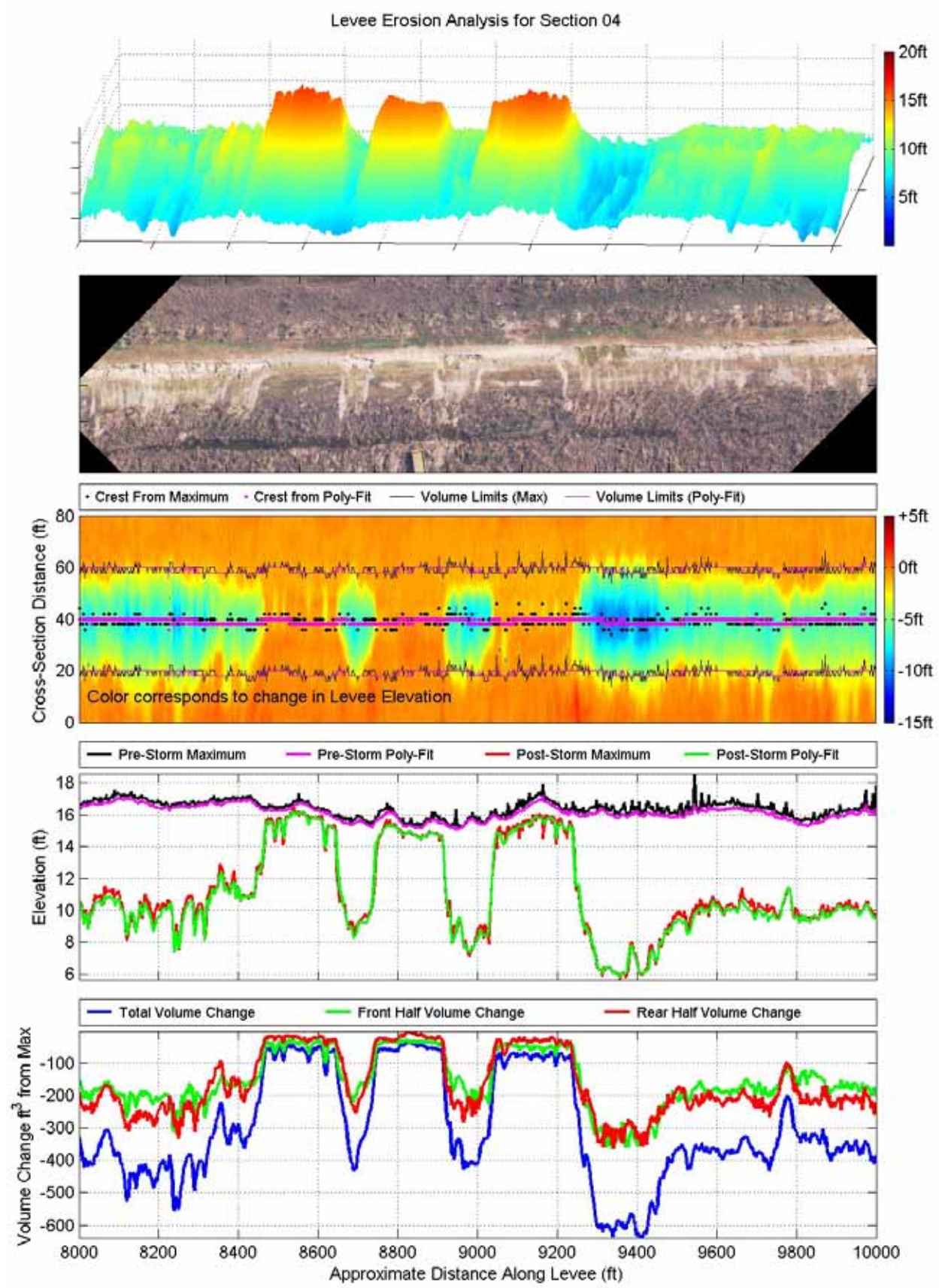

Levee Erosion Analysis for Section 00
20ft
15ft
10ft
5ft
Crest From Maximum
Crest from Poly-Fit
Volume Limits (Max)
Volume Limits (Poly-Fit)
Sheet Pile
Cross-Section Distance (ft)
Color corresponds to change in Levee Elevation
+5ft
0ft
-5ft
-10ft
-15ft
Pre-Storm Maximum
Pre-Storm Poly-Fit
Post-Storm Maximum
Post-Storm Poly-Fit
Elevation (ft)
Total Volume Change
Front Half Volume Change
Rear Half Volume Change
Volume Change ft3 from Max
Approximate Distance Along Levee (ft)

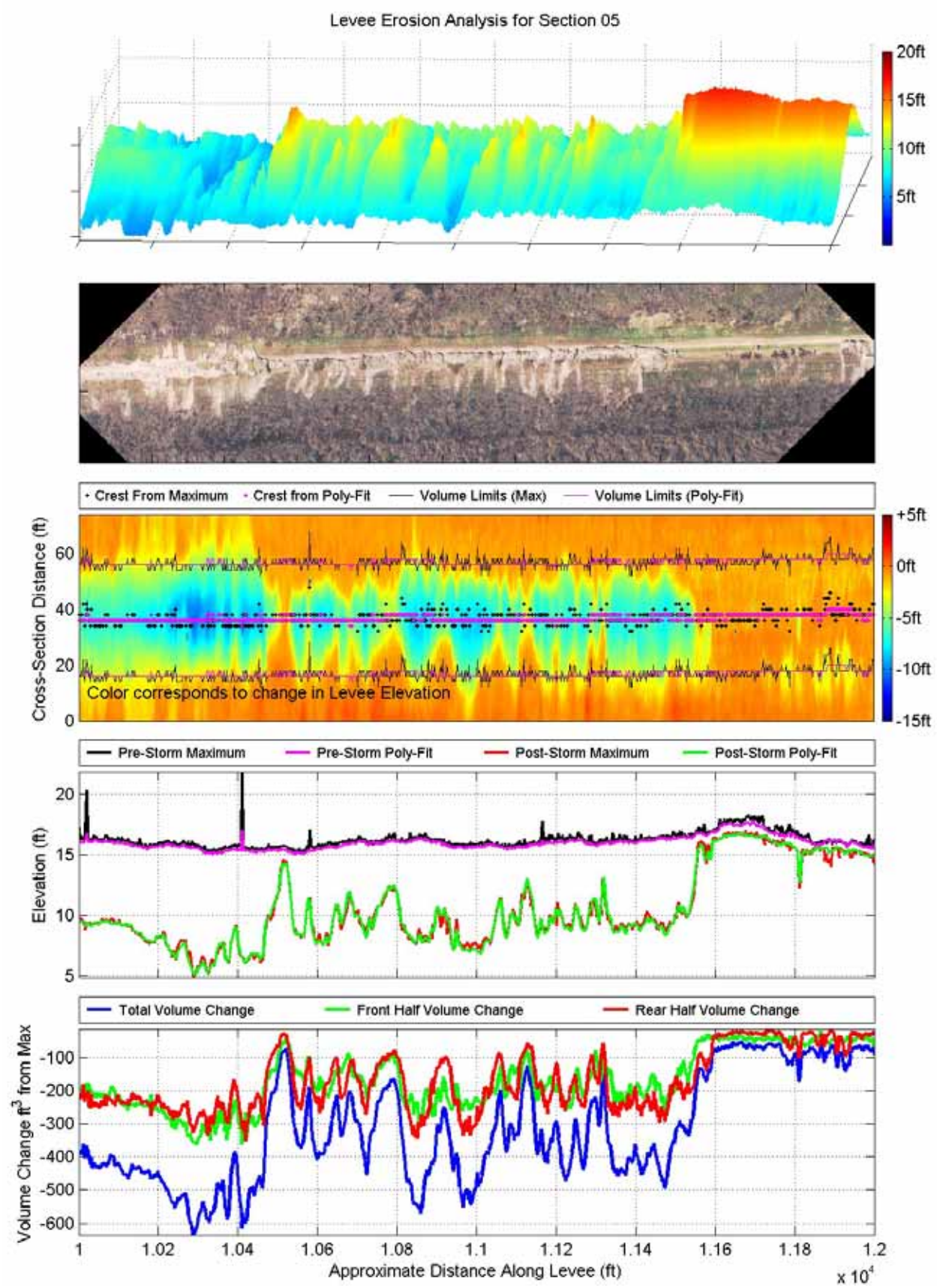

Levee Erosion Analysis for Section 01
20ft
15ft
10ft
5ft
Crest From Maximum
Crest from Poly-Fit
Volume Limits (Max)
Volume Limits (Poly-Fit)
Sheet Pile
Cross-Section Distance (ft)
80
60
40
20
0
+5ft
0ft
-5ft
-10ft
-15ft
Color corresponds to change in Levee Elevation
Pre-Storm Maximum
Pre-Storm Poly-Fit
Post-Storm Maximum
Post-Storm Poly-Fit
Elevation (ft)
20
15
10
5
Total Volume Change
Front Half Volume Change
Rear Half Volume Change
Volume Change ft3 from Max
-200
-400
-600
-800
2000
2200
2400
2600
2800
3000
3200
3400
3600
3800
4000
Approximate Distance Along Levee (ft)

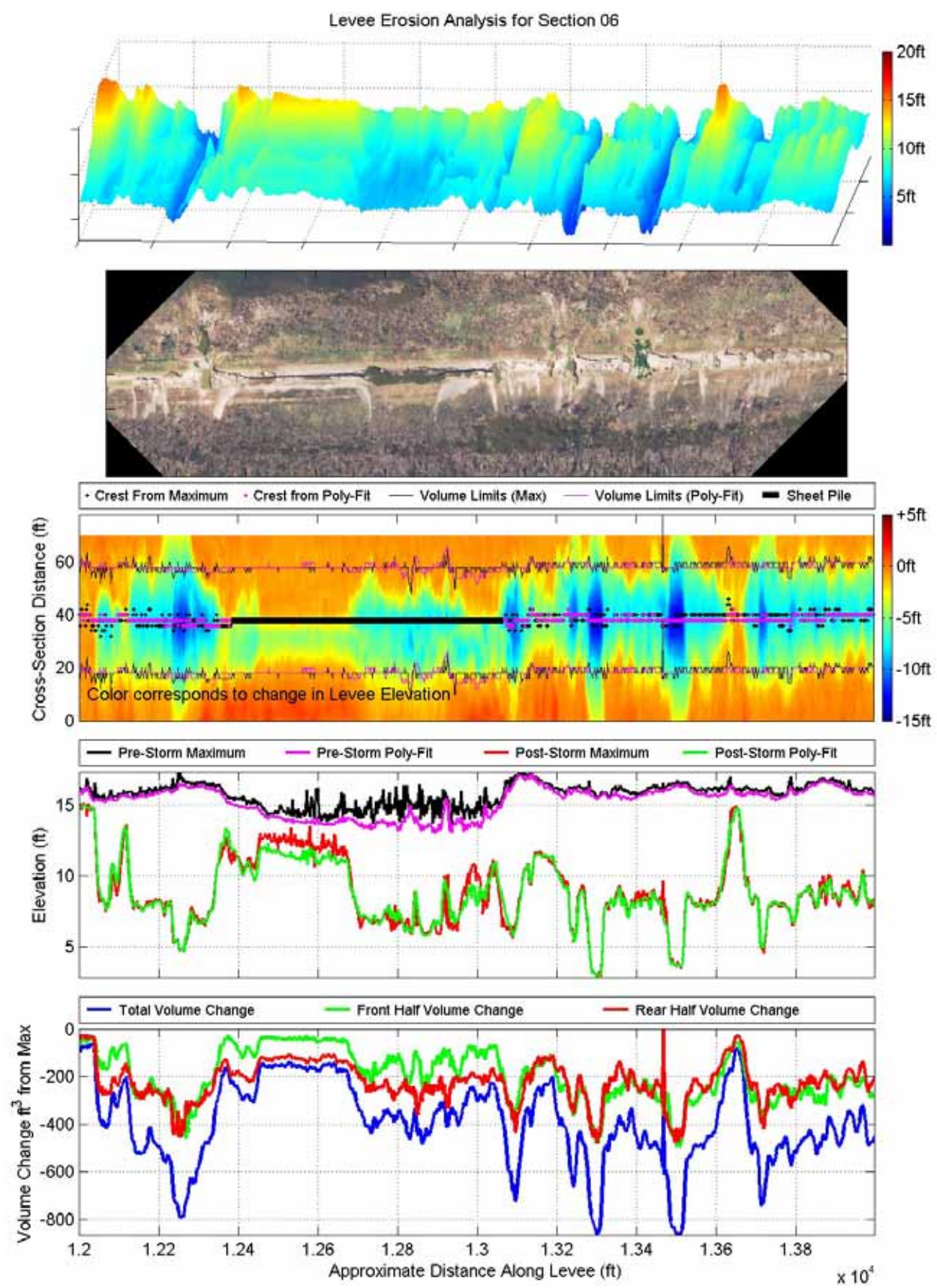

Levee Erosion Analysis for Section 02
20ft
15ft
10ft
5ft
Crest From Maximum
Crest from Poly-Fit
Volume Limits (Max)
Volume Limits (Poly-Fit)
Cross-Section Distance (ft)
100
50
0
Color corresponds to change in Levee Elevation
+5ft
0ft
-5ft
-10ft
-15ft
Pre-Storm Maximum
Pre-Storm Poly-Fit
Post-Storm Maximum
Post-Storm Poly-Fit
Elevation (ft)
15
10
5
0
Total Volume Change
Front Half Volume Change
Rear Half Volume Change
Volume Change ft3 from Max
0
-200
-400
-600
-800
4000
4200
4400
4600
4800
5000
5200
5400
5600
5800
6000
Approximate Distance Along Levee (ft)

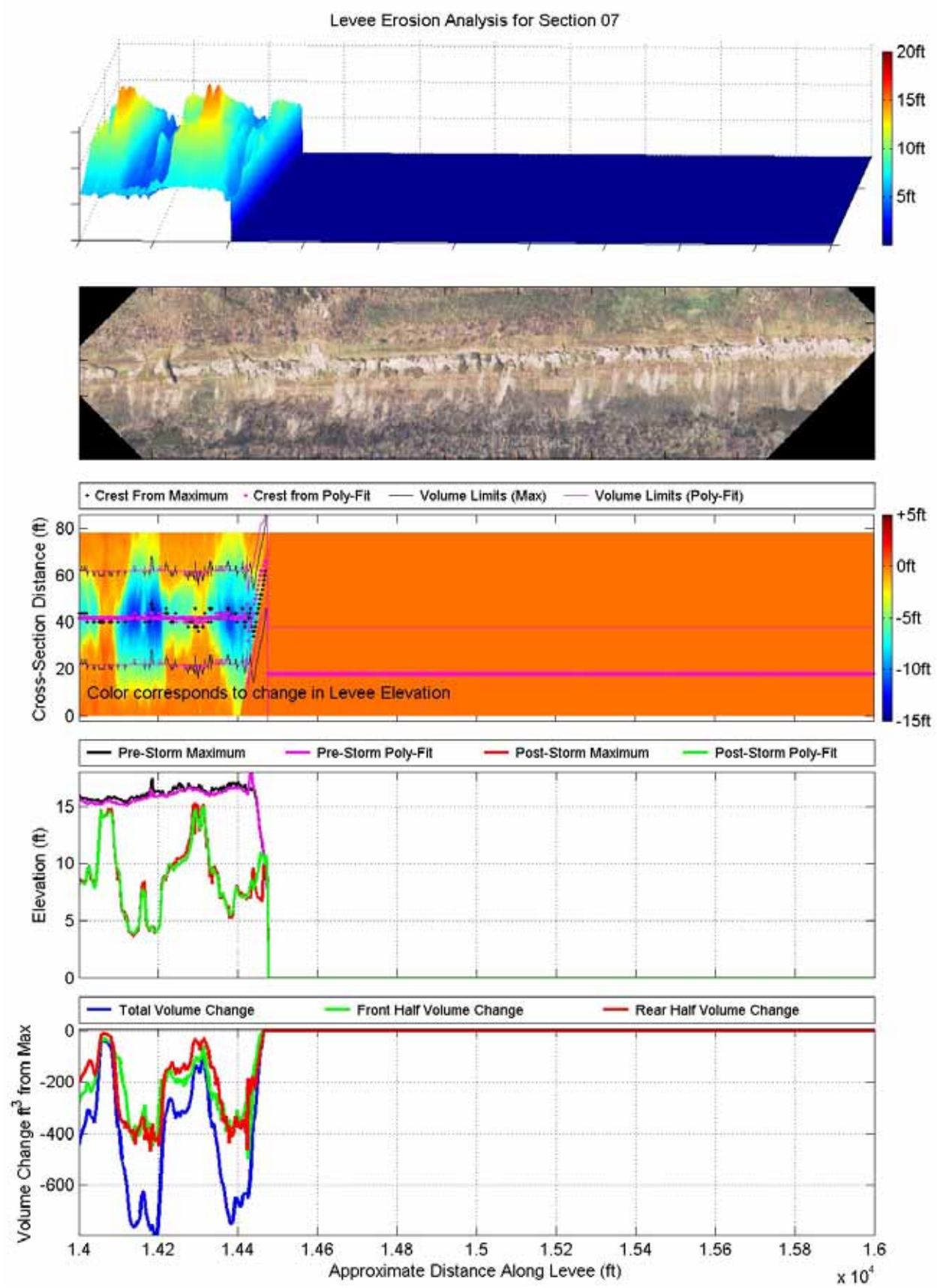
Levee Erosion Analysis for Section 03



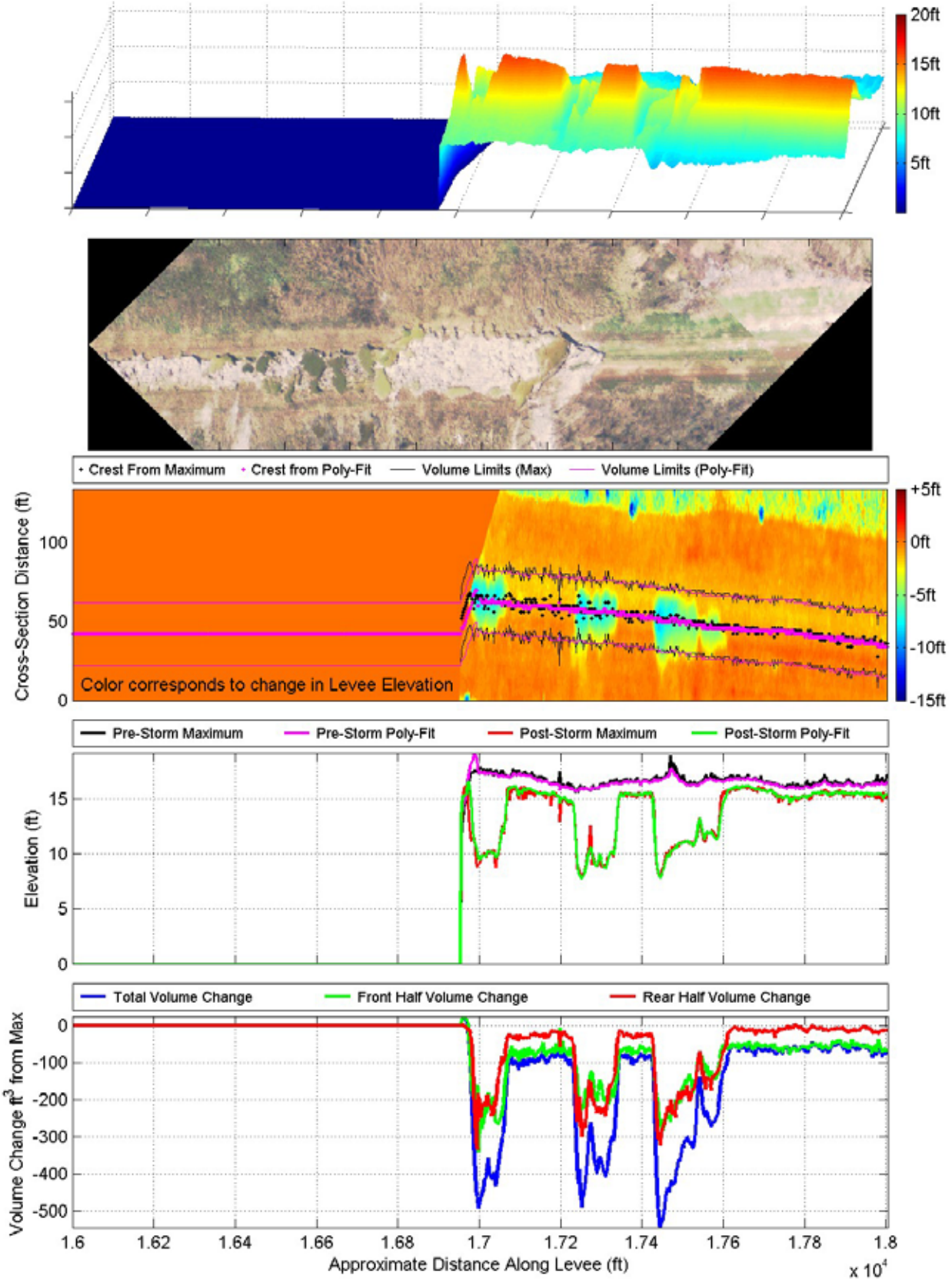

Levee Erosion Analysis for Section 04
20ft
15ft
10ft
5ft
Crest From Maximum
Crest from Poly-Fit
Volume Limits (Max)
Volume Limits (Poly-Fit)
Cross-Section Distance (ft)
80
60
40
20
0
+5ft
0ft
-5ft
-10ft
-15ft
Color corresponds to change in Levee Elevation
Pre-Storm Maximum
Pre-Storm Poly-Fit
Post-Storm Maximum
Post-Storm Poly-Fit
Elevation (ft)
18
16
14
12
10
8
6
Total Volume Change
Front Half Volume Change
Rear Half Volume Change
Volume Change ft3 from Max
-100
-200
-300
-400
-500
-600
8000
8200
8400
8600
8800
9000
9200
9400
9600
9800
10000
Approximate Distance Along Levee (ft)

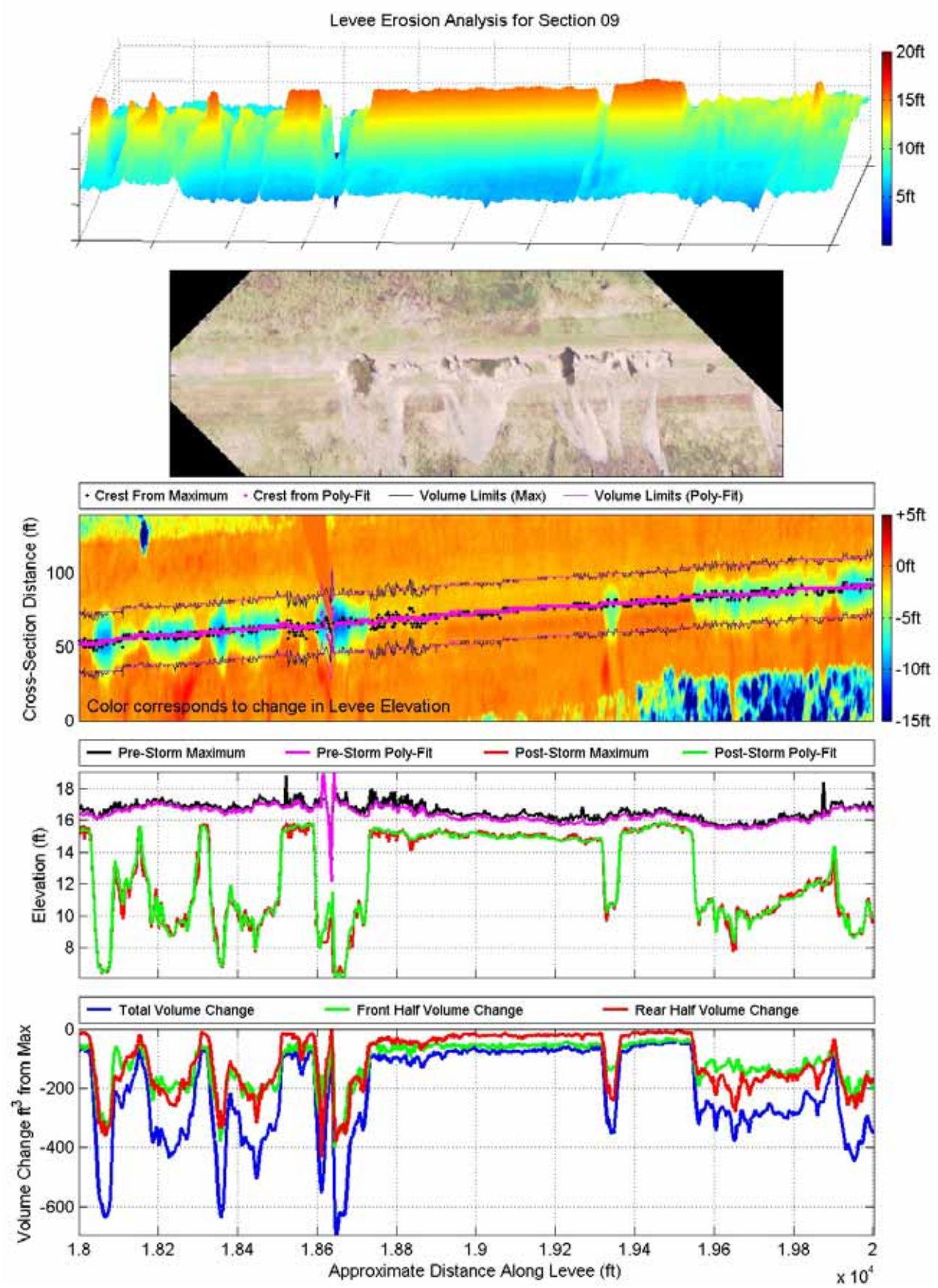

Levee Erosion Analysis for Section 05
20ft
15ft
10ft
5ft
Crest From Maximum
Crest from Poly-Fit
Volume Limits (Max)
Volume Limits (Poly-Fit)
Cross-Section Distance (ft)
60
40
20
0
+5ft
0ft
-5ft
-10ft
-15ft
Color corresponds to change in Levee Elevation
Pre-Storm Maximum
Pre-Storm Poly-Fit
Post-Storm Maximum
Post-Storm Poly-Fit
Elevation (ft)
20
15
10
5
Total Volume Change
Front Half Volume Change
Rear Half Volume Change
Volume Change ft3 from Max
-100
-200
-300
-400
-500
-600
1
1.02
1.04
1.06
1.08
1.1
1.12
1.14
1.16
1.18
1.2
Approximate Distance Along Levee (ft)
x 10^4

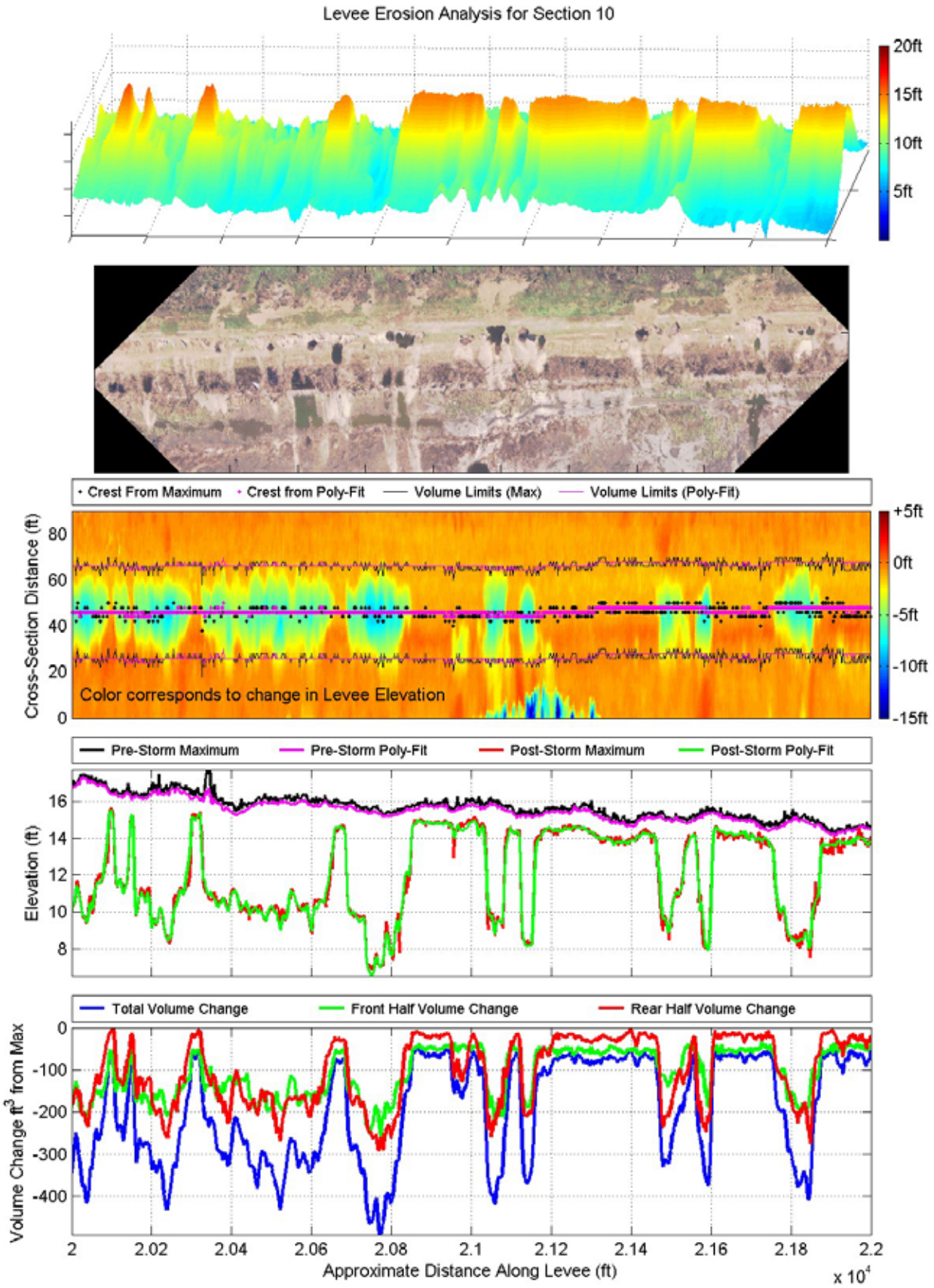

Levee Erosion Analysis for Section 06
20ft
15ft
10ft
5ft
Crest From Maximum
Crest from Poly-Fit
Volume Limits (Max)
Volume Limits (Poly-Fit)
Sheet Pile
Cross-Section Distance (ft)
60
40
20
0
+5ft
0ft
-5ft
-10ft
-15ft
Color corresponds to change in Levee Elevation
Pre-Storm Maximum
Pre-Storm Poly-Fit
Post-Storm Maximum
Post-Storm Poly-Fit
Elevation (ft)
15
10
5
Total Volume Change
Front Half Volume Change
Rear Half Volume Change
Volume Change ft3 from Max
0
-200
-400
-600
-800
1.2
1.22
1.24
1.26
1.28
1.3
1.32
1.34
1.36
1.38
Approximate Distance Along Levee (ft)
x 10^4

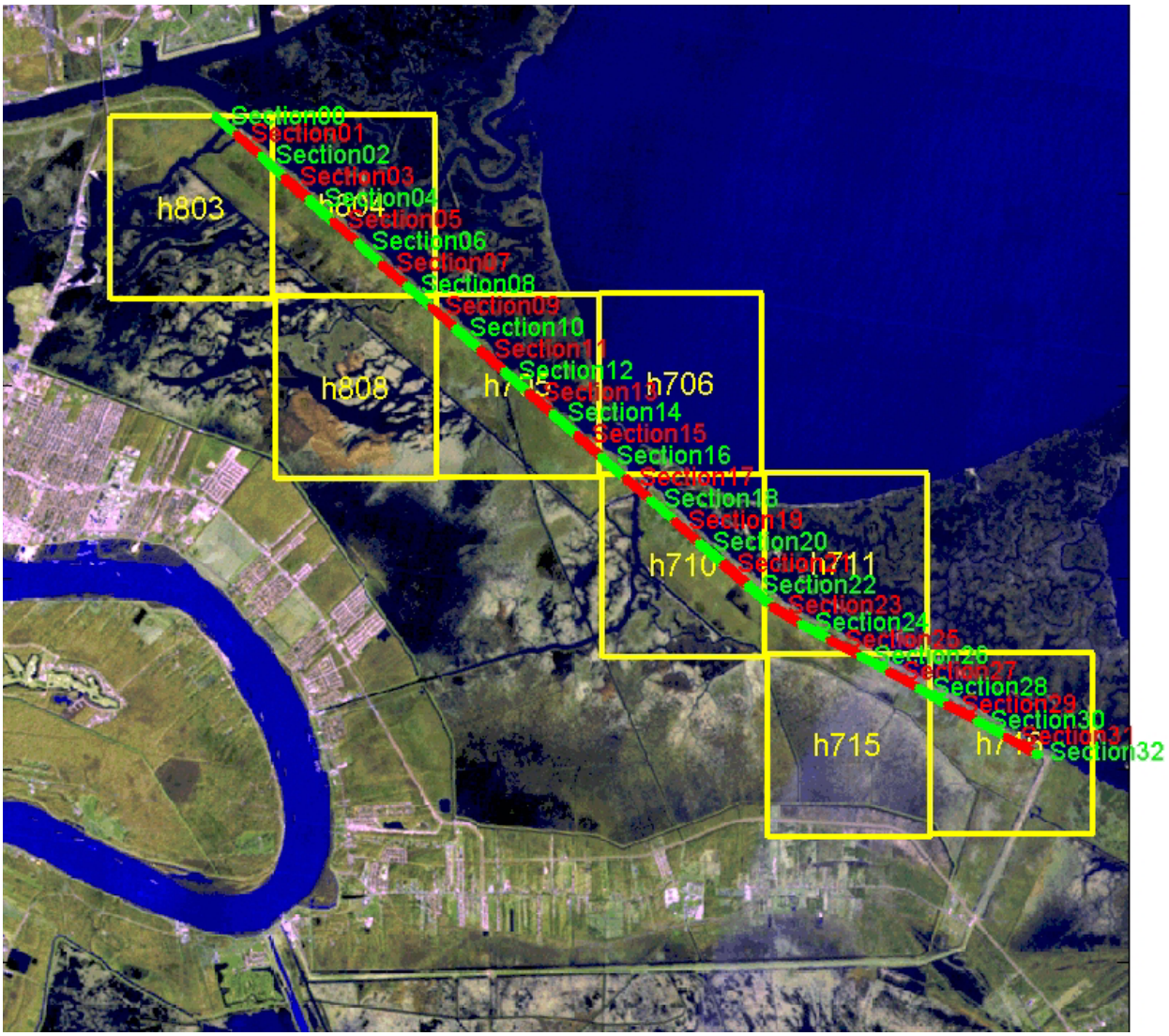

Levee Erosion Analysis for Section 07
20ft
15ft
10ft
5ft
Crest From Maximum
Crest from Poly-Fit
Volume Limits (Max)
Volume Limits (Poly-Fit)
Cross-Section Distance (ft)
80
60
40
20
0
Color corresponds to change in Levee Elevation
+5ft
0ft
-5ft
-10ft
-15ft
Pre-Storm Maximum
Pre-Storm Poly-Fit
Post-Storm Maximum
Post-Storm Poly-Fit
Elevation (ft)
15
10
5
0
Total Volume Change
Front Half Volume Change
Rear Half Volume Change
Volume Change ft3 from Max
0
-200
-400
-600
1.4
1.42
1.44
1.46
1.48
1.5
1.52
1.54
1.56
1.58
1.6
Approximate Distance Along Levee (ft)
x 10^4

Levee Erosion Analysis for Section 08

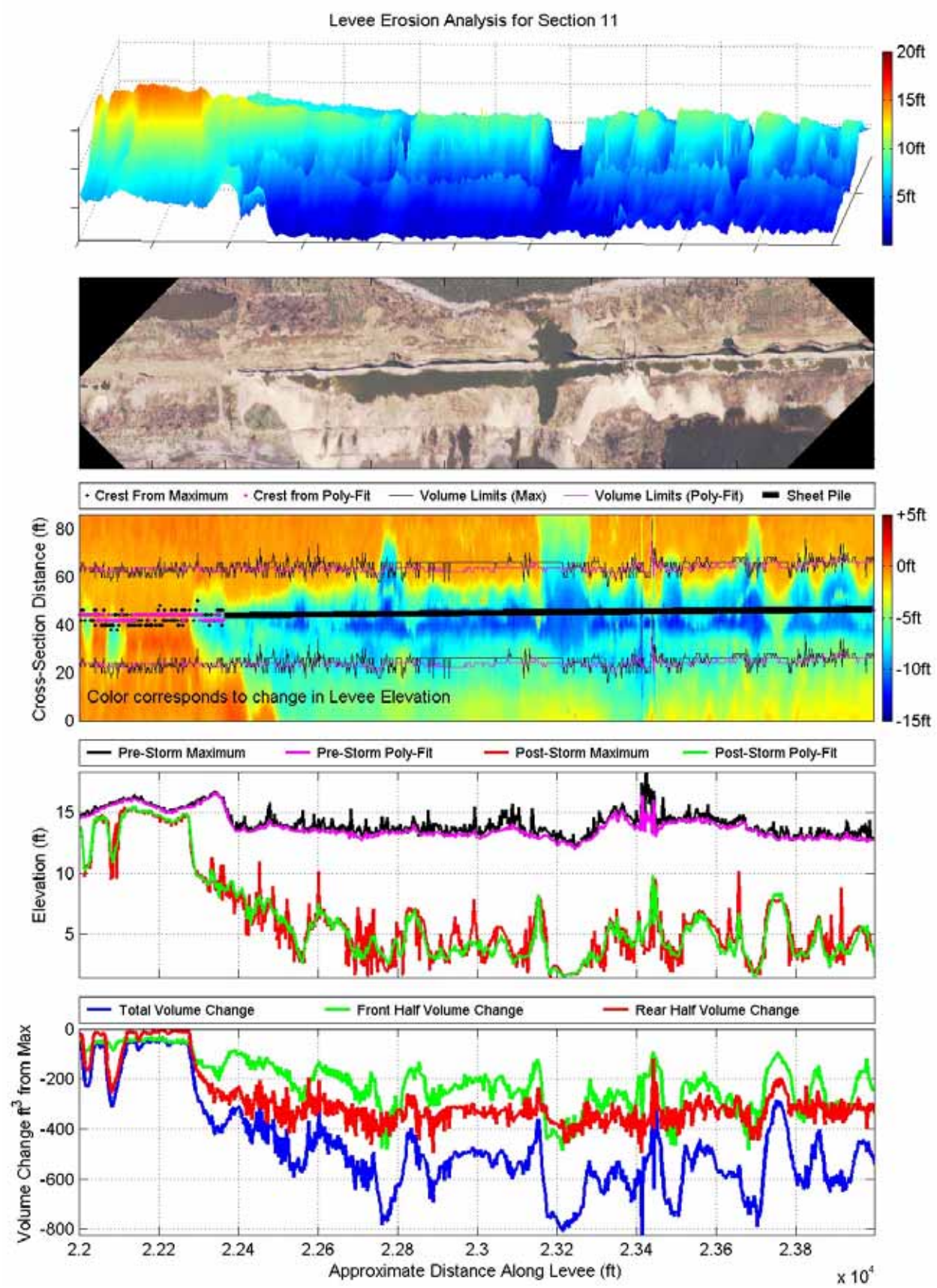


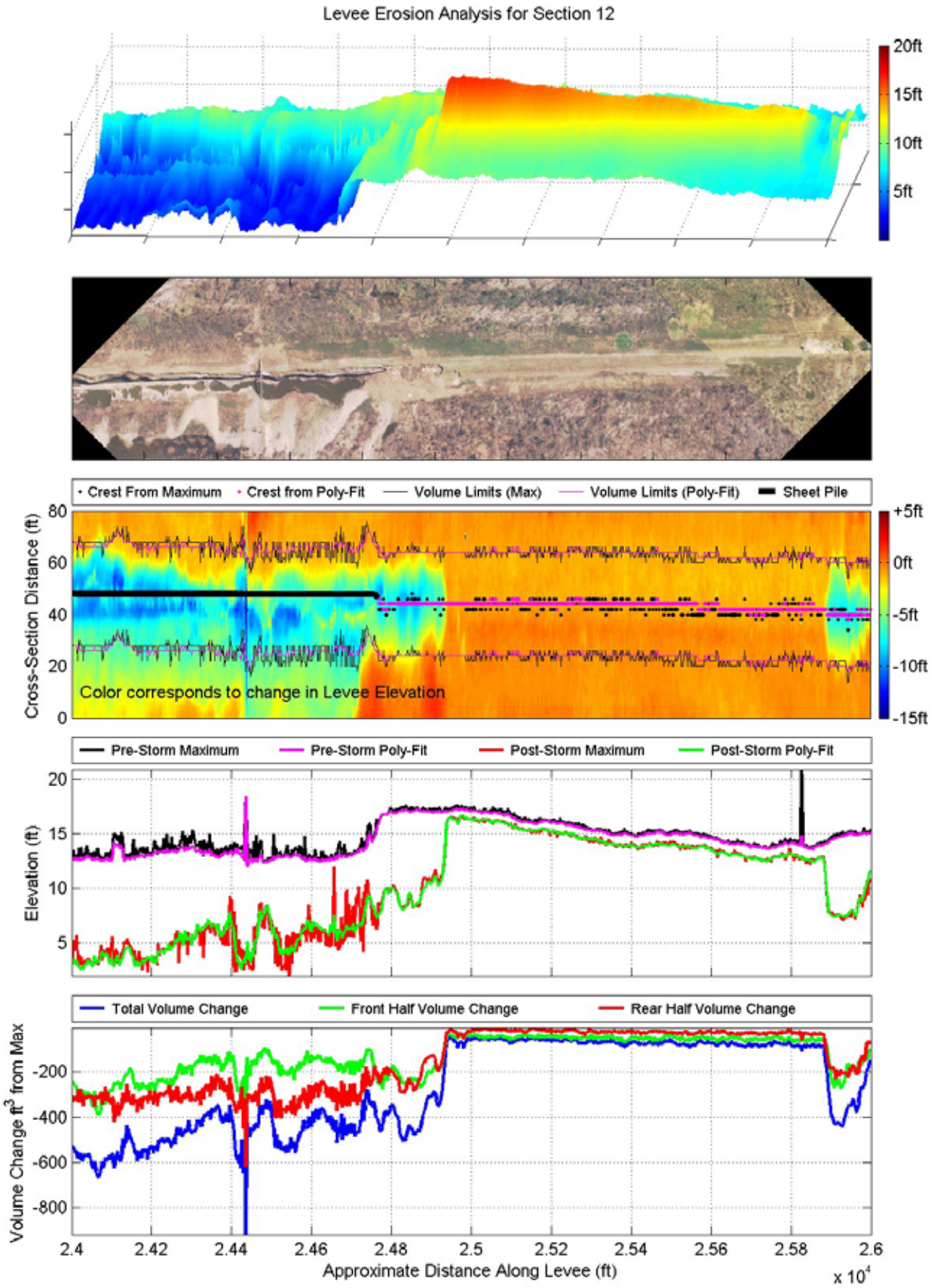

Levee Erosion Analysis for Section 09
20ft
15ft
10ft
5ft
Crest From Maximum
Crest from Poly-Fit
Volume Limits (Max)
Volume Limits (Poly-Fit)
Cross-Section Distance (ft)
100
50
0
+5ft
0ft
-5ft
-10ft
-15ft
Color corresponds to change in Levee Elevation
Pre-Storm Maximum
Pre-Storm Poly-Fit
Post-Storm Maximum
Post-Storm Poly-Fit
Elevation (ft)
18
16
14
12
10
8
Total Volume Change
Front Half Volume Change
Rear Half Volume Change
Volume Change ft3 from Max
0
-200
-400
-600
1.8
1.82
1.84
1.86
1.88
1.9
1.92
1.94
1.96
1.98
2
Approximate Distance Along Levee (ft)
x 10^4

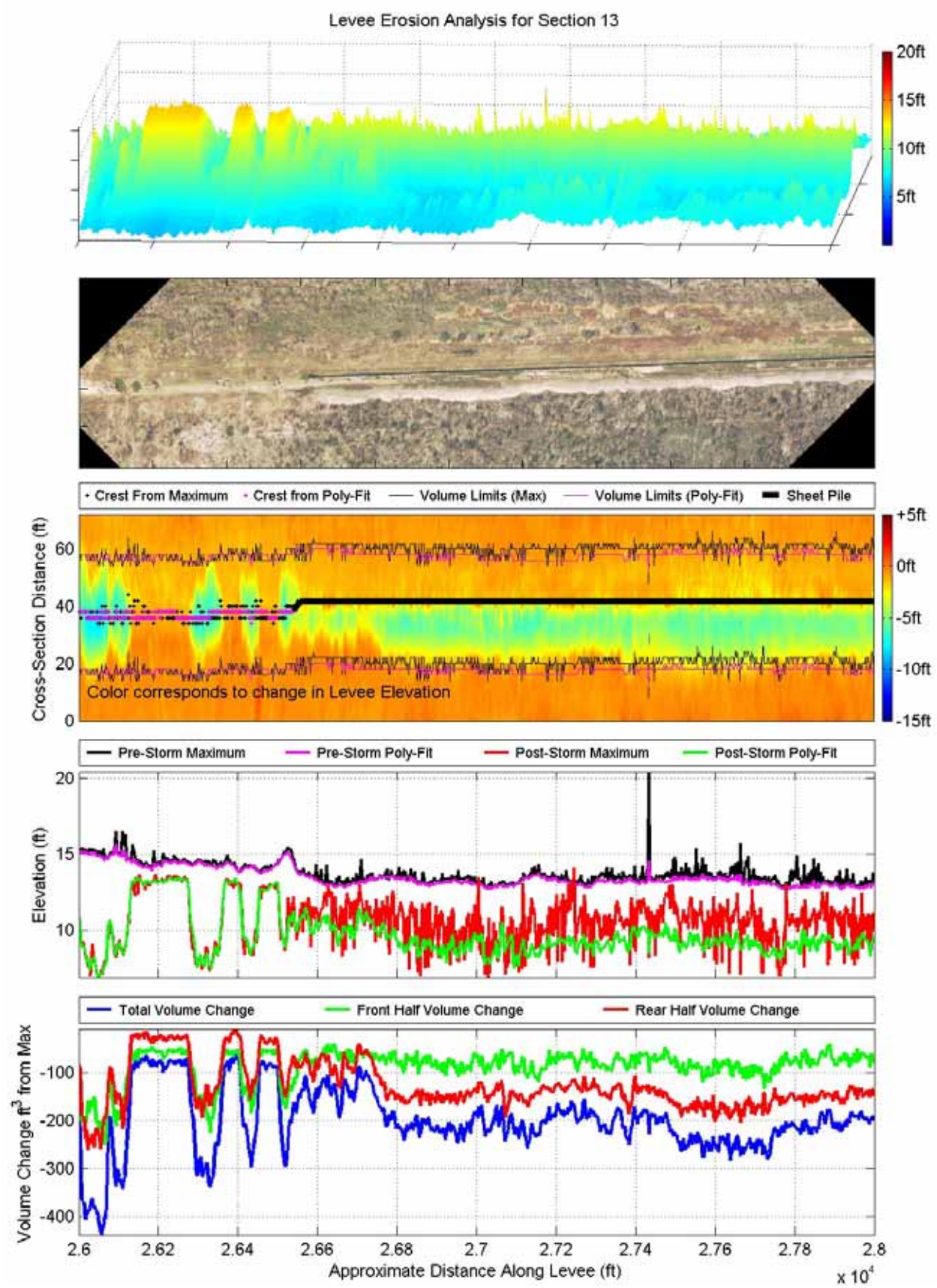

Levee Erosion Analysis for Section 10
20ft
15ft
10ft
5ft
Crest From Maximum
Crest from Poly-Fit
Volume Limits (Max)
Volume Limits (Poly-Fit)
Cross-Section Distance (ft)
80
60
40
20
0
+5ft
0ft
-5ft
-10ft
-15ft
Color corresponds to change in Levee Elevation
Pre-Storm Maximum
Pre-Storm Poly-Fit
Post-Storm Maximum
Post-Storm Poly-Fit
Elevation (ft)
16
14
12
10
8
Total Volume Change
Front Half Volume Change
Rear Half Volume Change
Volume Change ft3 from Max
0
-100
-200
-300
-400
2
2.02
2.04
2.06
2.08
2.1
2.12
2.14
2.16
2.18
2.2
Approximate Distance Along Levee (ft)
x 10^4

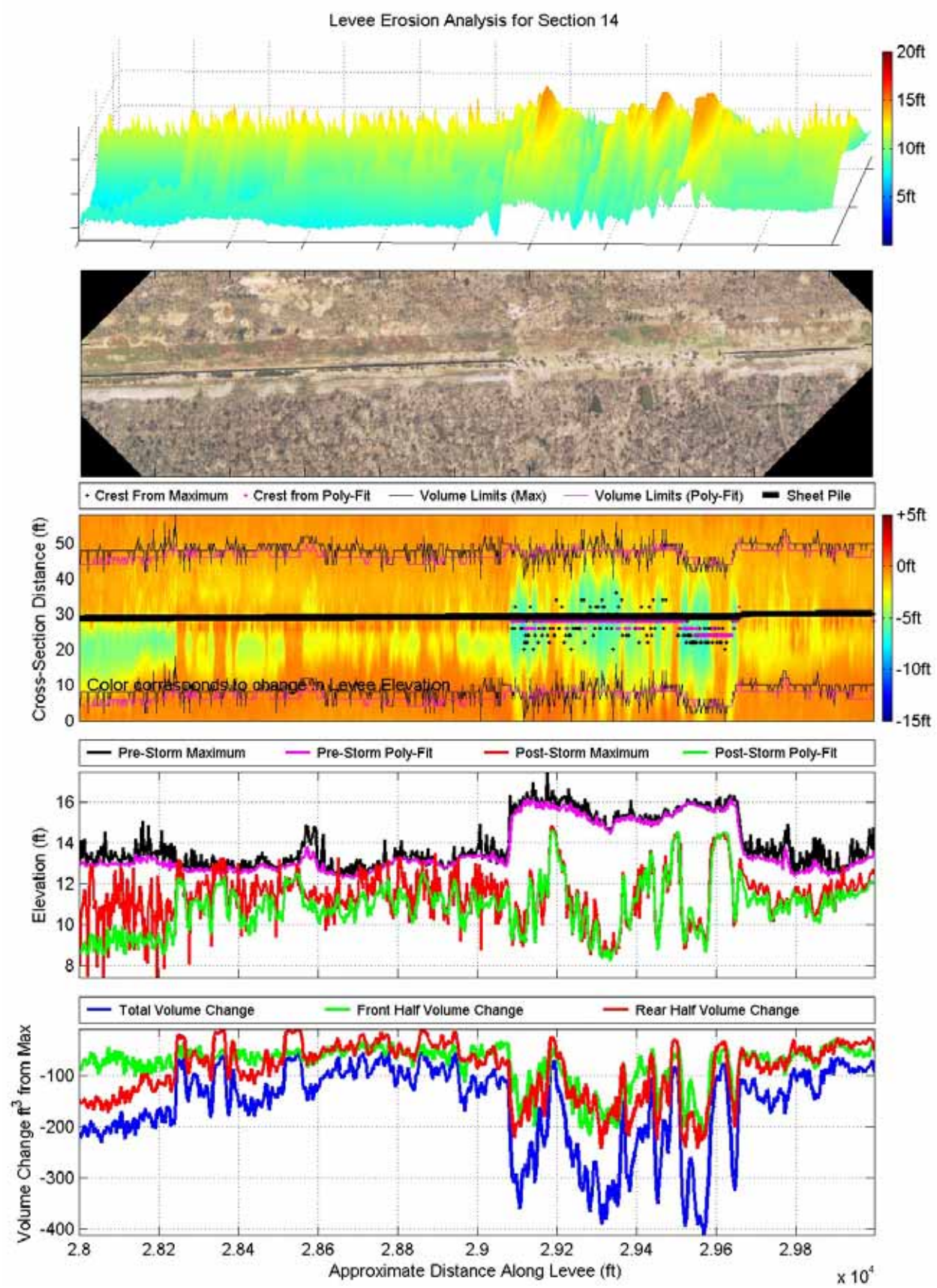


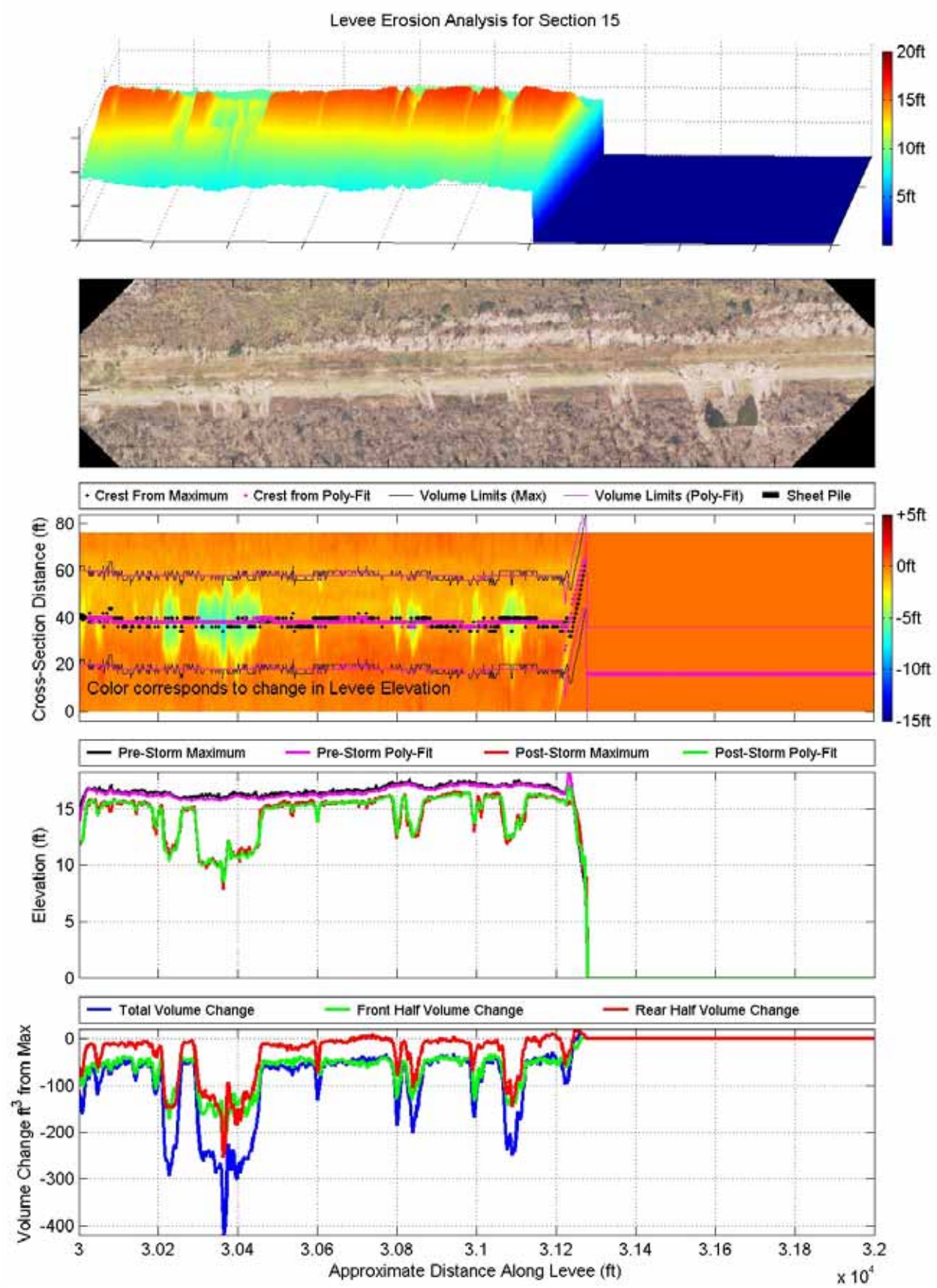
MRGO Levee sub-section locations.

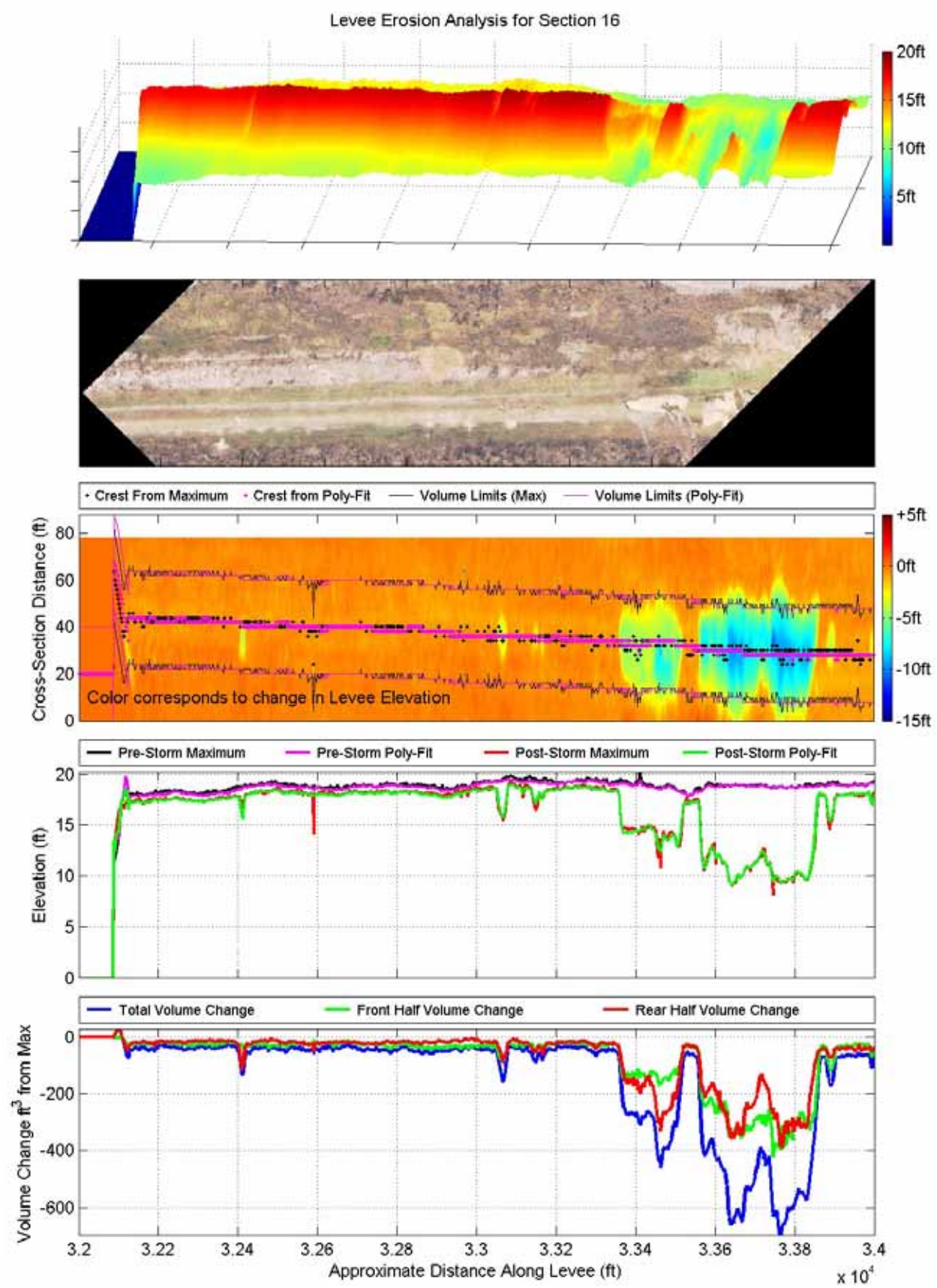

Levee Erosion Analysis for Section 11
20ft
15ft
10ft
5ft
Crest From Maximum
Crest from Poly-Fit
Volume Limits (Max)
Volume Limits (Poly-Fit)
Sheet Pile
Cross-Section Distance (ft)
80
60
40
20
0
+5ft
0ft
-5ft
-10ft
-15ft
Color corresponds to change in Levee Elevation
Pre-Storm Maximum
Pre-Storm Poly-Fit
Post-Storm Maximum
Post-Storm Poly-Fit
Elevation (ft)
15
10
5
Total Volume Change
Front Half Volume Change
Rear Half Volume Change
Volume Change ft3 from Max
0
-200
-400
-600
-800
2.2
2.22
2.24
2.26
2.28
2.3
2.32
2.34
2.36
2.38
Approximate Distance Along Levee (ft)
x 10^4

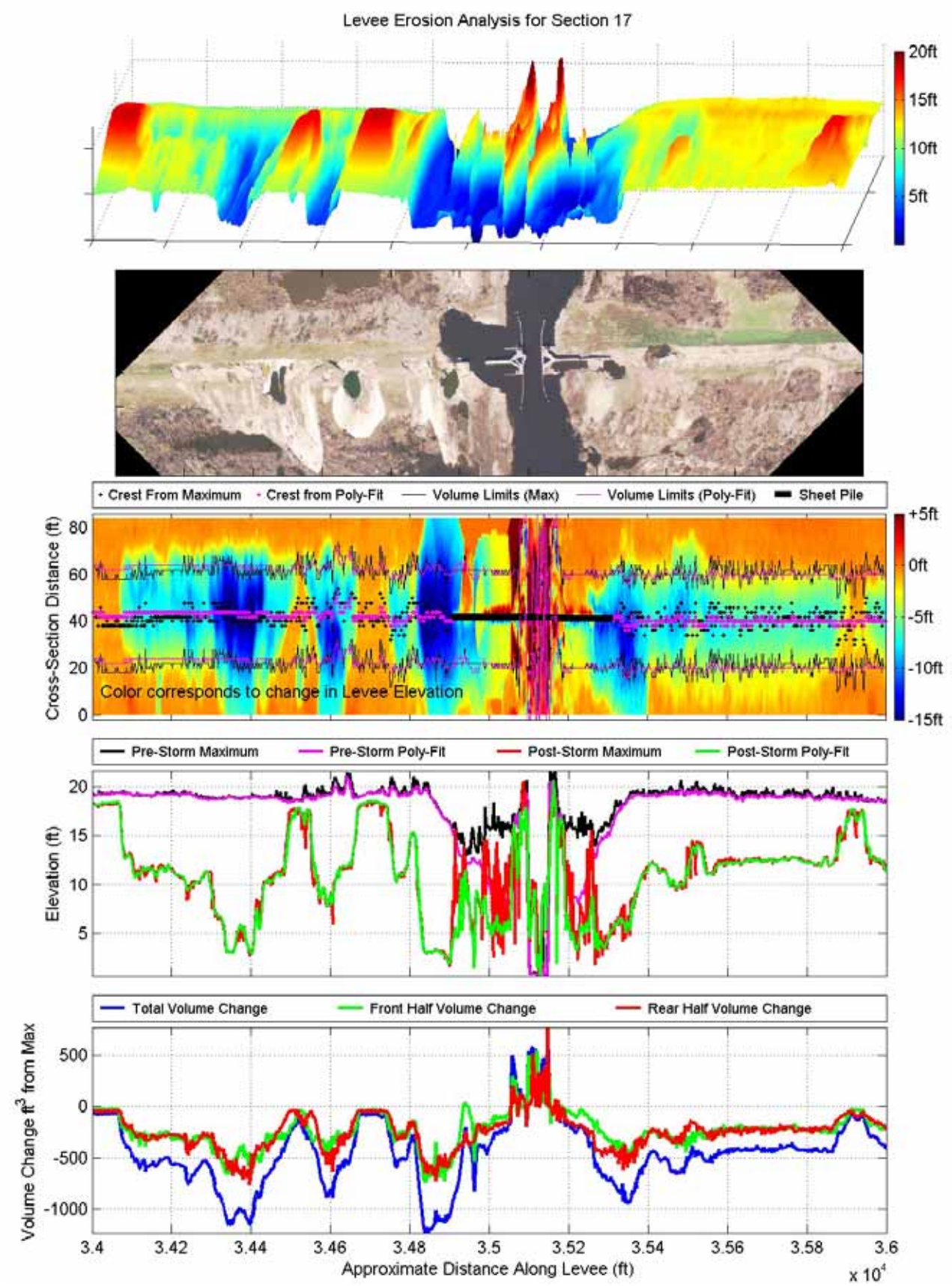

Levee Erosion Analysis for Section 12
20ft
15ft
10ft
5ft
Crest From Maximum
Crest from Poly-Fit
Volume Limits (Max)
Volume Limits (Poly-Fit)
Sheet Pile
Cross-Section Distance (ft)
80
60
40
20
0
+5ft
0ft
-5ft
-10ft
-15ft
Color corresponds to change in Levee Elevation
Pre-Storm Maximum
Pre-Storm Poly-Fit
Post-Storm Maximum
Post-Storm Poly-Fit
Elevation (ft)
20
15
10
5
Total Volume Change
Front Half Volume Change
Rear Half Volume Change
Volume Change ft3 from Max
-200
-400
-600
-800
2.4
2.42
2.44
2.46
2.48
2.5
2.52
2.54
2.56
2.58
2.6
Approximate Distance Along Levee (ft)
x 10^4

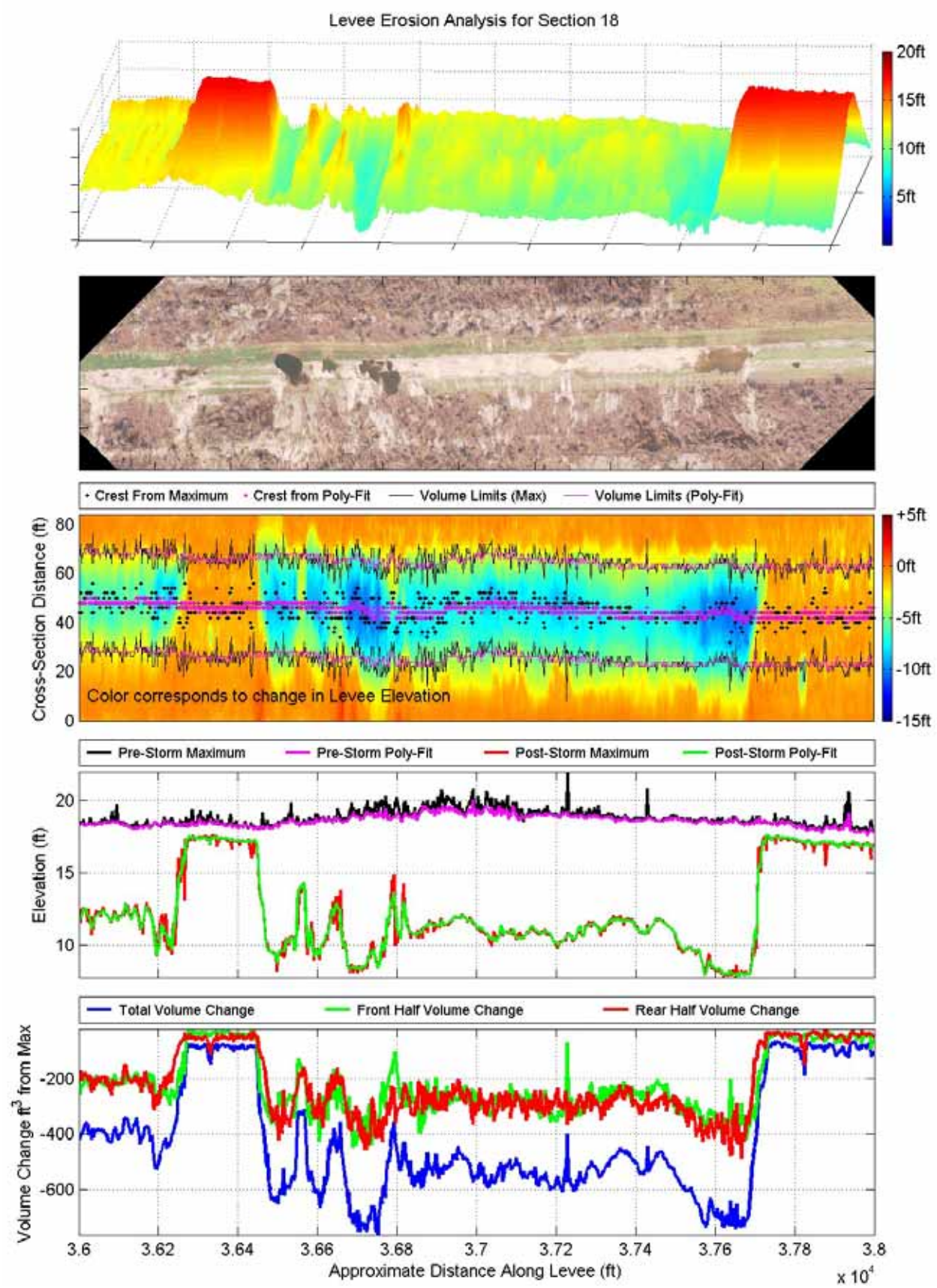

Levee Erosion Analysis for Section 13
20ft
15ft
10ft
5ft
Crest From Maximum
Crest from Poly-Fit
Volume Limits (Max)
Volume Limits (Poly-Fit)
Sheet Pile
Cross-Section Distance (ft)
60
40
20
0
+5ft
0ft
-5ft
-10ft
-15ft
Color corresponds to change in Levee Elevation
Pre-Storm Maximum
Pre-Storm Poly-Fit
Post-Storm Maximum
Post-Storm Poly-Fit
Elevation (ft)
20
15
10
Total Volume Change
Front Half Volume Change
Rear Half Volume Change
Volume Change ft3 from Max
-100
-200
-300
-400
2.6
2.62
2.64
2.66
2.68
2.7
2.72
2.74
2.76
2.78
2.8
Approximate Distance Along Levee (ft)
x 10^4

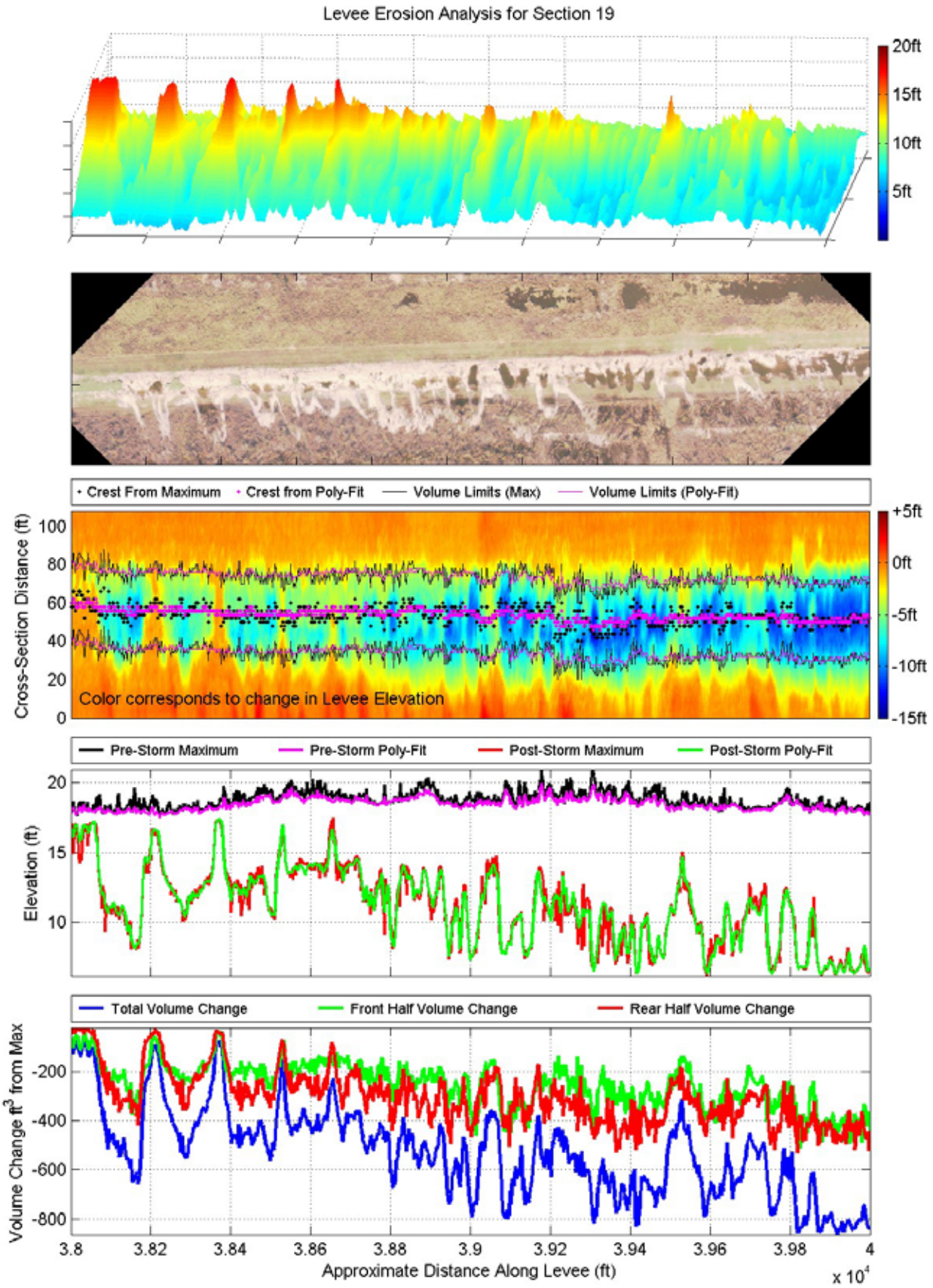

Levee Erosion Analysis for Section 14
20ft
15ft
10ft
5ft
Crest From Maximum
Crest from Poly-Fit
Volume Limits (Max)
Volume Limits (Poly-Fit)
Sheet Pile
Cross-Section Distance (ft)
50
40
30
20
10
0
Color corresponds to change in Levee Elevation
+5ft
0ft
-5ft
-10ft
-15ft
Pre-Storm Maximum
Pre-Storm Poly-Fit
Post-Storm Maximum
Post-Storm Poly-Fit
Elevation (ft)
16
14
12
10
8
Total Volume Change
Front Half Volume Change
Rear Half Volume Change
Volume Change ft3 from Max
-100
-200
-300
-400
2.8
2.82
2.84
2.86
2.88
2.9
2.92
2.94
2.96
2.98
Approximate Distance Along Levee (ft)
x 10^4

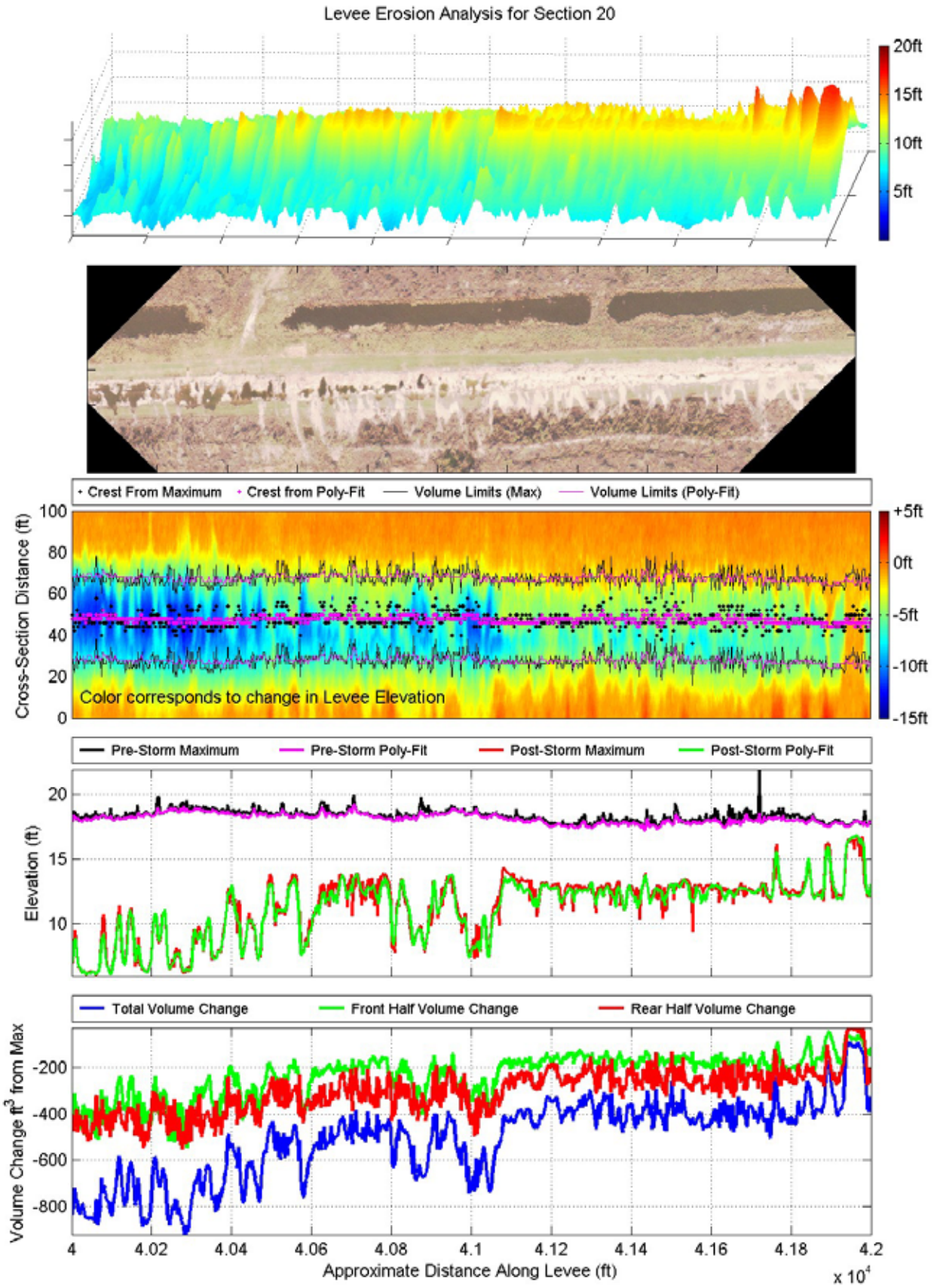

Levee Erosion Analysis for Section 15
20ft
15ft
10ft
5ft
Crest From Maximum
Crest from Poly-Fit
Volume Limits (Max)
Volume Limits (Poly-Fit)
Sheet Pile
Cross-Section Distance (ft)
80
60
40
20
0
+5ft
0ft
-5ft
-10ft
-15ft
Color corresponds to change in Levee Elevation
Pre-Storm Maximum
Pre-Storm Poly-Fit
Post-Storm Maximum
Post-Storm Poly-Fit
Elevation (ft)
15
10
5
0
Total Volume Change
Front Half Volume Change
Rear Half Volume Change
Volume Change ft3 from Max
0
-100
-200
-300
-400
3
3.02
3.04
3.06
3.08
3.1
3.12
3.14
3.16
3.18
3.2
Approximate Distance Along Levee (ft)
x 10^4

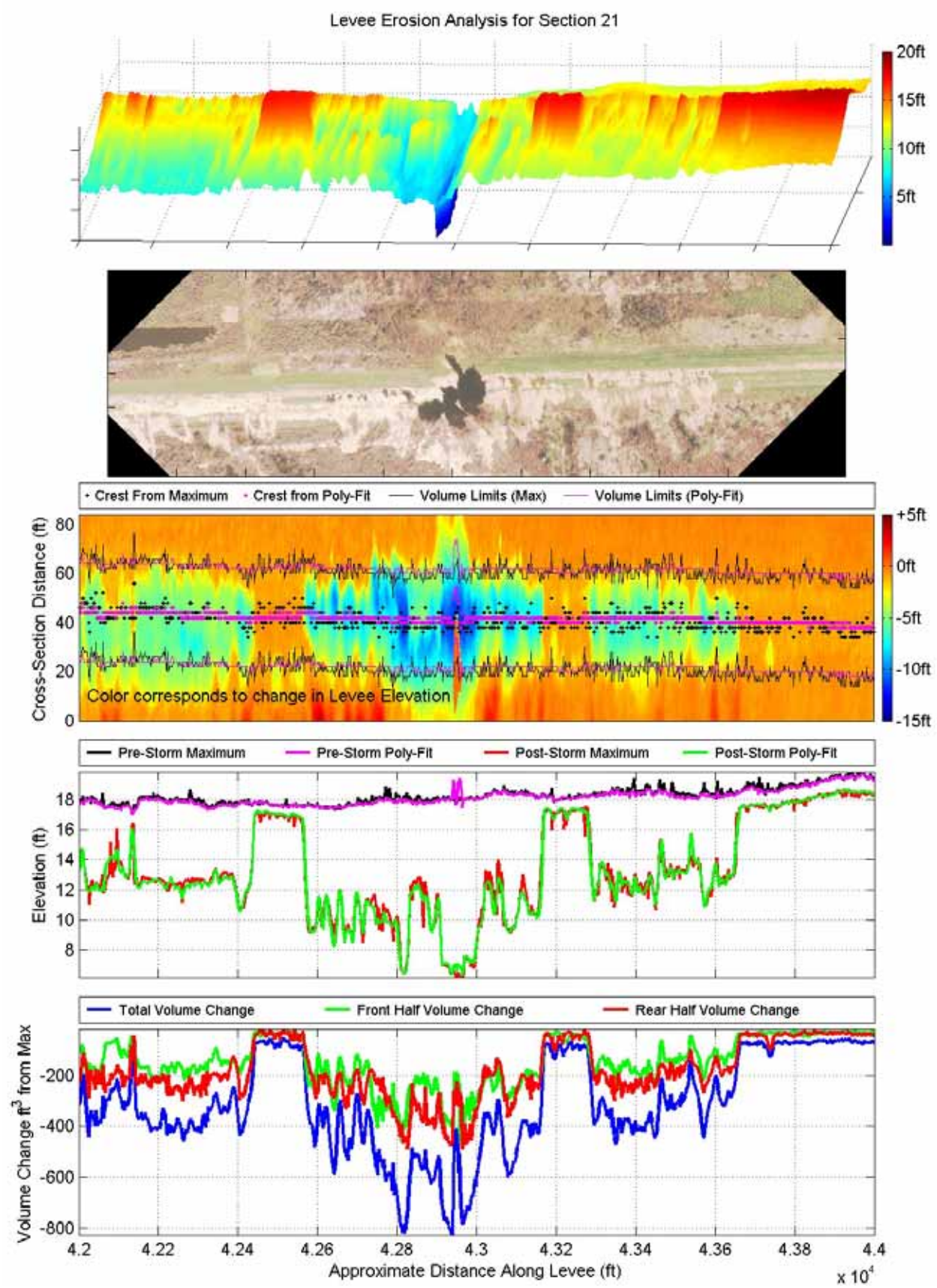

Levee Erosion Analysis for Section 16
20ft
15ft
10ft
5ft
Crest From Maximum
Crest from Poly-Fit
Volume Limits (Max)
Volume Limits (Poly-Fit)
Cross-Section Distance (ft)
80
60
40
20
0
Color corresponds to change in Levee Elevation
+5ft
0ft
-5ft
-10ft
-15ft
Pre-Storm Maximum
Pre-Storm Poly-Fit
Post-Storm Maximum
Post-Storm Poly-Fit
Elevation (ft)
20
15
10
5
0
Total Volume Change
Front Half Volume Change
Rear Half Volume Change
Volume Change ft3 from Max
0
-200
-400
-600
3.2
3.22
3.24
3.26
3.28
3.3
3.32
3.34
3.36
3.38
3.4
Approximate Distance Along Levee (ft)
x 10^4

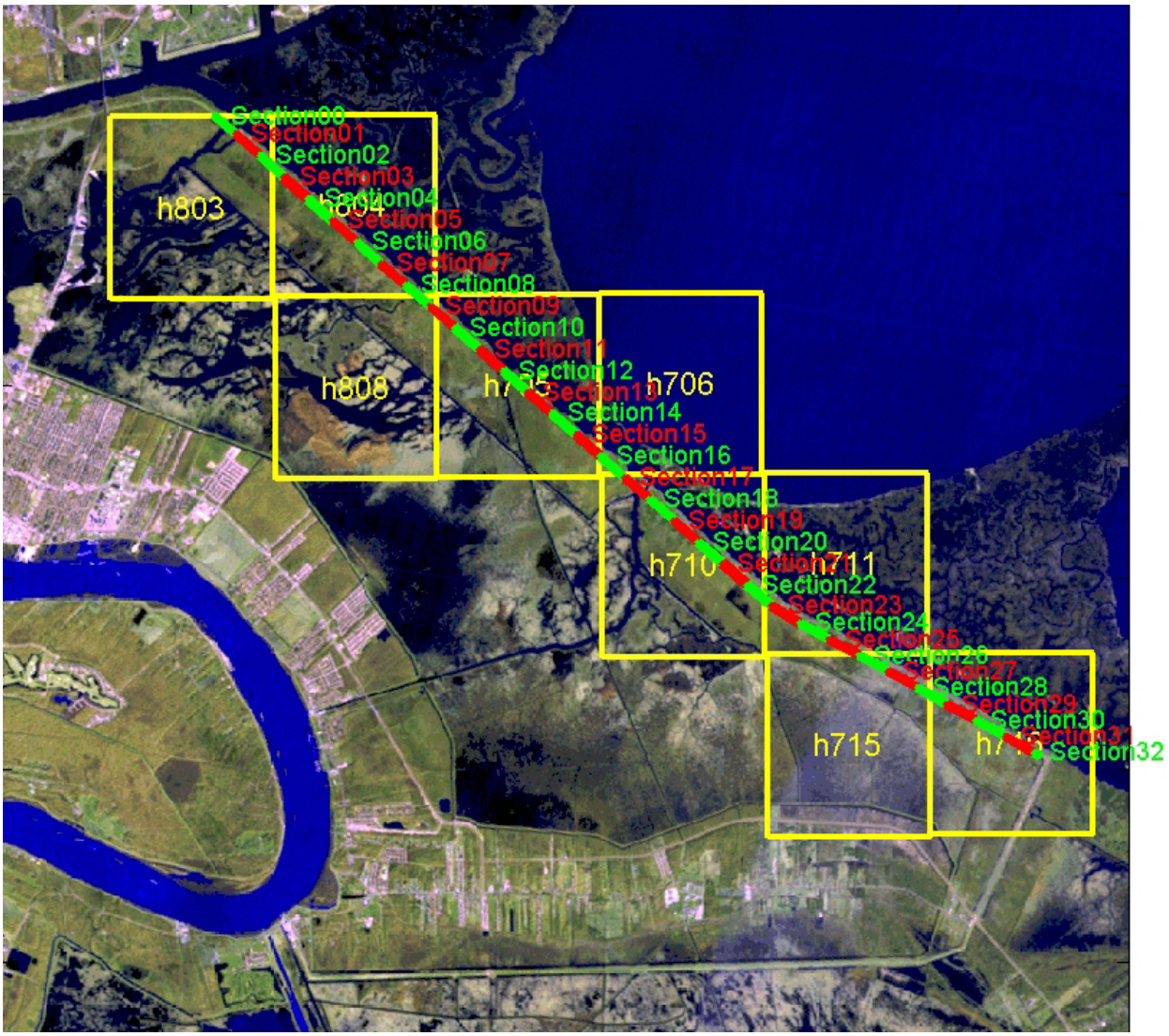

Levee Erosion Analysis for Section 17
20ft
15ft
10ft
5ft
Crest From Maximum
Crest from Poly-Fit
Volume Limits (Max)
Volume Limits (Poly-Fit)
Sheet Pile
Cross-Section Distance (ft)
80
60
40
20
0
Color corresponds to change in Levee Elevation
+5ft
0ft
-5ft
-10ft
-15ft
Pre-Storm Maximum
Pre-Storm Poly-Fit
Post-Storm Maximum
Post-Storm Poly-Fit
Elevation (ft)
20
15
10
5
Total Volume Change
Front Half Volume Change
Rear Half Volume Change
Volume Change ft3 from Max
500
0
-500
-1000
3.4
3.42
3.44
3.46
3.48
3.5
3.52
3.54
3.56
3.58
3.6
Approximate Distance Along Levee (ft)
x 10^4


Levee Erosion Analysis for Section 18
20ft
15ft
10ft
5ft
Crest From Maximum
Crest from Poly-Fit
Volume Limits (Max)
Volume Limits (Poly-Fit)
Cross-Section Distance (ft)
80
60
40
20
0
+5ft
0ft
-5ft
-10ft
-15ft
Color corresponds to change in Levee Elevation
Pre-Storm Maximum
Pre-Storm Poly-Fit
Post-Storm Maximum
Post-Storm Poly-Fit
Elevation (ft)
20
15
10
Total Volume Change
Front Half Volume Change
Rear Half Volume Change
Volume Change ft3 from Max
-200
-400
-600
3.6
3.62
3.64
3.66
3.68
3.7
3.72
3.74
3.76
3.78
3.8
Approximate Distance Along Levee (ft)
x 10^4

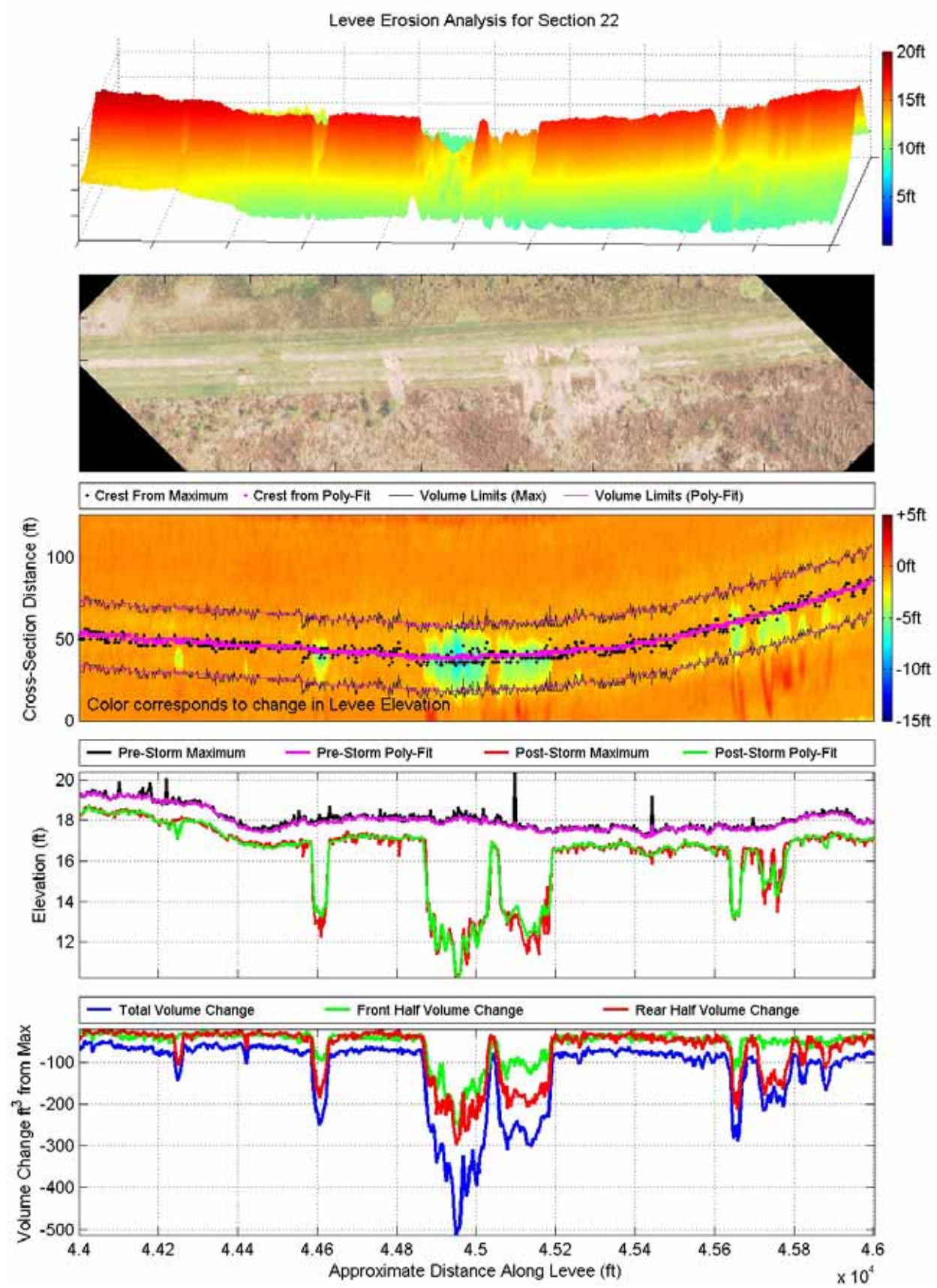

Levee Erosion Analysis for Section 19
20ft
15ft
10ft
5ft
Crest From Maximum
Crest from Poly-Fit
Volume Limits (Max)
Volume Limits (Poly-Fit)
Cross-Section Distance (ft)
100
80
60
40
20
0
+5ft
0ft
-5ft
-10ft
-15ft
Color corresponds to change in Levee Elevation
Pre-Storm Maximum
Pre-Storm Poly-Fit
Post-Storm Maximum
Post-Storm Poly-Fit
Elevation (ft)
20
15
10
Total Volume Change
Front Half Volume Change
Rear Half Volume Change
Volume Change ft3 from Max
-200
-400
-600
-800
3.8
3.82
3.84
3.86
3.88
3.9
3.92
3.94
3.96
3.98
4
Approximate Distance Along Levee (ft)
x 10^4

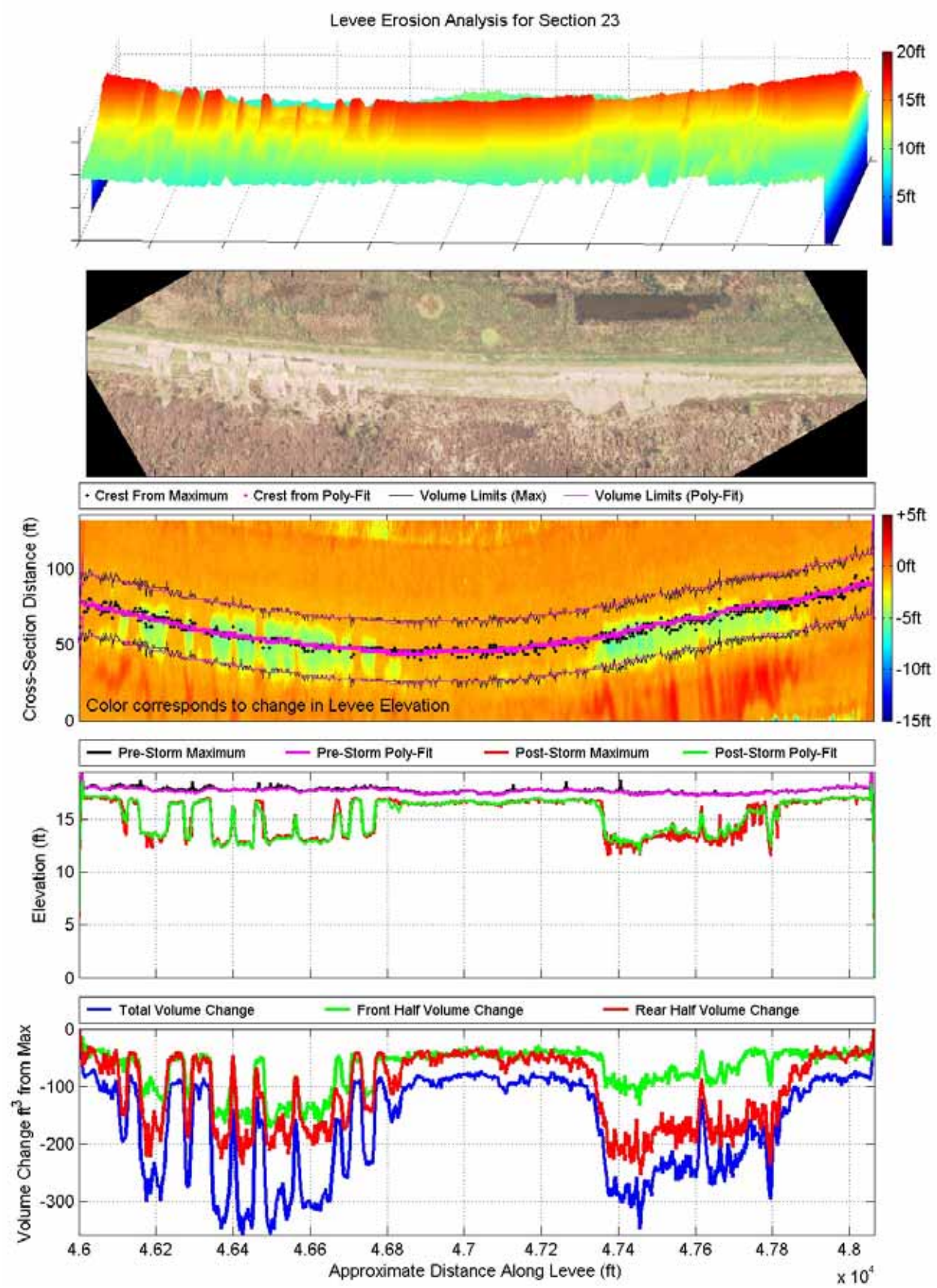

Levee Erosion Analysis for Section 20
20ft
15ft
10ft
5ft
Crest From Maximum
Crest from Poly-Fit
Volume Limits (Max)
Volume Limits (Poly-Fit)
Cross-Section Distance (ft)
100
80
60
40
20
0
+5ft
0ft
-5ft
-10ft
-15ft
Color corresponds to change in Levee Elevation
Pre-Storm Maximum
Pre-Storm Poly-Fit
Post-Storm Maximum
Post-Storm Poly-Fit
Elevation (ft)
20
15
10
Total Volume Change
Front Half Volume Change
Rear Half Volume Change
Volume Change ft3 from Max
-200
-400
-600
-800
4
4.02
4.04
4.06
4.08
4.1
4.12
4.14
4.16
4.18
4.2
Approximate Distance Along Levee (ft)
x 10^4

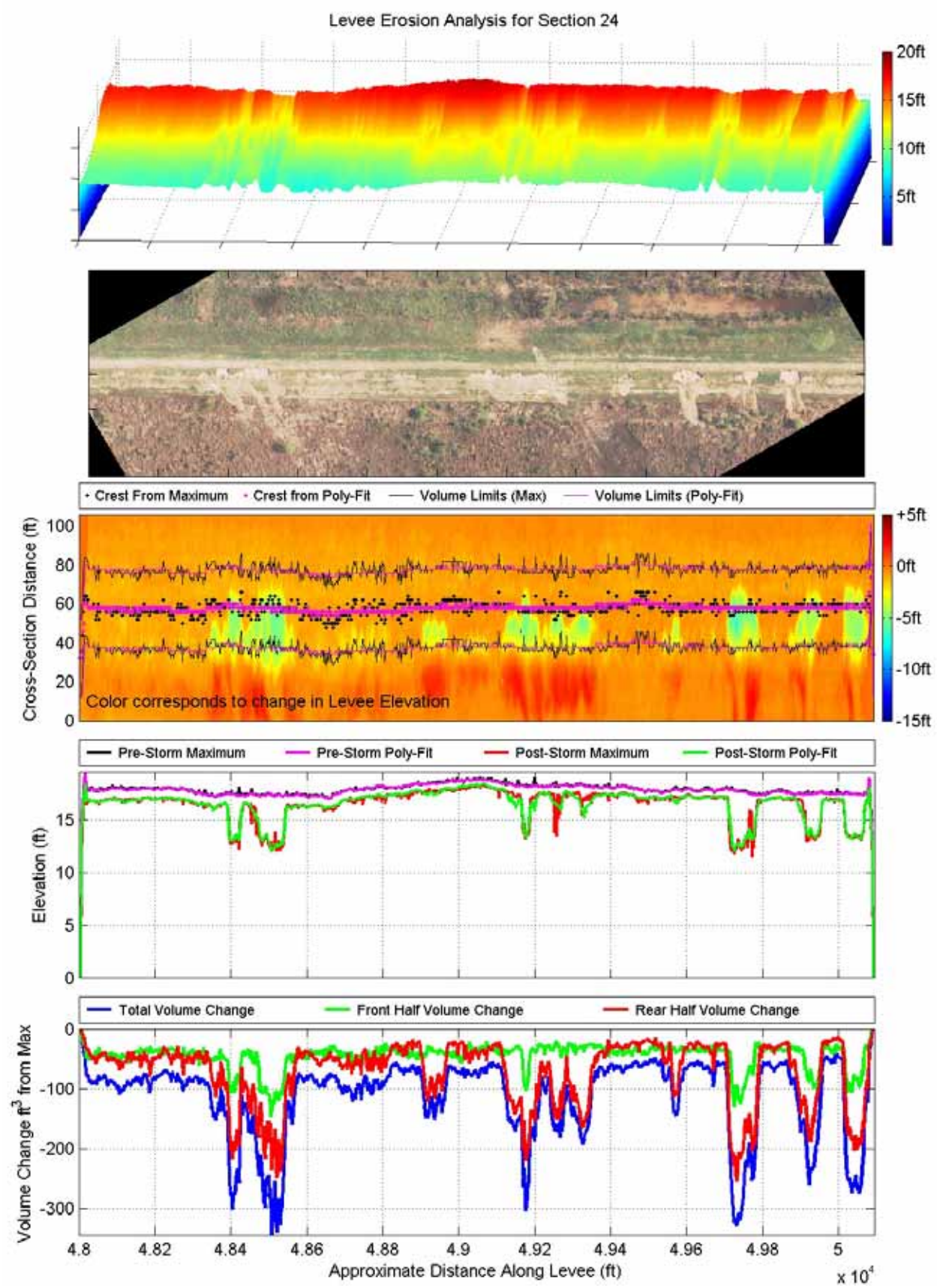

Levee Erosion Analysis for Section 21
20ft
15ft
10ft
5ft
Crest From Maximum
Crest from Poly-Fit
Volume Limits (Max)
Volume Limits (Poly-Fit)
Cross-Section Distance (ft)
80
60
40
20
0
+5ft
0ft
-5ft
-10ft
-15ft
Color corresponds to change in Levee Elevation
Pre-Storm Maximum
Pre-Storm Poly-Fit
Post-Storm Maximum
Post-Storm Poly-Fit
Elevation (ft)
18
16
14
12
10
8
Total Volume Change
Front Half Volume Change
Rear Half Volume Change
Volume Change ft3 from Max
-200
-400
-600
-800
4.2
4.22
4.24
4.26
4.28
4.3
4.32
4.34
4.36
4.38
4.4
Approximate Distance Along Levee (ft)
x 10^4

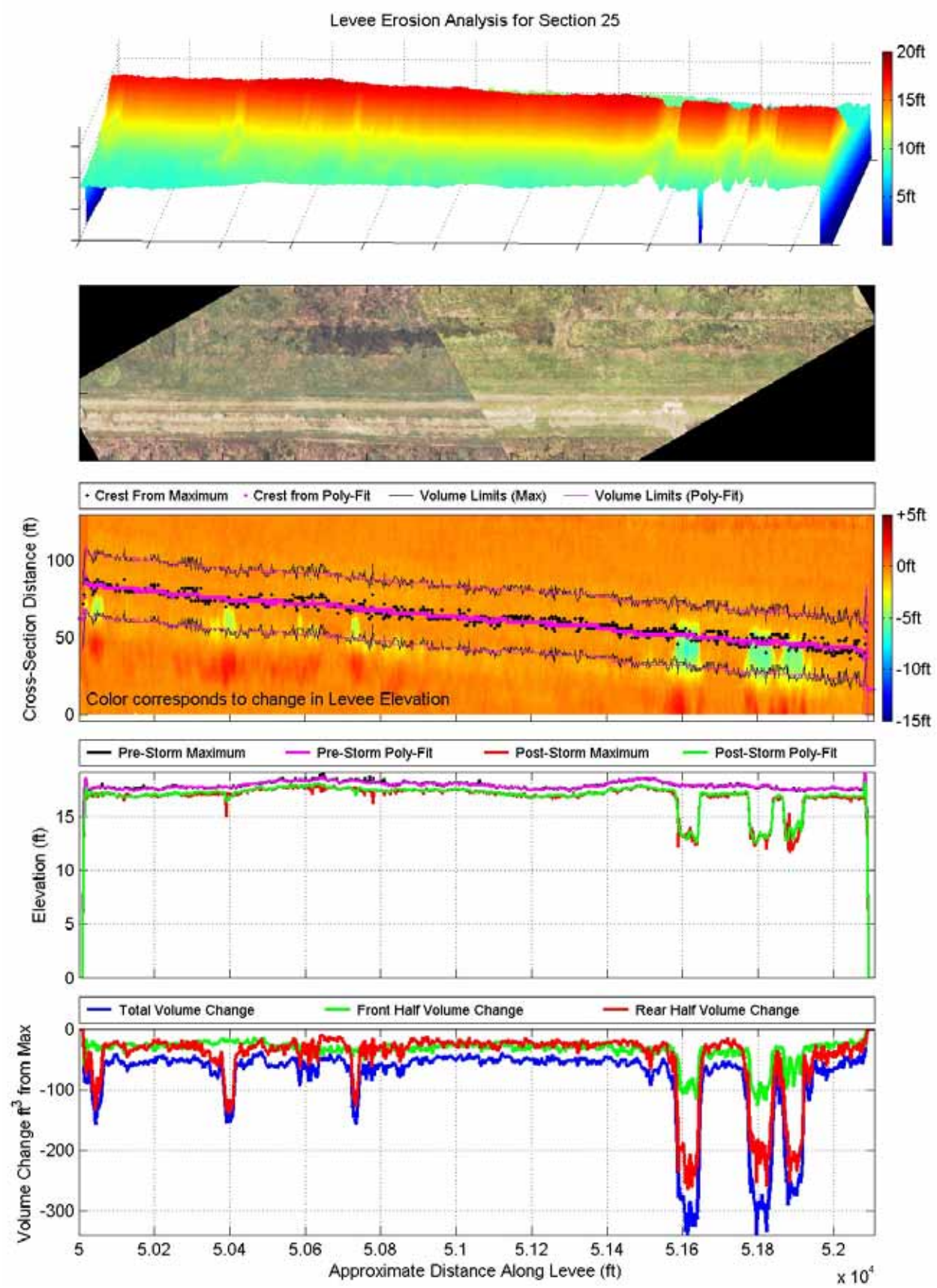


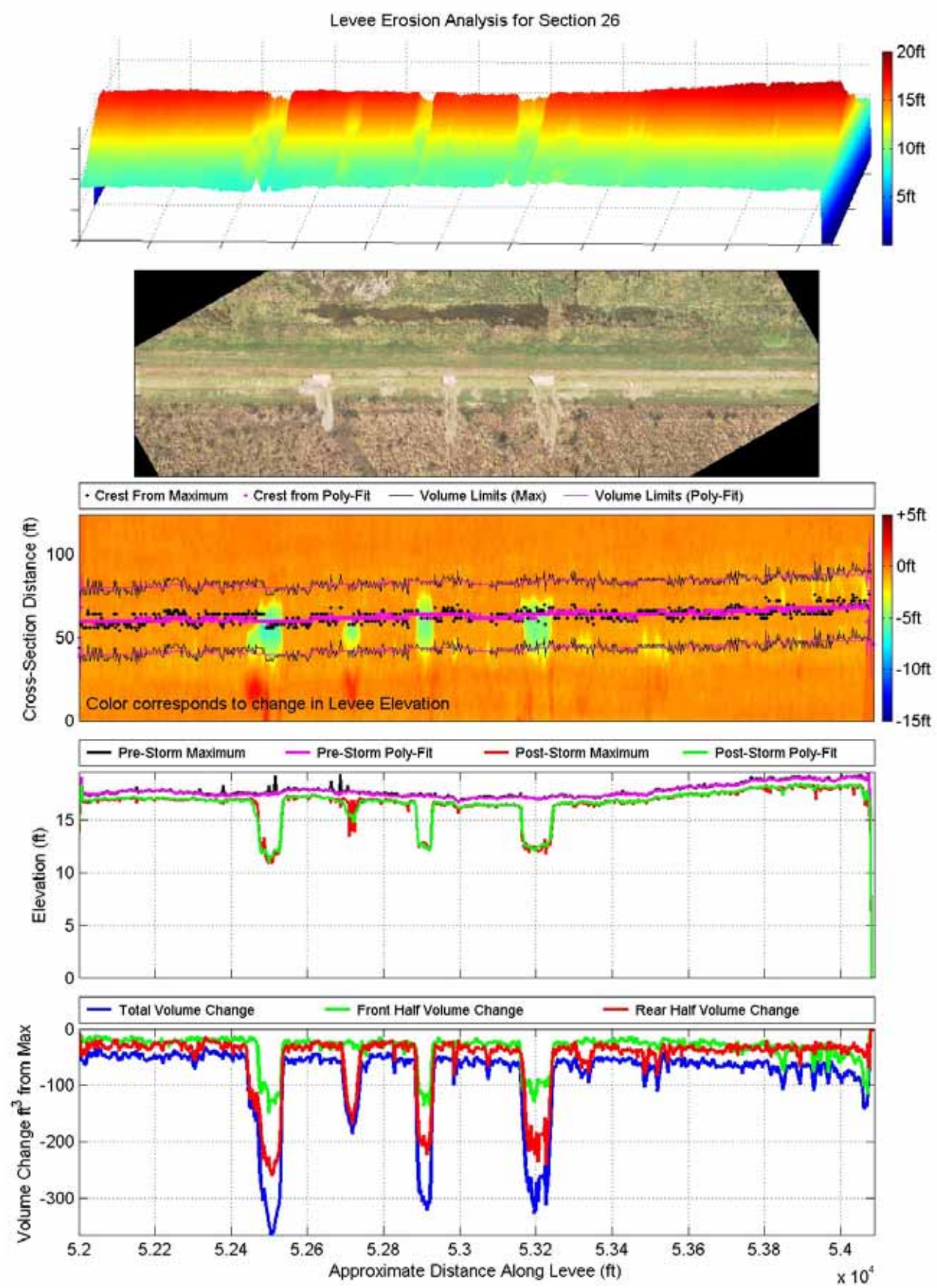
MRGO Levee sub-section locations.

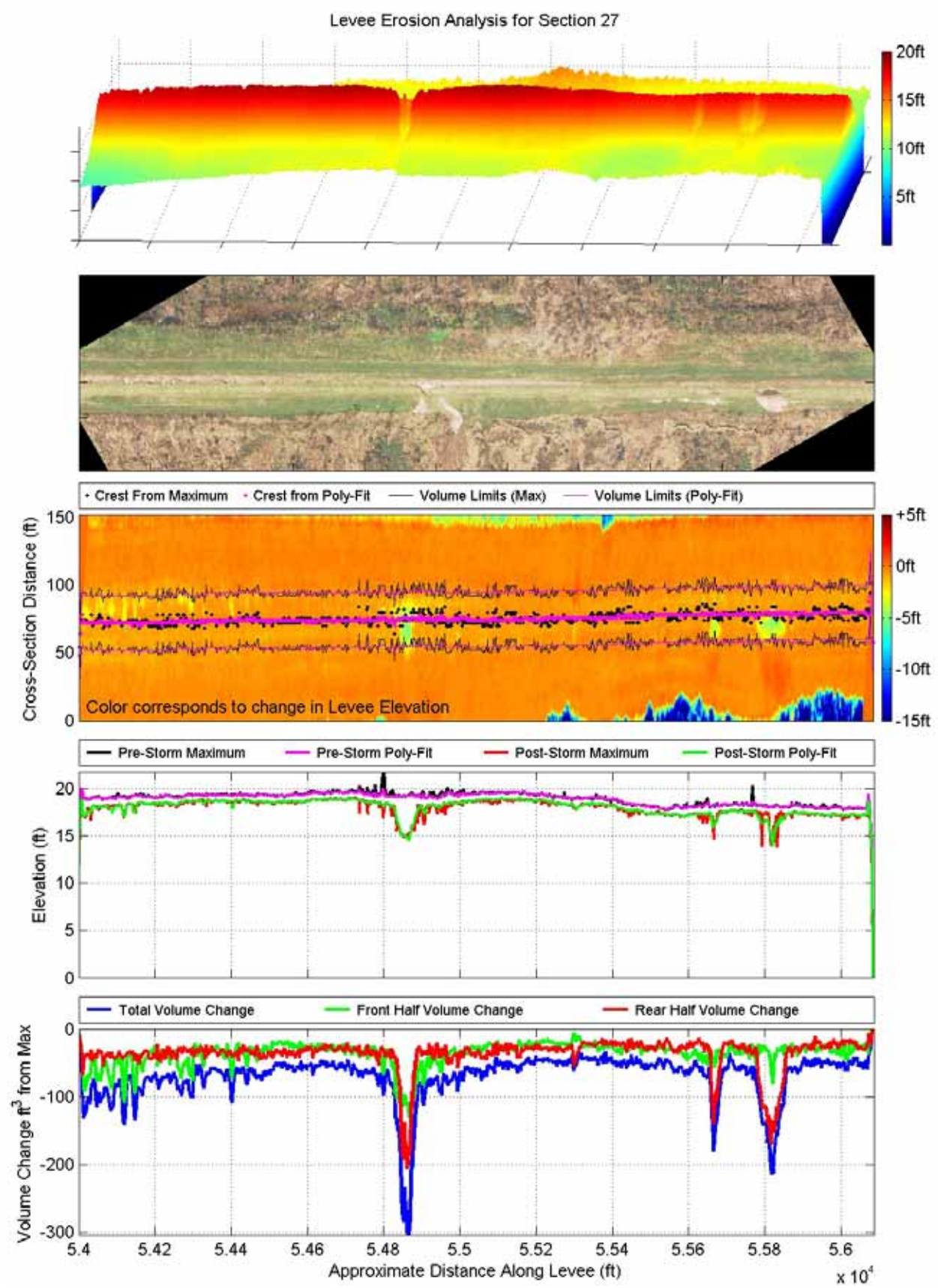

Levee Erosion Analysis for Section 22
20ft
15ft
10ft
5ft
Crest From Maximum
Crest from Poly-Fit
Volume Limits (Max)
Volume Limits (Poly-Fit)
Cross-Section Distance (ft)
100
50
0
+5ft
0ft
-5ft
-10ft
-15ft
Color corresponds to change in Levee Elevation
Pre-Storm Maximum
Pre-Storm Poly-Fit
Post-Storm Maximum
Post-Storm Poly-Fit
Elevation (ft)
20
18
16
14
12
Total Volume Change
Front Half Volume Change
Rear Half Volume Change
Volume Change ft3 from Max
-100
-200
-300
-400
-500
4.4
4.42
4.44
4.46
4.48
4.5
4.52
4.54
4.56
4.58
4.6
Approximate Distance Along Levee (ft)
x 10^4

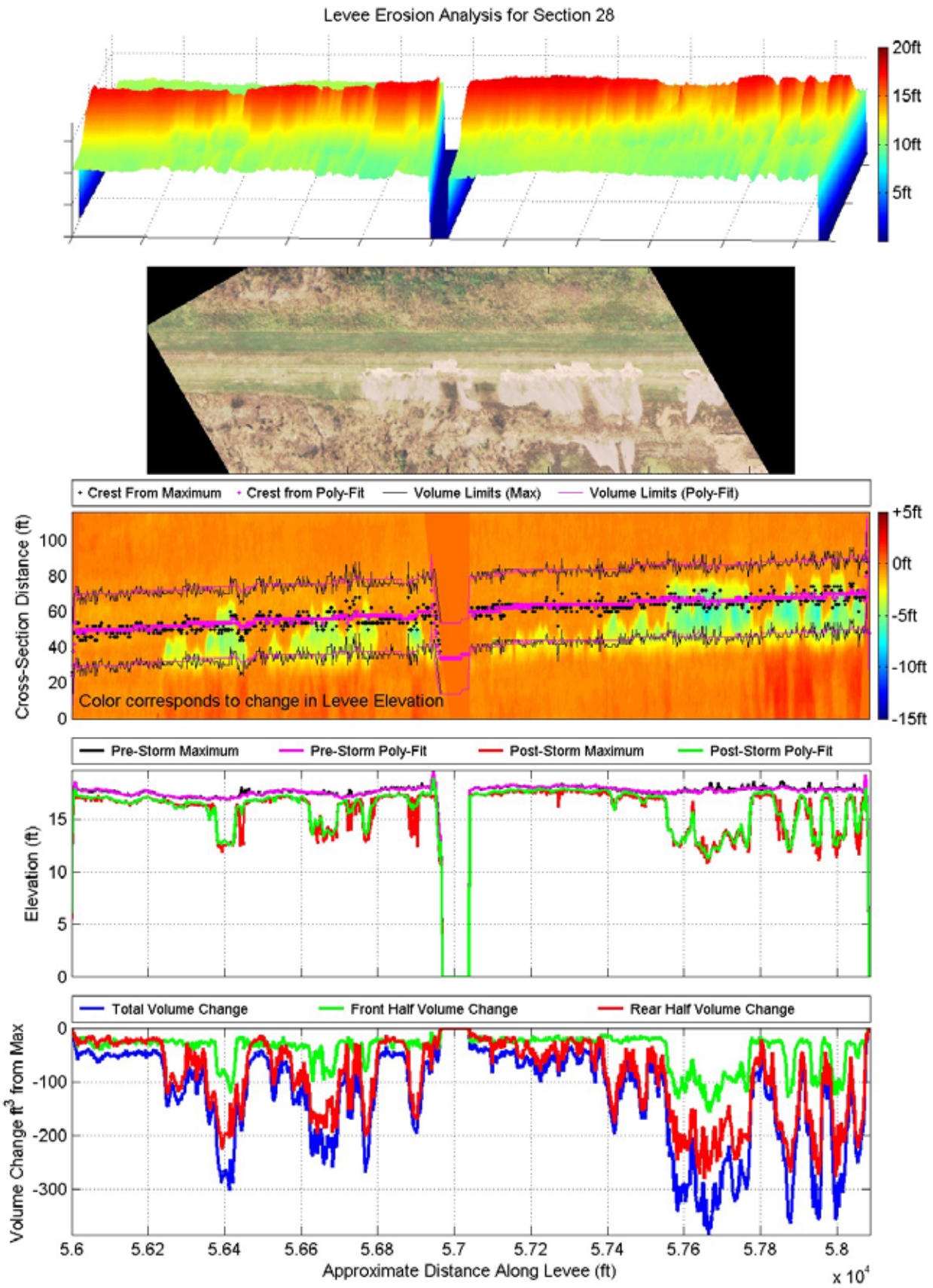

Levee Erosion Analysis for Section 23
20ft
15ft
10ft
5ft
Crest From Maximum
Crest from Poly-Fit
Volume Limits (Max)
Volume Limits (Poly-Fit)
Cross-Section Distance (ft)
100
50
0
+5ft
0ft
-5ft
-10ft
-15ft
Color corresponds to change in Levee Elevation
Pre-Storm Maximum
Pre-Storm Poly-Fit
Post-Storm Maximum
Post-Storm Poly-Fit
Elevation (ft)
15
10
5
0
Total Volume Change
Front Half Volume Change
Rear Half Volume Change
Volume Change ft3 from Max
0
-100
-200
-300
4.6
4.62
4.64
4.66
4.68
4.7
4.72
4.74
4.76
4.78
4.8
Approximate Distance Along Levee (ft)
x 10^4

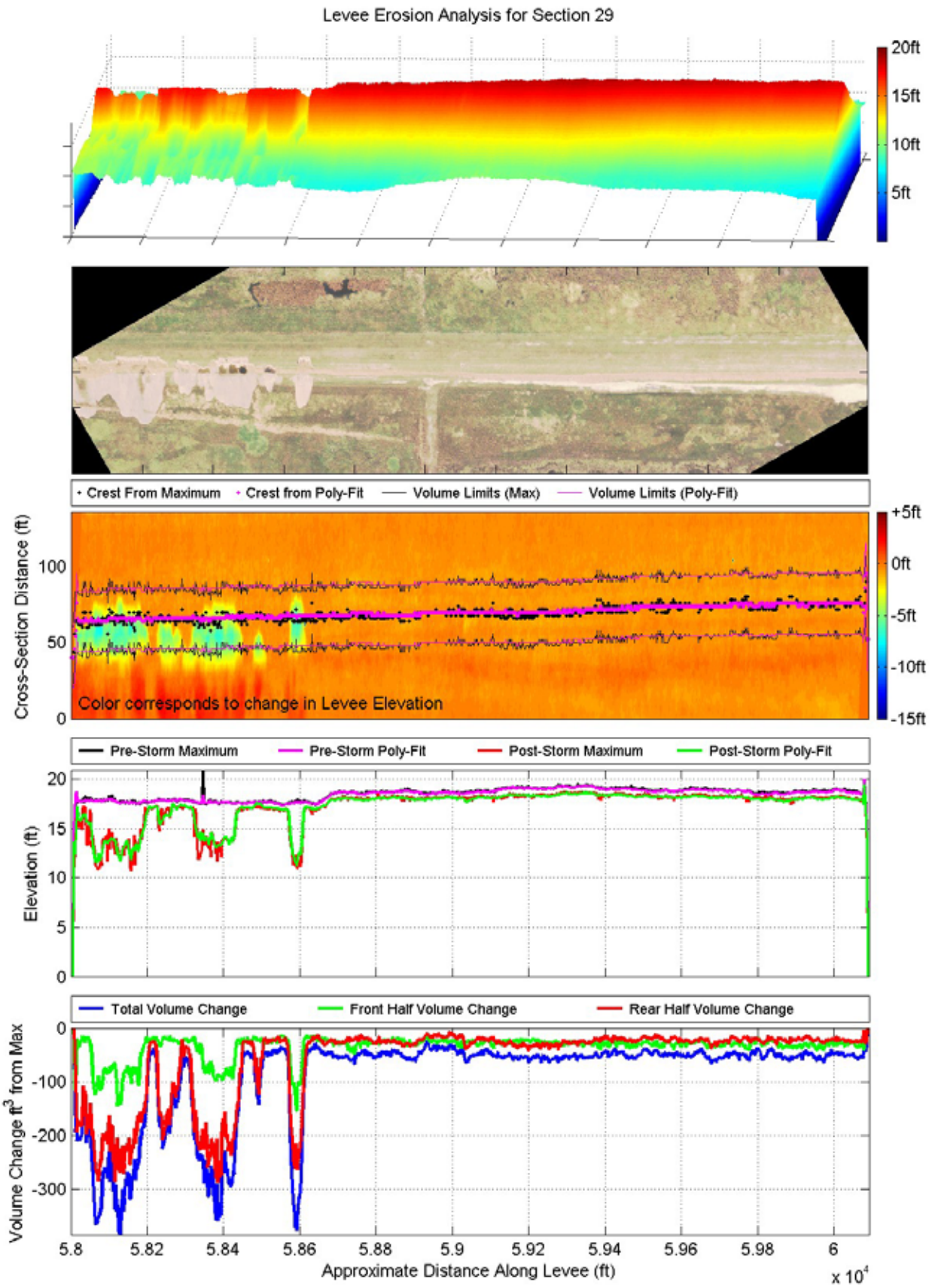

Levee Erosion Analysis for Section 24
20ft
15ft
10ft
5ft
Crest From Maximum
Crest from Poly-Fit
Volume Limits (Max)
Volume Limits (Poly-Fit)
Cross-Section Distance (ft)
100
80
60
40
20
0
+5ft
0ft
-5ft
-10ft
-15ft
Color corresponds to change in Levee Elevation
Pre-Storm Maximum
Pre-Storm Poly-Fit
Post-Storm Maximum
Post-Storm Poly-Fit
Elevation (ft)
15
10
5
0
Total Volume Change
Front Half Volume Change
Rear Half Volume Change
Volume Change ft3 from Max
0
-100
-200
-300
4.8
4.82
4.84
4.86
4.88
4.9
4.92
4.94
4.96
4.98
5
Approximate Distance Along Levee (ft)
x 10^4

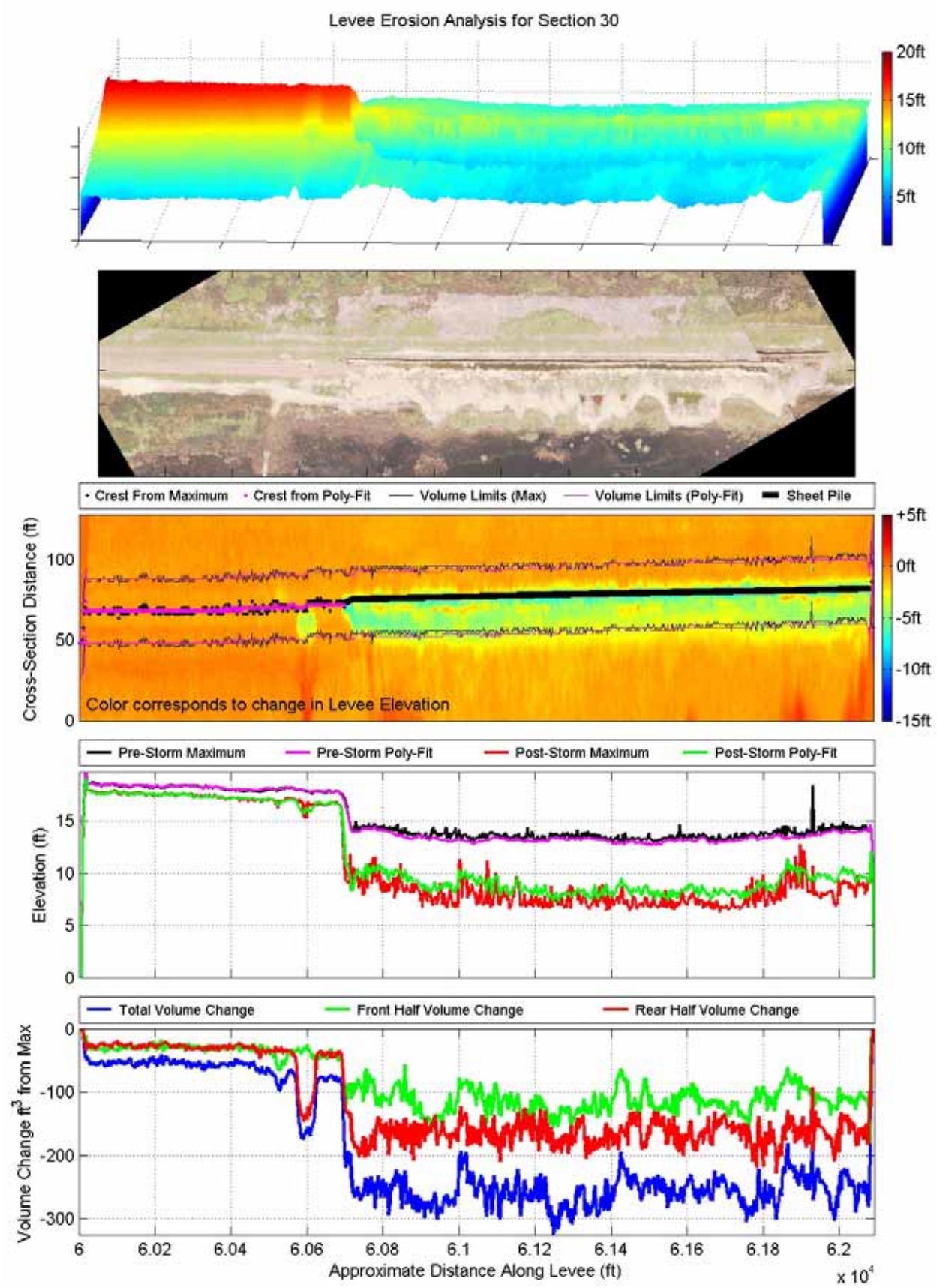

Levee Erosion Analysis for Section 25
20ft
15ft
10ft
5ft
Crest From Maximum
Crest from Poly-Fit
Volume Limits (Max)
Volume Limits (Poly-Fit)
Cross-Section Distance (ft)
100
50
0
Color corresponds to change in Levee Elevation
+5ft
0ft
-5ft
-10ft
-15ft
Pre-Storm Maximum
Pre-Storm Poly-Fit
Post-Storm Maximum
Post-Storm Poly-Fit
Elevation (ft)
15
10
5
0
Total Volume Change
Front Half Volume Change
Rear Half Volume Change
Volume Change ft3 from Max
0
-100
-200
-300
5
5.02
5.04
5.06
5.08
5.1
5.12
5.14
5.16
5.18
5.2
Approximate Distance Along Levee (ft)
x 10^4

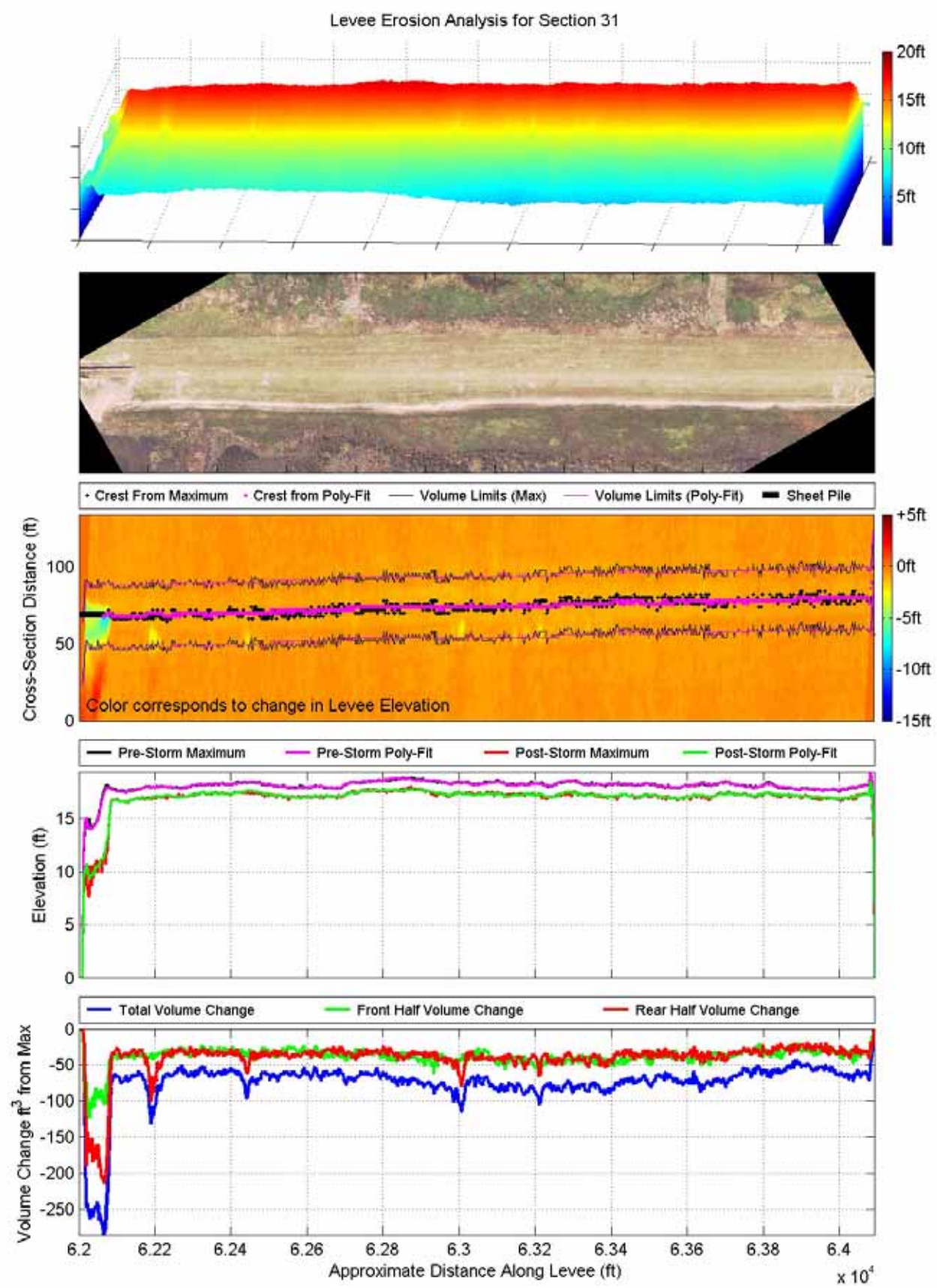

Levee Erosion Analysis for Section 26
20ft
15ft
10ft
5ft
Crest From Maximum
Crest from Poly-Fit
Volume Limits (Max)
Volume Limits (Poly-Fit)
Cross-Section Distance (ft)
100
50
0
Color corresponds to change in Levee Elevation
+5ft
0ft
-5ft
-10ft
-15ft
Pre-Storm Maximum
Pre-Storm Poly-Fit
Post-Storm Maximum
Post-Storm Poly-Fit
Elevation (ft)
15
10
5
0
Total Volume Change
Front Half Volume Change
Rear Half Volume Change
Volume Change ft3 from Max
0
-100
-200
-300
5.2
5.22
5.24
5.26
5.28
5.3
5.32
5.34
5.36
5.38
5.4
Approximate Distance Along Levee (ft)
x 10^4

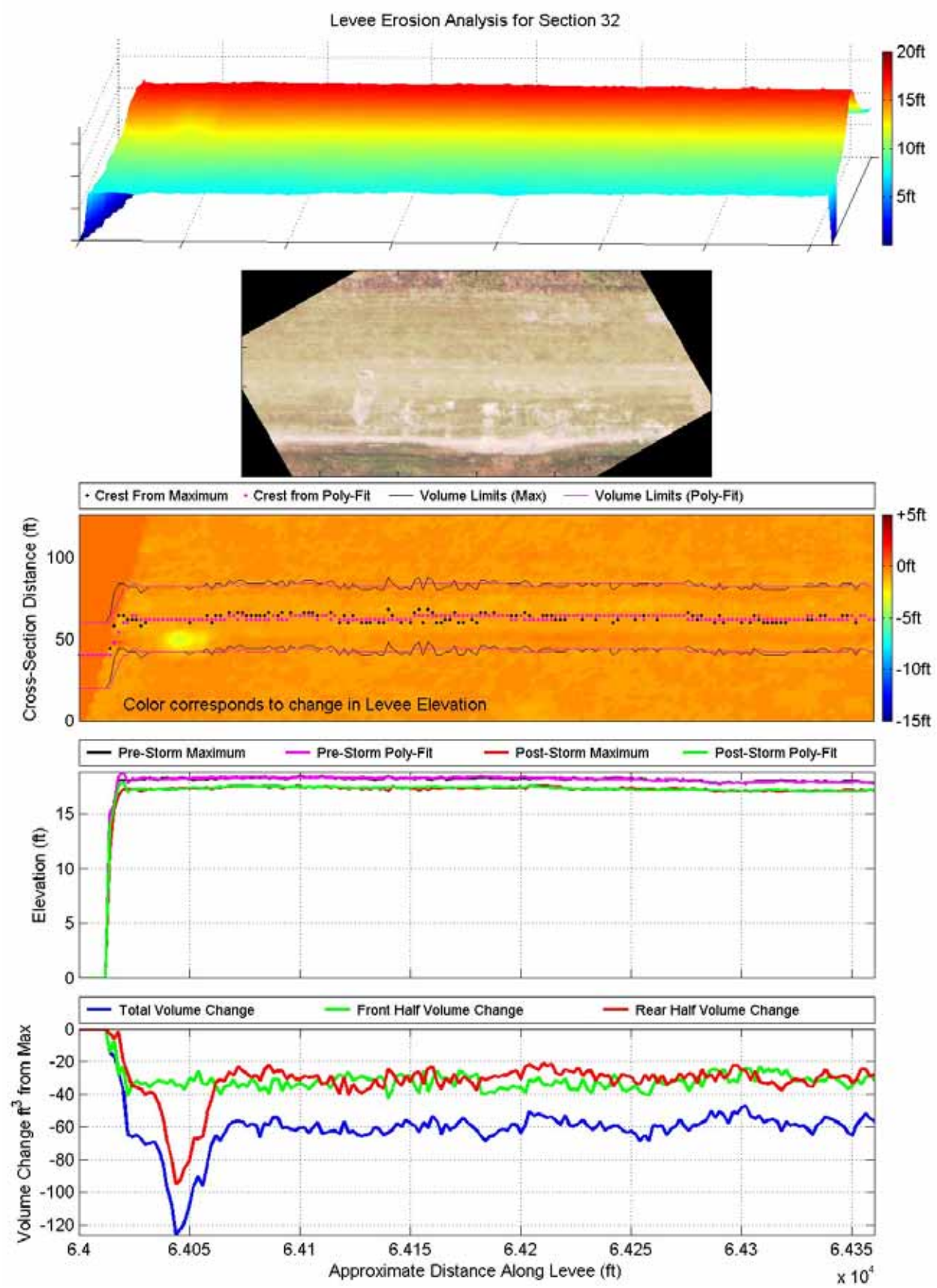

Levee Erosion Analysis for Section 27
20ft
15ft
10ft
5ft
Crest From Maximum
Crest from Poly-Fit
Volume Limits (Max)
Volume Limits (Poly-Fit)
Cross-Section Distance (ft)
150
100
50
0
Color corresponds to change in Levee Elevation
+5ft
0ft
-5ft
-10ft
-15ft
Pre-Storm Maximum
Pre-Storm Poly-Fit
Post-Storm Maximum
Post-Storm Poly-Fit
Elevation (ft)
20
15
10
5
0
Total Volume Change
Front Half Volume Change
Rear Half Volume Change
Volume Change ft3 from Max
0
-100
-200
-300
5.4
5.42
5.44
5.46
5.48
5.5
5.52
5.54
5.56
5.58
5.6
Approximate Distance Along Levee (ft)
x 10^4


Levee Erosion Analysis for Section 28
20ft
15ft
10ft
5ft
Crest From Maximum
Crest from Poly-Fit
Volume Limits (Max)
Volume Limits (Poly-Fit)
Cross-Section Distance (ft)
100
80
60
40
20
0
+5ft
0ft
-5ft
-10ft
-15ft
Color corresponds to change in Levee Elevation
Pre-Storm Maximum
Pre-Storm Poly-Fit
Post-Storm Maximum
Post-Storm Poly-Fit
Elevation (ft)
15
10
5
0
Total Volume Change
Front Half Volume Change
Rear Half Volume Change
Volume Change ft3 from Max
0
-100
-200
-300
5.6
5.62
5.64
5.66
5.68
5.7
5.72
5.74
5.76
5.78
5.8
Approximate Distance Along Levee (ft)
x 10^4


Levee Erosion Analysis for Section 29
20ft
15ft
10ft
5ft
Crest From Maximum
Crest from Poly-Fit
Volume Limits (Max)
Volume Limits (Poly-Fit)
Cross-Section Distance (ft)
100
50
0
+5ft
0ft
-5ft
-10ft
-15ft
Color corresponds to change in Levee Elevation
Pre-Storm Maximum
Pre-Storm Poly-Fit
Post-Storm Maximum
Post-Storm Poly-Fit
Elevation (ft)
20
15
10
5
0
Total Volume Change
Front Half Volume Change
Rear Half Volume Change
Volume Change ft3 from Max
0
-100
-200
-300
5.8
5.82
5.84
5.86
5.88
5.9
5.92
5.94
5.96
5.98
6
Approximate Distance Along Levee (ft)
x 10^4


Levee Erosion Analysis for Section 30
20ft
15ft
10ft
5ft
Crest From Maximum
Crest from Poly-Fit
Volume Limits (Max)
Volume Limits (Poly-Fit)
Sheet Pile
Cross-Section Distance (ft)
100
50
0
+5ft
0ft
-5ft
-10ft
-15ft
Color corresponds to change in Levee Elevation
Pre-Storm Maximum
Pre-Storm Poly-Fit
Post-Storm Maximum
Post-Storm Poly-Fit
Elevation (ft)
15
10
5
0
Total Volume Change
Front Half Volume Change
Rear Half Volume Change
Volume Change ft3 from Max
0
-100
-200
-300
6
6.02
6.04
6.06
6.08
6.1
6.12
6.14
6.16
6.18
6.2
Approximate Distance Along Levee (ft)
x 10^4


Levee Erosion Analysis for Section 31
20ft
15ft
10ft
5ft
Crest From Maximum
Crest from Poly-Fit
Volume Limits (Max)
Volume Limits (Poly-Fit)
Sheet Pile
Cross-Section Distance (ft)
100
50
0
Color corresponds to change in Levee Elevation
+5ft
0ft
-5ft
-10ft
-15ft
Pre-Storm Maximum
Pre-Storm Poly-Fit
Post-Storm Maximum
Post-Storm Poly-Fit
Elevation (ft)
15
10
5
0
Total Volume Change
Front Half Volume Change
Rear Half Volume Change
Volume Change ft3 from Max
0
-50
-100
-150
-200
-250
6.2
6.22
6.24
6.26
6.28
6.3
6.32
6.34
6.36
6.38
6.4
Approximate Distance Along Levee (ft)
x 10^4


Levee Erosion Analysis for Section 32
20ft
15ft
10ft
5ft
Crest From Maximum
Crest from Poly-Fit
Volume Limits (Max)
Volume Limits (Poly-Fit)
Cross-Section Distance (ft)
100
50
0
Color corresponds to change in Levee Elevation
+5ft
0ft
-5ft
-10ft
-15ft
Pre-Storm Maximum
Pre-Storm Poly-Fit
Post-Storm Maximum
Post-Storm Poly-Fit
Elevation (ft)
15
10
5
0
Total Volume Change
Front Half Volume Change
Rear Half Volume Change
Volume Change ft3 from Max
0
-20
-40
-60
-80
-100
-120
6.4
6.405
6.41
6.415
6.42
6.425
6.43
6.435
Approximate Distance Along Levee (ft)
x 10^4

APPENDIX D: Review of Levee Erosion Modeling Described in Declaration and Technical Reports by Robert Bea

The approach used by Robert Bea to model levee erosion on the front side has three primary components: 1) a method to compute shear stresses (or shear velocities derived from stresses) which act on the levee surface, i.e., the forcing; 2) a grass turf lift-off model which triggers erosion of levee sediments; and 3) computation of erosion using results from flume tests that involved unidirectional, steady flow conditions. The methods used for components 1) and 2) differ on the front and back sides of the levee. For the front side, Bea uses the LS-DYNA model to calculate shear velocities, and the grass lift-off model is related to the wave height. For the back-side, Bea uses an empirical method to calculate velocity and uses the velocity in the grass turf lift-off model.

Bea uses a number of computation methods, technical assumptions, and model inputs that are not justified or supported well with technical analysis or data; his approach does not properly treat a number of important physical processes that acted to erode the levee. The modeling approach was not properly validated with any independent levee response data set, or sets. It is unclear whether or not this modeling approach has ever been applied before to examine levee erosion under loading by hurricane surge and waves; and if it was, how successful was it in predicting erosion and observed levee response? In light of these technical deficiencies and an apparent lack of rigorous validation, results from Bea's erosion modeling are of questionable accuracy and are highly uncertain. Key technical deficiencies and limitations inherent to his modeling approach are discussed below.

Velocity Forcing

1) The LS-DYNA model is used to simulate surf zone wave transformation, breaking, run-up and overtopping at a levee that is subjected to extreme hurricane waves and water level conditions. Other models that simulate the same processes, and have a more extensive experience base, are applied in the coastal engineering profession and are available. The LS-DYNA model has not, to my knowledge, been successfully applied to simulate wave breaking in the surf zone, and run-up and overtopping of a sloping coastal levee or structure.

2) The LS-DYNA model is used to compute shear velocity. It is unclear if the LS-DYNA model has ever been validated for velocity profile predictions, or bottom velocity predictions, in the surf zone or in the overtopping zone. It is unclear if the LS-DYNA model has ever been validated in terms of water surface elevation variability in the surf zone. The velocity results often show considerable irregularity in peak velocity amplitude (see Figures 58 and 61, for example, in Bea 2008a), much more variability

than would be expected for the monochromatic waves (each wave has the same wave height) that are inputted to the model. Reasons for the variability in current speed are unclear. Rigorous validation should be done to examine model skill in predicting the hydrodynamic variables that are used in the erosion modeling, namely, velocity. There are many field and laboratory velocity data sets with which model accuracy can be evaluated. The COULWAVE model applied by the IPET has been validated against data sets of this type. The LS-DYNA model has never, to my knowledge, ever been validated to any of these data sets (laboratory and field).

3) Bea does not explain how time-averaged shear velocities are calculated with LS-DYNA. Is shear stress computed using the vertical velocity distribution calculated in the model? And if so how? The modeling description suggests that model resolution is 1.3 ft. This degree of vertical resolution is inadequate for accurately computing the vertical velocity profile for the wave and water level conditions considered (from which shear stress is presumably estimated). Or, is bottom velocity used to calculate shear stress using some other method? Has this method been validated? How has bottom roughness and bottom frictional influence of grass on flow been represented in the LS-DYNA modeling and in use of EFA flume results? How is shear stress and shear velocity computed in the EFA erosion flume? Is shear stress computed using the vertical velocity distribution calculated in the flume? And if so how? The method for doing so is not clear.

4) The bottom boundary layer for unsteady oscillatory flow on a grass-covered levee in the field under storm loadings is much different than the bottom boundary layer created by unidirectional steady flow in the narrow confines of the EFA erosion flume. Bea does not explain how the EFA velocities and shear stresses were computed and modified to reflect these differences, for use with the shear velocities computed using the LS-DYNA model.

5) Bea uses a monochromatic treatment of the incident waves, which assumes each incident wave has the same height and period. This is an unrealistic treatment of the irregular sea state experienced during hurricanes. Natural waves are highly irregular, in height and period. The velocity distribution created by irregular waves is quite different from that created by monochromatic waves. Use of this overly simplified method can lead to inaccurate estimates of the velocity regime and it introduces great uncertainty into the erosion modeling. Laboratory experiments involving erosion of sand beaches show that beach response for monochromatic wave incidence is dramatically different from beach erosion response for irregular, more natural incident wave conditions. The use of monochromatic waves in coastal processes modeling reflects an outdated technical approach, and introduces another source of considerable uncertainty into the modeling. How was the monochromatic wave height adjusted to accurately represent the actual energy contained in the directional spectrum computed with the SWAN model?

6) Computations of overtopping are unrealistically low. For example, values listed in Table 3 on page 48 of (Bea 2008a) show overtopping rates of only 0.2 cfs/ft for

conditions where the mean water surface is above the levee crest. Were these overtopping rates computed with the LS-DYNA model?

Lift-Off of Grass Turf

7) Erosion of grass must be a function of the sediment properties in which the grass is growing. Sediment must be eroded to enable grass to be removed from the levee surface. The erodability of the sediment used in Bea's grass lift-off model appears to be much less than the erodability of the underlying sediments using in the erosion modeling. This is an inconsistency.

8) Bea cites the grass lift-off model of Verheij et al (1997) and the work by Hewlett et al (1987) as the sources for development of his grass lift-off models. It is unclear what technical analysis was done to develop the Bea curves from the Hewlett curves and from the curves of Verheij et al? How subjective was this process, or is it founded in solid technical analysis. For example, the "quasi-steady" velocity required to lift off the turf in 1 hour from Bea's curve (Figure 69 in Bea 2008b) is 11, 18, and 33 ft/sec for poor, normal, and good turf, respectively. The results from Hewlett (Figure 68 in Bea 2008b) suggest 10, 12, and 15 ft/sec for poor, average, and good grass cover, i.e., much lower thresholds for normal and good grass cover. Bea does not explain these large differences.

Levee Erosion

9) Erodability at a time step is determined by using the time-averaged shear velocities, computed using LS-DYNA results, along with the relationship between gross-erosion rates and shear velocity (or shear stress) derived from EFA flume testing. Velocities in the surf zone vary significantly with the passage of each wave; the highest and most erosive velocities are associated with the passage of each wave crest. Data from the EFA flume tests indicate that vertical erosion rate is non-linearly related to shear velocity. In light of this nonlinear dependence, Bea's use of a time-averaged wave-induced shear velocity is unlikely to yield a correct erosion result. Assuming erosion is related to velocity cubed, it can be shown that when integrated in time over a wave period, the average of velocity-cubed is quite different than the cube of the average velocity. It is unclear how Bea addresses this important issue in his modeling.

10) Prediction of erosion extent (E) is related to the summation, or integration (through time), of erodability at a time step multiplied by the value of the time step (equation on pg 109 of Bea 2008b). In this equation, Bea relates horizontal or lateral erosion, or extent of erosion, directly to vertical erosion. Vertical erosion can only be directly related to horizontal erosion if the levee profile is assumed to retain its shape during the erosion process, and it simply translates horizontally throughout the process. How Bea relates vertical erosion to horizontal extent of erosion is unclear. It is unclear whether or not Bea accounts for changing levee cross-section throughout the levee degradation process; and, if so, how it's done. Realistic levee degradation modeling can not be done without

properly considering how the profile shape and the hydrodynamic loadings vary spatially and with time and interact with each other. Conceptually, Bea grossly oversimplifies the erosion and levee response processes, neglecting important processes. Realistic modeling must account for both bed load and suspended load modes of sediment transport, and the potential for sediment deposition, in addition to the process of erodability which is the only process accounted for in the EFA flume tests. These omissions in Bea's modeling cast serious doubt on the technical rigor and accuracy of the approach that he takes, and on the quality of his results.

11) To characterize erodability, Bea uses relationships between imposed shear velocity, or shear stress, and vertical gross-erosion rate for samples, S-4 (the extreme under-compacted sample), S-5 (the extreme under-compacted sample), and S-3 (relatively undisturbed core sample), from EFA flume tests. The relationships Bea used are shown in Figures 42 to 44 of Bea 2008a. Each sample was tested in the EFA erosion flume by the ILIT. Deficiencies of the EFA flume for simulating the actual hydrodynamic regimes that existed on either the front or back side of the levee are addressed in the main body of this expert report. Problems and limitations with the sample processing, testing performed by the ILIT on samples S-4 and S-5, and usefulness of results from those samples also are thoroughly discussed in the main text of this report. Results from the extreme low compaction S-4 and S-5 samples are of little to no use; it is likely that they grossly overestimate and over-exaggerate erodability of the intact, in-situ sediments at those two locations. Bea provides no quantitative evidence that the density of the under-compacted samples at S-4 and S-5 in any way accurately represented the density of the intact in-situ sediments at those two sites. Because it can not be shown, the ILIT authors recommended bounding any analysis using results for <u>both</u> extreme under- and over-compacted samples. Bea ignored this recommendation and only uses results for the extreme under-compacted S-4 sample, despite the availability of the extreme over-compacted S-4 sample results. By not using the high-compaction S-4 sample results, Bea biases his modeling towards an extreme over-prediction of erodability. For S-5, the only sample analyzed was extremely under-compacted, which also will bias results at this site. Sample S-3 was the only one that was acquired relatively intact during sampling, through use of sediment coring. Bea makes deterministic model calculations using results from the extreme under-compacted samples, despite the great variability in the erodability for the two extreme states of compaction. For example, at a shear velocity of 1 m/sec, the erodability for the extreme low and high states of compaction for Sample S-4 vary by more than 5 orders of magnitude, i.e., a factor of 100,000, and even more so for higher velocities. Bea provides no technical justification, backed up by analysis, for his decision to use only the extreme under-compacted samples in his erosion modeling.

12) To compensate for the erroneously high erosion rates associated with use of the severely under-compacted samples S-4 and S-5, Bea imposes an arbitrary upper bound on the relationship between erosion rate and shear velocity. The arbitrary caps are shown in Figures 45 to 47 of Bea (2008a). The choice of velocity at which to impose the cap for each sample differs (0.7 ft/sec for sample S-4, 1 m/sec for sample S-5, and greater than 5 m/sec for Sample S-3). Bea states that the rate was capped at a value twice the maximum EFA test result value. However, for the high erodability materials, he uses a cap value

that is more than a factor of 10 higher than the last test result, completely inconsistent with the other two samples. Bea states that the erodability ceiling is imposed because the water has a maximum sediment carrying capacity. However, there is no technical justification, or data analysis provided that supports this claim. The use of an arbitrary cap on erodability is a key assumption in the erosion modeling. Erosion model results are completely dependent upon the choice for this cap value, because it is imposed at such a low velocity. This renders the erosion modeling results highly suspect and uncertain.

14) The sediments analyzed by ILIT were all acquired at the surface, mostly within the upper 1 to 2 ft. Levees were degraded by amounts of up to 10 ft or more. Density of mixed sediments usually varies considerably with depth below the surface (more erodable near the surface and less erodable with increasing depth). Use of surface samples can bias results toward over-prediction of erosion. This is great source of uncertainty in any attempt to model levee erosion and degradation. This issue is not addressed at all by Bea.

References

Bea, R., 2008. "Declaration No. 1 – Engineering Forensic Studies of Performance of the Man-Made Features Bordering the Reach 2 of the Mississippi River-Gulf Outlet (MR-GO) During Hurricane Katrina," July 11, 2008.

Bea, R. and Storesund, R., 2008. "Technical Report No. 1 – Analysis of Breaching of MR-GO Reach 2 EBSBs During Hurricane Katrina & The 'Neutral' MR-GO Hurricane Katrina Conditions," July 11, 2008.

Bunya, S., Westerink, J., Dietrich, J.C., Westerink, H.J., Westerink, L.G., Atkinson, J., Ebersole, B., Smith, J.M., Resio, D., Jensen, R., Cialone, M.A., Luettich, R., Dawson, C., Roberts, H.J., and Ratcliff, J. 2008. A High Resolution Coupled Riverine Flow, Tide, Wind, Wind Wave and Storm Surge Model for Southern Louisiana and Mississippi: Part I – Model Development and Validation. *Submitted to* National Weather Review.

CivilTech Engineering, 2008. "Expert Opinion Report – Analysis of Flooding of the Lower Ninth Ward and St. Bernard Parish Hurricane Katrina August 2005 New Orleans, Louisiana," June 27, 2008. Prepared for Ingram Barge PSLC.

Dietrich, J.C., Bunya, S., Westerink, J.J., Ebersole, B.A., Smith, J.M., Atkinson, J.H., Jensen, R., Resio, D.T., Luettich, R.A., Dawson, C., Cardone, V.J., Cox, A.T., Powell, M.D., Westerink, H.J., and Roberts, H.J. 2008. A High-Resolution Coupled Riverine Flow, Tide, Wind, Wind Wave and Storm Surge Model for Southern Louisiana and Mississippi: Part II - Synoptic Description and Analysis of Hurricanes Katrina and Rita. *Submitted to* National Weather Review.

EM-1110-2-1100, U.S. Army Corps of Engineers, 2002. Coastal Engineering Manual, Washington, D.C. (in 6 volumes)

Eurotop 2007. "Wave Overtopping of Sea Defences and Related Structures: Assessment Manual," August 2007. http://www.overtopping-manual.com/EurOtop.pdf

Hewlett, H.W.M., Boorman, L.A., and Bramley, M.E., 1987. Design of Reinforced Grass Waterways, Construction Industry Research and Information Association (CIRIA)

Interagency Performance Evaluation Task Force, 2006. "Performance Evaluation of the New Orleans and Southeast Louisiana Hurricane Protection System, Volume IV, The Storm." (https://ipet.wes.army.mil/)

Interagency Performance Evaluation Task Force, 2007. "Performance Evaluation of the New Orleans and Southeast Louisiana Hurricane Protection System, Volume V, The Performance – Levees and Floodwalls." (https://ipet.wes.army.mil/)

Independent Levee Investigation Team, 2006, "New Orleans Systems, Hurricane Katrina, 2005, Chapter Nine: Erosion Tests on New Orleans Levee Samples." May 26, 2006.

Kok M., Aalberts M., Maaskant B., and de Wit, L., “Polder Flood Simulations for Greater New Orleans, Hurricane Katrina August 2005,” July 30, 2007.

Kok M., Aalberts M., Maaskant B., and de Wit, L., “Polder Flood Simulations for Greater New Orleans: the neutral MRGO scenario,” July 9, 2008.

Lick, W., Lijun, L., and Gailani, J. “Initiation of Movement of Quartz Particles” ASCE Journal of Hydraulic Engineering, August 2004, pp 755-761.

Seijffert, J.W., Verheij, H., Grass covers and reinforcement measures, Dike and revetments; design, maintenance and safety assessment. Edited by K.W. Pilarczyk, RWS-DWW, 1998.

TAW 1989, Guidelines for Design of River Dikes, Part 2 – Lower River Area, Technical Advisory Committee on Flood Defence, the Netherlands, Sep 1989.

TAW 2002, Technical Report: Wave Run-up and Wave Overtopping at Dikes, Technical Advisory Committee on Flood Defence, The Netherlands, May 2002.

URS Corporation. 2006. “Final Report – The Direct Impact of the MRGO on Hurricane Storm Surge,” February 2006, Prepared for the State of Louisiana, Department of Natural Resources.

de Wit, L., Maaskant B., Kok M., and Vrjiling, J.K., “Flow Modeling New Orleans – Mississippi River Gulf Outlet Hurricane Katrina August 2005: Final Report, Scenario 1, 2A, 2B, 2C, 2D, 3,” June 2008.

Curriculum Vitae

Education

University of Delaware, M.C.E., Civil Engineering, 1979
Specialization in Coastal Engineering, Formal coursework and training in: wave theory, coastal hydrodynamics and surf zone dynamics, modeling simulation techniques, geophysical fluid dynamics, hydromechanics, hydraulic engineering, ocean engineering, shoreline response and coastal engineering structures, littoral processes, physical oceanography. Research and thesis on numerical modeling of surf zone circulation and rip current generation.

University of Delaware, B.S.C.E., Civil Engineering, 1977

Professional Experience

2004-present
Chief, Flood & Storm Protection Division, Coastal and Hydraulics Laboratory, U.S. Army Engineer Research and Development Center, Vicksburg, MS. Responsible for basic and applied research and development program of $20M and 115 employees in these five technical branches: Coastal Processes, Estuarine Engineering, River Engineering, Hydrologic Systems, Field Data Collection and Analysis.

1988-2004
Chief, Coastal Processes Branch, Coastal and Hydraulics Laboratory, U.S. Army Engineer Research and Development Center, Vicksburg, MS. Responsible for research an development program of $6M and 20 engineers, scientists and support staff working in the following disciplines: tidal circulation and storm surge, wind wave generation and transformation, storm wave and water level prediction, surf zone dynamics, coastal inlet processes, coastal erosion and storm-induced morphology change, erodability of fine-grained and mixed sediments, design and maintenance of coastal storm damage reduction projects, beach fill design and performance evaluation, Design and evaluation of dredged material placement projects, prediction of dredged material stability, transport and fate, regional sediment management, heavy emphasis on numerical modeling of these coastal processes.

1979 -1988
Research Hydraulic Engineer, Coastal Processes Branch, Coastal and Hydraulics Laboratory, U.S. Army Engineer Research and Development Center, Vicksburg, MS (principal investigator responsible for research into tidal circulation and storm surge, nearshore wave propagation, transformation and surf zone wave breaking, shoreline and beach erosion processes, design and maintenance of coastal storm damage reduction projects including beach nourishment, numerical modeling of coastal processes)

Selected Publications Relevant to Subject Matter Addressed in this Report

Smith, E.R., Ebersole, B.A., Wang, P., and Zhang, J. "Dependence of longshore transport on incident waves and breaker type", *Accepted by* J. Coastal Research.

Wamsley, T.V., Cialone, M.C., Smith, J.M., Ebersole, B.A., and A.S. Grzegorzewski. "Influence of landscape restoration and degradation on storm surge and waves in southern Louisiana, *Submitted to* Journal of Natural Hazards.

Bunya, S., Westerink, J., Dietrich, J.C., Westerink, H.J., Westerink, L.G., Atkinson, J., Ebersole, B., Smith, J.M., Resio, D., Jensen, R., Cialone, M.A., Luettich, R., Dawson, C., Roberts, H.J., and Ratcliff, J. 2008. A High Resolution Coupled Riverine Flow, Tide, Wind, Wind Wave and Storm Surge Model for Southern Louisiana and Mississippi: Part I – Model Development and Validation. *Submitted to* National Weather Review.

Dietrich, J.C., Bunya, S., Westerink, J.J., Ebersole, B.A., Smith, J.M., Atkinson, J.H., Jensen, R., Resio, D.T., Luettich, R.A., Dawson, C., Cardone, V.J., Cox, A.T., Powell, M.D., Westerink, H.J., and Roberts, H.J. 2008. A High-Resolution Coupled Riverine Flow, Tide, Wind, Wind Wave and Storm Surge Model for Southern Louisiana and Mississippi: Part II - Synoptic Description and Analysis of Hurricanes Katrina and Rita. *Submitted to* National Weather Review.

Ebersole, B.A., Resio, D.T., and Westerink, J.J. 2006. A community approach to improved prediction and characterization of coastal storm hazards. Marine Technology Society Journal , Vol. 40, No. 3, pp 44-56.

Ebersole, B.A., Resio, D.T., Westerink , J.J., and Dean, R.G., "Performance Evaluation of the New Orleans and Southeast Hurricane Protection System, Report of the Interagency Performance Evaluation Task Force, Volume IV – The Storm," June 2006.

Svendsen, I.A., Qin, W., Ebersole, B.A., 2003, Modeling Waves and Currents in the LSTF Facility, Coastal Engineering, Vol. 50, pp 19-45.

Wang, P., Ebersole, B.A., Smith, E.R., and Johnson, B.D., Temporal and spatial variations of surf zone currents and suspended sediment concentration, Coastal Engineering 46 (2002) 175-211.

Ebersole, B.A., Gravens, M.B. Walton, T.L., Randall A. Wise. 2002. Beach Fill Design. In: Coastal Engineering Manual, Part V, Coastal Project Planning and Design, Chapter V-4, Engineer Manual 1110-2-1100, U.S. Army Corps of Engineers

A list of other publications can be provided.

Recent Professional Activities

- Lead U.S. Army Corps of Engineers representative to U.S. Interagency Working Group on Tropical Cyclone Research (current)

- Corps of Engineers Representative to U.S. Integrated Ocean Observing System, Modeling and Simulation Steering Committee (current)

- Invited Speaker, Joint Technical Commission for Oceanography and Marine Meteorology, 1st Scientific and Technical Symposium on Storm Surges, Korea, Oct 2007

- Interagency Performance Evaluation Task Force (IPET), Co-Leader, Regional Storm Surge and Waves Task, forensic study of hurricane protection system performance during Hurricane Katrina, 2005-2007

- Instructor, ASCE Webinar Series, B.A. Ebersole and D.T. Resio, Lessons Learned from Hurricane Katrina and Implications for the Civil Engineering Profession and Your Community, "Wave Forces and Overtopping" July 2007

- SEI Structures Conference, Presentation, "Hurricane Katrina Storm Surge and Waves" May 2007

- Corps of Engineers Guidance Update Teams, Engineering Regulation – Minimum Safety Requirements; I-Wall Engineering Circular; Levee Certification Engineering Technical Letter; 2007 to present

- Plenary Session Speaker, 4th Forensics Conference, "Forensic Study of New Orleans Hurricane Protection in Katrina" Oct 2006

- Plenary Session Speaker, Dam Safety Conference, "Forensic Study of New Orleans Hurricane Protection in Katrina" Sep 2006